

DISS. ETH NO.17551

**SILK FIBROIN SCAFFOLDING FOR GROWTH FACTOR
DELIVERY IN TISSUE REPAIR**

A dissertation submitted to

ETH ZURICH

Doctor of Sciences

presented by

LORENZ UEBERSAX

MSc molecular and cell biology, University Louis Pasteur of Strasbourg
Dipl. Biotech., University of Basel, Strasbourg, Freiburg and Karlsruhe (EUCOR)

born 20.02.1976

Citizen of Thörigen, Bern

accepted on the recommendation of

Prof. Dr. Hans P. Merkle, examiner

PD Dr. Dr. Lorenz Meinel, co-examiner

Prof. Dr. David L. Kaplan, co-examiner

Prof. Dr. Wendelin J. Stark, co-examiner

2008

To my parents

TABLE OF CONTENTS

ABBREVIATIONS AND NOTATIONS	II
BACKGROUND AND PURPOSE	1
ABSTRACT	9
ZUSAMMENFASSUNG	15
CHAPTER I	23
Biopolymer based growth factor delivery for tissue repair: From natural concepts to engineered systems	
CHAPTER II	97
Effect of scaffold design on bone morphology <i>in vitro</i>	
CHAPTER III	131
Biocompatibility and osteoconduction of macroporous silk fibroin implants in cortical defects in sheep	
CHAPTER IV	167
Insulin-like growth factor I releasing macroporous silk fibroin scaffolds inducing chondrogenic differentiation of human mesenchymal stem cells	
CHAPTER V	199
Silk fibroin matrices for the controlled release of nerve growth factor (NGF)	
CHAPTER VI	233
The support of adenosine release from adenosine kinase deficient ES cells by silk substrates	
GENERAL DISCUSSION AND CONCLUSION	263
CURRICULUM VITAE	273
ACKNOWLEDGEMENTS	281

ABBREVIATIONS

Adk (-/-)	Adenosine kinase deficiency
ALP	Alkaline phosphatase
ANOVA	Analysis of variance
ATTEMPTS	Antibody Targeted Triggered Electrically Modified Prodrug Type Strategy
AUC	Area under the curve
aFGF	Acidic fibroblast growth factor (FGF-1)
bFGF	Basic Fibroblast growth factor (FGF-2)
BS	Bone surface
BSA	Bovine serum albumin
BV	Bone volume
BMP-2 / 7	Bone morphogenic protein 2 / 7
BMSC	Bone marrow stromal cells
BSE	Bovine spongiform encephalopathy
CB	Calicified bone matrix
Col-1	Collagen type 1
CI	Confidence interval
DVS	Divinyl sulfone
DNA	Deoxyribonucleic acid
DMEM	Dulbecco's modified eagle medium
DSC	Differential scanning calorimetry
ECM	Extracellular matrix
ESC	Embryonic stem cells
ELISA	Enzyme linked immunosorbent assay
EDTA	Ethylene diamine tetraacetate
FACS	Fluorescence activated cell sorting
FBS	Fetal bovine serum
FCS	Fetal calf serum
FGF-1	Fibroblast growth factor 1 (aFGF)

FGF-2	Fibroblast growth factor 2 (bFGF)
FGFBP	Fibroblast growth factor binding protein
FTIR / FT-IR	Fourier-transformed infrared spectroscopy
GH	Growth hormone
GF	Growth factor
GAG	Glycosaminoglycans
GC (<i>chapter II</i>)	Gas chromatography
GC (<i>chapter III</i>)	Giant cells
GDNF	Glial derived nerve growth factor
GFAP	Glial fibrillary acidic protein
HA	Hydroxyapatite
HyA	Hyaluronic acid
H&E	Staining of nucleic acid and proteins by hematoxylin and eosin dyes
HBGF	Heparin-binding growth factors
HFIP	Hexafluoroisopropanol
HGF	Hepatocyte growth factor
HLGAGs	Heparin-like glycosaminoglycans
HPLC	High performance liquid chromatography
hMSC	Human mesenchymal stem cells
HRP	Horse radish peroxidase
IGF-I / II	Insulin-like growth factor I / II
IGFBP	Insulin-like growth factor binding protein
KGF	Keratinocyte growth factor
LAP	Latency-associated peptide
LCST	Lower critical solution temperature
LTBPs	Latent transforming growth factor-beta-binding proteins
LiBr	Lithium bromide
LLC	Large latent complex
LMWH	Low molecular weight heparin

LN	Laminin
MEM	Minimum essential medium
MFGCs	Multinuclear foreign body giant cells
MG63	Immature human osteoblasts cell line
mIFNbeta	Mouse interferon beta
MMP	Matrix metalloproteinase
MTT	3-(4,5-dimethylthiazol-2-yl)-2, 5-diphenyl tetrazolium bromide
MW	Molecular weight
MS	Mass spectrometry
MWCO	Molecular weight cut-off
NC	Nerve conduits
NGF	Nerve growth factor
2D	Two dimensional
3D	Three dimensional
OC	Osteocytes
OD	Optical density
OS	Osteoid
P1, 2, 3, ...	Passage 1, 2, ...
PBS	Phosphate buffer saline
PDGF	Platelet derived growth factor
P/S	Penicillin/streptomycin
PC12	Pheochromocytoma cells 12 (rat)
PEG	Poly(ethylene glycol)
p(LA-co-EO)	Poly(L-lactide-co-ethylene oxide)
p(HEMA-co-MMA)	Poly(2-hydroxyethyl methacrylate-co-methyl methacrylate)
PGA	Poly(glycolic acid)
PDLLA	Poly(D,L-lactide)
PLA	Poly(L-lactic acid)

PLLA	Poly(L-lactic acid)
PLGA	Poly(L-lactic-co-glycolic acid)
PlnDI	Perlecan domain I
PNIPAAm	Poly(N-isopropylacrylamide)
PO	Poly(L-ornithine)
PVA	Poly(vinyl alcohol)
PVDF	S-hydrophobic poly(vinylidene fluoride)
RGD	Cell adherence sequence from fibronectin
rhTGF-β1	Human recombinant transforming growth factor beta 1
rhBMP-2	Human recombinant bone morphogenic protein 2
RT	Room temperature
RP-HPLC	Reverse phase-high performance liquid chromatography
Safranin-O	Proteoglycan staining
SCID	Severe combined immunodeficiency
SD	Standard deviation
SD (<i>chapter III</i>)	Scaffold degradation
SEM	Scanning electron microscopy
SEC	Size exclusion chromatography
SDS	Sodium dodecyl sulfate
ShNC	S-hydrophilic nitrocellulose
SF	Silk fibroin
TCP (<i>chapter VI</i>)	Tissue culture plastic
TCP	Tricalcium phosphate
TFA	Trifluoroacetic acid
TGF-β / TGF-beta	Transforming growth factor beta
tTGase	Transglutaminase
tPA	Tissue-type plasminogen activator
Tukey-HST	Multiple post-hoc test for unequal sample size
UPW	Ultra purified water and SF scaffold produced by freeze drying of aqueous SF solution

VEGF	Vascular endothelial growth factor
von Kossa	Staining of calcium anion phosphate or carbonates based on silver nitrate solution
VS-PEG-VS	PEG-divinyl sulfone
wt	Wild type
w/w	weight over weight
XRD	X-ray diffraction
μCT	Micro-computed tomography

BACKGROUND & PURPOSE

Mammalian tissues mainly consist of differentiated eukaryotic cells embedded in a unique extracellular matrix (ECM). Both constituents contribute to the typical phenotype and topology of the tissue and determine its function(s) within the organism. Large variations between tissues exist with respect to their potential to regenerate after severe damage. Key for a successful regeneration of damaged tissue is its potential to induce sufficient proliferation of local tissue-specific cells and to prevent the invasion of unspecific cells from adjacent tissues, synonymous to the loss of its function. Some tissues such as blood, skin, bone and gut have high turnover rates, with “old” tissue being constantly replaced throughout our live time in contrast to brain, heart and muscle tissue, having lost their capacity for spontaneous regeneration [1]. In some instances lost tissue can be replaced by an activation of differentiated tissue specific cells, as in the case of hepatocytes [2], but in other cases activation of tissue associated undifferentiated stem cells is necessary [3]. In general, the potential for regeneration declines with age regardless of tissue type. In some tissues such as muscle, blood, liver and brain this decline could be directly associated to a loss of responsiveness of tissue-specific stem and progenitor cells. In other cases a drop in systemic factor availability and the age of the surrounding tissue seemed to be responsible [4]. Therefore, the critical level of tissue damage, where traditional medical treatments or surgery fail to restore lost tissue, is a function of the regenerative potential of a specific tissue in general, the size of the defect, the decrease of regenerative potential of tissue relative to the age of the patient, and other factors such as diseases, or long-term consumption of toxic agents [5, 6]. Hence, the continuous aging of our society and our excessive live style, including risky fun-sports, will drastically increase the need for more efficient interventions towards tissue repair in the future.

The aim of tissue engineering is, therefore, to provide new strategies for the restoration of critical tissue defects in order to prevent significant loss of function or severe physical disfiguration that are untreatable by conventional surgery.

Current strategies to replace lost tissue were by grafting of autologous or allogeneous tissue from a healthy donor site. However, the clinical outcomes of tissue grafts to restore skin, ligaments, bone, cartilage and nerves are difficult to control as the biological properties of the harvested tissue depend on the individual conditions of the patient. Complications such as pain, morbidity, and failure of tissue regeneration at the harvest-site have been reported, as well as necrosis of the grafted material and failure of its integration into the defect after implantation [7-10]. Such severe drawbacks can result in prolonged hospitalization and negatively affect the compliance of the patient. Therefore, the use of biomaterial scaffolds as substitutes for lost tissue after injuries or diseases has become an emerging alternative to traditional tissue grafts. Synthetic porous substitutes made of biocompatible materials share numerous advantages over autografts and allografts including their practically unlimited supply, straightforward sterilization and simple storage. They can be tailored to meet the individual needs of the patients and make second site surgery unnecessary. Besides synthetic materials such as polyesters and ceramics, natural biopolymers such as proteins and polysaccharides derived from human or animal ECM have been investigated as materials for tissue substitutes. At this point, only few biopolymers are commercially available and have been clinically administered such as collagen (INFUSE Bone Graft, Medtronic Inc., Minneapolis, MN, USA), hyaluronic acid (Hyaff-11, Fidia Advanced Biomaterials, Padova, Italy) and fibrin (TISSEEL, Baxter, Deerfield, IL, USA). Nevertheless, restricted manufacturing and fast biodegradation in combination with poor mechanical and load-bearing properties question their roles in physically supporting tissue regeneration. Silk fibroin (SF) derived from the silk worm *Bombyx mori* is a promising alternative to these biopolymers, as it provides comparable biocompatibility, but stronger mechanical strength and slower biodegradation. Scaffolding of SF may be under various conditions [11-13] such as from aqueous and non-aqueous solutions. In fact, SF have been successfully investigated for a wide range of biomedical applications and various tissues [14-17]. Its proven biocompatibility as well as the

good interaction between SF scaffolds and mesenchymal (adult) stem cells provides interesting opportunities to charge tissue defects with either sufficiently undifferentiated proliferating cells or with more differentiated, pre-organized tissue constructs from *in vitro* tissue cultures [18-20]. Nevertheless, expensive supplemental delivery of cytokines and other mediators for *in vitro* tissue culture, limited size of engineered tissue, and time are important economical and temporal constraints for this approach. Moreover, stem cell function is affected by age and, therefore, precautionary donations would be mandatory and urge for long-term quality assurance of donor cells under storage. Especially in elderly people, stem cell therapy may be less efficacious because an aged micro- as well as systemic environment may crucially affect the performance of progenitor cells [1]. Consequently, biomaterials suitable for tissue repair have to provide an environment similar to that in young and healthy tissue. With or without a combination with stem cells, such materials are to improve natural tissue regeneration and circumvent age related problems, time constraints and prolonged hospitalization, in order to improve patient compliance and reduce health care costs.

Important roles in both physiological tissue regeneration and the development of *in vitro* tissue engineering technologies are being played by growth factors (GFs) that regulate tissue maintenance by controlling proliferation as well as the cellular fate of progenitor and local cells [21-24]. During extracellular matrix formation, growth factors or their precursors are stored therein in form of inactive depots. Localization and storage is mediated by direct, low affinity binding of the GFs to ECM molecules or through specific binding molecules that provide stability and protect the proteins from degradation. Therefore, such GF depots represent stocks for important informational signals for tissue maintenance and growth within the ECM that can be liberated in response to physiological changes [21]. Consequently, to improve the biological activity of biomaterial implants it is important to endow the implant with signaling molecules such as GFs to activate regenerative processes in analogy to physiological tissue

self repair. The accommodation of GFs either on or in biomaterial scaffolds through covalent coupling, absorption or embedment have been demonstrated to provide successful strategies to enhance tissue regeneration [25-28]. However, the short biological half-life of GFs in the body, their limited physical and chemical stability during formulation and storage [29] as well as potential side effects [25-33] necessitate a rigorous control over the release of GFs. In some situations it turned out to be necessary to provide supraphysiological concentrations of exogenous GFs because of the inefficacy of physiological levels, in other cases physiological levels might be sufficient [34].

Recently, SF has been further developed as a platform for drug delivery both in the form of casted films [15] and as genetically engineered silk-elastine hydrogels [35, 36] that have been suggested as a promising material for the accommodation of bioactive compounds within a 3D implant. To further contribute to SF as a biomaterial, the purpose of this study was the development of novel scaffolding technologies and designs that allow to deliver bioactive compounds under spatiotemporal regimes that are beneficial for tissue regeneration in combination with suitable mechanical properties and adaptable implant design.

The first chapter of this PhD thesis summarizes different natural concepts of GF storage and stabilization in the ECM and the use of biopolymers as growth factor carriers to enhance tissue regeneration. Furthermore, rational approaches for the engineering of proteins and polysaccharides with enhanced GF stabilization properties and controlled release profiles will be presented, including the implementation of natural concepts for GF storage. In the first experimental chapter we introduce a novel scaffolding technology that was developed to fabricate porous SF scaffolds for skeletal tissue repair allowing for direct accommodation of (chemically and physically sensitive) GFs under comparably mild conditions in an aqueous system. Scaffolds with various pore sizes and interconnectivities were fabricated, and their ability investigated to guide bone formation by scaffold design using human mesenchymal stem cells (hMSC) that

were cultured under osteogenic conditions in bioreactors. In a second study, the performance of such SF scaffolds were further explored upon implantation into drill hole defects in cancellous bone of sheep. Both their biocompatibility and capacity to guide formation of new bone *in vivo* were tested in comparison to a previously established SF scaffolding protocol that required an organic solvent, hexafluoroisopropanol (HFIP). Subject of the third experimental study (chapter IV) of this thesis was the question whether the biological performance of SF scaffolds could be further improved by embedding insulin-like growth factor I (IGF-I). IGF-I release profiles as well as the bioactivity of released IGF-I were assessed over a time span of 4 weeks. Moreover, the outcome of IGF loaded SF scaffolds on chondrogenesis of hMSC was investigated in combination with TGF- β . To further enlarge the applicability of SF for drug delivery purposes the fifth experimental chapter of this PhD thesis deals with the successful water-based co-formulation of SF and nerve growth factor (NGF) as a GF delivery system to enhance peripheral nerve repair. For this aim, tubular NGF loaded SF nerve conduits (NC) were prepared by air-drying and freeze-drying. In a suitable *in vitro* model the formulations were tested as to the promise of NGF release and its biological potency - after release - for cellular differentiation. In the last experimental chapter we expanded the use of SF as prospective material for the encapsulation of therapeutic cells into semipermeable, biodegradable bioreactors. For this purpose SF was tested as a substrate for the cell-based delivery of adenosine to prevent epileptic seizures of the central nervous system. Adenosine kinase deficient glial precursor cells as derived from murine embryonic stem cells were seeded on SF substrates and their potential to differentiate into glial cells while producing relevant amounts of adenosine were explored. Such a strategy could further help to engineer sustained long term delivery systems for cell mediated therapies with small pharmaceuticals.

REFERENCES

1. T.A. Rando, Stem cells, ageing and the quest for immortality, *Nature* 441 (7097) (2006) 1080-6.
2. S.H. Sigal, S. Brill, A.S. Fiorino, L.M. Reid, The liver as a stem cell and lineage system, *Am J Physiol* 263 (2 Pt 1) (1992) G139-48.
3. J. Ehrhardt, J. Morgan, Regenerative capacity of skeletal muscle, *Curr Opin Neurol* 18 (5) (2005) 548-53.
4. I.M. Conboy, M.J. Conboy, A.J. Wagers, E.R. Girma, I.L. Weissman, T.A. Rando, Rejuvenation of aged progenitor cells by exposure to a young systemic environment, *Nature* 433 (7027) (2005) 760-4.
5. N. Chbinou, J. Frenette, Insulin-dependent diabetes impairs the inflammatory response and delays angiogenesis following Achilles tendon injury, *Am J Physiol Regul Integr Comp Physiol* 286 (5) (2004) R952-7.
6. L. Ma, L.W. Zheng, L.K. Cheung, Inhibitory effect of nicotine on bone regeneration in mandibular distraction osteogenesis, *Front Biosci* 12 (2007) 3256-62.
7. A.N. Kager, M. Marks, T. Bastrom, P.O. Newton, Morbidity of iliac crest bone graft harvesting in adolescent deformity surgery, *J Pediatr Orthop* 26 (1) (2006) 132-4.
8. S.N. Parikh, Bone graft substitutes: past, present, future, *J Postgrad Med* 48 (2) (2002) 142-8.
9. D. Bettin, H. Bohm, M. Clatworthy, D. Zurakowski, T.M. Link, Regeneration of the donor side after autogenous fibula transplantation in 53 patients: evaluation by dual x-ray absorptiometry, *Acta Orthop Scand* 74 (3) (2003) 332-6.
10. D.C. Rees, F.S. Haddad, Bone transplantation, *Hosp Med* 64 (4) (2003) 205-9.
11. L. Meinel, S. Hofmann, V. Karageorgiou, C. Kirker-Head, J. McCool, G. Gronowicz, L. Zichner, R. Langer, G. Vunjak-Novakovic, D.L. Kaplan, The inflammatory responses to silk films in vitro and in vivo, *Biomaterials* 26 (2) (2005) 147-55.
12. B. Panilaitis, G.H. Altman, J. Chen, H.J. Jin, V. Karageorgiou, D.L. Kaplan, Macrophage responses to silk, *Biomaterials* 24 (18) (2003) 3079-85.
13. G.H. Altman, F. Diaz, C. Jakuba, T. Calabro, R.L. Horan, J. Chen, H. Lu, J. Richmond, D.L. Kaplan, Silk-based biomaterials, *Biomaterials* 24 (3) (2003) 401-16.
14. L. Uebersax, D.E. Fedele, C. Schumacher, D.L. Kaplan, H.P. Merkle, D. Boison, L. Meinel, The support of adenosine release from adenosine kinase deficient ES cells by silk substrates, *Biomaterials* 27 (26) (2006) 4599-607.

15. S. Hofmann, C.T. Wong Po Foo, F. Rossetti, M. Textor, G. Vunjak-Novakovic, D.L. Kaplan, H.P. Merkle, L. Meinel, Silk fibroin as an organic polymer for controlled drug delivery, *J Control Release* 111 (1-2) (2006) 219-17.
16. L. Meinel, S. Hofmann, V. Karageorgiou, L. Zichner, R. Langer, D. Kaplan, G. Vunjak-Novakovic, Engineering cartilage-like tissue using human mesenchymal stem cells and silk protein scaffolds, *Biotechnol Bioeng* 88 (3) (2004) 379-91.
17. L. Meinel, V. Karageorgiou, R. Fajardo, B. Snyder, V. Shinde-Patil, L. Zichner, D. Kaplan, R. Langer, G. Vunjak-Novakovic, Bone tissue engineering using human mesenchymal stem cells: effects of scaffold material and medium flow, *Ann Biomed Eng* 32 (1) (2004) 112-22.
18. S. Hofmann, H. Hagenmuller, A.M. Koch, R. Muller, G. Vunjak-Novakovic, D.L. Kaplan, H.P. Merkle, L. Meinel, Control of in vitro tissue-engineered bone-like structures using human mesenchymal stem cells and porous silk scaffolds, *Biomaterials* 28 (6) (2007) 1152-62.
19. V. Karageorgiou, M. Tomkins, R. Fajardo, L. Meinel, B. Snyder, K. Wade, J. Chen, G. Vunjak-Novakovic, D.L. Kaplan, Porous silk fibroin 3-D scaffolds for delivery of bone morphogenetic protein-2 in vitro and in vivo, *J Biomed Mater Res A* 78 (2) (2006) 324-34.
20. L. Meinel, R. Fajardo, S. Hofmann, R. Langer, J. Chen, B. Snyder, G. Vunjak-Novakovic, D. Kaplan, Silk implants for the healing of critical size bone defects, *Bone* 37 (5) (2005) 688-98.
21. M.R. Tarla, F.S. Ramalho, L.N. Ramalho, E.S.T. Castro, D.F. Brandao, J. Ferreira, E.S.O. Castro, S. Zucoloto, A molecular view of liver regeneration, *Acta Cir Bras* 21 (2006) 58-62.
22. D.M. Bissell, Hepatic fibrosis as wound repair: a progress report, *J Gastroenterol* 33 (2) (1998) 295-302.
23. N. Sykaras, L.A. Opperman, Bone morphogenetic proteins (BMPs): how do they function and what can they offer the clinician? *J Oral Sci* 45 (2) (2003) 57-73.
24. S. Mohan, D.J. Baylink, Bone growth factors, *Clin Orthop Relat Res* (263) (1991) 30-48.
25. S.J. Lee, Cytokine delivery and tissue engineering, *Yonsei Med J* 41 (6) (2000) 704-19.
26. C.A. Kirker-Head, Potential applications and delivery strategies for bone morphogenetic proteins, *Adv Drug Deliv Rev* 43 (1) (2000) 65-92.

27. Y. Tabata, Tissue regeneration based on growth factor release, *Tissue Eng* 9 (Suppl 1) (2003) 5-15.
28. H. Seeherman, J. Wozney, R. Li, Bone morphogenetic protein delivery systems, *Spine* 27 (16 Suppl 1) (2002) 16-23.
29. R. Pawar, A. Ben-Ari, A.J. Domb, Protein and peptide parenteral controlled delivery, *Expert Opin Biol Ther* 4 (8) (2004) 1203-12.
30. D. Kaigler, J.A. Cirelli, W.V. Giannobile, Growth factor delivery for oral and periodontal tissue engineering, *Expert Opin Drug Deliv* 3 (5) (2006) 647-62.
31. J.R. Lieberman, A. Daluiski, T.A. Einhorn, The role of growth factors in the repair of bone. Biology and clinical applications, *J Bone Joint Surg Am* 84-A (6) (2002) 1032-44.
32. H. Seeherman, J.M. Wozney, Delivery of bone morphogenetic proteins for orthopedic tissue regeneration, *Cytokine Growth Factor Rev* 16 (3) (2005) 329-45.
33. M.C. Peters, B.C. Isenberg, J.A. Rowley, D.J. Mooney, Release from alginate enhances the biological activity of vascular endothelial growth factor, *J Biomater Sci Polym Ed* 9 (12) (1998) 1267-78.
34. V. Luginbuehl, E. Wenk, A. Koch, B. Gander, H.P. Merkle, L. Meinel, Insulin-like growth factor I-releasing alginate-tricalciumphosphate composites for bone regeneration, *Pharm Res* 22 (6) (2005) 940-50.
35. Z. Megeed, M. Haider, D. Li, B.W. O'Malley, Jr., J. Cappello, H. Ghandehari, In vitro and in vivo evaluation of recombinant silk-elastinlike hydrogels for cancer gene therapy, *J Control Release* 94 (2-3) (2004) 433-45.
36. Z. Megeed, J. Cappello, H. Ghandehari, Controlled release of plasmid DNA from a genetically engineered silk-elastinlike hydrogel, *Pharm Res* 19 (7) (2002) 954-9.

SUMMARY

For the clinical treatment of tissue defects, biomaterial scaffolds have become an emerging alternative to tissue grafts. They share various advantages over tissue autografts and allografts such as nearly unlimited supply, straightforward sterilization and storage, and make second site surgery unnecessary. However, in contrast to autologous tissue grafts, biomaterials *per se* lack the capacity to deliver intrinsic biological signals that stimulate the self-regeneration of damaged tissue. Growth factors (GFs) are soluble or matrix bound mitogenic and morphogenic factors that control cell proliferation, differentiation and migration during tissue development, regeneration and maintenance. A promising strategy, therefore, to improve the performance of biomaterials for tissue repair, is to endow biomaterial scaffolds with GFs in order to strengthen their biological outcome. Pivotal for the accommodation of GFs in biomaterial scaffolds is the development of suitable technologies that allow for an efficient loading of the scaffolds with GFs and, at the same time, sustain the potency and the release of the GFs *in vivo*. Silk fibroin (SF) derived from the silk worm *Bombyx mori* is an attractive biomaterial to be investigated for its capacity to accommodate GFs, as it exerts excellent biocompatibility, good mechanical strength, slow *in vivo* degradation and a flexible processability.

The extracellular matrix (ECM) of tissues is regarded as a physiological depot for various GFs, from where they are to be released into the surrounding tissue and play their natural roles in tissue regulation. In addition to autocrine and paracrine cell signalling, they provide specific extracellular information necessary to conduct tissue homeostasis and (re)generation. **Chapter I** of this PhD thesis reports on various physiological concepts that have evolved during evolution to control the activity of GFs in a specific manner through interaction with biopolymers of the ECM, and how such interactions may respond to systemic or cellular signals. A fundamental understanding of the extracellular storage of GFs and its control could provide important cues about the nature of GF interactions and improve the potency of current implantable biopolymers for GF delivery in

tissue repair. Therefore, in a second part of this review, nature-derived biopolymers will be discussed with respect to their availability, suitability for scaffolding, mechanical properties, and efficiency to sustain the activity and release of GFs. Furthermore, we will detail on rational modifications and engineering approaches to improve their applicability as delivery systems. In particular, we discuss biotechnology and chemical engineering tools to adapt natural concepts of GF depots for delivery purposes. In conclusion, the engineering of novel biopolymer platforms holds promise to enhance the biological performance of GF loaded artificial tissue substitutes in order to replace autologous and allogeneous tissue grafts for the treatment of critical tissue defects.

In **Chapter II** we introduce a novel scaffolding technology for SF with the aim to fabricate porous scaffolds for skeletal tissue repair allowing for direct accommodation of (chemically and physically sensitive) GFs under comparably mild conditions in an aqueous system. In particular, 3D scaffolds with various pore sizes and interconnectivities were fabricated through freeze drying of aqueous SF solution using paraffin spheres as porogen. Furthermore, their ability was tested to guide *in vitro* bone formation through scaffold architecture. For this purpose human mesenchymal stem cells (hMSC) were seeded onto the scaffolds and cultured under osteogenic conditions in bioreactors. Osteogenic differentiation of hMSC resulted in extensive mineralization, alkaline phosphatase activity, and the formation of interconnected trabecular- or cortical-like mineralized bone-like structures which was governed by the interconnective pore diameters of the SF scaffolds. As a result of the slow biodegradation inherent to silk fibroin, the scaffolds preserved their initial morphology and provided a stable template throughout the mineralization phase of the hMSC, also involving osteogenic differentiation and new extracellular matrix formation. The ability to direct bone morphology via scaffold design suggests a new option in the use of biodegradable scaffolds to control *in vitro* engineered bone tissue outcomes. Moreover, the novel scaffolding process allows for the accommodation of growth factors in the SF matrix during fabrication in an aqueous milieu.

The performance of novel SF scaffolds was further explored upon implantation into drill hole defects in cancellous bone of sheep (**Chapter III**). The goal of this study was to compare biocompatibility and cellular responses to porous SF scaffolds produced by (i) an ultrapurified water based (UPW) process with paraffin microspheres as porogen and (ii) a Hexafluorisopropanol (HFIP) based process using salt crystals as porogen, applying two different SF sources. For this purpose, SF scaffolds with pore sizes between 200 and 300 μm were implanted ($n=6$) into drill hole defects in cancellous sheep bone using tibiae and humeri. The scaffolds were macroscopically and histologically evaluated for biocompatibility, cell-scaffold interactions, cellular ingrowth and new bone formation after 8 weeks post implantation. For semiquantitative evaluation, the investigated parameters were scored and subjected to statistical analysis (ANOVA). All implants showed good biocompatibility as evidenced by low infiltration of inflammatory cells and absence of any encapsulation of the scaffolds into connective tissue. However, multinuclear foreign body giant cells (GCs) and macrophages were present in all parts of the scaffolds and shown to degrade the SF scaffolds. Cell ingrowth and vascularization of the scaffolds were uniform and independent of scaffold type and SF source except for the scaffolds produced by the HFIP process. In fact, HFIP scaffolds exhibited local regions of empty pores throughout their pore structure. The lack of tissue ingrowth into HFIP scaffolds appeared to correspond with their lower pore interconnectivity and interconnective pore diameter as compared to UPW scaffolds, which featured enlarged interconnectivity and interconnective pore diameters and improved osteoconduction indicated by local clusters of trabecular-like bone. Overall, because of slow biodegradation and good biocompatibility, SF scaffolds provide favourable opportunities for osteoconduction.

The improvement of the biological performance of the novel scaffold type through the embedment of growth factors was the aim of **Chapter IV** of this PhD thesis. Growth factor releasing scaffolds are an emerging alternative to autologous or allogeneous implants, providing a biologically active template for tissue

(re)generation. The goal of this study was to evaluate the feasibility of controlled insulin-like growth factor I (IGF-I) releasing silk SF scaffolds in the context of cartilage repair. The impact of manufacturing parameters (pH, methanol treatment and drug load) was correlated with IGF-I release kinetics using ELISA and potency tests. Methanol treatment induced water insolubility of SF scaffolds, allowed the control of bioactive IGF-I delivery and did not affect IGF-I potency. The cumulative drug release correlated linearly with the IGF-I load. To evaluate the chondrogenic potential of the scaffolds, hMSC were seeded on unloaded and IGF-I loaded scaffolds in TGF- β supplemented medium. Indeed, IGF-I loaded scaffolds showed chondrogenic differentiation of hMSC, starting after 2 weeks and more strongly after 3 weeks, whereas no chondrogenic responses were observed on unloaded control scaffolds. IGF-I loaded porous SF scaffolds have the potential to provide chondrogenic stimuli to hMSC. Evidence for *in vivo* cartilage (re)generation needs to be demonstrated by future, pre-clinical proof of concept studies.

Chapter V of this PhD thesis attempts to enlarge the applicability of SF for drug delivery purposes. Its focus is on the co-formulation of nerve growth factor (NGF) and aqueous SF solution to produce GF loaded nerve conduits (NC) aimed at the enhancement of peripheral nerve repair. NC for peripheral nerve repair should guide the sprouting axons and physically protect the axonal cone from any damage. The NC should also degrade after completion of its function to obviate the need of subsequent explantation and should optionally be suitable for controlled drug release of embedded growth factors to enhance nerve regeneration. As a biocompatible and slowly biodegradable biomaterial with excellent mechanical properties SF was assumed to meet the above stated requirements. *In vitro* tests with SF films showed that SF supported the adherence and metabolic activity of PC12 cells, and, in combination with NGF, fostered neurite outgrowth during PC12 cell differentiation. NGF-loaded SF-NC were prepared from aqueous solutions of NGF and SF (20%, w/w), which were air-dried or freeze-dried (freezing at -20 °C or -196 °C) in suitable molds. NGF release from the three

differently prepared SF-NC was prolonged over at least three weeks, but the total amount released depended on the drying procedure of the NC. The potency of released NGF was retained in all formulations. Validation experiments with differently dried NGF-lactose solutions presented no evidence for marked protein aggregation (SEC, HPLC), loss of ELISA-reactivity, or lack of PC12 cell bioactivity. Our study encourages a further exploitation of SF-NC for growth factor delivery and evaluation in peripheral nerve repair.

In the last experimental chapter (**Chapter VI**) this PhD thesis further expands the use of SF as prospective biomaterial for the encapsulation of therapeutic cells into semipermeable, biodegradable bioreactors. Adenosine kinase deficient (*Adk*^{-/-}) embryonic stem cells (ESC) encapsulated in synthetic polymers have previously been shown to provide therapeutic adenosine release and transient seizure suppression in epileptic rats. However, the previously used polymers were not biodegradable and would need to be explanted after the cells have lost their function. SF could be an ideal material to support the long term delivery of adenosine produced by encapsulated cells, as the material is highly permeable for nutritional components such as glucose and degrades slowly but completely after implantation. To assess the suitability of SF for this purpose, different materials were studied: (1) type I collagen (Col-1), (2) silk-fibroin (SF), and (3) poly(L-ornithine) (PO) coated tissue culture plastic. *Adk*^{-/-} or wild type (wt) ESC-derived glial precursor cells were seeded on these substrates and cultured either in proliferation medium containing GFs or in differentiation medium devoid of growth factors. In proliferation medium cell proliferation was higher and metabolic activity lower on Col-1 and PO substrates as compared to SF. Cells from both genotypes readily differentiated into astrocytes after growth factor removal on all substrates. *Adk*^{-/-} cells cultured on SF or PO released significantly more adenosine than their wt counterparts at all developmental stages. Adenosine release was similar on SF and PO substrates and the amounts released from *Adk*^{-/-} cells (>20 ng/ml) were considered to be of therapeutic relevance. Taken together, these results suggest that silk matrices are particularly suitable biomaterials for

ESC encapsulation and for the design of adenosine releasing bioreactors for the treatment of epilepsy. Such a strategy could further help to engineer sustained delivery systems for cell mediated therapies with small pharmaceuticals.

ZUSAMMENFASSUNG

Medizinprodukte aus Biomaterialien stellen für die klinische Behandlung von Gewebedefekten eine wachsende Alternative zur Transplantation von autologen Geweben dar. Solche Gerüste aus Biomaterialien stehen fast unbeschränkt zur Verfügung und können einfach sterilisiert und gelagert werden. Ihr Einsatz erübrigt die sonst notwendige chirurgische Entnahme von Gewebe aus einer gesunden Körperpartie. Im Gegensatz zu autologen Gewebe besitzen Biomaterialien jedoch keine biologisch aktiven Signale, welche die Regeneration von beschädigtem Gewebe anregen können. Solche Signale sind beispielsweise gelöste oder an die extrazelluläre Matrix (EZM) gebundene Wachstumsfaktoren (WF) mit mitogener und mutagener Aktivität, welche die Proliferation, Differenzierung und Migration von Zellen während der Entwicklung, Regeneration und Erhaltung von Geweben kontrollieren. Das Beladen von Biomaterialien mit WF stellt deshalb eine vielversprechende Strategie dar, die Effizienz der Reparatur des Gewebes zu steigern und somit die biologische Wirkung des künstlichen Gewebeersatzmaterials zu verbessern. Die erfolgreiche Einbettung von WF in Implantaten aus Biomaterialien benötigt geeignete Technologien, die eine effiziente Beladung mit WF ermöglichen und die Wirksamkeit des WFs während der Produktion, Lagerung und Freisetzung *in vivo* gewährleisten. Seidenfibroin (SF) vom Kokon des Seidenwurms *Bombyx mori* erscheint aufgrund seiner ausgezeichneten Biokompatibilität, seines langsamen Abbaus im Körper und seiner hervorragenden mechanischen Eigenschaften und flexiblen Verarbeitungsweise ein attraktives Trägermaterial für WF.

Die extrazelluläre Matrix (EZM) von Geweben kann als ein physiologisches Depot unterschiedlicher WF betrachtet werden, die in das umgebende Gewebe freigesetzt werden können, um ihre natürliche Funktion in der Geweberegulierung auszuüben. Zusätzlich zur autokrinen und parakrinen Signalgebung an Zellen steuern die in der EZM gespeicherten WF auch die Gewebemöostase. **Kapitel 1** dieser Dissertation beschreibt physiologische Konzepte, die sich während der Evolution entwickelt haben, um die Aktivität von

WF durch die Interaktion mit Biopolymeren der EZM spezifisch zu kontrollieren; das Kapitel zeigt auf, wie solche Interaktionen auf zelluläre und physiologische Signale reagieren können. Ein grundlegendes Verständnis der extrazellulären Speicherung von WF könnte wichtige Hinweise über die Natur der WF/EZM/Bipolymer-Interaktionen liefern und damit implantierbare biopolymere Gewebeersatzmaterialien mit verbesserten Eigenschaften und optimaler WF-Freisetzung ermöglichen. Im zweiten Teil dieser Übersicht werden natürliche Biopolymere bezüglich ihrer Verfügbarkeit, ihrer mechanischen Eigenschaften und ihrer Eignung zur Herstellung von Biopolymergerüsten beschrieben. Die Fähigkeit verschiedener Biopolymergerüste, die Aktivität von WF während einer verlängerten Freisetzung zu gewährleisten, wird hier besonders erörtert. WF-Freisetzungssysteme können beispielsweise durch rationale chemische Modifikationen existierender oder durch die Entwicklung neuartiger Biopolymeren verbessert werden. In diesem Zusammenhang erscheinen die biotechnologischen und chemischen Methoden erwähnenswert, welche natürliche Konzepte der WF-Speicherung für die Freisetzung aus Biopolymersystemen adaptieren. Die Steigerung der biologische Wirksamkeit von WF-beladenen künstlichen Gewebeersatzmaterialien durch die Entwicklung neuer Biopolymer-Plattformen stellt eine vielversprechende Möglichkeit dar, in Zukunft autologe und allogene Gewebetransplantate für die Behandlung kritischer Gewebedefekte zu ersetzen.

In **Kapitel II** stellen wir eine neue Technologie zur Herstellung von porösen SF Knochenimplantaten vor. Die Technologie ermöglicht, chemisch und physikalisch empfindliche WF in wässriger Lösung und unter vergleichbar milden Bedingungen in SF-Matrizen einzubetten. Gerüste mit verschiedenen Porengrößen und Durchmessern der Porenverbindungen wurden hergestellt. Die SF-Gerüste wurden mit humanen mesenchymalen Stammzellen (hMSZ) besiedelt und in Bioreaktoren unter knocheninduzierenden Bedingungen inkubiert. Die zentrale wissenschaftliche Fragestellung dieser Arbeit lautete, ob und in welchem Ausmass die Gerüstarchitektur der SF Matrizen die Knochenneubildung *in vitro*

steuern kann. Die osteogene Differenzierung von hMSZ führte zu ausgiebiger Mineralisierung und Alkalinphosphataseaktivität; zudem entwickelten sich trabekuläre oder kortikale knochenähnliche Strukturen, die anhand der Durchmesser der Porenverbindungen charakterisiert wurden. Dank des langsamen Abbaus des SF-Materials behielten die SF-Gerüste ihre ursprüngliche Architektur bei und boten den Stammzellen eine stabile Unterlage für die Mineralisierung während ihrer osteogenen Differenzierung. Unser Ansatz, Gewebestrukturen durch unterschiedliche Gerüstarchitekturen zu steuern, sollte die Nachbildung komplexer Gewebemorphologien ermöglichen. Zudem erlaubt das neue Herstellungsverfahren, WF in wässriger Lösung direkt während des Fabrikationsprozesses in Matrizen einzubetten.

Die neuen SF-Gerüste wurden dann *in vivo* auf ihre Biokompatibilität und knochenbildende Eigenschaften untersucht. Dazu wurden SF-Matrizen in Bohrlochdefekte in der Spongiosa von Schafen implantiert (**Kapitel III**). Die porösen SF-Gerüste mit einheitlichen Porengrößen zwischen 200-300 µm wurden auf zwei unterschiedliche Arten hergestellt: (i) aus einer wässrigen SF-Lösung und unter Verwendung von Paraffinkugeln definierter Größe als Porogen; (ii) aus einer SF-Lösung in Hexafluorisopropanol und unter Verwendung von Salzkristallen definierter Größe als Porogen. Die Implantate wurden zudem aus zwei Seiden unterschiedlicher Herkunft hergestellt. Die SF-Gerüste wurden in Bohrlochdefekte der Tibia und des Humerus von Schafen implantiert (n=6). Die Zellreaktionen auf die SF-Implantate wurden nach 8 Wochen makroskopisch und histologisch auf Biokompatibilität, Zell-Gerüst-Interaktion, Einwachsen von Zellen und Knochenbildung untersucht. Die ausgewählten Parameter wurden nach dem Ausmass der jeweiligen Zellreaktion in verschiedene Kategorien eingeteilt und daraus gewonnene semiquantitative Resultate statistisch analysiert (ANOVA). Die geringe Zahl von Entzündungszellen und das Fehlen makroskopischer Anzeichen einer Entzündung, wie beispielsweise das Einkapseln von Implantat in fibröses Bindegewebe, bestätigten die gute Biokompatibilität aller SF-Implantate. Multinukleäre Fremdkörper-Riesenzellen und Makrophagen waren trotz der guten

Biokompatibilität in allen Teilen der Gerüste präsent und bauten das SF-Material aktiv ab. Blutgefässe und Gewebe wuchsen, unabhängig vom Gerüsttyp, gleichmässig in diejenigen SF-Implantate ein, die aus wässriger SF-Lösung hergestellt wurden. In den porösen SF-Strukturen waren lokale Regionen mit leeren Poren jedoch überall erkennbar. Die Implantate, die aus Hexafluorisopropanol-Lösung hergestellt wurden, zeigten hingegen Bereiche mit geringem Einwachsen von Blutgefässen und Gewebezellen, was möglicherweise mit der geringeren Interkonnektivität und kleineren Durchmesser der Porenverbindungen zusammenhängt. Der grosse Durchmesser der Porenverbindungen in den SF-Gerüsten, die aus wässrigen Lösungen hergestellt wurden, erwies sich als entscheidend für die verbesserte Osteokonduktivität, welche vereinzelte Clusterbildung aus trabekulärem Knochen ermöglichte. Der langsame Abbau und die gute Biokompatibilität der SF-Gerüste begünstigten zudem die Osteokonduktivität *in vivo*.

Gegenstand von **Kapitel IV** ist die Verbesserung der biologischen Wirksamkeit der neuen SF-Gerüste durch Einbettung von WF. WF freisetzende Implantate stellen eine wachsende Alternative zu autologen und allogenen Geweben dar, da sie ein biologisch wirksames Substrat für die Geweberegeneration bereitstellen können. Ziel dieser Studie war die kontrollierte Freigabe von Insulin ähnlichem Wachstumsfaktor (IGF-I) aus SF-Gerüsten im Hinblick auf Anwendbarkeit in der Knorpelregeneration. Die Auswirkung von Prozessparametern wie pH der wässrigen SF-Lösung, Methanolbehandlung der SF-Gerüste und der Gehalt an IGF-I auf die IGF-I-Freisetzungs kinetik wurden mittels ELISA und Bioaktivitätstests analysiert. Die Methanolbehandlung machte die SF-Gerüste wasserunlöslich und verlängerte dadurch die Freisetzungsdauer von bioaktivem IGF-I, ohne jedoch dessen Bioaktivität zu beeinträchtigen. Die nach 29 Tagen insgesamt freigesetzte Menge IGF-I korrelierte linear mit der initialen IGF-I-Beladung der SF-Gerüste. Die Bedeutung der IGF-I-Freisetzung für die Chondrogenese wurde mit hMSZ geprüft, die auf IGF-I beladenen (40 µg pro ml SF-Lösung) und unbeladenen SF-Gerüsten in TGF-β enthaltendem Medium

kultiviert wurden. Auf mit IGF-I beladenen Gerüsten begann die chondrogene Differenzierung der hMSZ bereits nach 2 Wochen und verstärkte sich noch in der 3. Woche. Dagegen zeigte sich auf unbeladenen Gerüsten keine Chondrogenese der hMSZ. Folglich besitzen mit IGF-I beladene SF-Gerüste das Potenzial die Chondrogenese von hMSZ durch die kontinuierliche Freisetzung von IGF-I zu unterstützen.

Kapitel V dieser Dissertation befasst sich mit einem weiteren möglichen Anwendungsbereich von SF als Freisetzungssystem für Proteinwirkstoffe. Aus SF-Lösungen mit darin gelöstem nerve growth factor (NGF) gelang es, SF-Nervenleitkanäle (NK) herzustellen, die die Reparatur von durchtrennten oder beschädigten peripheren Nerven fördern sollten. NK aus Kollagen werden bereits klinisch zur Reparatur von peripheren Nerven eingesetzt. NK leiten die aus dem proximalen Nervenende austreibenden Axone in die gewünschte Richtung und schützen gleichzeitig den Wachstumskonus des Nervs vor Beschädigungen durch Kompression. Um eine später zwingende Explantation zu vermeiden, sollten NK sich nach der Nervenreparatur abbauen. Neuere Konzepte zielen auf NK, die eingebettete WF kontrolliert freisetzen können. Aufgrund der guten Biokompatibilität, dem langsamen Abbau und den hervorragenden mechanischen Eigenschaften von SF erscheint dieses Material für NK besonders geeignet. Die Ergebnisse unserer Untersuchungen zeigten, dass SF-Filme das Anhaften und die metabolische Aktivität von PC12-Zellen unterstützen und, in Kombination mit löslichem NGF, das Auswachsen von Neuriten während deren Differenzierung ermöglichen. Mit NGF beladene SF-NK wurden durch Lufttrocknen oder Gefriertrocknen (Einfriertemperatur -20 °C oder -196 °C) einer NGF enthaltenden, wässrigen SF-Lösung (20%, w/w) in einer geeigneten Form hergestellt. Die drei unterschiedlichen SF-NK setzten den eingebetteten NGF über mindestens 3 Wochen frei, wobei die total freigesetzte Menge von der jeweiligen Trocknungsmethode abhängig war. Die biologische NGF-Aktivität blieb in allen Formulierungen erhalten. Als Kontrolle wurde NGF in Laktose-Lösung unter identischen Trocknungsbedingungen verarbeitet und danach auf Stabilität

untersucht. Die Ergebnisse zeigten weder wesentliche Proteinaggregate (SEC, HPLC) noch Verlust an ELISA-Aktivität oder Bioaktivität. Die Ergebnisse ermutigen zu *in vivo* Experimenten, um die mit NGF beladenen SF-NK hinsichtlich einer Beschleunigung des peripheren Nervenwachstums am Tier zu untersuchen.

Das letzte experimentelle Kapitel (**Kapitel VI**) befasst sich mit der Anwendung von SF als Biomaterial zur Verkapselung therapeutischer Zellen in einem semipermeablen, bioabbaubaren Bioreaktor. Es konnte bereits früher gezeigt werden, dass embryonale adenosinkinase-defiziente Stammzellen (Adk-/-ES), die in synthetische Polymere verkapselt waren, Adenosin in therapeutischen Dosen freisetzen und dadurch epileptische Anfälle in Ratten unterdrücken können. Die dabei verwendeten synthetischen Materialien waren jedoch nicht degradierbar und mussten wieder explantiert werden, als die Funktion der eingekapselten Zellen erschöpft war. In unserer Arbeit betrachteten wir SF als geeignetes Material für die Verkapselung von Zellen und die verlängerte Freisetzung von Adenosin, welches durch die verkapselten Zellen produziert wurde. SF ist nämlich für Nährstoffe wie Glucose sehr gut permeabel und baut sich sehr langsam aber vollständig im Körper ab. Um die Anwendbarkeit von SF für diesen Zweck zu evaluieren, wurden zuerst unterschiedliche Materialien als Substrate für die Kultivierung von glialen Adk-/- und Vorläuferzellen vom Wildtyp (wt) verglichen: (i) Kollagen Typ I (Kol-I), (ii) SF, und (iii) Poly(L-Ornithin) (PO), alle jeweils als Filmschicht auf Zellkulturplatten. Die Zellproliferation war in Proliferationsmedium generell erhöht, die metabolische Aktivität auf Kol-I und PO jedoch geringer als auf SF. Die Differenzierung der Vorläuferzellen in Astrozyten erfolgte auf allen drei Substraten, unabhängig von den verwendeten Genotypen. Zur Bestimmung der Adenosinfreisetzung wurden die beiden ES-Zell-Genotypen auf SF und PO kultiviert. In jedem Entwicklungsstadium der Zellen war die von Adk-/- ES-Zellen freigesetzte Menge Adenosin gegenüber wt-Zellen auf beiden Substraten (SF und PO) signifikant erhöht und konnte in beiden Fällen als therapeutisch relevant eingestuft werden (>20 ng/ml). Diese Resultate zeichnen

SF als ein besonders geeignetes Biomaterial zur Verkapselung von Adenosin freisetzenden ES-Zellen aus. Auf der Grundlage dieser Arbeit könnten möglicherweise Bioreaktoren zur Behandlung von Epilepsie entwickelt werden. Generell sollte die hier erarbeitete Strategie die Entwicklung neuer Systeme ermöglichen, welche niedermolekulare Arzneistoffe lokal und zeitlich verlängert freisetzen.

CHAPTER I

Biopolymer based growth factor delivery for tissue repair: From natural concepts to engineered systems

Lorenz Uebersax, Hans P. Merkle, Lorenz Meinel

Institute of Pharmaceutical Sciences, ETH Zurich, Switzerland

ABSTRACT

The extracellular matrix (ECM) of tissues is regarded as a physiological depot for various growth factors, from where they are to be released into the surrounding tissue and play their natural roles in tissue regulation. In addition to autocrine and paracrine cell signalling, they provide specific extracellular information necessary to conduct tissue homeostasis and (re)generation. This review will detail on various physiological concepts that have evolved during evolution to control the activity of GFs in a specific manner through interaction with biopolymers of the ECM, and how such interactions may respond to systemic or cellular signals. A fundamental understanding of the extracellular storage and control of GFs could provide important cues about the nature of GF interactions and improve the potency of current implantable biopolymer systems for GF delivery in tissue repair. Therefore, in a second part of this review, current nature-derived biopolymers will be discussed with respect to their availability, suitability for scaffolding, mechanical properties, and efficiency to sustain the activity and release of GFs. Furthermore, we will detail on rational modifications and engineering approaches to improve their applicability as delivery systems. In particular, we discuss biotechnology and chemical engineering strategies to adapt natural concepts of GF depots for delivery purposes. In conclusion, the engineering of novel biopolymer platforms holds promise to enhance the biological performance of GF loaded artificial tissue substitutes in order to replace autologous and allogeneous tissue grafts for the treatment of critical tissue defects.

TABLE OF CONTENTS OF CHAPTER I

I. INTRODUCTION	26
II. NATURAL CONCEPTS FOR GROWTH FACTOR STORAGE IN THE EXTRACELLULAR MATRIX (ECM)	29
<i>AFFINITY BINDING OF GROWTH FACTORS TO ECM POLYSACCHARIDES AND PROTEINS</i>	29
Fibroblast growth factors.....	30
Hepatocyte growth factor	31
Bone morphogenic proteins.....	32
Vascular endothelial growth factor	33
<i>BINDING OF GROWTH FACTORS TO THE ECM VIA SPECIFIC BINDING PROTEINS OR PROFORMS</i>	34
Transforming growth factor beta.....	34
Bone morphogenic proteins.....	35
Insulin-like growth factors	35
Fibroblast growth factor	37
<i>LESSONS FROM NATURAL CONCEPTS FOR THE CONTROL OF GF ACTIVITY IN THE ECM</i>	37
III. NATURAL BIOPOLYMERS FOR GROWTH FACTOR DELIVERY IN TISSUE ENGINEERING.....	41
<i>POLYSACCHARIDE BASED GROWTH FACTOR DELIVERY PLATFORMS</i>	43
Heparin	43
Hyaluronic acid	44
Alginate	46
Chitosan.....	48
<i>PROTEIN BASED GROWTH FACTOR DELIVERY PLATFORMS</i>	50
Collagens.....	50
Fibrinogen / Fibrin.....	54
Albumin.....	55
Silk fibroin.....	56
IV. ENGINEERED BIOPOLYMER PLATFORMS FOR GROWTH FACTOR DELIVERY IN TISSUE REPAIR	60
<i>COMBINATION OF BIOPOLYMERS WITH SYNTHETIC MOLECULES</i>	61
<i>SYNTHESIS OF ANALOGOUS POLYSACCHARIDES AND PEPTIDES</i>	62
Heparin mimetics	62
Peptides and amino acid based polymers	64
<i>GENETIC ENGINEERING OF RECOMBINANT FIBROUS PROTEINS</i>	66
<i>DESIGN OF GF BINDING MEDIATORS</i>	69
V. CONCLUSIONS.....	76

I. INTRODUCTION

The extracellular matrix (ECM) of tissues is regarded as a physiological depot for various growth factors, from where they are to be released into the surrounding tissue and play their natural roles in tissue regulation and repair. Large variations exist among different tissues to self regenerate after damage. Blood, skin, bone, liver and gut possess relatively high regenerative potential after trauma in contrast to brain and heart tissue [1]. This capacity is mainly related to the potential of a tissue to attract or induce proliferation of tissue-specific cells upon damage, thereby avoiding the invasion of unspecific cells, and the loss of the original tissue and its associated functions. Tissue maintenance and regeneration can be provided by activation of differentiated cells, as in the case of hepatocytes [2], or associated undifferentiated stem cells present in all tissues [3]. In addition to variations between different tissues, self regeneration declines with age regardless of tissue type [4, 5]. In some tissues such as muscle, blood, liver and brain this decline has been attributed to a diminished responsiveness of tissue-specific stem and progenitor cells, but also to systemic factors and the age of adjacent tissue [4]. Therefore, the critical level of damage, when a tissue fails to be restored, is defined by the size of the defect, the regenerative potential of a specific tissue in general, and the age-related loss of regenerative potential. Hence, the continuous aging of our society and the growing interest in risky outdoor activities increases the need for novel biomedical approaches that replace or support surgical interventions. Traditionally, autologous tissue grafts have been used as a source of autologous cells and ECM including tissue specific growth factors (GFs). However, the availability of autologous material is limited and second site surgery can entail functional loss at the donor site as well as increase the risk of infection [6-9]. The biological activity of autologous bone grafts to induce regeneration is reduced in older patients and related to the decreased content of GFs in the harvest tissue upon aging [10]. Therefore, age related and individual variations in the biological activity of autologous tissue can result in unpredictable outcomes. The development of approaches that are unaffected by

such factors while providing stable biological activity would thus be beneficial and help to overcome logistical hurdles, e.g., caused by limited availability.

The aim of tissue engineering is to provide new approaches to critical tissue damages in order to prevent significant loss of function or physical disfiguration. To restore the physiological activity and performance of a damaged tissue, it is pivotal to reproduce the original tissue topology and phenotype [11-13]. Consequently, most tissue engineering approaches use biomaterial scaffolds to temporally fill the cavity of the defect and spatially support and guide tissue growth to regenerate the lost tissue. Adult stem cell based therapies in combination with biomaterial scaffolds are promising to further support the defect with sufficient tissue specific autologous cells or with pre-organized artificial tissue from *in vitro* cultures [14, 15]. The engineering of large tissue constructs is appealing but still limited by the time consuming *in vitro* expansion of donor cells and 3-D cultures, as well as ischemic conditions in the resulting engineered tissue, and hurdles related to implant-host tissue interaction. Furthermore, the consumption of large amounts of tissue culture media and expensive supplements in the course of *in vitro* culture pose economical constraints. As stem cells are affected by age, early harvest of autologous cells would be preferable, raising issues with logistics and economical matters due to the storage of donor cells. Especially the micro- as well as the systemic host environment of elderly people might provide low mitogenic and morphogenic stimuli to the implanted progenitor cells leaving stem cell treatments ineffective [1].

Important local factors to control cell proliferation and differentiation in healthy tissue are tissue-specific growth factors (GFs). GFs control the proliferation and differentiation of progenitor and stem cells or induce directly the growth of differentiated cells such as hepatocytes in the liver or osteoblasts in bone [16-19]. During matrix formation, some of these GFs or their pro-forms are expressed and locally stored in the ECM providing extracellular depots. GFs interact either directly with a specific ECM protein or polysaccharide, or via specific binding proteins, which are covalently or electrostatically linked to the

ECM. It is most likely that these strategies have developed separately during evolution with the overall aim to localize, stabilize, and control the GFs' efficacy in a specific tissue. In this context, the administration of GFs in combination with biomaterial scaffolds may be seen to enhance self regeneration of the injured tissue or the performance of implanted autologous cells. The short half-life of many GFs *in vivo* and major side effects, due to their high potency, often bars them from systemic administration. Consequently, they are administered as local parenteral depots integrated in tissue-conductive implants [20-28]. But their limited stability during formulation, storage and after implantation are major challenges to consider [29].

In nature, the protection and regulation of GFs is provided through their interaction with biopolymers of the ECM such as proteins and polysaccharides. In this review we report on natural concepts for GF storage in the ECM to control tissue regeneration and maintenance. We will further focus on nature derived biopolymers (e.g. proteins and polysaccharides) from different sources that were previously suggested as scaffolds to deliver GFs for enhanced tissue regeneration. In particular, we discuss the availability, processability and performance of selected biopolymers as delivery platform for GFs. Finally, strategies will be presented to improve GF binding, stabilization and release profiles, based on genetic engineering or chemical synthesis of novel biopolymers including the adaptation of natural concepts in biopolymer systems with improved GF delivery properties for tissue repair.

II. NATURAL CONCEPTS FOR GROWTH FACTOR STORAGE IN THE EXTRACELLULAR MATRIX (ECM)

Since the discovery of substantial quantities of GFs in the calcified matrix of bone and their implication in the control of local bone formation and regeneration, physiological GF depots have been discovered in almost any type of tissue [19, 30, 31]. For instance, GFs have been identified as biologically active components of decellularized autologous tissue. In case their biologic activity is retained during the preparation of the decellularized matrix they may stimulate the regenerative process in the defects [10, 19, 32]. The interaction of GFs with ECM is a basic prerequisite for the local sustainment and control of their potency in the extracellular environment providing a more persistent mode of action as compared to the same molecules in the fluid phase [33]. For that reason, independent concepts for GF storage have been developed during evolution that all provide tissue specific interactions for each individual GF. Consequently, the identification of biological concepts to accommodate GFs in the extracellular environment is likely to aid in engineering biopolymer systems for tissue repair with optimized GF-biomaterial interactions that help to sustain GFs in their most potent form. Therefore, different natural concepts for localization and release of GFs in the ECM are summarized in the following section including the identification of binding partners and the nature of their interactions.

Affinity binding of growth factors to ECM polysaccharides and proteins

ECM molecules are natural polysaccharides that belong to the family of glycosaminoglycans (GAGs) and show a broad spectrum of interactions with GFs. GAGs interact with each other or with extracellular proteins, such as collagen or fibronectin, and define the mechanical properties and the morphology of the tissue. The ratio between proteins and GAGs in the ECM strongly depends on the tissue type. Consequently, nature has developed strategies to store specific GFs through the interaction with either GAGs or ECM proteins of the specific tissue.

Fibroblast growth factors

Heparin is a sulfated GAG present in many tissues and well known to bind a variety of GFs denoted heparin binding growth factors (HBGFs), such as fibroblast growth factor 2 (FGF-2, basic FGF), hepatocyte growth factor (HGF), and vascular endothelial growth factor (VEGF) [34]. Binding and release of FGF-2 from heparin sulfates is implicated in the local growth regulation of various tissues. For example, FGF release triggered capillary blood vessel growth in normal and pathological situations [35] but was also reported to be involved in the mechanisms of endochondral ossification. The interaction of FGF-2 with GAGs stabilizes the growth factor or inhibits its binding to the receptor, thus controlling its activity. Heparin and dextran sulfate also enhanced the GF's activity by stabilizing the protein in solution and, therefore, allowing the GF to interact with the cell signalling receptor in a repetitive manner. The specific sulfation pattern of heparin is an important chemical feature for the interaction with FGF [36]. When desulfated, heparin-derivatives lose their stabilizing features and stimulatory capacity. The interaction of FGFs with GAGs can be abolished by enzymatic digestion of the matrix. Heparanase, a heparin digesting enzyme, is able to release bound FGF-2 from the endothelial matrix [30, 31]. Moreover, the overexpression of heparanase in transgenic mice enhanced active hair growth by activating the migration of follicular stem cell progeny through enhanced release of heparin-bound FGF [37]. Smooth muscle cell replication in heparanase treated muscle tissue could be rescued by co-formulation of FGF with endogenous heparin in contrast to FGF alone, which was unable to restore its original function. These findings indicate that heparin binding to FGF-2 is crucial for activating the proliferation of medial smooth muscle cells (SMC) following injury [38]. Perlecan is a proteoglycan of the growth plate in bone and consists of a chondroitin and a heparin chain. It has been reported that the enzymatic cleavage of the chondroitin chain increases the binding of perlecan bound FGF to its receptor whereas the bound heparin stabilizes the GF without interfering with the receptor binding [39]. Moreover, perlecan binds FGF-2 in cartilage tissue and can act as a mitogenic

signal for mechanotransduction. The activation of this pathway, upon compression, is dependent upon the pericellular concentration of FGF-2. FGF-2 can be released from the perlecan or alternatively brought into close proximity of the FGF-2 cell surface receptor during the compression of the matrix, triggering a cellular response whilst still attached to the heparin chain of perlecan [40]. An alternative to the release of FGF-2 through enzymatic cleavage of heparin or the proteoglycan matrix involves the competitive FGF binding by soluble FGF-binding proteins (FGFBPs). FGFBPs are secreted carrier proteins that have an affinity for FGFs, liberate them from the extracellular matrix, and thus enhance FGF activity. FGFBP has been shown to bind to FGF-1 (acidic FGF) and FGF-2 in a non-covalent, reversible manner [41, 42]. In addition to the interaction with heparin, FGF can bind matrix proteins and be stored in a proteinaceous matrix. Collagen I interacts with FGF-2 and was shown to stabilize bound FGF-2 protecting it from degradation [43, 44]. Moreover, FGF-2 was released during the degradation of a decellularized matrix of a natural bladder, which mainly consisted of collagen. The absence of heparin was suggested to represent an important contribution of the ECM protein collagen to the storage of FGF in this tissue type [43, 45]. FGF was also found to interact with fibrin. The cleavage of fibrinogen into fibrin is a crucial mechanism for blood coagulation and wound sealing. Binding of FGF-2 to fibrin after the digestion of fibrinogen is an important mechanism to increase the local concentration of FGF-2 in fibrin sealed wounds, which enhances the healing process by inducing the proliferation of endothelial cells and the formation of new blood vessels [46].

Hepatocyte growth factor

Hepatocyte growth factor (HGF) is a potent mitogen and morphogen for various epithelial cell types and known to bind to heparan sulfate proteoglycans in the ECM. Incubation of HGF with 0.1, 1, and 10 $\mu\text{g/ml}$ of heparin resulted in a concentration-dependent increase in mitogenic response in primary rat hepatocytes

without altering the binding isotherm of HGF for its receptor [47]. To investigate the underlying rationale for the interaction of HGF with heparin, the authors synthesized a series of chemically sulfated malto-oligosaccharides varying in unit size and charge. Di-, tri-, tetra-, and pentasaccharides did not significantly enhance HGF-dependent mitogenesis. However, larger oligosaccharides such as the sulfated hexa-, hepta- or a sulfated oligosaccharide mixture containing HGF stabilized by the addition of deca-saccharides, resulting in an approximately 2-, 4-, or 7-fold enhancement of receptor activation [47]. The interaction was only slightly affected by digestion with heparinase I or III, or by replacement of N-sulfates with N-acetyl groups. In contrast to FGF binding, which necessitates both 2-O-sulfates and N-sulfates for high affinity interaction [48], disaccharide analyses of various HGF-binding oligosaccharides indicated that affinity was more closely associated with 6-O-sulfation of GlcNSO₃ residues than with sulfation at any other position. The structural specificity of the HGF-HS interaction was thus shown to be radically different from that previously described for the FGF-2 interaction with heparin [48, 49].

Bone morphogenic proteins

One of the first tissues in which ECM storage and release of GFs has been observed and investigated is the calcified ECM of bone tissue, which is mainly composed of a mineralized collagen network. Bone cells produce substantial quantities of bone morphogenic proteins (BMPs) that are stored in their matrix [18, 19, 26]. BMPs are highly potent GFs and play a critical role in fetal development, organogenesis, and regeneration of damaged tissues. Therefore, specific mechanisms to control the local activity of such factors are crucial to respond to physiological changes. BMP-2 has been shown to bind specifically to a high-affinity binding site of the collagen triple helix of procollagen II, a collagen form mainly expressed in the matrix of cartilage [50]. The cystein-rich amino propeptide procollagen II alpha chain showed specific binding of BMP-2 and

TGF-beta but no affinity for other GFs such as FGF or IGF-I. Procollagen has an important function for the distribution of specific BMPs, belonging to the transforming growth factor (TGF) beta superfamily [51]. The interaction of BMP-2 with collagen II was increased by the presence of perlecan suggesting a synergistic interaction between ECM proteins and polysaccharides to control BMP-2 availability in the tissue [52]. Moreover, similar affinities of BMP-4 as well as BMP-2 for collagen IV, a main component of the basement membrane have been observed [53, 54].

Vascular endothelial growth factor

The non-covalent ligand-receptor-like binding of vascular endothelial growth factor (VEGF) to ECM molecules can depend on the extracellular pH acting like a pH sensitive sensor for VEGF release. Different isoforms of VEGF exist such as VEGF(165) and VEGF(121), whereof VEGF(165) binds heparin while VEGF(121) is known as non-heparin binder. However, when the pH dropped from 7 to 5.5 the latter transformed in a reversible manner into a heparin binding form. Moreover, binding of the VEGF isoforms VEGF(165) and VEGF(121) to fibronectin was increased at acidic pH values (pH 5.5-7.0). This transformation was reversible when the pH was increased. VEGF bound selectively to fibronectin in contrast to collagen I, representing a pH-controlled depot of VEGF on a specific ECM component. It could be envisioned that the affinity of VEGF to fibronectin would drop under hypoxic conditions thus guiding the migration of endothelial cells and the formation of new blood vessels in tissue with oxygen depletion [55]. VEGF also accumulates in wounds through binding to fibrin clots and induces the formation of new vasculature [46].

Binding of growth factors to the ECM via specific binding proteins or proforms

Transforming growth factor beta

One of the most complex and refined mechanisms to stabilize and store GF in an inactive form is the localization of transforming growth factor beta (TGF-beta) in the ECM through latent transforming growth factor-beta-binding proteins (LTBPs). TGF-beta is secreted as a large latent complex (LLC) in which it is bound to its cleaved prodomain, namely the latency-associated peptide (LAP). These prodomains can further bind to latent LTBPs and ECM glycoproteins in an inactive form. LTBPs are further covalently cross-linked to ECM proteins at their N-terminal region by transglutaminase (tTGase) [56]. The bound LAP can be cleaved through a number of proteases including plasmin and several matrix metalloproteinases (MMPs). The cleavage of the LAP results in a loss of affinity and release of active TGF-beta from the matrix. Fibronectin has been shown to be critical for the incorporation of LTBP1 and TGF-beta into the ECM of osteoblasts and fibroblasts, which represents the major mechanism for TGF-beta storage in bone tissue [57]. LTBP1 failed to assemble in embryonic fibroblasts lacking the gene for fibronectin. This suggests that for continued assembly of LTBP1 the presence of fibronectin is required leading to the localization of the inactive GF in a specific ECM [58]. In addition to the specificity of this localization, active GF is released exclusively in response to specific signals. In contrast to osteoblasts, isolated avian osteoclasts were able to cleave the complex through cell specific proteases and matrix metalloproteinases and released 90% of the latent TGF-beta bound in the bone matrix [59]. TGF-beta released by osteoclasts during bone resorption triggered the recruitment and proliferation of osteoblast precursors and mature osteoblasts. The proposed mechanism represents an extracellular sensor that can act as a fast forward loop in which LAP functions as a detector, LTBPs as a localizer and TGF-beta as an effector [57].

Bone morphogenic proteins

An alternative to direct low affinity binding of GFs to ECM proteins is the binding of the GF via specialized matrix associated GF binding proteins or parts of its cleaved proform. BMP-7, a member of the TGF-beta superfamily, is secreted as a noncovalent associate with the cleaved part of its proform, which is structurally similar to the small TGF-beta complex. The complex of BMP-7 with its prodomain, in contrast to the non-complexed GF, interacts with N-terminal regions of fibrillin-1, the major component of architectural elements in connective tissue denoted as microfibrils. Fibrillin-1 is colocalized with BMP-7 in the kidney capsule and skin in contrast to other tissues known to be active sites for BMP-7 signaling. This suggests that BMP-7 can be localized through different mechanisms depending on the tissue [60]. The BMP antagonist chordin was reported to show regulatory effects on endochondral ossification. The treatment with chordin delayed BMP-2 induced maturation of cultured chondrocytes, and the overexpression of chordin in chick limbs delayed the maturation of chondrocytes in developing skeletal elements of chick limbs [61].

Insulin-like growth factors

Upon synthesis by multiple cell types and release into the interstitial fluid insulin-like growth factor I and -II (IGF-I; IGF-II) circulate in relatively high concentrations in the plasma [62]. IGFs represent an abundant source of GFs in most fetal tissues stimulating the synthesis of collagen and GAGs, and play an important role during osteoclast driven bone remodeling [63, 64]. Binding of IGF-I to GAG protects the GF from degradation [65]. However, ECM storage and activity of IGFs are mostly regulated through the interaction with IGF binding proteins (IGFBP), which are expressed independently from the respective GF. IGFBPs are a family of six proteins that bind to IGF-I and -II with affinities that are between 2- and 50-fold stronger than to the IGF receptor, therefore controlling the local availability of the GF [62]. Some IGFBPs (IGFBP-2, -3 and -5) contain

the von Willebrand factor, which can bind to different ECM components such as collagen I, fibronectin, fibrin or heparin [66, 67]. Individual IGFs show selective affinities for IGFBPs, which on their part show different affinities for specific ECM molecules. IGFBPs can be cleaved by specific proteases or matrix metalloproteinases (MMPs) expressed by host cells of a particular tissue and, therefore, govern the availability of the GFs in response to cellular signals [62]. IGFBP-2 binds IGF-I and -II with high affinity but has little affinity for the ECM in its unbound state. However, IGFBP-2 in complex with IGF-II rather than IGF-I was found to increase the affinity of the complex to bind to heparin. This is in contrast to other ECM components such as type I collagen or fibronectin. The affinity of IGFBP-2 for a specific ECM molecule depends on bound GF and represents a unique, selective mechanism for the targeting of the anabolic IGF-II to heparin in bone [68]. Moreover, heparin-binding sites identified in IGFBP-2 bind heparin at the slightly acidic pH 6.0 and, more significantly, at pH 5.5, but are largely suppressed at pH 7.4. This effect suggests a further control element for IGF localization in bone tissue depending on the pH of the local environment [66]. IGFBP-3 binds IGF-1 with high affinity and is expressed in articular cartilage where it specifically binds to fibronectin and heparan sulfate proteoglycan but not to other ECM molecules, such as type VI collagen or tenascin-C. Therefore, local expression of IGFBP-3 in combination with fibronectin can regulate local levels of IGF-I in this tissue [69]. IGFBP-5 binds IGF-I at higher affinity than the IGF-receptor but lowers its affinity for IGF-I about 15-fold when bound to ECM molecules. The interaction of IGF-I/IGFBP-5 with the ECM allows for the release of IGF from its binding protein and interaction with the IGF receptor [62, 70, 71]. The described natural mechanism represents an astonishing concept for the control of local IGF-I and -II bioavailability and activity in response to the expressed ECM in a particular tissue [62].

Fibroblast growth factor

An alternative to fibroblast growth factor (FGF) release through enzymatic cleavage of heparin or the proteoglycan matrix involves the competitive binding of FGF by soluble FGF-binding proteins (FGFBPs). FGFBPs are secreted carrier proteins with affinity for FGF and liberate the GF from its extracellular matrix thus enhancing FGF activity. FGFBPs have been shown to bind to FGF-1 and -2 in a non-covalent, reversible manner and are preferentially expressed in normal human keratinocytes [41, 42].

Lessons from natural concepts for the control of GF activity in the ECM

Local cytokine networks are important to control tissue topography, homeostasis and regeneration [72]. Although the specific gene expression pattern of a tissue, developed during embryogenesis, and the cellular cross-talk between its host cells are pivotal for tissue regulation, local GF depots in the ECM may contribute additional extracellular control elements for tissue homeostasis and repair. After severe tissue damage, cell numbers in the defect are drastically reduced, and cellular cross-talk is interrupted. GF depots may act as crucial signal transmitters to rescue the compromised site, e.g., by cell attraction, and consequently replenish the available cell population to induce tissue regeneration. Therefore, we could argue that cell-independent release accelerates mitogenic and morphogenic responses, or both. The storage of GFs in the ECM allows for a better localization, regulation and sustainment of GF action as compared to the respective factor in solution which would quickly diffuse out of its location or lose its potency [33]. Consequently, GF depots may act as local extracellular signals and restrain specific cell development into the appropriate tissue. The mechanism of GF binding to ECM is highly specific and a key element for the extracellular regulation of GF functions during physiological processes (**Fig. 1**).

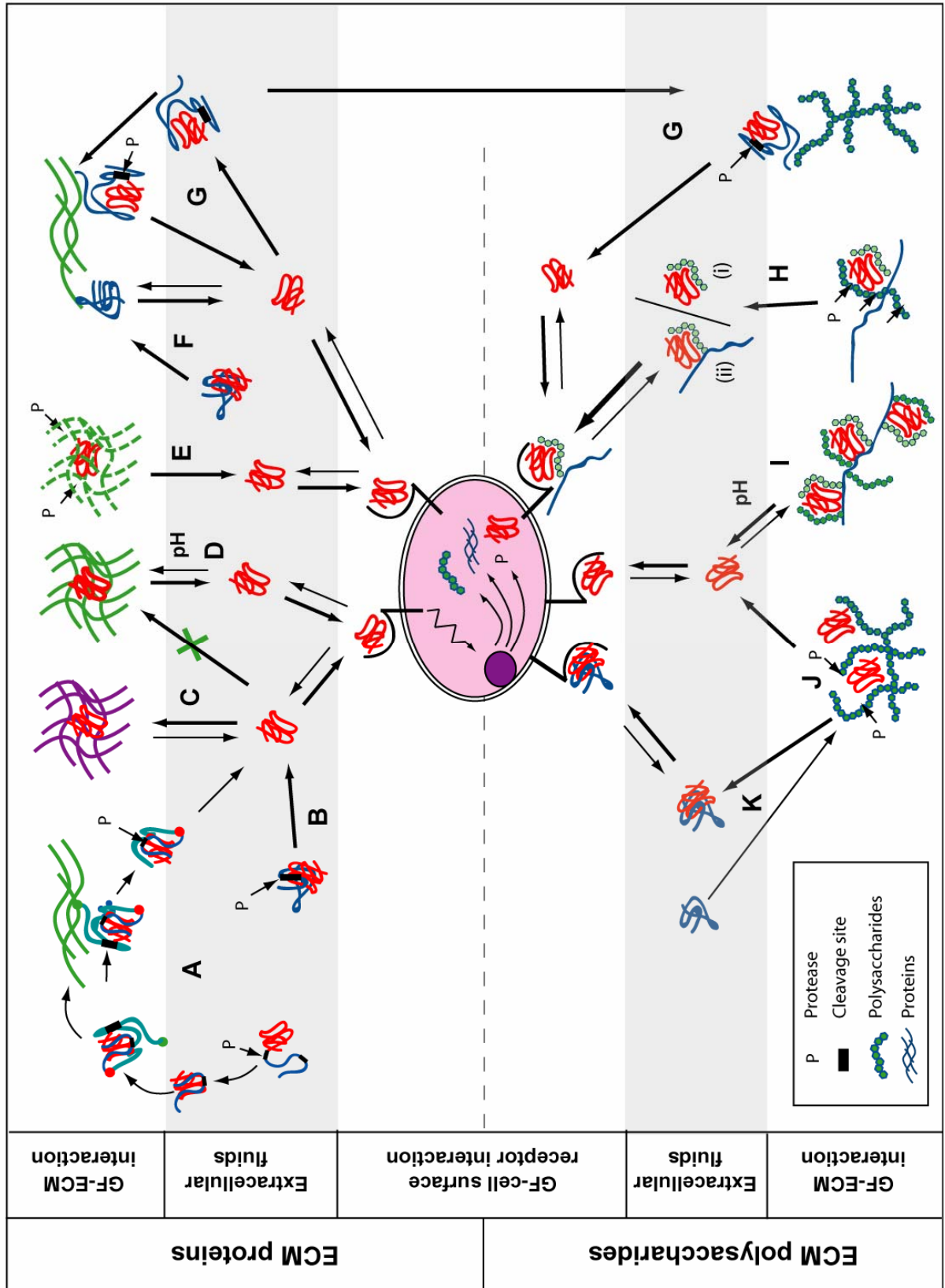


Fig. 1: Natural concepts for extracellular growth factor storage and release in the ECM. (A) TGF-beta binds to its cleaved prodomain LAP, which is covalently linked to the latent TGF-beta binding protein (LTBP) and together form the TGF-beta large latent complex (LLC). The LLC is further covalently linked to ECM molecules. The LLC is released from the ECM by protease cleavage and the TGF-beta is released from the LLC through cleavage of the LAP [56, 59]. (B) Soluble IGF-I binding proteins (IGFBP) bind IGFs in an inactive form, which can be released by enzymatic cleavage of IGFBP [62]. (C) TGF-beta and BMP-2 can bind to type IIa procollagen in cartilage [51]. FGF-2 or BMP-2 associated to collagen type I [44, 51, 73] or FGF-2 and VEGF can be accumulated in fibrin clots [46]. (D) Selective and pH dependent binding of VEGF to fibronectin at lower pH (5.5) [55]. (E) Release of GFs such as IGF-I from calcified collagen matrix of bone. (F) IGFBP-5 in complex with IGF-I reduces its affinity for IGF-I when bound to ECM proteins resulting in GF release at the target tissue [65]. (G) Binding of IGFBPs in complex with IGFs to specific ECM molecules such as collagen type I, fibronectin, fibrin or heparin. Release of IGFs by subsequent proteolytic cleavage of IGFBP [62, 66, 67]. (H) Control of GF activity by binding to different GAGs in the ECM: (i) Soluble heparin/FGF-2 complex stabilizes the GF and improves receptor binding [36, 38]. (ii) FGF-2 stabilized by the heparin part of perlecan can interact repeatedly with its cell surface receptor whilst still attached to the ECM [39]. Furthermore, FGF-2 bound to perlecan interacts with its cell surface receptor during compression of the tissue stimulating the growth of cartilage in this area [40]. (I) Reversible affinity binding of FGF-2 to heparin. (J) Possible protection of TGF-beta in hyaluronic acid matrix until degradation [74]. (K) FGF binding proteins (FGFBP) liberate FGF from its polysaccharide matrix and interact with the cell surface receptor [41, 42].

Therefore, we can consider a GF complexed with its binding partner in the ECM as one functional unit responsible for the localized mitogenic and morphogenic activity rather than the soluble GF alone. As most structural ECM proteins have evolved to provide tissue specific mechanical properties and mediate cell interaction and migration, their sequences are much conserved during evolution and do not allow for major adaptations of their structure. Therefore, nature brought forward various concepts for the extracellular localization of GFs providing tissue specific interaction between GFs and ECM molecules (**Fig. 1**). Such concepts mainly include the development of (i) different isoforms or

proforms of the GFs with different affinities for ECM molecules or (ii) different GF binding proteins which mediate their interaction with the ECM. Besides the localization of GFs, various concepts have evolved to control their interaction with cell surface receptors on demand in response to environmental changes or cellular signals in either a reversible or irreversible manner. In the case of cartilage, FGF bound to the ECM can interact reversibly with the cell surface receptor in response to compression of the tissue, thus promoting tissue growth at the compromised location [40]. Another mechanism is represented by the release of VEGF in response to pH changes induced under ischemic conditions triggering the growth of new blood vessels [55]. Growth factor depots can further be actively released in response to cellular signals, such as specific proteases, which irreversibly liberate the GF from its extracellular localization. The necessary control elements for this interactivity are implemented (i) directly in the GF or its proform, (ii) in the ECM molecule itself or (iii) in the GF binding protein and (iv) in synergistic patterns by all elements. The complexity of concepts for the storage and control of extracellular GFs in the ECM during tissue maintenance and (re)generation is intriguing and recommends to mimic such successful strategies by the use of natural or engineered biopolymers scaffolds for GF delivery in tissue repair.

III. NATURAL BIOPOLYMERS FOR GROWTH FACTOR DELIVERY IN TISSUE ENGINEERING

Taking natural concepts of GF storage in the ECM into consideration teaches us that the interactions between GFs and natural biopolymers are key for the localization and sustainment of their potency and function. GF delivery platforms based on biopolymers could provide a molecular, mechanical and physiological milieu similar to that found in the native ECM. Furthermore, many biopolymers are highly water soluble and, therefore, allow for a gentle processing of the GFs in an aqueous solution together with the biopolymer. Processing under mild conditions may help to sustain GF potency during manufacturing and release.

The choice of a specific biopolymer system for tissue repair depends on many factors, such as the mechanical requirements of the tissue, the defect size, but also on its performance to deliver a specific GF under the required regime. The temporospatial release of GFs from biopolymer matrices can be controlled to some degree by the loading concentration and the adjustment of matrix swelling and *in vivo* degradation, which in the end control the diffusional mobility of the embedded GFs. However, type and strength of GF-material interactions are pivotal to allow optimization of drug release kinetics and should be established early in the research and development process [73]. Finally, the availability as well as the processability of the biopolymer are two important factors which might further decide upon commercialization of a biopolymer system. The following part of this review will provide an overview (**Table 1**) over the characteristics of various biopolymers and their performance as scaffold materials in GF delivery platforms for tissue engineering and repair.

Table 1: Properties of biopolymersystems based growth factor delivery systems

	Natural Source	MW [kDa]	Charge	GF Affinity	Matrix	Mechanics	Mechanism of <i>in vivo</i> matrix degradation	<i>In vivo</i> matrix degradation time	Release mechanism
Collagen	Porcine Bovine Rat (Bone, Skin)	300	pI = 4.7	Specific BMP-2 (Col II)	Scaffolds Films Fibers Hydrogels	+++	Specific Proteases MMPs	Fast 1-2 month Dependant on cross linking	Desorption Diffusion Degradation
Gelatin	Porcine, Bovine, Rat (Bone, Skin)	5 - 100	pI = 4.8 - 9	Electrostatic	Scaffolds Films Fibers Hydrogels	+++	Specific Proteases MMPs	Fast 1-2 month Dependant on cross linking	Desorption Diffusion Degradation
Fibrinogen Fibrin	Bovine, Human (Plasma)	Fibrinogen: 350 fibrin dimer: 180	pI = 5.3 pI = 4.9 - 5.3	Specific FGF VEGF	Hydrogel Sealant	++	Specific Thrombin	7-14 days	Desorption Diffusion Degradation
Albumin	Bovine, Human (Plasma)	66.3	pI = 5.2		Gels Adjuvant	+	Proteases	n.d.	Desorption Diffusion Degradation
Silk fibroin	Spiders, Bombyx mori (cocoon, web)	H-chain: 350 L-chain: 25	pI = 4.2	Electrostatic	Fibers Scaffolds Hydrogels Films	++++	Unspecific Hydrolysis Proteases	6-12 month	Desorption Diffusion
Heparin	Bovine, Porcine, Human (Plasma)	10-14	pKa = 2.8 - 3.1	Specific Heparin binding GF	No matrix Additives	-	Specific Heparanases	No matrix	Desorption Diffusion Degradation
Hyaluronate	Bovine, Porcine (Joints, Cartilage)	5 - 20000	pKa = 2.8 - 2.9	Electrostatic	Scaffolds Hydrogels	++	Specific Hyaluronidases	2 - > 4 weeks dependant on cross-linking	Desorption Diffusion Degradation
Alginate	Seaweed Azobacter	30 - 270	Mannuronate: pKa = 4 Guluronate: pKa = 3.5	Electrostatic	Hydrogels Scaffolds / Poly-electrolyte complex)	+	Unspecific Enzymatic Hydrolysis Lysozyme	12 weeks	Desorption Diffusion Dissolution/Degradation
Chitosan	Shellfish	7 - 200	pKa = 6.3	Electrostatic	Scaffolds Hydrogels	+++	Unspecific Enzymatic hydrolysis Lysozyme	10 - 84 days Slower for higher degrees of deacetylation	Desorption Diffusion Degradation

Polysaccharide based growth factor delivery platforms

Natural polysaccharides have been successfully used as drug delivery scaffolds as they offer a large number of derivatizable groups, a wide range of molecular weights, varying chemical compositions, low toxicity, are biodegradable yet highly stable, and were approved as pharmaceutical excipients [75]. They can be derived from mammalian sources or other species such as shellfish, seaweed or bacteria.

Heparin

Heparin is a highly sulfated glycosaminoglycan widely used as an injectable anticoagulant or as an anticoagulant surface modification on various experimental and medical devices [76]. Pharmaceutical grade heparin is commonly derived from mucosal tissues of slaughtered animals such as porcine intestine or bovine lung [77] in the form of a strongly acidic 12 kDa to 15 kDa polymer. Heparin is very acidic because of its high content of covalently linked sulfate and carboxylic acid groups. As discussed earlier, heparin interacts and stabilizes GFs, in particular the group of heparin binding GFs (HBGF), and, therefore, has been widely used as GF delivery platform alone or to improve the properties of other biomaterials. For instance, the modification of fibrin with heparin increased the loading and the sustainment of FGF-2 release, which resulted in improved proliferation of fibroblasts and the ingrowth and formation of dense connective tissue *in vivo* [78]. FGF-2 released from the heparin modified fibrin matrices enhanced neurite extension from dorsal root ganglia by up to 100% [79]. Heparin was chemically modified with a silyl groups (silyl-heparin) to be adsorbed to hydrophobic surfaces by immersion or dip-coating. Silyl-heparins were found to be adsorbed onto a wide variety of substrates including polystyrene and poly(lactic-co-glycolic acid). Binding of FGF-2 to the adsorbed heparin was able to induce capillary tube formation of endothelial cells. Furthermore, FGF-2/Silyl-heparin coated to suture material increased the density of mesenchymal

cells in its proximity after the implantation in muscle tissue [80, 81]. Electrospun poly(ethylene glycol) (PEG) functionalized with low molecular weight heparins (LMWH) improved the binding of FGF-2 to the PEG fibers [82]. Heparin was modified with methacrylate groups to copolymerize with dimethacrylated PEG, which improved the adsorption of FGF-2 to the matrix of the copolymer. The heparin functionalized gels could deliver biologically active FGF-2 for up to 5 weeks and promoted adhesion, proliferation, and osteogenic differentiation of hMSC [83]. Heparin decorated collagen matrices increased the physical immobilization of VEGF and improved the angiogenic potential of collagenous matrices. The beneficial interaction between heparin and GFs has also been exploited for non HBGF. The pretreatment of BMP-2 with heparin, for example, has been shown to amplify the osteoinductive effects of BMP-2 *in vitro* [36]. A similar principle was used to localize the release of beta-nerve growth factor (beta-NGF). Although beta-NGF does not bind heparin with high affinity, heparin retained the GF and sustained its release from the delivery system. Immobilized heparin-fibrin matrices containing a large molar excess of heparin relative to GF, enhanced neurite extension by up to 100% relative to unmodified fibrin. Free neurotrophins within the fibrin matrix, in the absence of heparin, did not enhance neurite extension [84, 85]. Although heparin has the potential to improve and sustain the potency and the localization of GF it does not form mechanical stable matrices. Therefore, it has to be used in combination with other biomaterials.

Hyaluronic acid

Hyaluronic acid (HyA) is a non-sulfated glycosaminoglycan, which can be found in connective, epithelial, and neural tissues. It is a major component of the synovial fluids of articular cartilage and provides resilience to cartilage (i.e. mechanical resistance to compression). HyAs composed of D-glucuronic acid and D-N-acetylglucosamine, linked together via alternating β -1,4 and β -1,3 glycosidic bonds. The molecular weight (MW) of HyA can range between 5 to 20,000 kDa

and is mainly depending on the tissue [86]. HyA can interact with proteoglycans via a binding-region located at its NH₂-terminus or is associated with collagen fibers defining their thickness [87]. HyA with its versatile size provides attractive building blocks for new biocompatible and biodegradable drug delivery systems. Important new products based on HyA have already reached the marketplace [88]. High molecular weight HyA can be directly immobilized onto hydrophilic substrates without any chemical manipulation, allowing for the formation of ultra-thin chemisorbed layers that can interact with hydrophilic surfaces through hydrogen bonding between carboxylic acids, or through its hydroxyl groups with silanol, carboxylic acid or hydroxyl groups of the substrate. On glass or silicon oxide chemisorbed HyA layers remained stable for at least 7 days under physiological conditions. Furthermore, HyA can be immobilized on silicon and other dioxide surfaces in much higher quantities than other polysaccharides, including dextran sulfate, heparin, chondroitin sulfate, dermatan sulfate, or alginate. This feature is related to the molecular entanglement and intrinsic stiffness of HyA molecules as a result of strong internal and external hydrogen bonding as well as its high MW [89]. HyA hydrogels were synthesized by crosslinking HyA with divinyl sulfone (DVS) and PEG-divinyl sulfone (VS-PEG-VS) and investigated for their release of bovine serum albumin (BSA) as a model for anti-inflammatory protein drugs. After an initial burst, BSA was continuously released from both hydrogels for several days [90]. Furthermore, blends of poly(vinyl alcohol) (PVA) with HyA showed a linear release of growth hormone (GH) over 3 days, with the protein release increasing with increased HyA content [91]. Considerable potential to improve drug delivery properties of HyA lies in the derivatization of the biopolymer. A derivatized form of HyA (Hyaff-11) was used as vehicle for the delivery of recombinant human BMP-2 (rhBMP-2) in bone and cartilage repair. For GF loading the scaffolds were soaked with a rhBMP-2 solution. *In vitro* release kinetics revealed a sustained release of bioactive rhBMP-2 over 28 days with 32% of the initially loaded rhBMP-2 released and stimulating the differentiation of pluripotent stem cells. The retention of rhBMP-2 was

stronger with Hyaff-11 scaffolds than with collagen gels, which released most of the initially loaded rhBMP-2 within 14 days [92]. A novel injectable sustained release formulation of recombinant human growth hormone (rhGH), using sodium HyA as a stabilizer, was prepared in the form of solid microparticles by spray drying technology. The sustainment of the release could be further improved at higher HyA concentrations and continued for more than 72 hours. A single administration resulted in elevated serum IGF-I levels for 6 days demonstrating the feasibility of a once-a-week injection formulation for hGH delivery [93]. The interaction with HyA - in contrast to sulfated glycosaminoglycans - is able to suppress TGF-beta 1 activity, whereas subsequent treatment with hyaluronidase released active TGF-beta 1. Furthermore, when complexed with HyA the GF was protected from degradation by trypsin, in contrast to the free GF [74]. The aforementioned enzymatically controlled release of GF from HyA by hyaluronidases was further applied in form of gene delivery approaches, such as a hyaluronidase responsive matrix for the delivery of DNA from HyA-collagen hydrogels that was developed to stimulate cellular processes for tissue regeneration. Moreover, poly(ethylene imine) (PEI)/DNA complexes were immobilized on a HyA substrate; when incubated in hyaluronidase the release of PEI/DNA complex from the hydrogel substrate increased from 30% of the immobilized DNA to 50% [94]. Therefore, inhibitory and protective interactions of GF with HyA hold prospective applications for enzymatically controlled GF release by hyaluronidase in tissue such as cartilage.

Alginate

Alginates can be derived from brown seaweeds (*Phaeophyceae*, mainly *Laminaria*) or from distinct bacteria, notably the *Azotobacter* species. They are unbranched linear polymers containing D-mannuronic acid and L-guluronic acid residues. Given a basic milieu they may be extracted from their source, yielding high amounts of polymer [95]. Their molecular weights vary from 50 – 100'000

residues depending on the preparation. Water binding is increased with increasing MW of the polymer to suit different applications. Although alginates are not produced by mammalian species, they are established among the most versatile biopolymers used as excipients in drug products due to their gel-forming and stabilizing properties. Gels can be prepared in aqueous solution through hydration of alginic acid at low pH leading to the formation of high viscosity gels or by noncovalent crosslinking in the presence of divalent cations. The tensile strength of the gels can be improved by increasing amounts of glucuronic acid in the gels [96]. Various grades of alginate salts were manufactured in ultrapure form suitable as implant materials [97]. Because alginate is a foreign molecule to the human system, its biodegradation is unspecific and GF release from such gels are mainly driven by diffusion. VEGF, a potent stimulator of angiogenesis, has been embedded in spherical alginate beads in order to enhance the development of a vascular network within a three-dimensional matrix. Embedding efficiency of VEGF was 30 to 67%. Its *in vitro* release followed a constant rate of 5% per day for up to 14 days. The potency of released VEGF was three to five times higher as compared to VEGF which was directly added to the culture medium of endothelial cells [28]. VEGF was also embedded by extrusion and external gelation. The incorporation of VEGF at low concentrations of NaCl increased uptake rates to 97%; and VEGF release from the beads was sustained for 14 days [98]. Moreover, VEGF as well as bFGF loaded alginate gels promoted the formation of new blood vessel in the subcutaneous tissue of severe combined immunodeficiency (SCID) mice dependant on the VEGF dose [99]. The degradation rates of alginates were shown to be affected by gamma-irradiation; and the capacity for cell adherence and migration could be further improved by the decoration of the matrix with RGD-containing peptides in order to expose integrin specific adherence moieties to cells. Alginate gels are able to bind VEGF in a reversible manner and the hydrogels are capable of repeated deformation following compressional loading. Therefore, VEGF loaded alginate hydrogels were able to release growth factors in response to mechanical signals and upregulated the GF release during the

loading phase. Such a system could react to local mechanical stress and specifically guide tissue formation areas of compression [100]. Alginate gels could be further reinforced by mixing the polysaccharide with chitosan and heparin, which may increase the long-term supply of angiogenic growth factor [101]. A simultaneous release of BMP-2 and TGF-beta at protein concentrations that were more than one order of magnitude lower than doses reported previously to be necessary for bone formation, increased bone formation by transplanted hMSC [102].

Chitosan

Chitosan is a non-digestible aminopolysaccharide fiber derived from chitin in shellfish and besides alginate the most prominent polysaccharide used for drug delivery applications. Chitosans are non-toxic, biodegradable and biocompatible. Production is generally based on deacetylation of acetyl groups from chitin, yielding linear molecules of about 2000 saccharide monomers that consist of randomly distributed β -1,4-linked N-acetylglucosamine and N-acetyl-D-glucosamine. The degree of acetylation has a direct impact on the mechanical properties of chitosan and affect the adsorption of proteins [103, 104]. Grafting long chains of chitosan with 80 kDa chitosan branches can further enhance its tensile strength [105]. Sulfated chitosan finds a variety of applications in the biomedical sector and could provide improved biomaterials for GF interaction in analogy to sulfated polysaccharides of the ECM such as heparins [106]. Therefore, modifications of the biopolymer, using a specific isolation protocol, or derivatization of the isolated biopolymer, hold a certain potential to improve the biomaterial for GF delivery approaches. Chitosan has been used as a wound-healing accelerator in veterinary medicine promoting granulation and has proved to be beneficial for the treatment of large, open wounds in animals. Chitosan has also been successfully applied for GF delivery by surface adsorption or embedding. Platelet derived growth factor (PDGF) absorbed on a

chitosan/tricalcium phosphate (TCP) showed a high initial burst followed by a sustained release of GF in therapeutic concentrations, which enhanced bone regeneration in rat calvarial defects [107]. To increase the localization and the loading of GFs, BMP-2 was covalently linked directly onto the surface of chitosan nanofibres. The BMP-2-conjugated membrane surface retained its bioactivity for up to 4 weeks of incubation and increased osteoblastic cell attachment, proliferation and calcium deposition in contrast to adsorbed BMP-2 [108]. Chitosan is soluble in aqueous systems in comparison to most synthetic biomaterials. Therefore, GFs can be co-processed under quite mild condition in aqueous solution and directly embedded during matrix assembly. The preparation of freeze dried scaffolds by co-formulation of rhBMP-2 with PLLA in p-dioxane, an organic solvent, seriously deteriorated rhBMP-2, whereas rhBMP-2 formulated with chitosan in acetic acid retained its potency. The aqueous preparation of the GF with chitosan significantly enhanced its stability as well as the amount and the sustainment of GF release [109]. TGF-beta embedded in chitosan microparticles, fabricated by an emulsion-cross-linking method, was released within 7 days and increased glycosaminoglycan (GAG) production in chondrocyte cultures [110]. Furthermore, FGF-2 loaded chitosan hydrogels were immobilized on the surface of ischemic rabbit myocardium by UV-irradiation, thereby inducing angiogenesis, and increasing significantly the amount of viable myocardium blood vessels, protecting the myocardium from infarction in contrast to chitosan alone or other control groups [111]. Chitosans could be chemically modified to obtain derivatives with tailored molecular properties: FGF-2 embedded in freeze-dried hydroxypropylchitosan, a highly water soluble chitosan derivate, enhanced wound healing in genetically diabetic mice in contrast to unloaded films [112]. Another chitosan derivative featuring photocrosslinkable properties was used to embed FGF-2 in aqueous solution by short UV irradiation. FGF-2 retained its potency during photocrosslinking and was gradually released from the hydrogels upon *in vivo* biodegradation. The bioactivity of FGF-2 in the hydrogels was maintained for

more than 14 days and induced angiogenesis in ischemic rat limbs and in healing-impaired diabetic mice [113].

Protein based growth factor delivery platforms

Proteins are the major components of tissues that build up the structural backbone of the ECM. They provide mechanical strength while contributing to the local storage of GFs through direct interactions with GFs or through interaction with GF binding proteins. The use of ECM proteins derived from human tissue would be ideal to produce artificial tissue substitutes with GF delivery properties. However, they are costly and their availability is quite limited. Therefore, homologous proteins derived from other mammalian tissues such as from bovine or porcine origin are used instead, still providing acceptable biocompatibility. Moreover, proteins from other species than mammals have been investigated, such as silk fibroins (SF) from *Lepidoptera*, providing excellent availability, mechanical properties, biocompatibility and cellular interactions. Proteins in general offer a variable range of physiochemical properties, which may provide beneficial interactions with GFs and sustain their potency similar to the ECM proteins of native tissues (**Table 1**).

Collagens

Collagen type I, II and III are the most abundant collagens among the 12 existing collagen types, and are able to assemble into fibers and form macroscopic structures. Collagens I, II, III form rod-like right-handed triple helices consisting of three coiled subunits composed of two alpha and one beta chains [114]. Collagens are predominantly synthesized by fibroblasts, epithelial cells, osteoblasts and chondrocytes. Collagen I is the most abundant ECM protein (90 to 95% of total ECM) and can be harvested as a crude insoluble tissue isolate or as a soluble isolate after enzymatic cleavage of their telopeptides, important moieties for the cross-linking between different collagen triple helices [115]. Besides

providing structural and mechanical properties of tissue, collagens can interact with GFs and cytokines [44]. Upon implantation, collagens are degraded within several weeks. This issue can be overcome, at least to some extent, by physical cross-linking of collagen fibres, which sustains the mechanical properties after implantation and may support tissue (in)growth [116-118].

Native collagens

Because of their universal presence in almost any tissue, collagens have been widely used as a material for biomedical implants and delivery platforms for various GFs. The release of GFs from collagen matrices is generally controlled by the diffusion rate of the compound through the swollen matrices, but also by matrix interactions and enzymatic degradation, e.g., matrix resorption *in vivo*. Crosslinking of collagen by chemical or dehydrothermal treatments are widely used to reduce water uptake and degradation rates of the matrix in order to improve the sustainment of GF release [119, 120]. Until now, two collagen-based BMP delivery platforms have entered the market to treat non healing bone defects. For their fabrication human recombinant bone morphogenetic protein 7 (hrBMP-7 - OP-1; Stryker Biotech) was bound to a collagenous matrix through swelling in an aqueous medium containing BMP-7 [121]. INFUSE Bone Graft (from Medtronic Inc.) is another collagen sponge (ACS) platform to deliver absorbed recombinant human bone morphogenetic protein-2 (hrBMP-2). It is mainly applied in combination with a metal based device for spinal fusion in degenerative disc disease. BMP-2 loaded bovine type I collagen matrices were successfully used to heal large frontal bone defects in a 60-year-old man [122]. Moreover, collagen based BMP-2 platforms have been investigated for the treatment of cartilage defects, revealing good results in a 2 year study [123]. Collagens were further used as coatings to increase adsorption and release of rhBMP-2 from a PLGA membrane in rabbit mandibular defect [124] or coated on titanium membranes to promote wound healing through absorbed TGF-beta. Both coatings

significantly increased the sustainment of the GF release [125]. Collagen has also been shown to form an excellent delivery platform for naked plasmid vectors, the adenovirus vector, and for antisense DNA and DNA vaccines, protecting from DNA degradation by both chemical cleavage and enzymatic digestion [126]. Collagen matrices have been modified with heparin through chemical crosslinking, which further increased the immobilization of angiogenic vascular endothelial growth factor (VEGF) on the matrix. The loading of VEGF as well as its degradation could be affected by varying heparin concentrations [78, 81]. Although collagens can be easily isolated and purified in large quantities, risks of contamination with viruses or other pathogens exist. Furthermore, the use of bovine collagen bears risks of bovine spongiform encephalopathy (BSE) transmittance. Other sources, such as bullfrog skin yields 12.6% collagen devoid of the BSE threat. Therefore, bullfrog derived collagen was envisioned as a safe collagen source for biomedical applications, and successfully employed as a platform to release bovine serum albumin (BSA) from its matrix [127]. Certain GFs show a specific affinity to collagens fibers, which may depend on the isoforms of the respective GF. For example, proforms of BMP-2 can be cleaved into two different mature isoforms, a shorter and a more extended BMP-2. Homodimers and heterodimers of rhBMP-2 isoforms were produced and tested for their affinity to collagen matrices. The extended rhBMP-2 isoforms as well as heterogenous dimers changed their affinity to the collagen substrate depending on the pH. Overall, saturation of rhBMP-2 binding to collagen was higher than expected for monolayer adsorption, suggesting that rhBMP-2 forms multilayers [73]. The exploitation of GF isoforms with different affinities for collagens could provide versatile collagen-GF systems with tunable delivery properties.

Gelatine

Gelatin is derived from collagen and isolated through boiling of bones and skins. It has been traditionally used as the basis for glue production, food additives

and gelatine capsules. Its fabrication process dates back to the late 17th century. Nowadays, various processes have been developed to produce gelatin with various isoelectric points yielding either negatively charged acidic gelatin, or a positively charged basic gelatin at physiologic pH (7.4). This hypothetically allows electrostatic interactions to take place between gelatin and GFs of opposite net charges. The cross-linking density of gelatin hydrogels can further impact their enzymatic degradation and diffusional properties, thereby controlling *in vivo* release of GFs [128]. Gelatin hydrogels with different water contents were prepared through glutaraldehyde crosslinking, resulting in different BMP-2 retention in these matrixes. Gelatin hydrogels with a moderate retention capacity for BMP-2 maximized bone formation and ALP activity in contrast to a collagen sponge with either higher or lower BMP-2 retention. Hence, the control of GF sustainment by crosslinking of the matrix was beneficial for optimal bone formation [129]. Alternative crosslinking processes have been developed based on microwave treatments to crosslink gelatin, in order to overcome the toxicity of residual chemical crosslinking agents [130]. Gelatins as well as most other biopolymers can be processed as aqueous solutions, allowing for direct embedment of sensitive GFs into the matrix during processing, improving their loading and their capacity for retention. For example, rhBMP2-loaded dextran-co-gelatin hydrogel microspheres released the GF for more than 10 days and increased periodontal tissue regeneration in contrast to scaffolds that were simply soak-loaded with concentrated rhBMP2 aqueous solution [131]. Another approach to control release profiles is the embedment of GFs in multilayer coatings. Two-layered heterogeneously loaded and crosslinked gelatin coatings were used to obtain combined and sequential release of BMP-2 and IGF-I. Peak release from the top and bottom layers were located at 1 and 6 days, respectively. The initial burst was followed by an increase in BMP-2 and IGF-I release after 5 days and resulted in the largest deposition of mineralized matrix in CH3 cell cultures [132]. As aforementioned, different extraction processes can control the properties of gelatin and offer opportunities to modulate the interaction between gelatin and

GFs as well as its release characteristics. Denaturing collagen using trifluoroacetic acid (TFA) resulted in a more acidic gelatin and thus in a stronger and more sustained retention of FGF-2 (basic FGF) as compared to collagen denatured by heat. TFA-denatured gelatin progressively stimulated cell growth peaking at days 8 and 10 in contrast to heat denatured gelatin inducing cell growth exclusively during the first 5 days [133].

Fibrinogen / Fibrin

Fibrinogen is a large and complex fibrous glycoprotein consisting of three polypeptide chains linked together by 29 disulfide bonds. The complex is 45 nm in length, with globular domains at each end and connected by alpha-helical coiled-coil rods in mid section. Both strongly and weakly bound calcium ions are important to maintain the structure and function of fibrinogen. During homeostasis, soluble fibrinogen in the serum is cleaved by thrombin into insoluble fibrin polymer, resulting in the assembly of fibrin into staggered protofibrils. The protofibrils aggregate laterally to assemble in a three-dimensional network of fibers producing a fibrin clot that seals wounds. During the healing process, fibrin is further degraded through enzymatic cleavage of specific lysine residues in the fibrin protein by plasminogen [46]. The mechanical properties of such clots can be quite variable and are essential in homeostasis and wound healing [46, 134]. Fibrin has been used as wound sealant and surgical tissue adhesive as the assembly of fibrin into the gel is easily inducible by mixing fibrinogen with isolated thrombin prior to application. Fibrin sealant has been used as a haemostatic agent in cardiac, liver, and spleen surgery and is under investigation for its application as a slow-release drug delivery system and as a substrate for cellular growth and tissue engineering [135]. As mentioned in the first part of this review, fibrin undergoes interactions with many natural proteins, including fibronectin, albumin as well as IGFBPs, FGF-2, and VEGF, proteins that contain the von Willebrand factor. It therefore recommends itself as an interesting delivery platform for these GFs [46, 136]. Fibrin matrices have been used to deliver TFG-

beta directly to the joint cavity of articular cartilage defects. During the initial 5 days, 10 to 20% of the embedded TGF-beta was released per day, resulting in a total release of 68% after 25 days [137]. FGF-1 loaded fibrin matrices significantly improved the mechanical properties of the regenerated tissue in full-thickness wounds in rabbits after 2 weeks [138]. Furthermore, the strong interaction of FGF-2 with fibrin has been used to specifically localize the GF on fibrin surfaces. FGF-2 was printed with a custom inkjet printer on fibrin films in concentration modulated patterns including continuous concentration gradients. The immobilized FGF-2 was biologically active and the printed patterns persisted up to 10 days under cell culture conditions. Cell numbers as well as distribution increased according to the gradient [139]. The controlled surface deposition of GFs on biopolymer matrices holds potential for guiding tissue (re)generation by GF gradients.

Albumin

Serum albumin is the most abundant protein in animal sera and can be isolated and purified in large and cost effective amounts from animal blood. The primary structure of bovine serum albumin (BSA) is composed of 582 amino acid residues with an average molecular weight of 66.3 kDa. Its isoelectric point is around 5.2 and it contains 17 intrachain disulfide bridges and one sulfhydryl group. The charges of BSA are not uniformly distributed in the primary structure but become very uniform in the tertiary structure of the protein. Because of their strong intermolecular repulsion, BSA forms quite ordered and stable intermolecular structures in aqueous solutions under normal physiological conditions and responded like so-called colloidal crystals sinusoidal to linear strains [140]. BSA has been abundantly used to stabilize pharmaceutical proteins, such as GFs and monoclonal antibodies, in liquid formulations and protect such factors from unspecific adsorption and aggregation. In this context BSA was employed as an excipient to stabilize NGF and GDNF in synthetic nerve conduits [141] or for the stabilization of IGF and NGF upon encapsulation in PLGA

microspheres [142, 143]. In addition to its use as an excipient, it can be processed to form gels. Under heat treatment, BSA undergoes two structural modifications. In a first stage, occurring up to 65 °C, the protein undergoes a reversible denaturation followed by irreversible unfolding of its hydrophobic zones and exposure of cysteine residues resulting in hydrophobic interactions and disulfide bridges and, finally, formation of protein gels. BSA gels are typically prepared at concentrations ranging from 2 to 8 %. Their G' modulus increases with increasing protein concentration [144]. Albumins can undergo a reversible conformational transition when pH changes. This feature is very conserved among albumins of different species suggesting a major physiological role, possibly related to the function of albumin for the transport of small molecules including drugs as well as their stabilization [145, 146]. The change of pH from 4 to 2 decreased the alpha-helical content of albumin from 70% to 40% and could be restored by addition of sorbitol that resulted in the restoration of its initial conformation [146]. The transition of the structural feature of BSA upon pH change could be an interesting aspect for its further investigation as delivery platform for the controlled release of GFs.

Silk fibroin

Various insects and spiders produce silks for different applications, such as webs for hunting or cocoons to protect their larvae against predators and humidity during metamorphosis. Silk fibers are the strongest existing natural fibers rivaling synthetic fiber such as Kevlar in terms of elasticity and absorbed energy until break [147]. Although spider silks exert similar inflammatory reactions as compared to marketed wound dressings such as polyurethane film, collagen dressings, gauze pads [148], to date, silk fibroin (SF) from silkworm cocoons have been mainly investigated for biomedical use. Cocoons of the silk worm *Bombyx mori* represent a cost effective and straightforward source for SF, yielding high amounts of purified protein in either aqueous or organic solution. The molecular

structure of SF consists of a heavy chain (350 kDa), a light chain (26 kDa), and a glycoprotein (P25 - 25 kDa). The heavy and light chains are linked by a disulfide bond, and P25 associates with heavy and light chains by noncovalent interactions at a ratio of 1:6:6 to form an SF elementary unit, a large protein complex of approximately 2.3 MDa. The elementary unit further self-associates into fibers that are subsequently coated with sericin, a glue like glycoprotein, to form the silk fibers during spinning in the spinning ducts [149]. Pure SF can be obtained by boiling silk fibers to remove the water soluble sericin, which has been associated with an immune reaction of the host organism against implanted silk materials. The SF chains are composed of alternate arrays of crystalline and non-crystalline elements. The crystalline domains are characterized by repeats of highly conserved motifs consisting of perfect repeats of the unit peptide Gly-Ala-Gly-Ala-Gly-Ser. The Ser are replaced by Tyr in the non-crystalline domains and by irregular substitutions of Ala to Val or Tyr. The observed heterogeneities in numbers of repeats are probably a result of continuous unequal crossovers in a primordial gene during evolution and duplication or deletion of repetitive sequences [150]. The insolubility of SF fibers is provided by the formation of hydrophobic interactions between the SF molecules resulting in the formation and stacking of beta-sheets causing hydrophobic, intermolecular crosslinking. Silk fibers have been used for decades as biomedical suture material [151], and first attempts to apply silks as biomedical implant for tendon replacements were already reported in the early 20th century [152]. Since then, existing biocompatibility concerns were attributed to residual sericin in the SF preparations and were resolved by purification. SF purified from sericin leads to mild inflammatory reactions, which are comparable to other biomaterials such as collagen or poly(lactic-co-glycolic acid) [151, 153, 154].

Various technologies have been employed to produce 3-D porous SF scaffolds including foaming, particle leaching and electrospinning [155-158]. SF scaffolds have been investigated for application in various tissues such as tendon, bone, cartilage and neural tissues [15, 155, 159-163]. The excellent mechanical

properties of SF and its slow biodegradation [164] are most beneficial for tissue engineering when compared to other faster degrading biomaterials, such as collagen [165]. However, its potential as a material for the delivery of GFs has only been recently explored. Given the abundant chemistry for side chain substitutions of amino acids, there are manifold opportunities to functionalize and decorate SF with bioactive proteins [166]. BMP-2 was directly immobilized on SF films and induced osteogenesis of adherent human mesenchymal stem cells (hMSC) in contrast to pure SF films. Using cell culture inserts, it has been demonstrated that the observed differentiation was induced by the immobilized bioactive protein rather than the release of the active GF into the culture medium [167]. BMP-2 was adsorbed onto porous silk fibroin scaffolds by soaking in concentrated BMP-2 solution. 75% of the loaded BMP-2 was released under dynamic culture conditions (spinner flasks) and induced osteogenesis of hMSCs in contrast to unloaded scaffolds. The GF loaded scaffolds caused significant bone ingrowth after implantation in critical sized cranial defects in mice independent of whether the scaffolds were seeded with hMSC or left unseeded [168]. Dextrans of different molecular weights, as well as proteins, were physically entrapped into films produced from aqueous SF solutions. Drug release kinetics were evaluated as a function of dextran molecular weight and film crystallinity. Treatments with methanol resulted in an increased beta-sheet content thus augmenting hydrophobicity. Elevated beta-sheet conformation reduced the burst release and sustained the subsequent release of dextrans and bioactive proteins [169]. BMP-2 loaded nanofibrous silk fibroin scaffolds have been produced via electrospinning and applied for *in vitro* bone formation from human bone marrow-derived hMSCs. BMP-2 retained its bioactivity during the water-based electrospinning process and enhanced calcium deposition and bone-specific markers in cultured hMSCs for up to 31 days [170]. Previously, our group developed a process for the fabrication of porous SF scaffolds based on freeze-drying of highly concentrated SF solutions exerting customized control over pore size and pore interconnectivity [155]. IGF-I was directly embedded into the porous SF matrix, namely by dissolution of IGF-I

in an aqueous SF solution before freeze-drying, leading to sustained release of bioactive GF from the freeze-dried scaffolds over 4 weeks. Methanol treatments of SF, to induce crystallinity and insolubility, respectively, did not adversely affect the bioactivity of the released IGF-I, indicating a stabilization of the GF through interaction with SF. Released IGF-I, in combination with low concentrations of TGF-beta in chondrogenic medium, supported the chondrogenesis of adherent hMSC, producing tissue of cartilage-like morphology in contrast to unloaded scaffolds [171]. In a similar approach and aimed at the application for peripheral nerve repair, nerve growth factor (NGF) was embedded in tubular SF nerve conduits (NC) produced by air drying of films or freeze-drying of aqueous SF solutions in tubular molds. The bioactivity of NGF was retained in all formulations; however, magnitude and kinetics of release were dependent on the drying process and the freezing temperature used. These results suggested an important impact of the scaffolding process on the release kinetics and potency of the GF. The GF seemed to interfere with SF, which reduced the total cumulative release of the initially loaded GF [172]. As an alternative platform aiming at a localized delivery of GFs, SF microspheres were developed using lipid vesicles as templates, to form depots for GF release either in combination or without a biomaterial scaffold. Upon formation of the vesicles residual lipids were removed by treatments with methanol or sodium chloride, which induced beta-sheet formation and water-insolubility of SF. Horseradish peroxidase (HRP) was encapsulated as a model protein resulting in sustained release from the microspheres for up to 1 to 2 weeks, depending on the β -sheet content that was controlled by the time period used for the salt treatment [173]. To introduce hydrophilic properties and boost the total release of bioactive proteins from SF substrates, SF was blended with solutions of soluble or suspensions of insoluble collagen type I at a ratio of 90:10. The total cumulative release of HRP embedded in such blends was enhanced in contrast to pure SF films, which released 80% of the initial loading in 14 days, in contrast to 15%, respectively (Uebersax et al., unpublished data). The blending of SF with other biopolymers, such as collagens,

heparins or hyaluronic acid could further help to adapt the delivery properties to a specific GF and tailor GF release according to the needs of a particular tissue defect (Uebersax, unpublished data; Garcia-Fuentes, unpublished data). Another opportunity to tune SF-GF interactions lies in the functionalization of tyrosine residues. Sulfation of SF is also envisaged to improve the hydrophilicity of SF and enhance the binding of positively charged GFs, such as FGF-2, to the scaffold.

IV. ENGINEERED BIOPOLYMER PLATFORMS FOR GROWTH FACTOR DELIVERY IN TISSUE REPAIR

Although biopolymers can be readily harvested from natural sources in relevant amounts the availability of engineered biopolymers for biomedical use is severely limited by the pharmaceutical quality and purity of the primary materials. Furthermore, the endowment of biopolymers with new functional elements to control self assembly, biodegradation, GF loading and GF release in order to meet specific clinical applications adds to the complexity of such materials. In addition to passive release control, through tailoring the swelling rate and kinetics of biodegradation of the biopolymer's matrix, its performance may be further controlled by the implementation of elements that respond to physiological parameters such as pH or enzymatic activity. Natural concepts for GF storage and release could help to guide the rational design of biopolymer systems for GF delivery. In this context, we will summarize some strategies that hold promising potential to customize biopolymers for GF delivery in tissue repair, including the blending of biopolymers with synthetic polymers, the chemical synthesis of peptides and polysaccharides, and the genetic engineering of recombinant fibrous proteins and GF binding mediators (**Fig. 2**).

Combination of biopolymers with synthetic molecules

Many commercially available synthetic polymers show physicochemical and mechanical properties comparable to those of biological tissues. However, their biocompatibility and biodegradability are often insufficient, limiting their potential for the clinic. Therefore, the blending of well defined synthetic materials with biopolymers in bioartificial polymeric systems could improve, e.g., the physical properties, the release profile and the capacity of self-assembly, while still preserving the intrinsic biocompatibility and biodegradation of the biopolymer component [12, 13, 174]. For instance, blending collagen and HyA with poly(vinyl alcohol) (PVA) [91] enhanced their mechanical properties. Moreover, blends with higher concentrations of either of the two biopolymers significantly improved the matrix release of growth hormone (GH). In order to combine biocompatibility, biodegradability and biological functions with responsiveness to external stimuli, e.g., for site directed drug delivery in tissue repair, polysaccharides such as chitosan, alginate, cellulose, dextran and their derivatives have been grafted or blended with thermo-sensitive polymers such as poly(N-isopropylacrylamide) (PNIPAAm). Such negatively thermo-reversible hydrogels can be tuned into liquids at room temperature (20-25 °C) but undergo gelation when brought in contact with body fluids that warm them up above their lower critical solution temperature (LCST, 36-37 °C) [175]. Furthermore, gels of alginate, dextran or chitosan in combination with PNIPAAm showed shrunk pore sizes and decreased perfusion when heated above their LCST (32 °C) resulting in diffusional hindrance and sustained release of embedded proteins [13, 176]. Consequently, in a bioartificial polymeric system, the loading of GFs can be increased by the use of the biopolymer component and the sustainment of the release by the thermo-responsive synthetic component (e.g. PNIPAAm). To control the gelation of chitosan this polysaccharide was grafted with poly(ethylenglycol) (PEG) chains [13]. At body temperature the PEGylated chitosan transformed from an aqueous solution to a semisolid hydrogel after

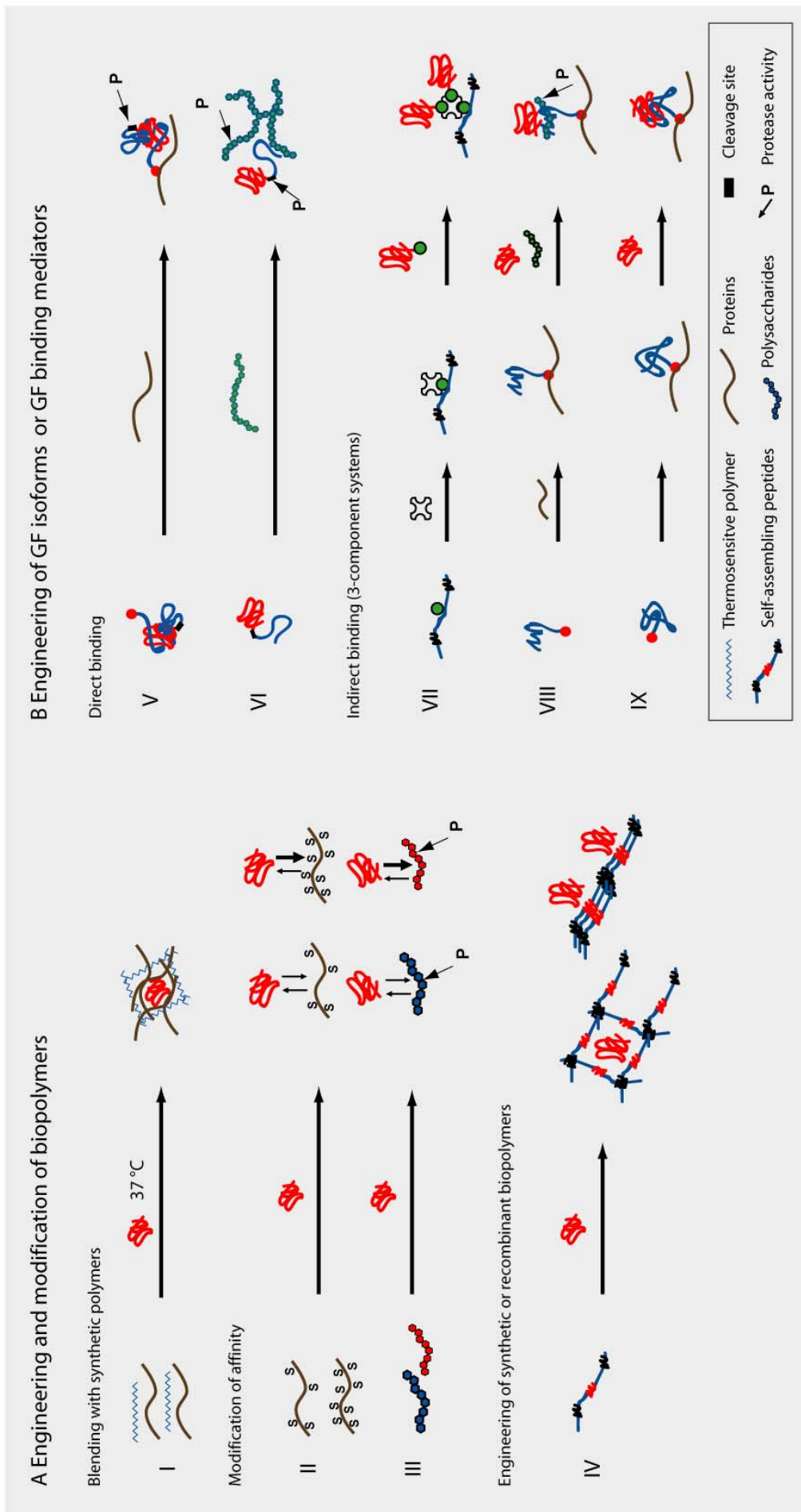
injection. Crosslinking of the hydrogel further prolonged the in situ release of embedded BSA for up to 40 days.

Synthesis of analogous polysaccharides and peptides

Heparin mimetics

Since glycosaminoglycans (GAG), especially heparins, control local GF levels and receptor binding, they have been under investigation for their potential to generate GF delivery platforms with customized properties for tissue repair. Although heparin-like glycosaminoglycans (HLGAGs) are complex carbohydrates and difficult to synthesize, recent developments in oligosaccharide synthesis greatly accelerated the complete synthesis of stereoselective heparin oligosaccharides derivatives [177]. Still, the structure-function relationships of GAGs are poorly understood owing to the chemical complexity and heterogeneity of the biopolymer.

Fig. 2: Engineering biopolymer systems with controlled GF interaction. (A) Engineering and modification of biopolymers: (I) Blending of biopolymers with thermo-responsive, synthetic polymers for GF embedment during in situ gel formation at body temperature. (II) Modification of affinity by chemical modification of proteins (heparin mimetics), e.g. sulfation (S). (III) Design of oligosaccharides with tailorable affinity for GFs. (IV) Genetic or chemical engineering of peptides with integrated moieties for GF interaction. (B) Engineering of GF isoforms or GF binding proteins: (V) Engineering of GF isoforms with integrated moieties for protease cleavage and cross linking to the biopolymer matrix. (VI) Engineering of GF isoforms with integrated moieties for protease cleavage and enhanced affinity for the biopolymer matrix. (VII) Streptavidin binder for the linkage of biotin modified GF to biotin modified biopolymer matrices. (VIII) Modification of biopolymer with perlecan derived peptides, which bind heparin to enhance the binding of HBGF to the biopolymer matrix. (IX) Cross-linking GF binding proteins to biopolymer matrices.



The interaction of GFs with heparins depends on the amount and the positions of the O-sulfate groups in the polymer (iduronyl 2-O-sulfates, glucosaminyl 6-O- and 3-O-sulfates) that form binding sites for the proteins. The specific sulfation patterns of heparin is mediated by enzymes such as sulfotransferases involved in heparin biosynthesis [178, 179]. With these tools, a library of octasaccharides with different sulfation patterns was produced and subjected to affinity chromatography to test for interactions with FGF-2, -4, -7, -8, -10, and -18, HGF, BMP-6, and VEGF. The study allowed to classify the interactions between GFs and heparin into five groups: group 1 needed 2-O-sulfate but not 6-O-sulfate (FGF-2); group 2 needed 6-O-sulfate but not 2-O-sulfate (FGF-10); group 3 had affinity to both 2-O-sulfate and 6-O-sulfate but preferred 2-O-sulfate (FGF-18, HGF); group 4 required both 2-O-sulfate and 6-O-sulfate (FGF-4, FGF-7); and group 5 hardly bound to any of the octasaccharides (FGF-8, BMP-6, VEGF) [180]. The fast screening and quantification of GF affinities for oligosaccharide has potential to further enhance the development of a next generation of GF binding polymeric platforms. In this context, an array of synthetic heparin oligosaccharides was successfully developed that yielded defined binding partners for FGF-1 and FGF-2 exerting different affinities [181]. A library of rationally designed heparin mimetics with specific GF affinities allowed to tailor materials with controlled sustainment of GF release that may help to provide GFs in specific regimens adapted to meet clinical needs.

Peptides and amino acid based polymers

Small synthetic peptides have been reported to serve as biomaterial scaffolds for tissue engineering of cartilage, blood vessels, and other tissues by mimicking the self assembly process of natural fibers [182]. The synthesis of peptide-based fibers inspired by alpha-helices and the collagen triple helix as building blocks for self-assembly, may lead to promising candidates to mimic collagen function and interaction with GFs [182]. Such mimics were demonstrated

to produce complex fibrous structures and provide moieties that could be easily functionalized [183]. Synthetic peptides have been successfully used as injectable self-assembled substrates to guide neurite outgrowth and synapse formation [184, 185]. However, improvement in their GF binding has not yet been addressed. To custom design proteinaceous biomaterials that are structurally related to natural proteins, amino acids or dipeptides have been used as building blocks. Among the class of poly(amino acid)s, only a small number of poly(γ -substituted glutamates) and copolymers have been identified as promising candidate materials for biomedical applications [186]. Serum proteins such as fibrinogen, or extracellular matrix proteins such as fibronectin adsorbed strongly onto surfaces of tyrosine-derived polycarbonates, providing the basis for cell adhesion in tissue culture. One of the advantages of poly(amino acids) is that they produce only minor amounts of acidic degradation products during bioresorption of the material as compared to synthetic polyesters [187]. Their peptide-type backbone may engage in strong hydrogen bonding with peptide drugs in order to increase the drugs' stability and avoid a burst release. In this context tyrosine-derived polyarylates were found to be particularly useful. The screening of polyarylate libraries facilitated the identification of strong interactions with any given target peptide. A sustained release system for the heptapeptide integrilin was developed on the basis of poly(desamino-tyrosyl-tyrosine ethyl ester adipate), poly(DTE adipate), that showed particularly strong hydrogen bonding with Integrilin. Integrilin incorporated into a poly(DTE adipate) matrix was hardly released during a 50 day incubation period under physiological conditions (pH 7.4, 37 °C) [188]. In analogy to the recent developments in heparin synthesis, peptides have been developed to mimic sulfated glycosaminoglycan heparin and offer binding of HBGFs. Peptide-based heparin mimetics would be particularly attractive, given the ease of peptide synthesis and modification. In this context, a library of some 6600 sulfated tetrapeptides was engineered and analyzed on-resin for VEGF binding. The top binder exerted a 100-fold stronger binding to VEGF than the polysaccharide based heparin mimic suramin [189].

Genetic engineering of recombinant fibrous proteins

Over the past 20 years, significant advances in genetic engineering and the understanding of protein secondary and tertiary structures allowed for the engineering and production of novel polypeptides in biological organisms. The biotechnological production of recombinant biopolymers can assure constant quality, minimizes purification process and batch variations and reduces the production costs of the material. The precision with which these polymers can be synthesized allows to incorporate motifs for gel-formation, stimuli-sensitivity, biodegradation, and biorecognition [190, 191]. The introduction of novel properties in biopolymers by genetic engineering are, in particular, interesting for controlled delivery of GFs. The genetic engineering of polysaccharides is much more demanding and less predictable. The outcomes are mainly controlled by the up- or downregulation of enzymes involved in the anabolic pathways of the specific polysaccharide or by adaptation of nutrition factors rather than the modification of one single gene. Therefore, we will exclusively focus on the genetic engineering of recombinant proteins based on sequences from natural fibrous proteins. The engineering and application of thermally associating polypeptides based on sequences related to elastin, silk and collagen, as injectable drug delivery vehicles, has recently been extensively reviewed by Hart et al. [191] and will not further be detailed in this review. Hence, we will focus on genetically engineered peptides that form fibres with prospective applications as structural scaffold material for GF delivery in tissue repair. Recombinant collagens can self assemble into ordered structures or fibrils and can be expressed in mammalian cells, insect cells, yeast, *Escherichia coli*, transgenic tobacco, mice and silkworms for various biological applications [192]. Mammalian cells are still the preferred expression system for collagen-type peptides as they provide hydroxylation of prolines to hydroxyprolines, which is intrinsic to native collagen. In other organisms the hydroxylation has to be achieved by co-expression of hydroxylase or by chemical modification after downstream processing [192]. However, recombinant gelatin (HU4) was produced in *E.coli*, featuring part of the amino

acid sequence of the $\alpha 1$ -chain of human type I collagen, was modified with methacrylate residues for chemical crosslinking and gel formation. Lysozyme and trypsin inhibitor were embedded in the matrix during gel formation providing sustained release of the embedded proteins over several days [193]. The implementation of the GF binding site into these peptides could help to better control GF release from such peptide systems.

Silks represent a further family of fibrous proteins with excellent mechanical properties, slow *in vivo* degradation and good but unspecific interaction with GFs and cells [151, 159, 161, 163, 165, 172]. It is attractive to exploit the excellent mechanical properties of this protein family and their intrinsic sequences for self assembly to produce customized recombinant peptides that self assemble. Such peptides may further feature motifs from mammalian ECM proteins to improve their biological performance. Recombinant proteins based on various types of silk sequences have been genetically engineered and successfully expressed in different host cells [194, 195]. The silk worm larva from *Bombyx mori* itself represents an optimal expression system for recombinant fibrous proteins. Specialized cells at the posterior end of its silk glands devote 85% of their protein synthesis actively to silk production, corresponding to a productivity of $80 \mu\text{g protein cell}^{-1} \text{ day}^{-1}$. By comparison, the best recombinant high-yield mammalian cell culture system only produces $50 \text{ pg protein cell}^{-1} \text{ day}^{-1}$, which rather limits this system [196, 197]. As aforementioned, genetically modified silk worm larvae have been used to produce fusion proteins containing collagen type III derived sequences that could be easily harvested in high amounts from the silk worm cocoons [198, 199]. In this context, chimeric SF proteins were produced in silk worm larvae by baculovirus-mediated homologous recombination of a foreign gene downstream from a powerful SF promoter [200, 201]. Silk-like proteins based on SF from the wild silk worm *Samia cynthia ricini* were produced in *E. coli* including the cell adherence sequences from fibronectin (RGD) and an additional sequence from elastin [202]. The RGD sequences incorporated in the silk-like protein significantly improved the adherence and proliferation of seeded

cells, confirming the retained accessibility and function of the adhesion motifs after self-assembly, whereas the elastin sequences reduced the crystallinity of the protein. Among the different silks, spider silk constitutes the strongest fiber that even rivals synthetic fibers such as Kevlar [147]. However, the availability of spider silk is limited and the spider itself is not a feasible organism for the production of recombinant silk in relevant amounts. Consequently, spider silk-elastin fusion proteins have been produced in transgenic plants using straightforward extraction from the leaf material, with high protein yields [203, 204]. Bacteria are still the most successful and versatile hosts for the transgenic expression of recombinant proteins, allowing simple introduction of foreign genes and cost efficient production of recombinant spider silks and collagens [195, 205, 206]. In this context, silk-elastin chimeric proteins produced in bacteria were applied as platform for the controlled release of plasmid DNA and adenoviral vectors. The delivery of DNA in such a hydrogel increased transfection rates in a murine model of human breast cancer by 1 to 3 orders of magnitude, as compared to naked DNA. The release of a bioactive adenoviral vector could be controlled by the concentration of the polymer in the hydrogel [207-209]. Up to now, silk modifications have shown to affect assembly, crystallinity and swelling behavior of recombinant protein matrices. However, the implementation of protein domains that respond to extracellular cues such as pH or protease activity, or control the release of GF have not yet been addressed. The introduction of degradable motifs into SF could further help to control the biodegradation of SF *in vivo*, which - in its unmodified form - undergoes rather slow biodegradation (6–12 months). Moreover, the introduction of GF binding sites derived from ECM molecules, GF-receptors, GF-binding proteins or moieties identified by affinity screenings of peptide libraries could further improve the materials and open the field for the application of more specialized biopolymers for GF delivery. Nevertheless, reliable prediction of tertiary and quaternary structures is pivotal to assure the accessibility and the function of the introduced elements after protein assembly.

Design of GF binding mediators

The implementation of signals for self assembly and optimized GF interaction in a single biopolymer with appropriate mechanical strength is a challenging objective. Even if successfully accomplished such developments are likely to lead to highly specialized indications. As the development of new biomaterials is time consuming and expensive, it may be strategically more promising to design modular systems in which the GF binding domain is separately developed from the load bearing sections of the scaffold. This approach would facilitate the introduction of regulatory elements to control GF release and potency by their response to cellular signals in analogy to natural GF binding proteins. Such binding intermediates could probably be adapted to different scaffold materials, designs, and mechanics, and would allow an optimized setup of each component before assembly. In a model study, tetravalent streptavidin was used to mediate the conjunction between biotinylated IGF-I and equally biotinylated self-assembling peptides for injection upon cardiac injury. When injected such nanofibers provided sustained IGF-I delivery for 28 days *in vivo*, and, in combination with seeded autologous myoblasts, improved systolic function after experimental myocardial infarction [210]. Heparin was used to mediate FGF-2 binding to PLGA nanofibers. For this purpose heparin was covalently coupled via a PEG linker to electrospun PLGA nanofibres. This approach led to a 3-fold improvement in the immobilization of FGF-2 in the tissue resulting in a more homogenous distribution of the GF on the fiber surface [211]. Furthermore, keratinocyte growth factor (KGF) was covalently linked to a peptide containing a fibrin binding motif (factor XII). Expectedly the GF-peptide complexes bound readily to the fibrin matrices and enhanced their wound healing properties. KGF release occurred primarily in response to the cell-associated enzymatic degradation of the fibrin matrix [212]. In another approach, a chimeric peptide carrying a N-terminal transglutaminase substrate and a C-terminal heparin-binding domain (factor XIIIa based on antithrombin III) was synthesized, and covalently cross-linked to fibrin matrices by transglutaminase, which was added during

coagulation of fibrinogen through thrombin. The C-terminal heparin binding domain caused an electrostatic immobilization of heparin on the matrix of the peptide. Bound heparin enhanced both the adsorption and retention of beta-NGF, a brain-derived neurotrophic factor, and neurotrophin-3 to the fibrin matrix and slowed down the passive release of the GFs. The active release of GFs in response to the biodegradation of heparin and fibrin through cellular proteases clearly dominated the release kinetics. Immobilization of GFs on heparin increased neurite extension by 100% in comparison to unbound neurotrophic factors [79]. In a similar approach, a recombinant fragment of perlecan, a natural heparan sulfate proteoglycan, was coupled via EDC/NHS chemistry to electrospun collagen or gelatin fibers. The heparin chains bound to perlecan domain I (PInDI) and improved FGF-2 binding to the biopolymer [213]. PLGA scaffolds coated with collagen II fibrils in combination with PInDI improved BMP-2 binding as well as the retention of the GF, inducing chondrogenesis in multipotential mouse embryonic mesenchymal cells in contrast to uncoated scaffolds or collagen II coated scaffolds [52]. Another approach included the insertion of enzymatic cleavage sites into the binding peptides to provide a cell-demanded release of the GF from the matrix. In the context of a physiological GF release control, a latent form of mouse interferon beta (mIFNbeta) was engineered by fusing the cytokine to the LAP of TGF-beta1. To achieve cell-demanded release of the GF, the LAP included a cleavage site for MMP-1 or MMP-3 matrix metalloproteinases (MMPs). The LAP domain of the fusion protein protected the activity of the cytokine and prevented the interaction with its receptors until cleavage [214].

Alternative to the engineering of GF binding mediators is the direct implementation of binding sites and sequences for enzymatic cleavage into recombinant GF variants. VEGF121 was immobilized on fibrin matrices by introducing a sequence (alpha2PI(1-8)) providing enzymatic cross linkage of the GF to fibrin during thrombin induced coagulation. To release GF on demand, the VEGF isoform was further equipped with a plasmin cleavage site [215].

To enhance the binding of BMP-2 to demineralized bone scaffolds, a collagen-binding peptide was fused to the N-terminus of BMP-2. The resulting collagen-targeted BMP-2 (rhBMP2-v) showed increased binding to the scaffold and improved the bone inductive capacity of such matrices in contrast to matrices loaded with regular BMP-2 being less efficacious [216]. These and other modifications are generally aimed to improve the retention and the localization of the GF in the defect, preventing washout and premature loss of GF during tissue regeneration. Dissociation constants for the binding between GFs and their binding proteins may be further optimized by screening phage display peptide libraries in combination with a directed evolution approach [42]. This has potential to tailor GF release kinetics by choice or combination of binding proteins (**Fig. 3**).

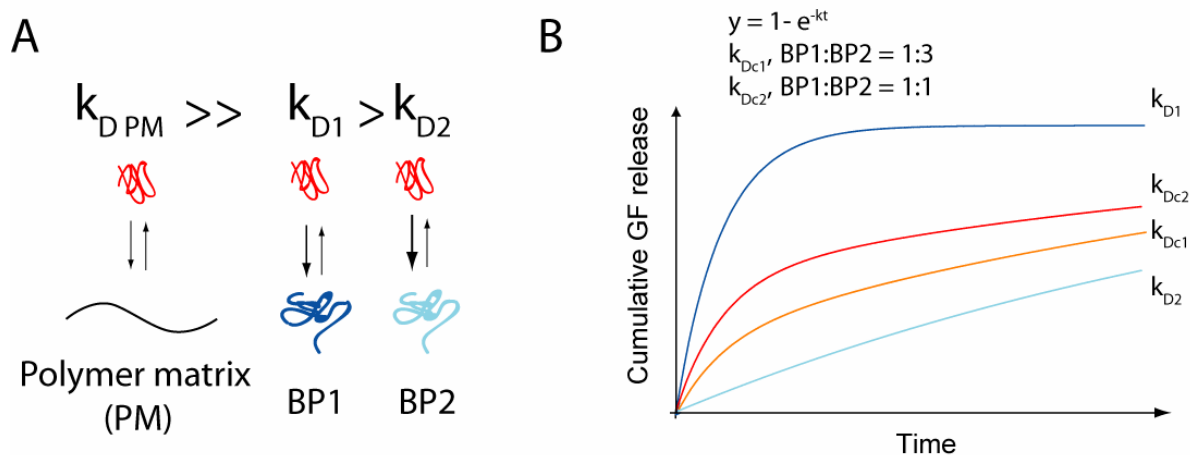


Fig. 3: Bioengineering of GF binders with tunable GF affinities to control GF release from biopolymer matrices. (A) GF binding proteins (BP1, BP2) with tunable dissociation constants (k_{D1} , k_{D2}) below the k_D for the polymer matrix ($k_{DPM} \gg k_{D1}$ and k_{D2}) are produced by affinity screening of peptide libraries or directed evolution. (B) The combination of GF binding proteins (BP1, BP2) with different k_D (k_{D1} , k_{D2}) in different ratios control the overall dissociation constant (k_{Dc1} , k_{Dc2}) of biopolymer system.

By such means, whole libraries of GF binders may be accessible. Further libraries may be created consisting of molecules carrying moieties with high binding affinities to or for cross linking with the scaffold material, in order to link the GF interactive part to the mechanically supportive part of the scaffold (**Fig. 4**).

By means of a specific linker, the two libraries may be combined to endow the scaffold with optimized mechanical and GF delivery properties which are similar strategies may be exploited for the systemic administration of inactive drugs that are exclusively activated in the specific target tissue. This approach was taken for the targeted delivery of tissue-type plasminogen activator (tPA) for thrombolytic therapy, termed ATTEMPTS (Antibody Targeted Triggered Electrically Modified Prodrug Type Strategy). More specifically, tPA was genetically engineered to bind heparin in an inactive state. This complex was further linked to a fibrin specific antibody which – upon systemic administration - targeted the enzyme to fibrin clots for subsequent thrombolysis. tPA can be released at the target site through enzymatic cleavage of heparin, or by the administration of protamin, a strong, competitive binder of heparin [217-220]. Further strategies to release GFs from an inactive state on a binding protein are by exploiting the specific enzymatic activity or pH at the target site. For that purpose, the identification of physiological patterns during tissue regeneration, such as temporospatial enzymatic activity or changes in pH, is pivotal to engineer responsive biopolymer system for controlled GF release (**Fig. 5**). Similar strategies for targeted delivery of protected GFs have been developed by nature. For example, IGFBP-5 was observed to bind IGF-I with higher affinity than the IGF-receptor, but lowered its affinity for IGF-I when bound to ECM molecules. Therefore, binding of IGFBP-5 to the ECM caused IGF-I to be released at the target site and interact with the IGF receptor [62, 70, 71].

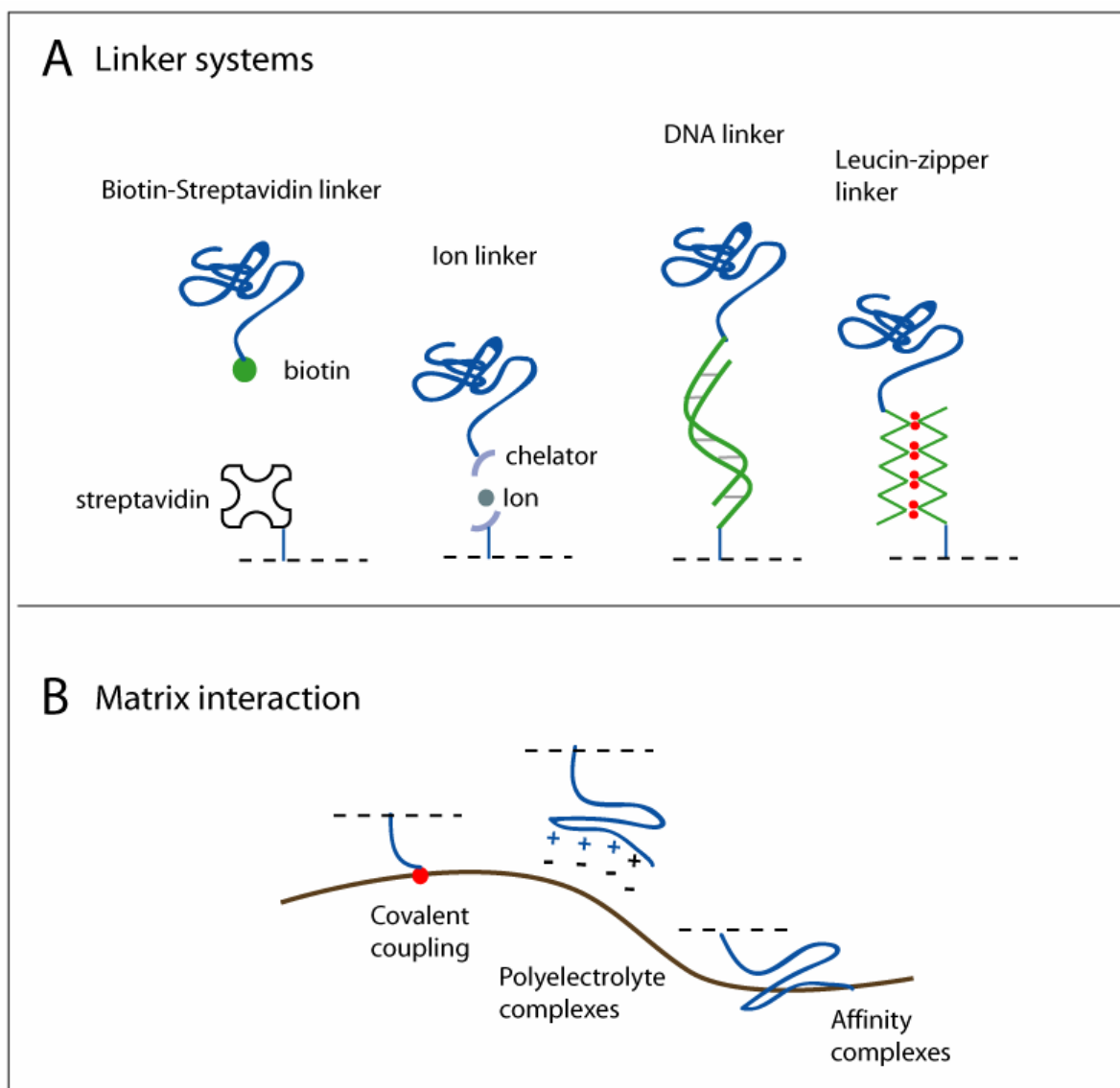


Fig. 4: The combination of independent GF binders and polymer matrices by molecular linkers to design adjustable GF delivery systems (4 component systems). (A) The interaction of GF binding proteins (BP) with polymer matrix can be mediated by the integration of moieties for covalent coupling, strong electrostatic interaction (polyelectrolyte complexes) or strong affinity for the matrix. (B) The use of molecular linkers allows the straightforward loading of the polymer matrix, containing the binding partner of the linker, with the desired GF/BP combination. Moieties for protease or pH triggered release can be integrated in the BP.

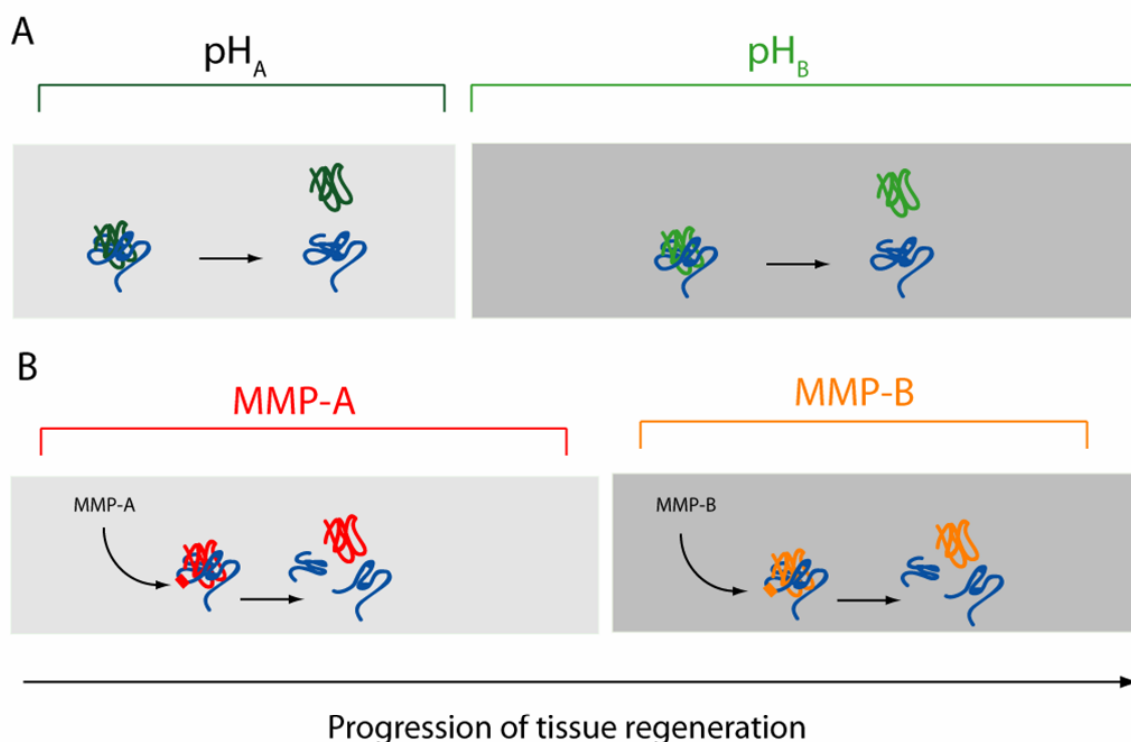


Fig. 5: Exploiting physiological changes during tissue (re)generation for sequential release of specific GFs. (A) pH driven GF release: The initial pH_A at the defect site is lowered due to ischemic conditions in damaged tissue or inflammation. The lower pH triggers the release of GFs involved in vascularization (VEGF, FGF-2), anti-inflammatory factors (IGF-1) or factors important in the initial regeneration phase. After the physiological pH in the tissue has reestablished (pH_B) a second set of GFs are released to support the tissue regeneration. (B) GF release driven by protease activity: Matrix metalloproteinase (MMP) expression during the regeneration phase triggers sequential release of one type or multiple types of GFs through the cleavage of the specific GF binding protein (GFBP).

The adaptation of such strategies may be exploited to target a locally or systemically administered GF to a specific ECM molecule or implanted biomaterial. The use of GF binding mediators with specific affinity for the implant material would then allow to load or reload an implanted matrix *in vivo* during tissue regeneration, or administer different GFs under a given temporospatial regime and so support tissue regeneration with mitogenic factors until completion (**Fig. 6**).

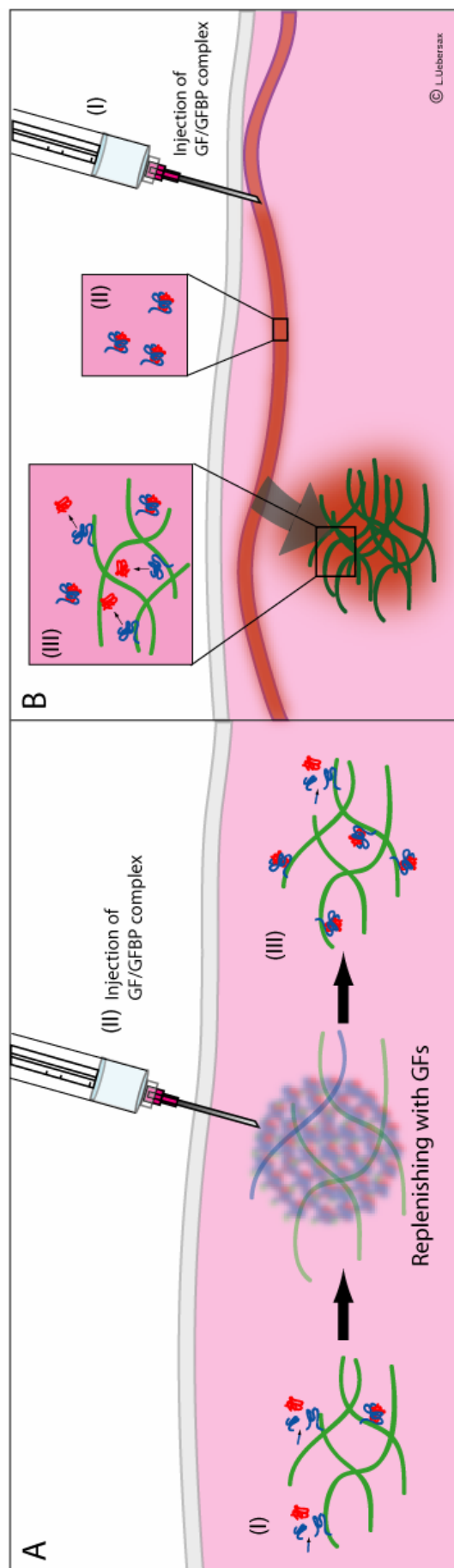


Fig. 6: In situ GF (re)loading of implants during tissue (re)generation. (A) In situ loading of implanted scaffold with specific GFs by local administration of GF/GFBP complexes; (I) The accommodated GF is released from the implanted matrix. (II) GF/GFBP complexes with high affinity for the implant material are locally injected to replenish the depletion of GFs in the scaffold or to provide a second GF type. (III) GF/GFBP bound to the scaffold and GFs can be released through enzymatic cleavage or dissociation from the complex. (B) Accumulation of systemically administered GFBP/GF complexes and release of unbound GF at the defect site through targeting of the implant material mimicking the IGF-I/IGBP-5 complex: (I) GF/GFBP complexes are systemically injected. (II) The GFBP protects the GF from degradation and prevents its interaction with cell surface receptors until arrival at the target tissue. (III) The interaction of GFBP/GF complex with the implant material leads to the disintegration of the complex and consequently the liberation of the active GF in the target tissue.

V. CONCLUSIONS

As components of the ECM, proteins and polysaccharides contribute to the physiological storage of GFs in tissue. Through their interactions with GFs they provide extracellular accumulation of these mutagenic and morphogenic factors and control their activity as well as their release upon demand. In this context, GFs are part of a tightly regulated and interdependent extracellular system, composed of biopolymers that store and control vital chemical information crucial for tissue development, maintenance and (re)generation [34, 221]. In recent years, the delivery of GFs has become more and more evident to form a key element in stimulating the proliferation of implanted or host cells and promoting the regeneration of critical tissue defects treated with biomaterial scaffolds [20, 22, 23, 25]. However, the high costs of GFs demand for delivery systems, which minimize GF waste and provide the GFs in optimal kinetics with maximal biological potency. Much effort has been spent to address this task by improving formulation parameters and protocols as well as the sustainment of the GFs' release by controlling swelling behavior and degradation time of the matrix. However, natural concepts for GF storage in the ECM suggest that the nature and strength of GF–biopolymer interaction play a key role in the protection of GF potency and the regulation of their activation on demand. Consequently, these concepts can provide general paradigms that assist in the engineering of novel biopolymer systems, aiming at the enhancement of the biological impact of accommodated GFs in target tissue. The independent development of the load bearing polymeric component of an implant, from the components providing optimal GF interactions, would facilitate their individual design, manufacturing and storage and help to prolong their life cycle, increasing their field of application and consequently reducing overall development costs. The implementation of a universal and straightforward system to link the two components in various combinations (**Figure 4**) could concede implants with optimal mechanics and design as well as tailorable GF loading, release kinetics

and mechanisms. Yet, little is known about optimal GF regimes for the treatment of individual tissue defects. Therefore, the chronological impact of specific GFs during (re)generation of a specific tissue has to be elucidated in the context of individual factors such as the initial cause of the damage, defect size, age and genetic predestination of the patient. Therefore, flexible and highly potent GF delivery systems will be necessary to transform such findings into clinical treatments.

REFERENCES

1. T.A. Rando, Stem cells, ageing and the quest for immortality, *Nature* 441 (7097) (2006) 1080-6.
2. S.H. Sigal, S. Brill, A.S. Fiorino, L.M. Reid, The liver as a stem cell and lineage system, *Am J Physiol* 263 (2 Pt 1) (1992) G139-48.
3. J. Ehrhardt, J. Morgan, Regenerative capacity of skeletal muscle, *Curr Opin Neurol* 18 (5) (2005) 548-53.
4. I.M. Conboy, M.J. Conboy, A.J. Wagers, E.R. Girma, I.L. Weissman, T.A. Rando, Rejuvenation of aged progenitor cells by exposure to a young systemic environment, *Nature* 433 (7027) (2005) 760-4.
5. I.M. Conboy, T.A. Rando, Aging, stem cells and tissue regeneration: lessons from muscle, *Cell Cycle* 4 (3) (2005) 407-10.
6. S.N. Parikh, Bone graft substitutes: past, present, future, *J Postgrad Med* 48 (2) (2002) 142-8.
7. D. Bettin, H. Bohm, M. Clatworthy, D. Zurakowski, T.M. Link, Regeneration of the donor side after autogenous fibula transplantation in 53 patients: evaluation by dual x-ray absorptiometry, *Acta Orthop Scand* 74 (3) (2003) 332-6.
8. D.C. Rees, F.S. Haddad, Bone transplantation, *Hosp Med* 64 (4) (2003) 205-9.
9. A.N. Kager, M. Marks, T. Bastrom, P.O. Newton, Morbidity of iliac crest bone graft harvesting in adolescent deformity surgery, *J Pediatr Orthop* 26 (1) (2006) 132-4.
10. S. Honsawek, D. Dhitiseith, Content of bone morphogenetic protein-4 in human demineralized bone: relationship to donor age and ability to induce new bone formation, *J Med Assoc Thai* 88 (Suppl 4) (2005) 260-5.
11. R. Toni, C.D. Casa, G. Spaletta, G. Marchetti, P. Mazzoni, M. Bodria, S. Ravera, D. Dallatana, S. Castorina, V. Riccioli, E.G. Castorina, S. Antoci, E. Campanile, G. Scalise, R. Rossio, G. Ugolotto, A. Martorella, E. Rot, F. Sgallari, A. Pinchera, The bioartificial thyroid: a biotechnological perspective in endocrine organ engineering for transplantation replacement, *Acta Biomed* 78 (Suppl 1) (2007) 129-55.
12. M.G. Cascone, N. Barbani, C. Cristallini, P. Giusti, G. Ciardelli, L. Lazzeri, Bioartificial polymeric materials based on polysaccharides, *J Biomater Sci Polym Ed* 12 (3) (2001) 267-81.

13. N. Bhattarai, H.R. Ramay, J. Gunn, F.A. Matsen, M. Zhang, PEG-grafted chitosan as an injectable thermosensitive hydrogel for sustained protein release, *J Control Release* 103 (3) (2005) 609-24.
14. V. Viateau, G. Guillemin, V. Bousson, K. Oudina, D. Hannouche, L. Sedel, D. Logeart-Avramoglou, H. Petite, Long-bone critical-size defects treated with tissue-engineered grafts: a study on sheep, *J Orthop Res* 25 (6) (2007) 741-9.
15. L. Meinel, R. Fajardo, S. Hofmann, R. Langer, J. Chen, B. Snyder, G. Vunjak-Novakovic, D. Kaplan, Silk implants for the healing of critical size bone defects, *Bone* 37 (5) (2005) 688-98.
16. M.R. Tarla, F.S. Ramalho, L.N. Ramalho, E.S.T. Castro, D.F. Brandao, J. Ferreira, E.S.O. Castro, S. Zucoloto, A molecular view of liver regeneration, *Acta Cir Bras* 21 (2006) 58-62.
17. D.M. Bissell, Hepatic fibrosis as wound repair: a progress report, *J Gastroenterol* 33 (2) (1998) 295-302.
18. N. Sykaras, L.A. Opperman, Bone morphogenetic proteins (BMPs): how do they function and what can they offer the clinician? *J Oral Sci* 45 (2) (2003) 57-73.
19. S. Mohan, D.J. Baylink, Bone growth factors, *Clin Orthop Relat Res* (263) (1991) 30-48.
20. V. Luginbuehl, L. Meinel, H.P. Merkle, B. Gander, Localized delivery of growth factors for bone repair, *Eur J Pharm Biopharm* 58 (2) (2004) 197-208.
21. D. Kaigler, J.A. Cirelli, W.V. Giannobile, Growth factor delivery for oral and periodontal tissue engineering, *Expert Opin Drug Deliv* 3 (5) (2006) 647-62.
22. C.A. Kirker-Head, Potential applications and delivery strategies for bone morphogenetic proteins, *Adv Drug Deliv Rev* 43 (1) (2000) 65-92.
23. S.J. Lee, Cytokine delivery and tissue engineering, *Yonsei Med J* 41 (6) (2000) 704-19.
24. J.R. Lieberman, A. Daluiski, T.A. Einhorn, The role of growth factors in the repair of bone. Biology and clinical applications, *J Bone Joint Surg Am* 84-A (6) (2002) 1032-44.
25. H. Seeherman, J. Wozney, R. Li, Bone morphogenetic protein delivery systems, *Spine* 27 (16 Suppl 1) (2002) S16-23.
26. H. Seeherman, J.M. Wozney, Delivery of bone morphogenetic proteins for orthopedic tissue regeneration, *Cytokine Growth Factor Rev* 16 (3) (2005) 329-45.

27. Y. Tabata, Tissue regeneration based on growth factor release, *Tissue Eng* 9 (Suppl 1) (2003) S5-15.
28. M.C. Peters, B.C. Isenberg, J.A. Rowley, D.J. Mooney, Release from alginate enhances the biological activity of vascular endothelial growth factor, *J Biomater Sci Polym Ed* 9 (12) (1998) 1267-78.
29. R. Pawar, A. Ben-Ari, A.J. Domb, Protein and peptide parenteral controlled delivery, *Expert Opin Biol Ther* 4 (8) (2004) 1203-12.
30. P. Bashkin, S. Doctrow, M. Klagsbrun, C.M. Svahn, J. Folkman, I. Vlodavsky, Basic fibroblast growth factor binds to subendothelial extracellular matrix and is released by heparitinase and heparin-like molecules, *Biochemistry* 28 (4) (1989) 1737-43.
31. R. Ishai-Michaeli, A. Eldor, I. Vlodavsky, Heparanase activity expressed by platelets, neutrophils, and lymphoma cells releases active fibroblast growth factor from extracellular matrix, *Cell Regul* 1 (11) (1990) 833-42.
32. B. Han, Z. Yang, M. Nimni, Effects of moisture and temperature on the osteoinductivity of demineralized bone matrix, *J Orthop Res* 23 (4) (2005) 855-61.
33. I. Vlodavsky, G. Korner, R. Ishai-Michaeli, P. Bashkin, R. Bar-Shavit, Z. Fuks, Extracellular matrix-resident growth factors and enzymes: possible involvement in tumor metastasis and angiogenesis, *Cancer Metastasis Rev* 9 (3) (1990) 203-26.
34. E. Schonherr, H.J. Hausser, Extracellular matrix and cytokines: a functional unit, *Dev Immunol* 7 (2-4) (2000) 89-101.
35. I. Vlodavsky, R. Bar-Shavit, R. Ishai-Michaeli, P. Bashkin, Z. Fuks, Extracellular sequestration and release of fibroblast growth factor: a regulatory mechanism? *Trends Biochem Sci* 16 (7) (1991) 268-71.
36. T. Takada, T. Katagiri, M. Ifuku, N. Morimura, M. Kobayashi, K. Hasegawa, A. Ogamo, R. Kamijo, Sulfated polysaccharides enhance the biological activities of bone morphogenetic proteins, *J Biol Chem* 278 (44) (2003) 43229-35.
37. E. Zcharia, D. Philp, E. Edovitsky, H. Aingorn, S. Metzger, H.K. Kleinman, I. Vlodavsky, M. Elkin, Heparanase regulates murine hair growth, *Am J Pathol* 166 (4) (2005) 999-1008.
38. M.G. Kinsella, C. Irvin, M.A. Reidy, T.N. Wight, Removal of heparan sulfate by heparinase treatment inhibits FGF-2-dependent smooth muscle cell proliferation in injured rat carotid arteries, *Atherosclerosis* 175 (1) (2004) 51-7.

39. S.M. Smith, L.A. West, P. Govindraj, X. Zhang, D.M. Ornitz, J.R. Hassell, Heparan and chondroitin sulfate on growth plate perlecan mediate binding and delivery of FGF-2 to FGF receptors, *Matrix Biol* 26(3) (2007) 175-84.
40. T.L. Vincent, C.J. McLean, L.E. Full, D. Peston, J. Saklatvala, FGF-2 is bound to perlecan in the pericellular matrix of articular cartilage, where it acts as a chondrocyte mechanotransducer, *Osteoarthritis Cartilage* 15 (7) (2007) 752-63.
41. D.Q. Wu, M.K. Kan, G.H. Sato, T. Okamoto, J.D. Sato, Characterization and molecular cloning of a putative binding protein for heparin-binding growth factors, *J Biol Chem* 266 (25) (1991) 16778-85.
42. B. Xie, E. Tassi, M.R. Swift, K. McDonnell, E.T. Bowden, S. Wang, Y. Ueda, Y. Tomita, A.T. Riegel, A. Wellstein, Identification of the fibroblast growth factor (FGF)-interacting domain in a secreted FGF-binding protein by phage display, *J Biol Chem* 281 (2) (2006) 1137-44.
43. A. Kanematsu, S. Yamamoto, M. Ozeki, T. Noguchi, I. Kanatani, O. Ogawa, Y. Tabata, Collagenous matrices as release carriers of exogenous growth factors, *Biomaterials* 25 (18) (2004) 4513-20.
44. A. Kanematsu, A. Marui, S. Yamamoto, M. Ozeki, Y. Hirano, M. Yamamoto, O. Ogawa, M. Komeda, Y. Tabata, Type I collagen can function as a reservoir of basic fibroblast growth factor, *J Control Release* 99 (2) (2004) 281-92.
45. A. Kanematsu, S. Yamamoto, T. Noguchi, M. Ozeki, Y. Tabata, O. Ogawa, Bladder regeneration by bladder acellular matrix combined with sustained release of exogenous growth factor, *J Urol* 170 (4 Pt 2) (2003) 1633-8.
46. J.W. Weisel, Fibrinogen and fibrin, *Adv Protein Chem* 70 (2005) 247-99.
47. T.F. Zioncheck, L. Richardson, J. Liu, L. Chang, K.L. King, G.L. Bennett, P. Fugedi, S.M. Chamow, R.H. Schwall, R.J. Stack, Sulfated oligosaccharides promote hepatocyte growth factor association and govern its mitogenic activity, *J Biol Chem* 270 (28) (1995) 16871-8.
48. M. Maccarana, B. Casu, U. Lindahl, Minimal sequence in heparin/heparan sulfate required for binding of basic fibroblast growth factor, *J Biol Chem* 268 (32) (1993) 23898-905.
49. M. Lyon, J.A. Deakin, K. Mizuno, T. Nakamura, J.T. Gallagher, Interaction of hepatocyte growth factor with heparan sulfate. Elucidation of the major heparan sulfate structural determinants, *J Biol Chem* 269 (15) (1994) 11216-23.

50. A.L. Sieron, N. Louneva, A. Fertala, Site-specific interaction of bone morphogenetic protein 2 with procollagen II, *Cytokine* 18 (4) (2002) 214-21.
51. Y. Zhu, A. Oganessian, D.R. Keene, L.J. Sandell, Type IIA procollagen containing the cysteine-rich amino propeptide is deposited in the extracellular matrix of prechondrogenic tissue and binds to TGF-beta1 and BMP-2, *J Cell Biol* 144 (5) (1999) 1069-80.
52. W. Yang, R.R. Gomes, A.J. Brown, A.R. Burdett, M. Alicknavitch, M.C. Farach-Carson, D.D. Carson, Chondrogenic differentiation on perlecan domain I, collagen II, and bone morphogenetic protein-2-based matrices, *Tissue Eng* 12 (7) (2006) 2009-24.
53. V.M. Paralkar, B.S. Weeks, Y.M. Yu, H.K. Kleinman, A.H. Reddi, Recombinant human bone morphogenetic protein 2B stimulates PC12 cell differentiation: potentiation and binding to type IV collagen, *J Cell Biol* 119 (6) (1992) 1721-8.
54. A.H. Reddi, Morphogenetic messages are in the extracellular matrix: biotechnology from bench to bedside, *Biochem Soc Trans* 28 (4) (2000) 345-9.
55. A.L. Goerges, M.A. Nugent, pH regulates vascular endothelial growth factor binding to fibronectin: a mechanism for control of extracellular matrix storage and release, *J Biol Chem* 279 (3) (2004) 2307-15.
56. J.P. Annes, J.S. Munger, D.B. Rifkin, Making sense of latent TGFbeta activation, *J Cell Sci* 116 (Pt 2) (2003) 217-24.
57. G. Ge, D.S. Greenspan, BMP1 controls TGFbeta1 activation via cleavage of latent TGFbeta-binding protein, *J Cell Biol* 175 (1) (2006) 111-20.
58. S.L. Dallas, P. Sivakumar, C.J. Jones, Q. Chen, D.M. Peters, D.F. Mosher, M.J. Humphries, C.M. Kielty, Fibronectin regulates latent transforming growth factor-beta (TGF beta) by controlling matrix assembly of latent TGF beta-binding protein-1, *J Biol Chem* 280 (19) (2005) 18871-80.
59. S.L. Dallas, J.L. Rosser, G.R. Mundy, L.F. Bonewald, Proteolysis of latent transforming growth factor-beta (TGF-beta)-binding protein-1 by osteoclasts. A cellular mechanism for release of TGF-beta from bone matrix, *J Biol Chem* 277 (24) (2002) 21352-60.
60. K.E. Gregory, R.N. Ono, N.L. Charbonneau, C.L. Kuo, D.R. Keene, H.P. Bachinger, L.Y. Sakai, The prodomain of BMP-7 targets the BMP-7 complex to the extracellular matrix, *J Biol Chem* 280 (30) (2005) 27970-80.

61. D. Zhang, C.M. Ferguson, R.J. O'Keefe, J.E. Puzas, R.N. Rosier, P.R. Reynolds, A role for the BMP antagonist chordin in endochondral ossification, *J Bone Miner Res* 17 (2) (2002) 293-300.
62. D.R. Clemmons, Role of insulin-like growth factor binding proteins in controlling IGF actions, *Mol Cell Endocrinol* 140 (1-2) (1998) 19-24.
63. J. Palka, E. Banikowski, S. Jaworski, An accumulation of IGF-I and IGF-binding proteins in human umbilical cord, *Mol Cell Biochem* 206 (1-2) (2000) 133-9.
64. E. Bankowski, J. Palka, S. Jaworski, Pre-eclampsia-induced alterations in IGF-I of human umbilical cord, *Eur J Clin Invest* 30 (5) (2000) 389-96.
65. T. Arai, A. Arai, W.H. Busby, Jr., D.R. Clemmons, Glycosaminoglycans inhibit degradation of insulin-like growth factor-binding protein-5, *Endocrinology* 135 (6) (1994) 2358-63.
66. Z. Kuang, S. Yao, D.W. Keizer, C.C. Wang, L.A. Bach, B.E. Forbes, J.C. Wallace, R.S. Norton, Structure, dynamics and heparin binding of the C-terminal domain of insulin-like growth factor-binding protein-2 (IGFBP-2), *J Mol Biol* 364 (4) (2006) 690-704.
67. M. Milne, J.M. Quail, C.J. Rosen, D.T. Baran, Insulin-like growth factor binding proteins in femoral and vertebral bone marrow stromal cells: expression and regulation by thyroid hormone and dexamethasone, *J Cell Biochem* 81 (2) (2001) 229-40.
68. C.A. Conover, S. Khosla, Role of extracellular matrix in insulin-like growth factor (IGF) binding protein-2 regulation of IGF-II action in normal human osteoblasts, *Growth Horm IGF Res* 13 (6) (2003) 328-35.
69. J.A. Martin, B.A. Miller, M.B. Scherb, L.A. Lembke, J.A. Buckwalter, Co-localization of insulin-like growth factor binding protein 3 and fibronectin in human articular cartilage, *Osteoarthritis Cartilage* 10 (7) (2002) 556-63.
70. T. Arai, A. Parker, W. Busby, Jr., D.R. Clemmons, Heparin, heparan sulfate, and dermatan sulfate regulate formation of the insulin-like growth factor-I and insulin-like growth factor-binding protein complexes, *J Biol Chem* 269 (32) (1994) 20388-93.
71. T.J. Nam, W.H. Busby, Jr., D.R. Clemmons, Human fibroblasts secrete a serine protease that cleaves insulin-like growth factor-binding protein-5, *Endocrinology* 135 (4) (1994) 1385-91.

72. Y. Yamaguchi, V.J. Hearing, S. Itami, K. Yoshikawa, I. Katayama, Mesenchymal-epithelial interactions in the skin: aiming for site-specific tissue regeneration, *J Dermatol Sci* 40 (1) (2005) 1-9.
73. R. Morin, D. Kaplan, B. Perez-Ramirez, Bone morphogenetic protein-2 binds as multilayers to a collagen delivery matrix: an equilibrium thermodynamic analysis, *Biomacromolecules* 7 (1) (2006) 131-8.
74. P. Locci, L. Marinucci, C. Lilli, D. Martinese, E. Becchetti, Transforming growth factor beta 1-hyaluronic acid interaction, *Cell Tissue Res* 281 (2) (1995) 317-24.
75. M.K. Chourasia, S.K. Jain, Polysaccharides for colon targeted drug delivery, *Drug Deliv* 11 (2) (2004) 129-48.
76. I. Bjork, U. Lindahl, Mechanism of the anticoagulant action of heparin, *Mol Cell Biochem* 48 (3) (1982) 161-82.
77. R.J. Linhardt, N.S. Gunay, Production and chemical processing of low molecular weight heparins, *Semin Thromb Hemost* 25 (Suppl 3) (1999) 5-16.
78. C. DeBlois, M.F. Cote, C.J. Doillon, Heparin-fibroblast growth factor-fibrin complex: in vitro and in vivo applications to collagen-based materials, *Biomaterials* 15 (9) (1994) 665-72.
79. S.E. Sakiyama-Elbert, J.A. Hubbell, Development of fibrin derivatives for controlled release of heparin-binding growth factors, *J Control Release* 65 (3) (2000) 389-402.
80. P.O. Zamora, R. Tsang, L.A. Pena, S. Osaki, P. Som, Local delivery of basic fibroblast growth factor (bFGF) using adsorbed silyl-heparin, benzyl-bis(dimethylsilylmethyl)oxycarbamoyl-heparin, *Bioconjug Chem* 13 (5) (2002) 920-6.
81. G.C. Steffens, C. Yao, P. Prevel, M. Markowicz, P. Schenck, E.M. Noah, N. Pallua, Modulation of angiogenic potential of collagen matrices by covalent incorporation of heparin and loading with vascular endothelial growth factor, *Tissue Eng* 10 (9-10) (2004) 1502-9.
82. C.L. Casper, N. Yamaguchi, K.L. Kiick, J.F. Rabolt, Functionalizing electrospun fibers with biologically relevant macromolecules, *Biomacromolecules* 6 (4) (2005) 1998-2007.
83. D.S. Benoit, K.S. Anseth, Heparin functionalized PEG gels that modulate protein adsorption for hMSC adhesion and differentiation, *Acta Biomater* 1 (4) (2005) 461-70.

84. A.C. Lee, V.M. Yu, J.B. Lowe, 3rd, M.J. Brenner, D.A. Hunter, S.E. Mackinnon, S.E. Sakiyama-Elbert, Controlled release of nerve growth factor enhances sciatic nerve regeneration, *Exp Neurol* 184 (1) (2003) 295-303.
85. S.E. Sakiyama-Elbert, J.A. Hubbell, Controlled release of nerve growth factor from a heparin-containing fibrin-based cell ingrowth matrix, *J Control Release* 69 (1) (2000) 149-58.
86. H. Saari, Y.T. Konttinen, C. Friman, T. Sorsa, Differential effects of reactive oxygen species on native synovial fluid and purified human umbilical cord hyaluronate, *Inflammation* 17 (4) (1993) 403-15.
87. M. Paulsson, M. Morgelin, H. Wiedemann, M. Beardmore-Gray, D. Dunham, T. Hardingham, D. Heinegard, R. Timpl, J. Engel, Extended and globular protein domains in cartilage proteoglycans, *Biochem J* 245 (3) (1987) 763-72.
88. K.P. Vercruyse, G.D. Prestwich, Hyaluronate derivatives in drug delivery, *Crit Rev Ther Drug Carrier Syst* 15 (5) (1998) 513-55.
89. K.Y. Suh, J.M. Yang, A. Khademhosseini, D. Berry, T.N. Tran, H. Park, R. Langer, Characterization of chemisorbed hyaluronic acid directly immobilized on solid substrates, *J Biomed Mater Res B Appl Biomater* 72 (2) (2005) 292-8.
90. S.K. Hahn, S. Jelacic, R.V. Maier, P.S. Stayton, A.S. Hoffman, Anti-inflammatory drug delivery from hyaluronic acid hydrogels, *J Biomater Sci Polym Ed* 15 (9) (2004) 1111-9.
91. M.G. Cascone, B. Sim, S. Downes, Blends of synthetic and natural polymers as drug delivery systems for growth hormone, *Biomaterials* 16 (7) (1995) 569-74.
92. H.D. Kim, R.F. Valentini, Retention and activity of BMP-2 in hyaluronic acid-based scaffolds in vitro, *J Biomed Mater Res* 59 (3) (2002) 573-84.
93. S.J. Kim, S.K. Hahn, M.J. Kim, D.H. Kim, Y.P. Lee, Development of a novel sustained release formulation of recombinant human growth hormone using sodium hyaluronate microparticles, *J Control Release* 104 (2) (2005) 323-35.
94. T. Segura, P.H. Chung, L.D. Shea, DNA delivery from hyaluronic acid-collagen hydrogels via a substrate-mediated approach, *Biomaterials* 26 (13) (2005) 1575-84.
95. A. Jork, F. Thurmer, H. Cramer, G. Zimmermann, P. Gessner, K. Hamel, G. Hofmann, B. Kuttler, H.J. Hahn, O. Josimovic-Alasevic, K.G. Fritsch, U. Zimmermann, Biocompatible alginate from freshly collected *Laminaria pallida* for implantation, *Appl Microbiol Biotechnol* 53 (2) (2000) 224-9.

96. J.L. Drury, R.G. Dennis, D.J. Mooney, The tensile properties of alginate hydrogels, *Biomaterials* 25 (16) (2004) 3187-99.
97. H.H. Tonnesen, J. Karlsen, Alginate in drug delivery systems, *Drug Dev Ind Pharm* 28 (6) (2002) 621-30.
98. F. Gu, B. Amsden, R. Neufeld, Sustained delivery of vascular endothelial growth factor with alginate beads, *J Control Release* 96 (3) (2004) 463-72.
99. K.Y. Lee, M.C. Peters, D.J. Mooney, Comparison of vascular endothelial growth factor and basic fibroblast growth factor on angiogenesis in SCID mice, *J Control Release* 87 (1-3) (2003) 49-56.
100. K.Y. Lee, M.C. Peters, K.W. Anderson, D.J. Mooney, Controlled growth factor release from synthetic extracellular matrices, *Nature* 408 (6815) (2000) 998-1000.
101. K.W. Lee, J.J. Yoon, J.H. Lee, S.Y. Kim, H.J. Jung, S.J. Kim, J.W. Joh, H.H. Lee, D.S. Lee, S.K. Lee, Sustained release of vascular endothelial growth factor from calcium-induced alginate hydrogels reinforced by heparin and chitosan, *Transplant Proc* 36 (8) (2004) 2464-5.
102. C.A. Simmons, E. Alsberg, S. Hsiong, W.J. Kim, D.J. Mooney, Dual growth factor delivery and controlled scaffold degradation enhance in vivo bone formation by transplanted bone marrow stromal cells, *Bone* 35 (2) (2004) 562-9.
103. N.G. Schipper, K.M. Varum, P. Artursson, Chitosans as absorption enhancers for poorly absorbable drugs. 1: Influence of molecular weight and degree of acetylation on drug transport across human intestinal epithelial (Caco-2) cells, *Pharm Res* 13 (11) (1996) 1686-92.
104. M. Rinaudo, M. Milas, P. Le Dung, Characterization of chitosan. Influence of ionic strength and degree of acetylation on chain expansion, *Int J Biol Macromol* 15 (5) (1993) 281-5.
105. D. Aggarwal, H.W. Matthew, Branched chitosans: Effects of branching parameters on rheological and mechanical properties, *J Biomed Mater Res A* 2007)
106. R. Jayakumar, N. Nwe, S. Tokura, H. Tamura, Sulfated chitin and chitosan as novel biomaterials, *Int J Biol Macromol* 40 (3) (2007) 175-81
107. Y.M. Lee, Y.J. Park, S.J. Lee, Y. Ku, S.B. Han, P.R. Klokkevold, C.P. Chung, The bone regenerative effect of platelet-derived growth factor-BB delivered with a chitosan/tricalcium phosphate sponge carrier, *J Periodontol* 71 (3) (2000) 418-24.
108. Y.J. Park, K.H. Kim, J.Y. Lee, Y. Ku, S.J. Lee, B.M. Min, C.P. Chung, Immobilization of bone morphogenetic protein-2 on a nanofibrous chitosan

- membrane for enhanced guided bone regeneration, *Biotechnol Appl Biochem* 43 (Pt 1) (2006) 17-24.
109. C.Y. Hsieh, H.J. Hsieh, H.C. Liu, D.M. Wang, L.T. Hou, Fabrication and release behavior of a novel freeze-gelled chitosan/gamma-PGA scaffold as a carrier for rhBMP-2, *Dent Mater* 22 (7) (2006) 622-9.
110. J.E. Lee, K.E. Kim, I.C. Kwon, H.J. Ahn, S.H. Lee, H. Cho, H.J. Kim, S.C. Seong, M.C. Lee, Effects of the controlled-released TGF-beta 1 from chitosan microspheres on chondrocytes cultured in a collagen/chitosan/glycosaminoglycan scaffold, *Biomaterials* 25 (18) (2004) 4163-73.
111. M. Fujita, M. Ishihara, Y. Morimoto, M. Simizu, Y. Saito, H. Yura, T. Matsui, B. Takase, H. Hattori, Y. Kanatani, M. Kikuchi, T. Maehara, Efficacy of photocrosslinkable chitosan hydrogel containing fibroblast growth factor-2 in a rabbit model of chronic myocardial infarction, *J Surg Res* 126 (1) (2005) 27-33.
112. K. Mizuno, K. Yamamura, K. Yano, T. Osada, S. Saeki, N. Takimoto, T. Sakurai, Y. Nimura, Effect of chitosan film containing basic fibroblast growth factor on wound healing in genetically diabetic mice, *J Biomed Mater Res A* 64 (1) (2003) 177-81.
113. M. Ishihara, M. Fujita, K. Obara, H. Hattori, S. Nakamura, M. Nambu, T. Kiyosawa, Y. Kanatani, B. Takase, M. Kikuchi, T. Maehara, Controlled releases of FGF-2 and paclitaxel from chitosan hydrogels and their subsequent effects on wound repair, angiogenesis, and tumor growth, *Curr Drug Deliv* 3 (4) (2006) 351-8.
114. D.J. Hulmes, A. Miller, D.A. Parry, K.A. Piez, J. Woodhead-Galloway, Analysis of the primary structure of collagen for the origins of molecular packing, *J Mol Biol* 79 (1) (1973) 137-48.
115. D.L. Helseth, Jr., A. Veis, Collagen self-assembly in vitro. Differentiating specific telopeptide-dependent interactions using selective enzyme modification and the addition of free amino telopeptide, *J Biol Chem* 256 (14) (1981) 7118-28.
116. S. Itoh, K. Takakuda, S. Kawabata, Y. Aso, K. Kasai, H. Itoh, K. Shinomiya, Evaluation of cross-linking procedures of collagen tubes used in peripheral nerve repair, *Biomaterials* 23 (23) (2002) 4475-81.
117. F. Everaerts, M. Torrianni, M. Hendriks, J. Feijen, Quantification of carboxyl groups in carbodiimide cross-linked collagen sponges, *J Biomed Mater Res A* 83 (4) (2007) 1176-83.
118. B. Hafemann, K. Ghofrani, H.G. Gattner, H. Stieve, N. Pallua, Cross-linking by 1-ethyl-3-(3-dimethylaminopropyl)-carbodiimide (EDC) of a collagen/elastin

- membrane meant to be used as a dermal substitute: effects on physical, biochemical and biological features in vitro, *J Mater Sci Mater Med* 12 (5) (2001) 437-46.
119. F.A. Radu, M. Bause, P. Knabner, G.W. Lee, W.C. Friess, Modeling of drug release from collagen matrices, *J Pharm Sci* 91 (4) (2002) 964-72.
 120. M. Geiger, R.H. Li, W. Friess, Collagen sponges for bone regeneration with rhBMP-2, *Adv Drug Deliv Rev* 55 (12) (2003) 1613-29.
 121. G.E. Friedlaender, C.R. Perry, J.D. Cole, S.D. Cook, G. Cierny, G.F. Muschler, G.A. Zych, J.H. Calhoun, A.J. LaForte, S. Yin, Osteogenic protein-1 (bone morphogenetic protein-7) in the treatment of tibial nonunions, *J Bone Joint Surg Am* 83-A Suppl 1 (Pt 2) (2001) 151-8.
 122. C. Arnander, A. Westermarck, R. Veltheim, A.C. Docherty-Skog, J. Hilborn, T. Engstrand, Three-dimensional technology and bone morphogenetic protein in frontal bone reconstruction, *J Craniofac Surg* 17 (2) (2006) 275-9.
 123. R.S. Sellers, R. Zhang, S.S. Glasson, H.D. Kim, D. Peluso, D.A. D'Augusta, K. Beckwith, E.A. Morris, Repair of articular cartilage defects one year after treatment with recombinant human bone morphogenetic protein-2 (rhBMP-2), *J Bone Joint Surg Am* 82 (2) (2000) 151-60.
 124. N. Okafuji, T. Shimizu, T. Watanabe, A. Kimura, S. Kurihara, K. Furusawa, H. Hasegawa, T. Kawakami, Tissue reaction to poly (lactic-co-glycolic acid) copolymer membrane in rhBMP used rabbit experimental mandibular reconstruction, *Eur J Med Res* 11 (9) (2006) 394-6.
 125. J.M. McPherson, The utility of collagen-based vehicles in delivery of growth factors for hard and soft tissue wound repair, *Clin Mater* 9 (3-4) (1992) 225-34.
 126. A. Sano, M. Maeda, S. Nagahara, T. Ochiya, K. Honma, H. Itoh, T. Miyata, K. Fujioka, Atelocollagen for protein and gene delivery, *Adv Drug Deliv Rev* 55 (12) (2003) 1651-77.
 127. H. Li, D. Wang, S. Li, B. Liu, L. Gao, Sustained release of BSA from a novel drug delivery matrix -- bullfrog skin collagen film, *Macromol Biosci* 4 (4) (2004) 454-7.
 128. S. Young, M. Wong, Y. Tabata, A.G. Mikos, Gelatin as a delivery vehicle for the controlled release of bioactive molecules, *J Control Release* 109 (1-3) (2005) 256-74.
 129. M. Yamamoto, Y. Takahashi, Y. Tabata, Controlled release by biodegradable hydrogels enhances the ectopic bone formation of bone morphogenetic protein, *Biomaterials* 24 (24) (2003) 4375-83.

130. M.A. Vandelli, M. Romagnoli, A. Monti, M. Gozzi, P. Guerra, F. Rivasi, F. Forni, Microwave-treated gelatin microspheres as drug delivery system, *J Control Release* 96 (1) (2004) 67-84.
131. F. Chen, Z. Wu, Q. Wang, H. Wu, Y. Zhang, X. Nie, Y. Jin, Preparation and biological characteristics of recombinant human bone morphogenetic protein-2-loaded dextran-co-gelatin hydrogel microspheres, *in vitro* and *in vivo* studies, *Pharmacology* 75 (3) (2005) 133-44.
132. A.T. Raiche, D.A. Puleo, *In vitro* effects of combined and sequential delivery of two bone growth factors, *Biomaterials* 25 (4) (2004) 677-85.
133. M.F. Cote, G. Laroche, E. Gagnon, P. Chevallier, C.J. Doillon, Denatured collagen as support for a FGF-2 delivery system: physicochemical characterizations and *in vitro* release kinetics and bioactivity, *Biomaterials* 25 (17) (2004) 3761-72.
134. J.D. Ferry, The Mechanism of Polymerization of Fibrinogen, *Proc Natl Acad Sci USA* 38 (7) (1952) 566-9.
135. W.D. Spotnitz, R. Prabhu, Fibrin sealant tissue adhesive--review and update, *J Long Term Eff Med Implants* 15 (3) (2005) 245-70.
136. S.H. Park, S.R. Park, S.I. Chung, K.S. Pai, B.H. Min, Tissue-engineered cartilage using fibrin/hyaluronan composite gel and its *in vivo* implantation, *Artif Organs* 29 (10) (2005) 838-45.
137. P. Giannoni, E.B. Hunziker, Release kinetics of transforming growth factor-beta1 from fibrin clots, *Biotechnol Bioeng* 83 (1) (2003) 121-3.
138. A.S. Pandit, D.J. Wilson, D.S. Feldman, Fibrin scaffold as an effective vehicle for the delivery of acidic fibroblast growth factor (FGF-1), *J Biomater Appl* 14 (3) (2000) 229-42.
139. P.G. Campbell, E.D. Miller, G.W. Fisher, L.M. Walker, L.E. Weiss, Engineered spatial patterns of FGF-2 immobilized on fibrin direct cell organization, *Biomaterials* 26 (33) (2005) 6762-70.
140. S. Ikeda, K. Nishinari, Intermolecular forces in bovine serum albumin solutions exhibiting solidlike mechanical behaviors, *Biomacromolecules* 1 (4) (2000) 757-63.
141. E.G. Fine, I. Decosterd, M. Papaloizos, A.D. Zurn, P. Aebischer, GDNF and NGF released by synthetic guidance channels support sciatic nerve regeneration across a long gap, *Eur J Neurosci* 15 (4) (2002) 589-601.

142. T.A. Hadlock, T. Sheahan, M.L. Cheney, J.P. Vacanti, C.A. Sundback, Biologic activity of nerve growth factor slowly released from microspheres, *J Reconstr Microsurg* 19 (3) (2003) 179-84; discussion 185-6.
143. L. Meinel, O.E. Illi, J. Zapf, M. Malfanti, H. Peter Merkle, B. Gander, Stabilizing insulin-like growth factor-I in poly(D,L-lactide-co-glycolide) microspheres, *J Control Release* 70 (1-2) (2001) 193-202.
144. L. Donato, C. Garnier, B. Novales, S. Durand, J.L. Dublier, Heat-induced gelation of bovine serum albumin/low-methoxyl pectin systems and the effect of calcium ions, *Biomacromolecules* 6 (1) (2005) 374-85.
145. D.P. Mikhailidis, A.M. Mikhailidis, P. Dandona, Effect of human plasma proteins on stabilisation of platelet anti-aggregatory activity of prostacyclin, *Ann Clin Biochem* 19 (Pt 4) (1982) 241-4.
146. N. El Kadi, N. Taulier, J.Y. Le Huerou, M. Gindre, W. Urbach, I. Nwigwe, P.C. Kahn, M. Waks, Unfolding and refolding of bovine serum albumin at acid pH: ultrasound and structural studies, *Biophys J* 91 (9) (2006) 3397-404.
147. P.M. Cunniff, S.A. Fossey, M.A. Auerbach, J.W. Song, D.L. Kaplan, W. Adams, R.K. Eby, D. Mahoney, D. Deborah, D.L. Vezie, Mechanical and thermal properties of Dragline Silk from the Spider *Nephila cavipes*, *Polymers for Advanced Technologies* 5 (1994) 401-410.
148. F. Vollrath, P. Barth, A. Basedow, W. Engstrom, H. List, Local tolerance to spider silks and protein polymers in vivo, *In Vivo* 16 (4) (2002) 229-34.
149. S. Inoue, K. Tanaka, F. Arisaka, S. Kimura, K. Ohtomo, S. Mizuno, Silk fibroin of *Bombyx mori* is secreted, assembling a high molecular mass elementary unit consisting of H-chain, L-chain, and P25, with a 6:6:1 molar ratio, *J Biol Chem* 275 (51) (2000) 40517-28.
150. K. Mita, S. Ichimura, T.C. James, Highly repetitive structure and its organization of the silk fibroin gene, *J Mol Evol* 38 (6) (1994) 583-92.
151. G.H. Altman, F. Diaz, C. Jakuba, T. Calabro, R.L. Horan, J. Chen, H. Lu, J. Richmond, D.L. Kaplan, Silk-based biomaterials, *Biomaterials* 24 (3) (2003) 401-16.
152. F. Lange, Künstliche Bänder aus Seide., *Münch Med Wochenschr* (17) (1907) 834-836.
153. L. Meinel, S. Hofmann, V. Karageorgiou, C. Kirker-Head, J. McCool, G. Gronowicz, L. Zichner, R. Langer, G. Vunjak-Novakovic, D.L. Kaplan, The inflammatory responses to silk films in vitro and in vivo, *Biomaterials* 26 (2) (2005) 147-55.

154. B. Panilaitis, G.H. Altman, J. Chen, H.J. Jin, V. Karageorgiou, D.L. Kaplan, Macrophage responses to silk, *Biomaterials* 24 (18) (2003) 3079-85.
155. L. Uebersax, H. Hagemuller, S. Hofmann, E. Gruenblatt, R. Muller, G. Vunjaknovakovic, D.L. Kaplan, H.P. Merkle, L. Meinel, Effect of Scaffold Design on Bone Morphology in Vitro, *Tissue Eng* 12 (12) (2006) 3417-29.
156. R. Nazarov, H.J. Jin, D.L. Kaplan, Porous 3-D scaffolds from regenerated silk fibroin, *Biomacromolecules* 5 (3) (2004) 718-26.
157. H.J. Jin, S.V. Fridrikh, G.C. Rutledge, D.L. Kaplan, Electrospinning *Bombyx mori* silk with poly(ethylene oxide), *Biomacromolecules* 3 (6) (2002) 1233-9.
158. Y. Wang, U.J. Kim, D.J. Blasioli, H.J. Kim, D.L. Kaplan, In vitro cartilage tissue engineering with 3D porous aqueous-derived silk scaffolds and mesenchymal stem cells, *Biomaterials* 26 (34) (2005) 7082-94.
159. G.H. Altman, R.L. Horan, H.H. Lu, J. Moreau, I. Martin, J.C. Richmond, D.L. Kaplan, Silk matrix for tissue engineered anterior cruciate ligaments, *Biomaterials* 23 (20) (2002) 4131-41.
160. L. Meinel, V. Karageorgiou, S. Hofmann, R. Fajardo, B. Snyder, C. Li, L. Zichner, R. Langer, G. Vunjak-Novakovic, D.L. Kaplan, Engineering bone-like tissue in vitro using human bone marrow stem cells and silk scaffolds, *J Biomed Mater Res A* 71 (1) (2004) 25-34.
161. L. Meinel, V. Karageorgiou, R. Fajardo, B. Snyder, V. Shinde-Patil, L. Zichner, D. Kaplan, R. Langer, G. Vunjak-Novakovic, Bone tissue engineering using human mesenchymal stem cells: effects of scaffold material and medium flow, *Ann Biomed Eng* 32 (1) (2004) 112-22.
162. S. Hofmann, H. Hagemuller, A.M. Koch, R. Muller, G. Vunjak-Novakovic, D.L. Kaplan, H.P. Merkle, L. Meinel, Control of in vitro tissue-engineered bone-like structures using human mesenchymal stem cells and porous silk scaffolds, *Biomaterials* 28 (6) (2007) 1152-62.
163. L. Uebersax, D.E. Fedele, C. Schumacher, D.L. Kaplan, H.P. Merkle, D. Boison, L. Meinel, The support of adenosine release from adenosine kinase deficient ES cells by silk substrates, *Biomaterials* 27 (26) (2006) 4599-607.
164. R.L. Horan, K. Antle, A.L. Collette, Y. Wang, J. Huang, J.E. Moreau, V. Volloch, D.L. Kaplan, G.H. Altman, In vitro degradation of silk fibroin, *Biomaterials* 26 (17) (2005) 3385-93.

165. L. Meinel, S. Hofmann, V. Karageorgiou, L. Zichner, R. Langer, D. Kaplan, G. Vunjak-Novakovic, Engineering cartilage-like tissue using human mesenchymal stem cells and silk protein scaffolds, *Biotechnol Bioeng* 88 (3) (2004) 379-91.
166. S. Sofia, M.B. McCarthy, G. Gronowicz, D.L. Kaplan, Functionalized silk-based biomaterials for bone formation, *J Biomed Mater Res* 54 (1) (2001) 139-48.
167. V. Karageorgiou, L. Meinel, S. Hofmann, A. Malhotra, V. Volloch, D. Kaplan, Bone morphogenetic protein-2 decorated silk fibroin films induce osteogenic differentiation of human bone marrow stromal cells, *J Biomed Mater Res A* 71 (3) (2004) 528-37.
168. V. Karageorgiou, M. Tomkins, R. Fajardo, L. Meinel, B. Snyder, K. Wade, J. Chen, G. Vunjak-Novakovic, D.L. Kaplan, Porous silk fibroin 3-D scaffolds for delivery of bone morphogenetic protein-2 in vitro and in vivo, *J Biomed Mater Res A* 78 (2) (2006) 324-34.
169. S. Hofmann, C.T. Wong Po Foo, F. Rossetti, M. Textor, G. Vunjak-Novakovic, D.L. Kaplan, H.P. Merkle, L. Meinel, Silk fibroin as an organic polymer for controlled drug delivery, *J Control Release* 111(1-2) (2006) 219-27
170. C. Li, C. Vepari, H.J. Jin, H.J. Kim, D.L. Kaplan, Electrospun silk-BMP-2 scaffolds for bone tissue engineering, *Biomaterials* 27 (16) (2006) 3115-24.
171. L. Uebersax, H.P. Merkle, L. Meinel, Insulin-like growth factor I releasing silk fibroin scaffolds induce chondrogenic differentiation of human mesenchymal stem cells, *J Control Release* 127 (1) (2008) 12-21.
172. L. Uebersax, M. Mattotti, M. Papaloizos, H.P. Merkle, B. Gander, L. Meinel, Silk fibroin matrices for the controlled release of nerve growth factor (NGF), *Biomaterials* 28 (30) (2007) 4449-60
173. X. Wang, E. Wenk, A. Matsumoto, L. Meinel, C. Li, D.L. Kaplan, Silk microspheres for encapsulation and controlled release, *J Control Release* 117 (3) (2007) 360-70.
174. P. Giusti, L. Lazzeri, S. De Petris, M. Palla, M.G. Cascone, Collagen-based new bioartificial polymeric materials, *Biomaterials* 15 (15) (1994) 1229-33.
175. M. Prabaharan, J.F. Mano, Stimuli-responsive hydrogels based on polysaccharides incorporated with thermo-responsive polymers as novel biomaterials, *Macromol Biosci* 6 (12) (2006) 991-1008.
176. X. Huang, T.L. Lowe, Biodegradable thermoresponsive hydrogels for aqueous encapsulation and controlled release of hydrophilic model drugs, *Biomacromolecules* 6 (4) (2005) 2131-9.

177. D.B. Werz, P.H. Seeberger, Carbohydrates as the next frontier in pharmaceutical research, *Chemistry* 11 (11) (2005) 3194-206.
178. C. Freeman, L. Liu, M.G. Banwell, K.J. Brown, A. Bezos, V. Ferro, C.R. Parish, Use of sulfated linked cyclitols as heparan sulfate mimetics to probe the heparin/heparan sulfate binding specificity of proteins, *J Biol Chem* 280 (10) (2005) 8842-9.
179. P. Jemth, E. Smeds, A.T. Do, H. Habuchi, K. Kimata, U. Lindahl, M. Kusche-Gullberg, Oligosaccharide library-based assessment of heparan sulfate 6-O-sulfotransferase substrate specificity, *J Biol Chem* 278 (27) (2003) 24371-6.
180. S. Ashikari-Hada, H. Habuchi, Y. Kariya, N. Itoh, A.H. Reddi, K. Kimata, Characterization of growth factor-binding structures in heparin/heparan sulfate using an octasaccharide library, *J Biol Chem* 279 (13) (2004) 12346-54.
181. J.L. de Paz, C. Noti, P.H. Seeberger, Microarrays of synthetic heparin oligosaccharides, *J Am Chem Soc* 128 (9) (2006) 2766-7.
182. T. Koide, Triple helical collagen-like peptides: engineering and applications in matrix biology, *Connect Tissue Res* 46 (3) (2005) 131-41.
183. D.N. Woolfson, M.G. Ryadnov, Peptide-based fibrous biomaterials: Some things old, new and borrowed, *Curr Opin Chem Biol* 10 (6) (2006) 559-67.
184. T.C. Holmes, S. de Lacalle, X. Su, G. Liu, A. Rich, S. Zhang, Extensive neurite outgrowth and active synapse formation on self-assembling peptide scaffolds, *Proc Natl Acad Sci U S A* 97 (12) (2000) 6728-33.
185. L. Gentilucci, A. Tolomelli, F. Squassabia, Peptides and peptidomimetics in medicine, surgery and biotechnology, *Curr Med Chem* 13 (20) (2006) 2449-66.
186. K.R. Sidman, W.D. Steber, A.D. Schwope, G.R. Schnaper, Controlled release of macromolecules and pharmaceuticals from synthetic polypeptides based on glutamic acid, *Biopolymers* 22 (1) (1983) 547-56.
187. S.L. Bourke, J. Kohn, Polymers derived from the amino acid L-tyrosine: polycarbonates, polyarylates and copolymers with poly(ethylene glycol), *Adv Drug Deliv Rev* 55 (4) (2003) 447-66.
188. D.M. Schachter, J. Kohn, A synthetic polymer matrix for the delayed or pulsatile release of water-soluble peptides, *J Control Release* 78 (1-3) (2002) 143-53.
189. H.D. Maynard, J.A. Hubbell, Discovery of a sulfated tetrapeptide that binds to vascular endothelial growth factor, *Acta Biomater* 1 (4) (2005) 451-9.

190. Z. Megeed, J. Cappello, H. Ghandehari, Genetically engineered silk-elastinlike protein polymers for controlled drug delivery, *Adv Drug Deliv Rev* 54 (8) (2002) 1075-91.
191. D.S. Hart, S.H. Gehrke, Thermally associating polypeptides designed for drug delivery produced by genetically engineered cells, *J Pharm Sci* 96 (3) (2006) 484-516.
192. D. Olsen, C. Yang, M. Bodo, R. Chang, S. Leigh, J. Baez, D. Carmichael, M. Perala, E.R. Hamalainen, M. Jarvinen, J. Polarek, Recombinant collagen and gelatin for drug delivery, *Adv Drug Deliv Rev* 55 (12) (2003) 1547-67.
193. M. Sutter, J. Siepmann, W.E. Hennink, W. Jiskoot, Recombinant gelatin hydrogels for the sustained release of proteins, *J Control Release* 119 (3) (2007) 301-12.
194. H. Heslot, Artificial fibrous proteins: a review, *Biochimie* 80 (1) (1998) 19-31.
195. C. Wong Po Foo, D.L. Kaplan, Genetic engineering of fibrous proteins: spider dragline silk and collagen, *Adv Drug Deliv Rev* 54 (8) (2002) 1131-43.
196. F.M. Wurm, Human therapeutic proteins from silkworms, *Nat Biotechnol* 21 (1) (2003) 34-5.
197. B. Griffiths, F.M. Wurm, Mammalian Cell Culture, *Encyclopedia of Physical Sciences and Technology* 9 (in: R.A Meyers (ed. 3)) (2002) 31-47.
198. M. Tomita, H. Munetsuna, T. Sato, T. Adachi, R. Hino, M. Hayashi, K. Shimizu, N. Nakamura, T. Tamura, K. Yoshizato, Transgenic silkworms produce recombinant human type III procollagen in cocoons, *Nat Biotechnol* 21 (1) (2003) 52-6.
199. T. Adachi, M. Tomita, K. Shimizu, S. Ogawa, K. Yoshizato, Generation of hybrid transgenic silkworms that express *Bombyx mori* prolyl-hydroxylase alpha-subunits and human collagens in posterior silk glands: Production of cocoons that contained collagens with hydroxylated proline residues, *J Biotechnol* 126 (2) (2006) 205-19.
200. H. Mori, M. Tsukada, New silk protein: modification of silk protein by gene engineering for production of biomaterials, *J Biotechnol* 74 (2) (2000) 95-103.
201. M. Yamamoto, M. Yamao, H. Nishiyama, S. Sugihara, S. Nagaoka, M. Tomita, K. Yoshizato, T. Tamura, H. Mori, New and highly efficient method for silkworm transgenesis using *Autographa californica* nucleopolyhedrovirus and piggyBac transposable elements, *Biotechnol Bioeng* 88 (7) (2004) 849-53.
202. M. Yang, C. Tanaka, K. Yamauchi, K. Ohgo, M. Kurokawa, T. Asakura, Silklike materials constructed from sequences of *Bombyx mori* silk fibroin, fibronectin, and elastin, *J Biomed Mater Res* 84(2) (2008) 353-63.

203. J. Scheller, U. Conrad, Plant-based material, protein and biodegradable plastic, *Curr Opin Plant Biol* 8 (2) (2005) 188-96.
204. J. Scheller, D. Henggeler, A. Viviani, U. Conrad, Purification of spider silk-elastin from transgenic plants and application for human chondrocyte proliferation, *Transgenic Res* 13 (1) (2004) 51-7.
205. M. Li, G. Tu, Z. Huang, X. Huang, [Study on the conditions of high density fermentation for the engineering bacterial strain with RGD spider silk protein gene], *Sheng Wu Yi Xue Gong Cheng Xue Za Zhi* 22 (6) (2005) 1206-9.
206. J. Yao, S. Yanagisawa, T. Asakura, Design, expression and characterization of collagen-like proteins based on the cell adhesive and crosslinking sequences derived from native collagens, *J Biochem (Tokyo)* 136 (5) (2004) 643-9.
207. J. Cappello, J. Crissman, M. Dorman, M. Mikolajczak, G. Textor, M. Marquet, F. Ferrari, Genetic engineering of structural protein polymers, *Biotechnol Prog* 6 (3) (1990) 198-202.
208. Z. Megeed, M. Haider, D. Li, B.W. O'Malley, Jr., J. Cappello, H. Ghandehari, In vitro and in vivo evaluation of recombinant silk-elastinlike hydrogels for cancer gene therapy, *J Control Release* 94 (2-3) (2004) 433-45.
209. M. Haider, V. Leung, F. Ferrari, J. Crissman, J. Powell, J. Cappello, H. Ghandehari, Molecular engineering of silk-elastinlike polymers for matrix-mediated gene delivery: biosynthesis and characterization, *Mol Pharm* 2 (2) (2005) 139-50.
210. M.E. Davis, P.C. Hsieh, T. Takahashi, Q. Song, S. Zhang, R.D. Kamm, A.J. Grodzinsky, P. Anversa, R.T. Lee, Local myocardial insulin-like growth factor 1 (IGF-1) delivery with biotinylated peptide nanofibers improves cell therapy for myocardial infarction, *Proc Natl Acad Sci U S A* 103 (21) (2006) 8155-60.
211. S. Patel, K. Kurpinski, R. Quigley, H. Gao, B.S. Hsiao, M.M. Poo, S. Li, Bioactive nanofibers: synergistic effects of nanotopography and chemical signaling on cell guidance, *Nano Lett* 7 (7) (2007) 2122-8.
212. D.J. Geer, D.D. Swartz, S.T. Andreadis, Biomimetic delivery of keratinocyte growth factor upon cellular demand for accelerated wound healing in vitro and in vivo, *Am J Pathol* 167 (6) (2005) 1575-86.
213. C.L. Casper, W. Yang, M.C. Farach-Carson, J.F. Rabolt, Coating Electrospun Collagen and Gelatin Fibers with Perlecan Domain I for Increased Growth Factor Binding, *Biomacromolecules* 8 (4) (2007) 1116-23.

214. S. Vessillier, G. Adams, Y. Chernajovsky, Latent cytokines: development of novel cleavage sites and kinetic analysis of their differential sensitivity to MMP-1 and MMP-3, *Protein Eng Des Sel* 17 (12) (2004) 829-35.
215. M. Ehrbar, A. Metters, P. Zammaretti, J.A. Hubbell, A.H. Zisch, Endothelial cell proliferation and progenitor maturation by fibrin-bound VEGF variants with differential susceptibilities to local cellular activity, *J Control Release* 101 (1-3) (2005) 93-109.
216. B. Chen, H. Lin, Y. Zhao, B. Wang, Y. Zhao, Y. Liu, Z. Liu, J. Dai, Activation of demineralized bone matrix by genetically engineered human bone morphogenetic protein-2 with a collagen binding domain derived from von Willebrand factor propolypeptide, *J Biomed Mater Res A* 80 (2) (2007) 428-34.
217. V.C. Yang, S.S. Naik, H. Song, A.A. Dombkowski, G. Crippen, J.F. Liang, Construction and characterization of a t-PA mutant for use in ATTEMPTS: a drug delivery system for achieving targeted thrombolysis, *J Control Release* 110 (1) (2005) 164-76.
218. Y.J. Park, J.F. Liang, H. Song, Y.T. Li, S. Naik, V.C. Yang, ATTEMPTS: a heparin/protamine-based triggered release system for the delivery of enzyme drugs without associated side-effects, *Adv Drug Deliv Rev* 55 (2) (2003) 251-65.
219. J.F. Liang, Y.J. Park, H. Song, Y.T. Li, V.C. Yang, ATTEMPTS: a heparin/protamine-based prodrug approach for delivery of thrombolytic drugs, *J Control Release* 72 (1-3) (2001) 145-56.
220. J.F. Liang, Y.T. Li, V.C. Yang, A novel approach for delivery of enzyme drugs: preliminary demonstration of feasibility and utility in vitro, *Int J Pharm* 202 (1-2) (2000) 11-20.
221. F. Ramirez, D.B. Rifkin, Cell signaling events: a view from the matrix, *Matrix Biol* 22 (2) (2003) 101-7.

CHAPTER II

Effect of scaffold design on bone morphology in vitro

*Lorenz Uebersax¹, Henri Hagenmüller^{1,2}, Sandra Hofmann¹, Emanuel Gruenblatt¹,
Ralph Müller², Gordana Vunjak-Novakovic^{3,4} David L. Kaplan⁵, H.P.Merkle¹
Lorenz Meinel^{1,4,5}*

¹*Institute of Pharmaceutical Sciences, ETH Zurich, Zurich, Switzerland*

²*Institute for Biomedical Engineering, University and ETH Zurich, Zurich, Switzerland*

³*Department of Biomedical Engineering, Columbia University, New York, NY*

⁴*Harvard-MIT Division of Health Sciences and Technology, Cambridge, MA*

⁵*Department for Biomedical Engineering, Tufts University, Medford, MA*

ABSTRACT

Silk fibroin (SF) is an important polymer for scaffold designs, forming biocompatible and mechanically robust biomaterials for bone, cartilage and ligament tissue engineering. In the present work, 3D biomaterial matrices were fabricated from SF with controlled pore diameter and pore interconnectivity, and utilized to engineer bone starting from human mesenchymal stem cells (hMSC). Osteogenic differentiation of hMSC seeded on these scaffolds resulted in extensive mineralization, alkaline phosphatase activity, and the formation of interconnected trabecular- or cortical-like mineralized networks as a function of the scaffold design utilized; allowing mineralized features of the tissue engineered bone to be dictated by the scaffold features used initially in the cell culture process. This approach to scaffold predictors of tissue structure expands the window of applications for SF based biomaterials into the realm of directing the formation of complex tissue architecture. As a result of slow degradation inherent to SF, scaffolds preserved their initial morphology and provided a stable template during the mineralization phase of stem cells progressing through osteogenic differentiation and new extracellular matrix formation. The slow degradation feature also facilitated transport throughout the 3D scaffolds to foster improved homogeneity of new tissue; avoiding regions with decreased cellular density. The ability to direct bone morphology via scaffold design suggests new options in the use of biodegradable scaffolds to control *in vitro* engineered bone tissue outcomes.

INTRODUCTION

Scaffolds used for bone tissue engineering have to address biological, mechanical and architectural needs to foster functional tissue outcomes. These factors, along with requirements for biocompatibility and maintenance of a suitable environment for cells to thrive impose an impressive array of challenges and constraints. Optimal porosity, pore interconnectivity and control of pore diameter are just some of the important features that can impact mechanical properties, cell responses and new tissue ingrowth.

The impact of porosity and pore diameter were previously detailed for various biomaterials including polyHIPE polymer [1], collagen and hydroxyapatite (HA) [2] and shown to effect cellular proliferation and osteogenic differentiation [3]. For *in vivo* applications, the minimum recommended pore size is suggested to be approximately 100 μm [4] and maximum pore size around 500 μm , with larger pores resulting in the formation of fibroblastic tissue [3, 5] indicating the relevance of scaffold geometry and lineage restriction. Other considerations for such designs revolve around mechanical properties and biocompatibility. For example, degradable, synthetic polymers such as poly(L-lactic acid) (PLA) and poly(L-lactic-co-glycolic acid) (PLGA) can induce inflammation due to the localized acidity of hydrolysis products and also find difficulty in matching the mechanical properties of native bone [1, 6-9]. Collagens remain problematic due to concerns with bioburdens as well as rapid degradation [10, 11].

Silks, which represent the strongest natural fibers known, may contribute to this important niche in biomaterial needs due to their remarkable mechanical properties and well documented biocompatibility [12-15]. Recent studies with silk films and fiber matrices have shown a wide range of potential biomedical applications [16-20] and detailed the low inflammatory potential both *in vitro* and *in vivo* [14]. Furthermore, silk fibers have been used for decades in suture formats, thus, there is a long history of biomedical materials experience with this protein polymer [21, 22].

Some current protocols for scaffold preparation start from silk fibroin (SF) solutions in organic solvent such as hexafluoroisopropanol (HFIP) or water and frequently use sodium chloride (NaCl) crystals as a porogen to generate the pores in the 3D structures upon processing [23-26]. Both the use of organic solvents as well as the salt crystals can potentially restrict the application of SF based biomaterials one of which would be the embedding of growth factors to support osteoinduction. Some growth factors were reported to be prone to high ionic strength (local remnants of NaCl crystals) or to the presence of some organic solvents [27].

This study presents a process replacing ‘exploratory’ organic solvent with unknown ICH classification by well known organic solvents and water, to minimize possible side effects related to this uncertainty and to further move SF scaffolds towards clinical application [28]. Paraffin has been used previously together with PLA and PLGA processing. The use of paraffin is attractive as it allows precise control of pore diameter and morphological features through controlled melting of the paraffin porogen and has demonstrated its use during manufacture and has been found an acceptable raw material [29, 30].

In the present study the use of paraffin porogens was integrated into the formation of silk scaffolds and different porogen diameters (100-200 μm , 200-300 μm , 300-400 μm) were considered. Different heat treatments to control the interconnectivity of pores were also considered by careful and controlled melting of paraffin porogen thereby forming different levels of interconnectivity. Osteogenic differentiation of human bone marrow derived mesenchymal stem cells (hMSC) was evaluated on these scaffolds (**Table 1**) to assess impact on bone-related features, through the use of biochemical assays, mechanical characterization, histology and micro-computed tomography (μCT) imaging. The results suggest that a significant level of control of bone geometries can be achieved *in vitro* through the ability to manipulate scaffold designs with the methods described herein.

Table 1: Experimental groups for bone tissue engineering *in vitro*

Scaffold type	Pore size	Culture system	Medium
37 scaffold	200 - 300 μm	Spinner flask	Control medium
37 scaffold	200 - 300 μm	Spinner flask	Osteogenic medium
RT scaffold	200 - 300 μm	Spinner flask	Osteogenic medium

MATERIALS AND METHODS

Materials

Paraffin with a melting temperature of 54-56 °C, lithium bromide, Na₂CO₃, polyethylene glycol (PEG) (MW 6000), formalin, alkaline phosphatase substrate (p-nitro-phenyl-phosphate), ascorbic acid, dexamethasone and β -glycerolphosphate were purchased from Sigma-Aldrich (St. Louis, MO). Potassium bromide was from Merck (Darmstadt, Germany). All antibodies, CD44 (endothelial cells), CD34 (sialomucin/hematopoietic progenitors), CD71 (transferring receptor/proliferating cells), and CD105 (endoglin), anti-CD44, anti-CD14 conjugated with fluoresceine isothiocyanate (CD44-FITC, CD14-FITC), anti-CD31 conjugated with phycoerythrin (CD31-PE), anti-CD34 conjugated with allophycocyanine (CD34-APC), anti-CD71-APC and anti-CD105 with the exception of secondary rat-antimouse IgG-FITC antibody (Neomarkers, Fremont, CA) were purchased from BD Bioscience (Maryland, MD). RPMI1640, Dulbecco's modified eagle medium (DMEM), fetal bovine serum (FBS), bFGF, Pen-Strep, fungizone, insulin and TGF β 1 were from Gibco (Palo Alto, CA). BMP-2 was kindly provided by Wyeth (Madison, NJ). Papain solution and Matrigel were from BD Bioscience (Maryland, MD). The kit to assess calcium concentration was from Rolf Greiner BioChemica (Vienna, Austria). Osmium tetroxide was purchased from Electron Microscopy Science (Hatfield, PA).

Hexane and N,N-Dimethylformamid was from EGT Chemie AG (Tägerig, Switzerland).

Preparation of paraffin globules

Paraffin globules were prepared in an emulsion process using water, gelatin and paraffin. Gelatin was dissolved in hot ultra purified water (UPW) (80 °C) at a concentration of 30 mg/ml and paraffin (melting temperature 54-56 °C) was carefully heated at a concentration of 200 g/l. Phases were emulsified by stirring at 9,000 rpm for 10 minutes and poured into ice-cold water. The solidified paraffin globules were harvested and washed with UPW. After filtering through 12-25 µm pore filter paper (Schleicher & Schuell, Switzerland) and drying, the globules were classified with standard sieves (Retsch, Haan, Germany). Fractions of >500 µm, 400-500 µm, 300-400 µm, 200-300 µm, 100-200 µm were separated and stored at 4 °C.

Preparation of SF solution

SF solution was prepared as described previously [19]. Briefly, cocoons from *Bombyx mori* (Trudel, Zurich, Switzerland), were boiled in 0.02 M Na₂CO₃ solution, rinsed and dissolved in 9 M LiBr for 3 h at 55 °C to generate a 10% (w/v) solution. The solution was dialyzed (Pierce, molecular weight cut-off 3,500 g/mol) in 1.5 l of UPW. The UPW was exchanged 5 times in 72 h resulting in a SF concentration of 3% (w/v).

Heat treatment of paraffin mold

The paraffin globules, 1.2 g, were loaded into 20 ml falcon syringes (BD Bioscience, Maryland, MD). The surface was evened by the use of a pistil and the syringes were left at RT or incubated at either 37 °C or 45 °C (Thermocenter, salvis OAKTON Instruments, Vernon Hills, NY) for 50 minutes. After heat treatment the mold was left to cool to RT.

Preparation and freeze drying of SF scaffolds

Freshly prepared SF in UPW was transferred to a dialysis chamber and further dialyzed against a 13.3% (w/v) PEG 6000 solution in UPW overnight resulting in a 20% (w/v) SF solution. One ml of this solution was soaked in the prepared paraffin mold so that the SF filled all pores between the porogen. This material was then flash frozen in liquid nitrogen for 1 min. The scaffolds were freeze dried at -30 °C under temperature control for 48 h (LYOVAC GT2, FINN-AQUA, Hurth, Germany). Scaffolds were immersed in 90% (v/v) methanol for 30 minutes and then air dried. The paraffin was extracted in hexane. Hexane was replaced after 12 and 24 h and the leached scaffolds were dried under vacuum for 12 h.

Differential scanning calorimetry (DSC)

For DSC analysis, nitrogen flow was 20 ml/min and baseline optimization was set between 105-250 °C. Calibration was performed with indium (~5 mg). Each sample (1 mg) was encapsulated in an aluminum pan, dried under a nitrogen flow at 105 °C for 10 minutes and then heated at a rate of 10 °C/min up to 250 °C and held at 250 °C for one minute [31].

Fourier-transformed infrared spectroscopy (FTIR)

For FTIR, a mortar and pestle was used to grind 5 mg of scaffold that was then mixed with 300 mg potassium bromide, and pressed into a pellet with 10 tons under vacuum for one minute. A 2000 FT-IR Spectrum V3,01 (Perkin Elmer, Bosten, MA) was used to analyze the materials.

Dissolution study

Water solubility was assessed using samples of 20 mg each (n=6), placed in 1 ml reaction tubes containing 1 ml of UPW and incubated at 37 °C. For each time point the supernatants were collected and the samples were dried under vacuum in

a speed-vac SC110 (Savant Instruments, Farmingdale, NY). The dry weight was assed over a total of 14 days using an analytical balance (Mettler-Toledo AX205 Deltarange, Greifensee, Switzerland).

Mechanical testing

Scaffolds (18 mm in diameter) were cut into cylinders with parallel surfaces (thickness 6-7 mm). Compressive testing between two parallel plates was performed at room temperature using a Zwick 1456 (Zwick Testing Machines Ltd, Kennesaw, GA) for material testing. Preload was set to 2 N and compression speed was 2 mm/minute. The compressive force and travel were graphed and the Young's modulus was determined using a 2% off set criterion.

Scanning electron microscopy images (SEM)

Scaffolds were cut into slices (1-2 mm height), dried, platinum-coated and analyzed by scanning electron microscopy (SEM, Zeiss Leo Gemini 1530, Zeiss, Germany).

Head space gas chromatography (GC) for the determination of residual solvents

Residual solvents in SF scaffolds after the hexane leaching were determined according to the US pharmacopeia [32]. 350 mg of leached and dried scaffold material was dissolved in 10 ml of 9 M Lithium bromide solution. 990 μ l of diluted SF scaffold in LiBr was mixed with 10 μ l of N,N- Dimethylformamide containing 0, 250, 500 and 1000 ppm of hexane and sealed in 10 ml headspace vials. The solution was preheated for 10 minutes at 60 °C and 1 ml of the gas phase was injected in the gas chromatograph equipped with a flame ionization detector heated at 260 °C (HP5890Agilent, Wilmington, DE, USA). GC was carried out using a HP-Fast residual solvents Col 3 column (Agilent, Wilmington, DE, USA). Helium flow rate was set to 6 ml/min, inlet temperature set at 180 °C

and splitless time set to 1 min with a split ratio of 1:6. The oven temperature was increased from 40 to 45 °C at 2 °C/min and from 45 to 250 °C at 30 °C/min.

Isolation, expansion and characterization of human mesenchymal stem cells (hMSC)

Cell isolation was performed as previously described [18]. Briefly, samples of bone marrow, of a single donor, were diluted in 100 ml of isolation medium (RPMI1640 supplemented with 5% FBS). The cells were centrifuged at 300 x g for 10 minutes. Cells were pelleted and suspended in expansion medium (DMEM, 10% FBS, 1 ng/ml bFGF) and seeded in 75 cm² flasks at a density of 5 x10⁴ cells/cm². The adherent cells were allowed to reach 80% confluence (12–17 days for the first passage, 6 days for later passages). Cells were trypsinized and replated every 6–8 days at 80% confluence. The second passage (P2) cells were used, if not otherwise stated. The hMSCs were characterized with respect to (i) the expression of surface antigens and (ii) the ability to selectively differentiate along the chondrogenic or osteogenic lineages. The expression of the following six surface antigens was characterized by fluorescence-activated cell sorting (FACS; Facscalibur, BD Bioscience, Maryland, MD) analysis, as described before [19], using the following marker proteins: CD44 (endothelial cells), CD34 (sialomucin/hematopoietic progenitors), CD71 (transferring receptor/proliferating cells), and CD105 (endoglin). Cells were detached with 0.05% (w/v) trypsin, pelleted, and resuspended at a concentration of 1x10⁷ cells/ml. Fifty-microliter aliquots of the cell suspension were incubated (30 min on ice) with 2 µl of each of the following antibodies: anti-CD44 and anti-CD14 conjugated with fluoresceine isothiocyanate (CD44-FITC, CD14-FITC), anti-CD31 conjugated with phycoerythrin (CD31-PE), anti-CD34 conjugated with allophycocyanine (CD34-APC), anti-CD71-APC, and anti-CD105 with a secondary rat-anti mouse IgG-FITC antibody. Cells were washed, suspended in 100 ml of 2% formalin and subjected to FACS analysis. To assess the potential of hMSC for osteogenic

differentiation, the cells were cultured in 12 well plates as micromass cultures (5 drops of 15 μ l of 2×10^7 cells/ml per well) in either control medium (DMEM supplemented with 10% FBS, penicillin/streptomycin and Fungizone) or osteogenic medium (control medium supplemented with 50 μ g/ml ascorbic acid-2-phosphate, 10 nM dexamethasone, 7 mM β -glycerolphosphate, and 1 μ g/ml BMP-2). Medium was exchanged every 2–3 days. After 2 weeks of culture the amounts of calcium were measured, as described before [18].

Cultivation in Bioreactor (spinner flask)

Methanol treated scaffolds, prepared with porogen treated at 37 °C (37-scaffold) and at RT (RT-scaffold), were cut into discs (thickness 1-2 mm) and scaffolds of 12 mm diameter were punched from this material. Matrigel matrix (BD Bioscience, Maryland, MD) was thawed overnight at 4 °C. Cells were trypsinized and cell number was assessed using a Neubauer hemocytometer (Brand GmbH, Wertheim, Germany). Five million cells were aliquoted and resuspended in 20 μ l of Matrigel and the cell suspension was seeded on the scaffolds in a Falcon non tissue culture treated 12 well plate (BD Bioscience, Maryland, MD). Scaffolds were incubated for 15 minutes (37 °C and 5% CO₂) until gelation of the Matrigel. The seeded scaffolds were then fixed with needles in the spinner between plastic stoppers (3x3 mm squares), which were cut from tubing (Norton Manufacturing Company, Fostoria, OH). The spinner was closed and 150 ml of media was added. For the control, DMEM containing 10% FBS 1% penicillin/streptomycin and 1% fungizone was used. For the differentiation along the osteogenic lineage, bone medium was prepared containing DMEM, 10% FBS, 1% penicillin/streptomycin, 1% fungizone, 50 μ g/ml ascorbic acid, 10 nM dexamethasone, 10 mM β -glycerol phosphate di-sodium salt hydrate and 1 μ g/ml BMP-2. Half of the medium was replaced every 2-3 days with osteogenic replacement medium containing DMEM, 10% FBS, 1% penicillin/streptomycin, 1% fungizone, 100 μ g/ml ascorbic acid, 20 nM dexamethasone, 20 mM β -glycerol

phosphate di-sodium salt hydrate and 2 $\mu\text{g/ml}$ BMP-2. Total culture time was 4 weeks.

Biochemical Assays

Constructs were harvested after 4 weeks. Scaffolds (n=4) were cut into halves, using one half for the assessment of ALP activity and DNA content and the other for quantification of total calcium. The wet weights of the scaffold halves were recorded (Mettler-Toledo® AX205 Deltarange®) and transferred into 2 ml tubes (Fisher Scientific, Pittsburgh, PA, US) for analytical evaluation.

Alkaline phosphatase (ALP) activity

For the assessment of ALP, halves of scaffolds (n=4) were incubated with 1 ml 0.2% (v/v) Triton-X100, 5 mM MgCl_2 and disintegrated using steel balls and a Minibead-beater (Biospec, Bartlesville, OK). After centrifugation at 300 x g for 10 minutes (4 °C), 80 μl of sample were transferred to a new tube. Alkaline phosphatase (ALP) activity (n=5) was measured using a biochemical assay from (Sigma-Aldrich, Inc., MO, US), based on ALP dependant conversion of *p*-nitrophenyl phosphate to *p*-nitrophenol and read spectrophotometrically at 405 nm in a microplate reader (Molecular Devices Corporation, Sunnyvale, CA).

DNA-Assay

DNA content (n=4) was measured by the PicoGreen assay (Molecular Probes, Eugene, OR), according to the protocols of the manufacturer. Samples were measured fluorometrically at an excitation wavelength of 480 nm and an emission wavelength of 528 nm (Packard instrument, Downes Gore, IL).

Calcium-Assay

To measure the amount of calcium, scaffold halves (n=4) were immersed in 1 ml of 5% trichloroacetic acid and disintegrated using steel balls and a Minibead-

beater. The debris was re-extracted with another 1 ml and the solutions were combined. Calcium content was determined spectrophotometrically at 575 nm (Microplate reader, Molecular Devices Corporation, Sunnyvale, CA), according to the manufacturer's protocol.

Histology

For histology, constructs (n=4) were fixed in 10% (v/v) neutral-buffered formalin (24 h at 4 °C), dehydrated in graded ethanol solutions, embedded in paraffin, bisected through the center, and cut into 5- μ m-thick sections. In order to visualize hMSCs in the scaffold cross sections, H&E staining was carried out after deparaffinization through graded ethanol series. For calcium visualization, von Kossa staining was performed. Briefly, deparaffinized sections were immersed in a 5% silver nitrate solution exposed to a 60 Watt lamp for 1 h. The sections were rinsed 3 times with UPW and fixed in a 5% sodium thiosulfate solution for 5 minutes. After washing, the stained sections were dehydrated with increasing concentration of ethanol and finally rinsed with xylene before the samples were covered with a glass plate.

X-ray Diffraction (XRD) of tissue engineered bone

XRD patterns of scaffolds after spinner flasks cultivation in osteogenic or control medium were obtained by means of a Stoe STADIP powder diffractometer equipped with a curved position sensitive detector covering 45 deg. in 2Theta. The radiation source was CuK α 1 (λ =1.54059 Angstrom, Ge-monochromator).

Micro-computed Tomography (μ CT)

μ CT was employed for the calculation of scaffold porosity and visualization of morphology of tissue engineered bone.

For assessment of scaffold porosity by μ CT scaffolds were stained in 25 mg/ml osmium tetroxide solution for 48 h and left under the hood until completely

dried. For the assessment of bone-like tissue morphology, constructs were cultured in spinner flasks, scaffolds were fixed in 10% formalin solution prior to the measurement.

Stained scaffolds (n=3) or constructs of tissue engineered bone (n=4) were analyzed by micro-computed tomography on a micro-CT40 imaging system (Scanco Medical, Bassersdorf, Switzerland) providing an isotropic resolution of 12 μm and 15 μm , respectively. A constrained Gaussian filter was used to partly suppress noise. Stained scaffolds or mineralized tissue were segmented from background using a global thresholding procedure [33]. All samples were processed by using the same filter width (1.2) and filter support (1). Quantitative morphometry was performed to calculate the porosity of stained scaffold and bone volume, bone surface and bone surface-to-volume ratio for mineralized tissue, respectively, using direct microstructural bone analysis [34]. Three-dimensional visualization was generated using in-house software [35].

Statistics

Statistical data analysis was performed by one-way analysis of variance (ANOVA) and Tukey-HST test for *post hoc* comparison using Minitab® Release 14 for Windows. $p < 0.05$ was considered statistically significant.

RESULTS

Characterization of scaffolds

Changes in SF crystallinity in response to methanol treatment were analyzed by FT-IR (**Fig. 1A**). The treatment with methanol resulted in an absorption at 1232 cm^{-1} and a visible shoulder at 1262 cm^{-1} (amide III band shift - assigned to the β -sheet conformation of SF and absent in untreated scaffolds [36]). From analysis by DSC, a shift in endothermic peaks to higher temperatures was visible after methanol treatment (**Fig. 1B**). Untreated SF scaffolds showed an

endothermic peak at 199.6 °C and methanol treated silk fibroin scaffolds at 213.6 °C. A brownish coloration and visual evidence of decomposition were observed at these temperatures using a polarization microscope (**Data not shown**), suggesting higher stability of the SF network after methanol treatment. Mass loss of methanol treated SF scaffolds in water at 37 °C was 4.9% after 5 days and remained constant until the end of the experiment (14 days), demonstrating the integrity of the scaffold over time, as a prerequisite to provide a stable template for bone-like tissue formation. The mass loss of untreated scaffolds was high during the first two days and kept on until 36% of the mass was lost after 14 days (**Fig. 1C**).

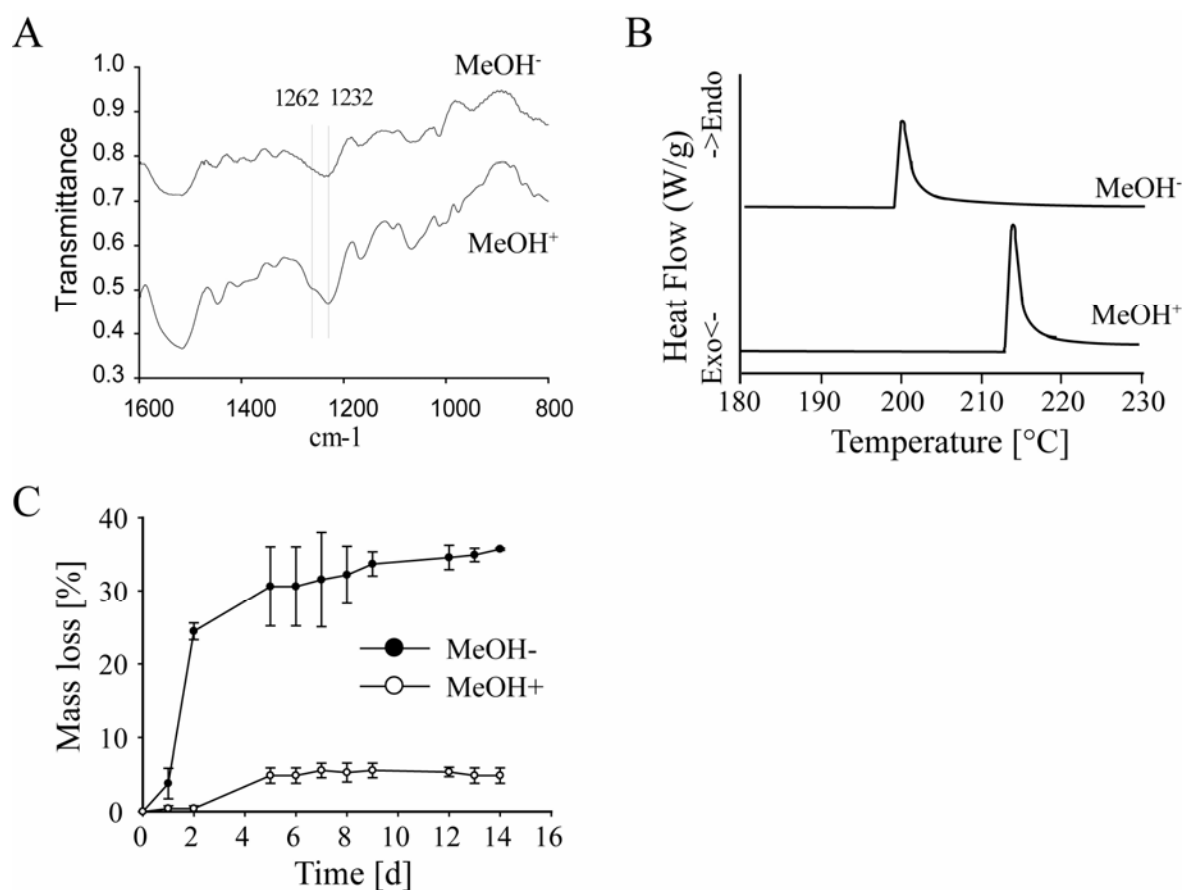


Fig. 1: (A) Fourier transformed infrared spectroscopy, and (B) differential scanning calorimetry thermograms from untreated freeze dried scaffolds or scaffolds treated with 90% methanol. (C) Mass loss in % of untreated and methanol treated scaffolds over time.

Scanning electron microscope images were taken from scaffolds prepared with 100-200 μm , 200-300 μm and 300-400 μm paraffin globules used as porogen. The treatment of the paraffin globules at room temperature (RT-scaffold), 37 $^{\circ}\text{C}$ (37-scaffold) and 45 $^{\circ}\text{C}$ (45-scaffold), prior to the addition of aqueous 20% silk SF solution (w/w) into the paraffin mold, resulted in different pore interconnectivities (**Fig. 2**). Overall distributions revealed an interconnected network for the treatments at 37 $^{\circ}\text{C}$ and 45 $^{\circ}\text{C}$ (**Fig. 2**). Treatments at room temperature did not show apparent interconnectivity, based on qualitative observations. Pore interconnectivity increased for materials based on paraffin treated at 37 $^{\circ}\text{C}$ and 45 $^{\circ}\text{C}$, resulting in average pore-pore connections between 50-80 μm in diameter for treatments at 37 $^{\circ}\text{C}$, and 120-200 μm for treatment at 45 $^{\circ}\text{C}$, as qualitatively assessed for pore sizes of 200- 300 μm . Porosity, as calculated from μCT data, was not significantly increased by the treatment of the porogen at higher temperature but depended on the pore size used (**Table 2**).

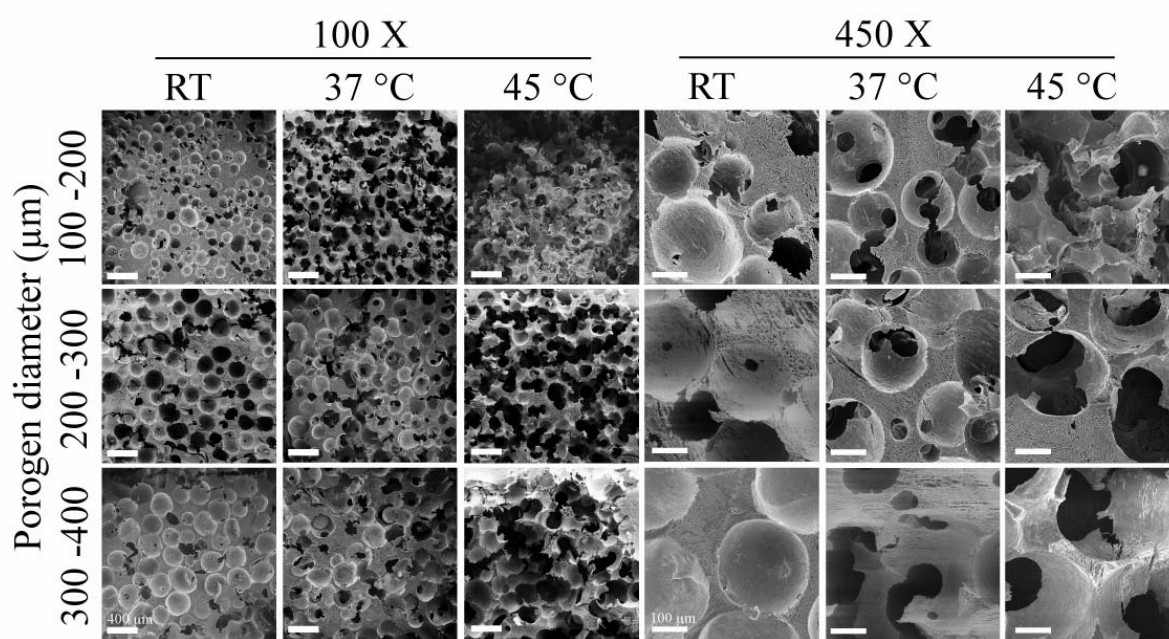


Fig. 2: Scanning electron microscopy images taken from silk fibroin (SF) scaffolds prepared with porogens of different diameters (100-200 μm , 200-300 μm , 300-400 μm). Interconnectivity was controlled by melting of the paraffin porogen at room temperature (RT), 37 $^{\circ}\text{C}$ or 45 $^{\circ}\text{C}$ prior to addition of the SF solution.

Table 2: Scaffold porosity [%]

	100 - 200 μm	200 - 300 μm	300 - 400 μm
RT	93.28 \pm 7.61	81.99 \pm 1.45	75.08 \pm 1.05
37 $^{\circ}\text{C}$	88.89 \pm 2.28	80.13 \pm 4.03	76.06 \pm 1.78
45 $^{\circ}\text{C}$	93.27 \pm 2.32	85.77 \pm 1.12	76.85 \pm 2.03

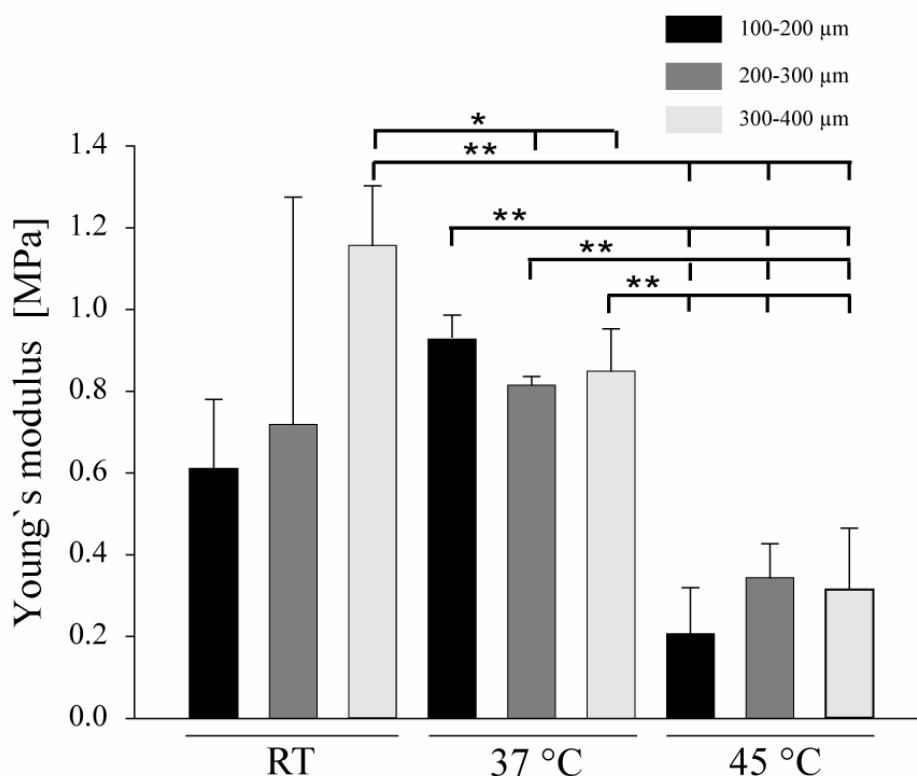


Fig. 3: Compressive strength (Young's modulus) of silk fibroin (SF) scaffolds as a function of porogen diameter (100-200 μm , 200-300 μm , 300-400 μm) and temperature of processing during porogen removal (room temperature (RT), 37 $^{\circ}\text{C}$, 45 $^{\circ}\text{C}$) prior to the addition of SF solution (** $p < 0.01$; * $p < 0.05$).

Nevertheless, the mechanical properties of the scaffolds were significantly influenced by the treatment of the porogen at different temperatures prior to the addition of the SF solution, ranging from 0.35 MPa for scaffolds prepared with 45 $^{\circ}\text{C}$ treatment and 1.1 MPa for scaffolds prepared with 37 $^{\circ}\text{C}$ (**Fig. 3**). Significant inter group differences in Young's modulus were recorded for the 37 $^{\circ}\text{C}$ porogen treatment when compared to scaffolds resulting from 45 $^{\circ}\text{C}$

porogen treatments ($p < 0.01$) and for 300-400 μm diameter RT-treatment, when compared to 37-scaffolds - ($p < 0.05$), or 45-scaffolds ($p < 0.01$). Absolute values were well below cancellous bone (200 MPa) or cartilage (20 MPa) [37].

Gas chromatography was used to detect traces of residual solvents used in the scaffolding process, such as hexane and methanol. Traces of hexane were 208.93 ± 26.9 ppm. Methanol was below the detection limits.

Characterization of isolated mesenchymal stem cells from bone marrow

For the characterization of the bone marrow isolates, cells were investigated for their expression of surface markers by FACS analysis. The expression of the surface antigens CD34 and CD31 was negative, suggesting the absence of hematopoietic progenitor cells and cells of endothelial origin, respectively. Most cells expressed CD71, a surface antigen commonly present in proliferating cells, and CD44, the transmembrane hyaluronate receptor for osteopontin, ankyrin, and fibronectin. Furthermore, the expression of CD105/endoglin, a putative marker for MSCs and $\alpha\text{v}\beta\text{1}$, a ligand for osteopontin, were positively expressed. The potential of isolated cells to differentiate into the osteogenic lineage was tested in a micromass culture. The isolated cells treated with osteogenic medium, containing BMP-2, showed a significant deposition of calcium and the activity alkaline phosphatase was elevated as compared to the control, after 2 weeks of culture (**Data not shown**).

Biochemical, histological and micro tomographic evaluation of osteogenic differentiation of hMSC seeded on silk fibroin (SF) scaffolds in spinner flask cultures

DNA content in RT- and 37-scaffolds, prepared with the identical porogen size (diameter 200-300 μm) was not significant different after cultivation of hMSCs for 4 weeks in osteoinductive medium (Fig. 5A). hMSCs cultured on 37 °C treated SF scaffolds with the same pore diameter (200-300 μm) in control

medium resulted in significantly higher levels of DNA ($p < 0.05$) when compared to the osteogenic medium.

Alkaline phosphatase (ALP) activity, measured by the conversion of p-nitrophenylphosphate to p-nitrophenol per DNA, was significantly higher for constructs grown in osteogenic medium when compared to control medium ($p < 0.05$) (**Fig. 4B**). No differences in ALP activity/DNA were observed for scaffolds with different interconnectivities. Calcium deposition per DNA was significantly increased for RT-scaffolds ($p < 0.05$) or 37-scaffolds ($p < 0.01$) when compared to the controls, with no significant differences between these two scaffold geometries (**Fig. 4B**).

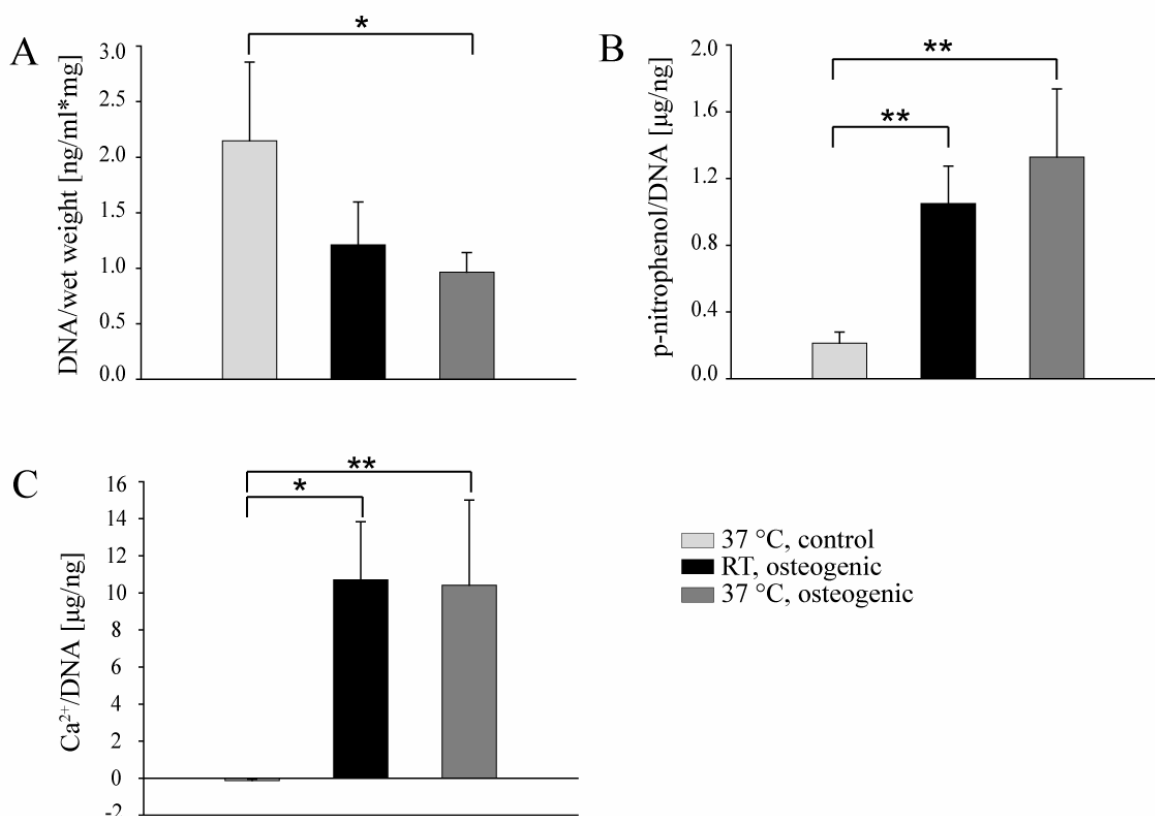


Fig. 4: Biochemical characterization of SF constructs seeded with hMSCs after 4 weeks of culture in bioreactors with osteogenic (scaffolds prepared at RT or 37 °C) or control medium, respectively (scaffolds prepared at 37 °C). (A) DNA normalized to mg wet weight of the construct ($\text{ng} \times \text{ml}^{-1} \times \text{mg}^{-1}$), (B) alkaline phosphatase activity expressed as p-nitrophenol conversion/DNA ($\mu\text{g}/\text{ng}$), and (C) calcium deposition normalized per DNA content ($\mu\text{g}/\text{ng}$) (** $p < 0.01$; * $p < 0.05$).

Cellular ingrowth in RT-scaffolds was confined to single pores and prominent at the scaffold surface, whereas complete in-growth was observed in the 37-scaffolds resulting in a dense cellular network after 4 weeks of culture in osteogenic medium (**Fig. 5B, C**). This was corroborated by von Kossa staining (calcium staining) (**Fig. 5D, E**). Mineralization observed on RT-scaffolds (small interconnectivity) was confined to disconnected clusters of bone-like tissue (**Fig. 5D**). Staining of 37-scaffolds resulted in homogenous mineralization of constructs with an interconnected trabecular network of bone-like tissue (**Fig. 5E**).

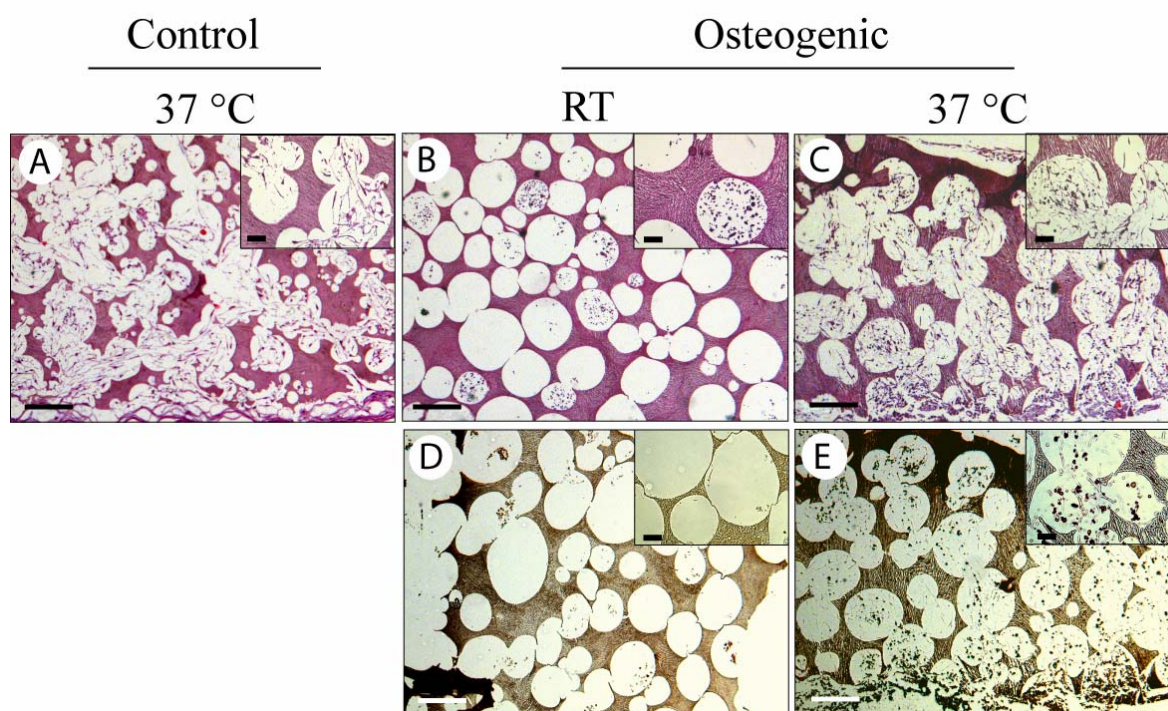
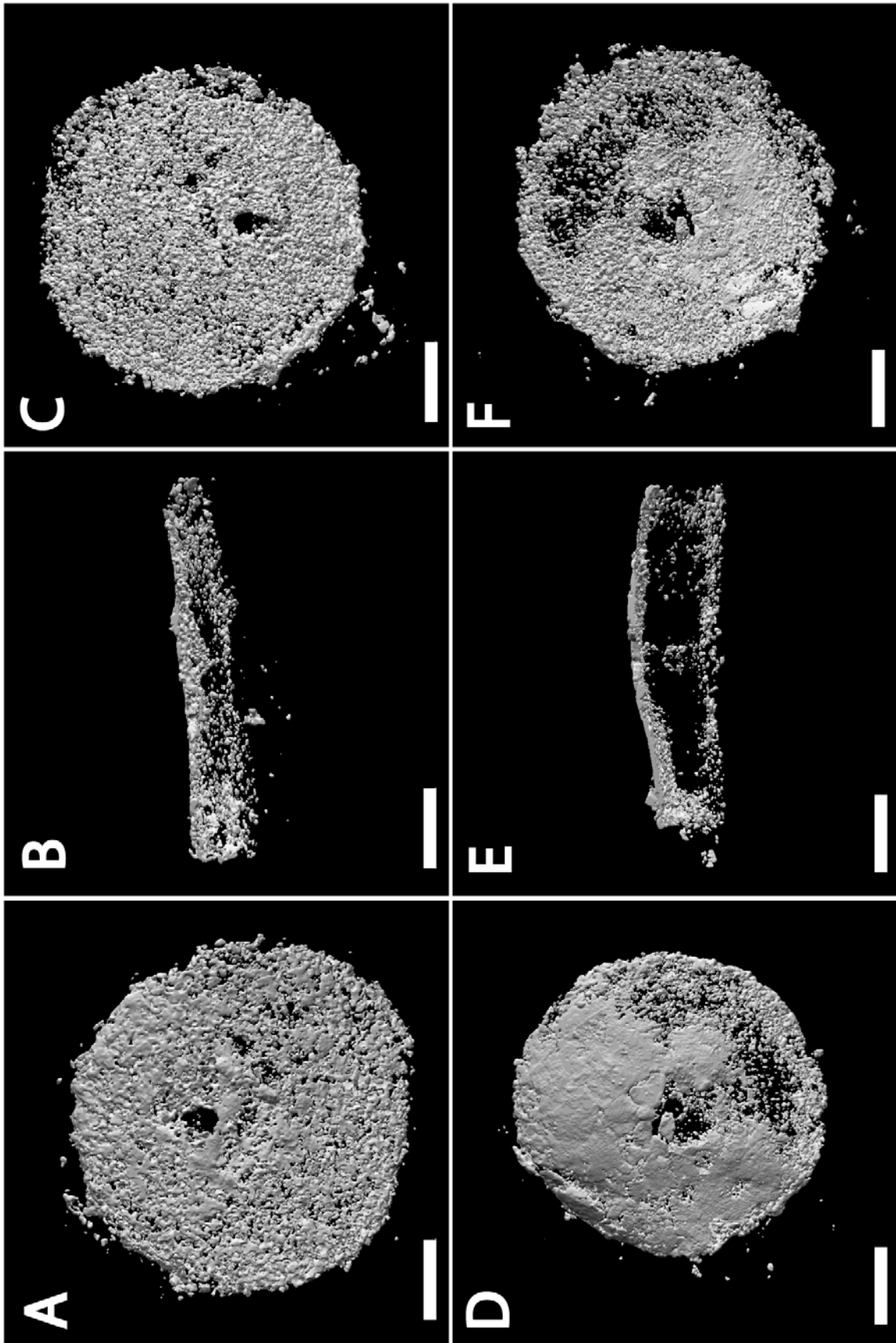


Fig. 5: Histological sections taken from silk fibroin constructs prepared with porogen treated at room temperature (RT-scaffold) (B, D) and 37 °C (37-scaffold; C, E). Constructs were seeded with hMSC and cultured for 4 weeks in osteogenic (RT- and 37-scaffolds; B-E) or control medium (37-scaffolds; A). H&E staining (A-C) and von Kossa staining (D, E); bar length 200 μm for whole images 50 μm for close-ups.

The calcium staining was confirmed by micro-computed tomography (μ CT) showing top view, center-cross view and bottom views of bone-like structures deposited on 37-scaffolds (**Fig. 6A, B, C**) and RT-scaffolds (**Fig. 6D-F**) after 4 weeks culture in bioreactors using osteoinductive medium. The bone formed as observed in the top view of 37-scaffolds; (**Fig. 6, 7A**) was characterized by a trabecular bone-like structure including focally restricted areas of plate-like bone. The bottom view of the scaffolds exhibited the same characteristics (**Fig. 6C**). The center cross-view (**Fig. 6B**) through the scaffold center revealed a gradual transition of trabecular-like bone into non-connected bone clusters from top to center. The top and bottom views of bone-like tissue on the RT-scaffolds showed the formation of plate-like bone (**Fig. 6D, F**). Bone formation was not observed in the center of the construct, with the exception of the small band coinciding with the location of the needle pin, holding the construct in place during culture (**Fig. 6E**). Calculated bone volumes and surfaces revealed no significant difference between the RT-scaffolds and 37-scaffolds (**Fig. 6A, B**). Bone surface to volume ratio was significantly increased for the 37-scaffolds when compared to RT-scaffolds (**Fig. 6C**). BS and BV but not BS/BV are normalized by the wet weight of constructs, a source of additional systemic error, which is circumvented by the measure BS/BV resulting in significant difference.

Fig. 6: Morphology of tissue engineered bone on silk fibroin (SF) scaffolds seeded with hMSCs after 4 weeks of culture in bioreactors with osteogenic medium as determined by micro-computed tomography (μ CT). Porogen diameter was 200-300 μ m, and exposed to 37 °C (A-C) or room temperature (RT; D-F) for 50 minutes prior to addition of SF solution. Top view (A, D), center-cross view (B, E) and bottom view (C, F). Bar length = 2mm.



To verify the bone-like nature of the deposited tissue, the scaffolds were characterized by XRD. In spectras obtained from scaffolds cultured with hMSC in osteogenic condition, in contrast to scaffold cultured in control medium, characteristic 2Theta values of 26° and 40° could be detected corresponding to Miller indices of (0 0 2) and (3 1 0), respectively. Those bands and an additional broader band between 30° and 35° fitted the pattern of cortical bone [38] indicating a hydroxyl apatite structure of the tissue engineered bone.

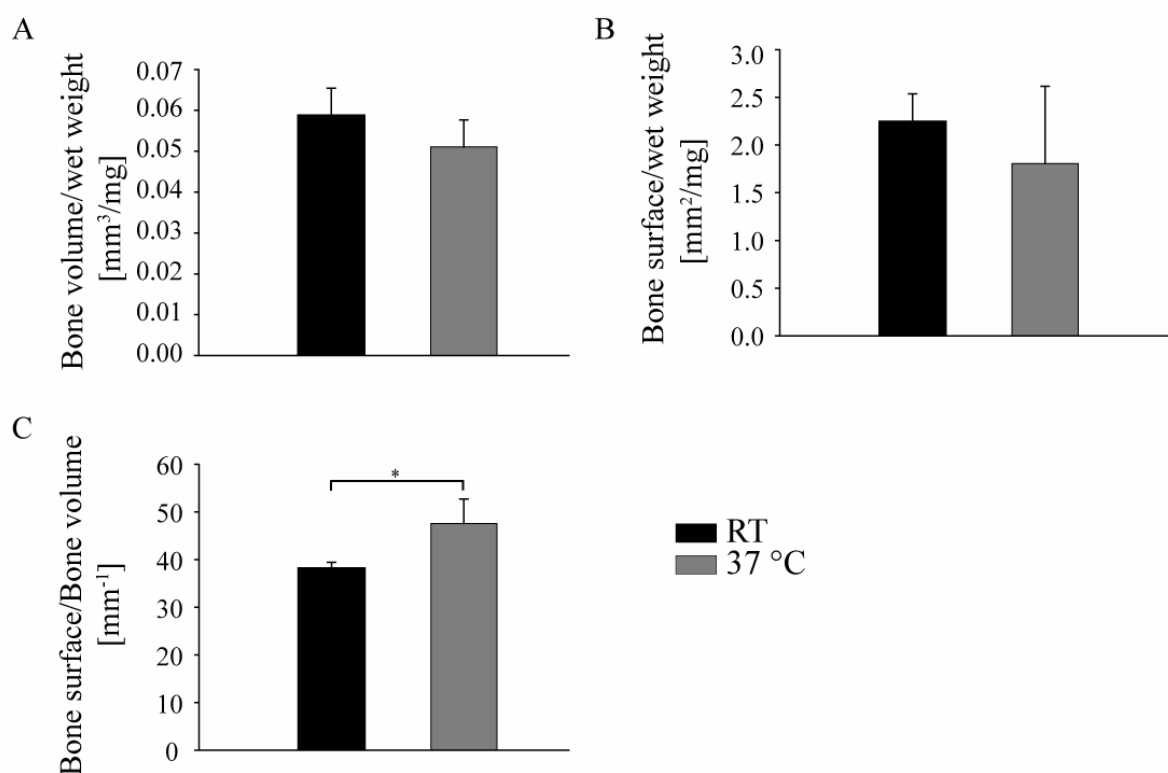


Fig. 7: Effect of interconnectivity on total bone volume (A), bone surface (B) and bone surface/volume (C) of hMSC seeded on constructs (pore diameter 200-300 μm ; treated at room temperature (RT-scaffold) and at 37 $^\circ\text{C}$ (37-scaffold) in osteoinductive medium.

DISCUSSION

Scaffolds used for bone tissue engineering and repair have to fulfill various requirements such as biological, mechanical and architectural aspects. They should be biocompatible, enable the adherence of cells, be slowly degradable and provide a physical support but display highly interconnected pores to allow a homogenous ingrowth of cells, tissue and a sufficient vascularization at the implant site. Therefore, strategies to address these criteria should include on one hand the quest for an ideal biomaterial and on the other hand for a suitable fabrication technology to control the porosity and biomechanical strength of the implant. To expand the available options of silk fibroin (SF) scaffolds starting from aqueous SF solutions, a novel process was used to generate 3D biomaterials with control of pore size and interconnectivity. The pore porosity of our scaffolds was mainly influenced by the diameter of the porogen used but did not impact the mechanical structure. The new process circumvents the use of NaCl and the use of non-ICH organic solvents (e.g. HFIP) [28] during the assembly of the SF (**Fig. 8**). These scaffolds offer mechanical strength and control over pore size and interconnectivity. This approach adds versatility and options to prior methods of preparing 3D SF scaffolds in which organic solvents of unknown safety, and salt with associated conditions of high ionic strength, were required. hMSCs seeded scaffolds with pore sizes between 200-300 μm exhibited substantially higher interconnectivity of the deposited bone clusters, when the material was prepared at 37 °C as compared to RT.

The results suggest that the process for the preparation of aqueous based SF scaffolds by freeze-drying and the use of paraffin as porogen can direct the morphology of bone-like tissue resulting in deposition of plate-like bone prominent at the surface (RT-scaffold) or an interconnected network of bone trabeculae throughout the construct (37-scaffold). These findings are important as other biodegradable polymeric biomaterial scaffolds do not offer the same level of control of this type of outcome, even aside from the unique mechanical features of silk-based biomaterials.

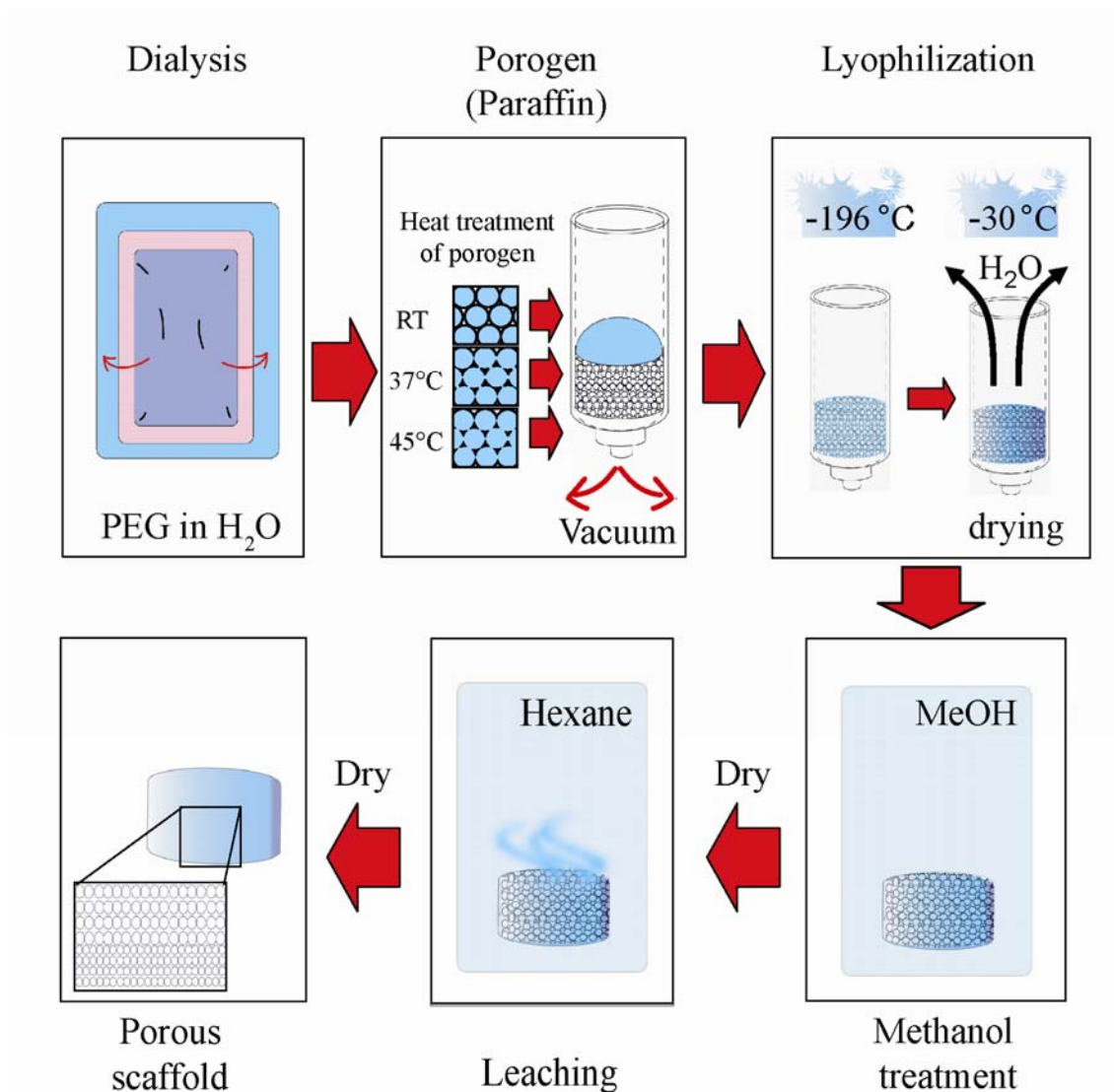


Fig. 8: Schematic illustration of the production process starting from aqueous silk fibroin (SF) solutions.

For example, collagen sponges degrade too rapidly to maintain the required template features as we have shown earlier in osteogenic studies [18]. While cross-linking helps in this regard, a negative impact on the desired biological functions due to cross-linking has been shown [39, 40]. Similarly, PLA systems remain limited due to failure in meeting mechanical demands at the implantation site and acidic by-products as typically released during degradation [6, 7].

Methanol treatment induced β -sheet crystallinity as indicated by an additional shoulder at 1262 cm^{-1} as compared to the chromatogram taken from

non-methanol treated SF scaffolds. This shoulder is due to a shift of the amide III band and indicative for a conformational shift of SF into β -sheet structure (**Fig. 2A**) [41, 42]. The increase in crystallinity for methanol treated scaffolds was reflected in an increase in decomposition temperature as shown in the DSC thermogram (**Fig. 2B**). However, for a detailed analysis of changes in crystallinity as a consequence of methanol treatment, further studies should be conducted. FTIR is sensitive to changes in short-range changes – on the functional group level - and less suited for an analysis of supramolecular assembly. Changes in long range crystallinity of SF films and fibers as a consequence of methanol treatment have been detailed before using X-ray diffractometry studies [43, 44]. The observed changes in crystallinity by both, FTIR and DSC are in line with the substantial decrease in water solubility for methanol treated versus untreated scaffolds, respectively (**Fig. 2C**).

The methanol and hexane content in the scaffolds was assessed by head space gas chromatography. Residual methanol was not present in the scaffold but 208.93 ± 26.9 ppm of hexane were detected. According to ICH limit for residual solvents pharmaceutical products, the permitted daily exposure (PDE) of hexane is 2.9 mg/day corresponding to a daily administration of 10 g product containing 290 ppm of hexane [28]. Scaffolds prepared according to the presented protocols are well below ICH limits and, therefore, are generally considered as safe for this parameter.

Microarchitectural parameters were related to compressive mechanical properties [45]. The porosity of scaffolds with different pore sizes (100-200 μm , 200-300 μm , 300-400 μm) and for each treatment regimen (RT, 37 $^{\circ}\text{C}$ and 45 $^{\circ}\text{C}$) was identified by μCT (**Table 1**). The porosity was particularly influenced by the diameter of the porogen among groups manufactured with different porogen diameters but not the mode of temperature treatment, i.e. interconnectivity of the pores within a group manufactured with identical porogen diameters. Therefore, the mechanical properties were mainly influenced by the architecture of the pores and not by the porosity. Heat treatment of the porogen at 45 $^{\circ}\text{C}$ transformed the

resulting scaffold architecture from separated or connected single pore voids observed at RT and 37 °C, respectively, to fused pores forming larger and weaker frameworks (**Fig. 3**). Scaffolds with low pore interconnectivities did not result in improved mechanical properties, with the exception of pore sizes of 300-400 μm , which displayed laminar cracks and structural inhomogeneities after freeze-drying, most likely the result of higher porogen mobility during soaking of the aqueous SF solution and freezing. Therefore, microarchitectural parameters affect mechanical properties as well as the reproducibility of the production process. The results did not reveal an influence of pore size on the mechanical properties as described in other models [46-48].

Cells isolated from bone marrow showed an expression of CD105/endoglin (a putative marker of MSCs [49, 50]), and CD71 (a receptor expressed in proliferating cells [51, 52]) as well as the lack of expression of CD31 and CD34 (markers for cells that are of endothelial [53] or hematopoietic origin [53-55]) that indicated the MSC nature of these cells. Furthermore, cells showed the ability to undergo osteogenic differentiation in micromass cultures using osteogenic medium (**data not shown**).

The formation of bone-like tissue by hMSC cultured in spinner flasks on different scaffold designs was further investigated by micro-computed tomography (μCT) and demonstrated that different morphologies of bone-like tissues can be engineered as a function of scaffold design. This control of geometry extends the design of mechanically stable bone constructs, directing the formation of different bone structures by tissue engineering. The nature of the deposited bone, as a result of scaffold geometry, was further reflected in morphometric analysis (**Fig. 8A**). Bone surface-to-volume ratio was significantly increased in scaffolds prepared with porogen treated at 37 °C, suggesting a shift to trabecular bone-like tissue. This could be a function of diffusional hindrance for nutrients and gases to enter scaffolds with lower interconnectivity, resulting in impaired deposition of bone and cellular proliferation in more central parts of the constructs, as has been observed for other biomaterials [56-58].

In summary, a new fabrication protocol for the preparation of SF scaffolds was identified that circumvents the use of organic solvents not generally recognized as safe [28] and provides control of mechanical properties, pore size and interconnectivity. The geometry of the engineered bone, as a result of calcium deposition during osteogenic differentiation of hMSCs, was guided or templated by the scaffold design. This relationship resulted in more plate-like or trabecular-like geometries and degrees of cellular penetration into the scaffold centers correlated to the scaffold features used in the cell cultivation process. Future studies will focus on combining the mechanical advantages of SF scaffolds with drug delivery through co-encapsulation of growth factors to impact cell proliferation and differentiation *in vitro* and/or *in vivo* [3, 59-63].

ACKNOWLEDGMENTS

We thank Trudel (Zurich, Switzerland) for silk cocoons, Wyeth Biopharmaceuticals (Andover, MA) for BMP-2 supply and the group of Prof. Altorfer (ETH Zurich) for access to their DSC equipment. We further thank Prof. Amadò and Thomas Schärer (ILW, ETH Zurich) for the access and the help with the GC analysis and Chunmei Li (IPW, ETH Zurich) for the help with the XRD. Financial support was from the AO Foundation (AO Biotechnology Research Grant 2003), Association for Orthopaedic Research, ETH Zurich (TH 26.04-1), the US National Science Foundation (Grant Nr. 0436490) and the National Institute of Health (P41 - EB002520) is gratefully acknowledged.

REFERENCES

1. G. Akay, M.A. Birch, M.A. Bokhari, Microcellular polyHIPE polymer supports osteoblast growth and bone formation in vitro, *Biomaterials* 25 (18) (2004) 3991-4000.
2. E. Tsuruga, H. Takita, H. Itoh, Y. Wakisaka, Y. Kuboki, Pore size of porous hydroxyapatite as the cell-substratum controls BMP-induced osteogenesis, *J Biochem (Tokyo)* 121 (2) (1997) 317-24.
3. V. Karageorgiou, D. Kaplan, Porosity of 3D biomaterial scaffolds and osteogenesis, *Biomaterials* 26 (27) (2005) 5474-91.
4. S.F. Hulbert, F.A. Young, R.S. Mathews, J.J. Klawitter, C.D. Talbert, F.H. Stelling, Potential of ceramic materials as permanently implantable skeletal prostheses, *J Biomed Mater Res* 4 (3) (1970) 433-56.
5. M.C. Wake, C.W. Patrick, Jr., A.G. Mikos, Pore morphology effects on the fibrovascular tissue growth in porous polymer substrates, *Cell Transplant* 3 (4) (1994) 339-43.
6. K.A. Athanasiou, G.G. Niederauer, C.M. Agrawal, Sterilization, toxicity, biocompatibility and clinical applications of polylactic acid/polyglycolic acid copolymers, *Biomaterials* 17 (2) (1996) 93-102.
7. J.O. Hollinger, J. Brekke, E. Gruskin, D. Lee, Role of bone substitutes, *Clin Orthop Relat Res* (324) (1996) 55-65.
8. L.D. Harris, B.S. Kim, D.J. Mooney, Open pore biodegradable matrices formed with gas foaming, *J Biomed Mater Res* 42 (3) (1998) 396-402.
9. H. Suh, Recent advances in biomaterials, *Yonsei Med J* 39 (2) (1998) 87-96.
10. F. DeLustro, J. Dasch, J. Keefe, L. Ellingsworth, Immune responses to allogeneic and xenogeneic implants of collagen and collagen derivatives, *Clin Orthop Relat Res* (260) (1990) 263-79.
11. S. Srivastava, S.D. Gorham, D.A. French, A.A. Shivas, J.M. Courtney, In vivo evaluation and comparison of collagen, acetylated collagen and collagen/glycosaminoglycan composite films and sponges as candidate biomaterials, *Biomaterials* 11 (3) (1990) 155-61.
12. P.M. Cunniff, S.A. Fossey, M.A. Auerbach, J.W. Song, D.L. Kaplan, W. Adams, R.K. Eby, D. Mahoney, D. Deborah, D.L. Vezie, Mechanical and thermal properties

- of Dragline Silk from the Spider *Nephila cavipes*, *Polymers for Advanced Technologies* 5 (1994) 401-410.
13. S. Sofia, M.B. McCarthy, G. Gronowicz, D.L. Kaplan, Functionalized silk-based biomaterials for bone formation, *J Biomed Mater Res* 54 (1) (2001) 139-48.
 14. L. Meinel, S. Hofmann, V. Karageorgiou, C. Kirker-Head, J. McCool, G. Gronowicz, L. Zichner, R. Langer, G. Vunjak-Novakovic, D.L. Kaplan, The inflammatory responses to silk films in vitro and in vivo, *Biomaterials* 26 (2) (2005) 147-55.
 15. B. Panilaitis, G.H. Altman, J. Chen, H.J. Jin, V. Karageorgiou, D.L. Kaplan, Macrophage responses to silk, *Biomaterials* 24 (18) (2003) 3079-85.
 16. G.H. Altman, F. Diaz, C. Jakuba, T. Calabro, R.L. Horan, J. Chen, H. Lu, J. Richmond, D.L. Kaplan, Silk-based biomaterials, *Biomaterials* 24 (3) (2003) 401-16.
 17. L. Meinel, S. Hofmann, V. Karageorgiou, L. Zichner, R. Langer, D. Kaplan, G. Vunjak-Novakovic, Engineering cartilage-like tissue using human mesenchymal stem cells and silk protein scaffolds, *Biotechnol Bioeng* 88 (3) (2004) 379-91.
 18. L. Meinel, V. Karageorgiou, R. Fajardo, B. Snyder, V. Shinde-Patil, L. Zichner, D. Kaplan, R. Langer, G. Vunjak-Novakovic, Bone tissue engineering using human mesenchymal stem cells: effects of scaffold material and medium flow, *Ann Biomed Eng* 32 (1) (2004) 112-22.
 19. L. Meinel, V. Karageorgiou, S. Hofmann, R. Fajardo, B. Snyder, C. Li, L. Zichner, R. Langer, G. Vunjak-Novakovic, D.L. Kaplan, Engineering bone-like tissue in vitro using human bone marrow stem cells and silk scaffolds, *J Biomed Mater Res A* 71 (1) (2004) 25-34.
 20. N. Minoura, S. Aiba, M. Higuchi, Y. Gotoh, M. Tsukada, Y. Imai, Attachment and growth of fibroblast cells on silk fibroin, *Biochem Biophys Res Commun* 208 (2) (1995) 511-6.
 21. F. Lange, Ueber die Sehnenplastik, *Verh Dtsch Orthop* 2 (1903) 10-12.
 22. F. Lange, Künstliche Bänder aus Seide., *Münch Med Wochenschr* (17) (1907) 834-836.
 23. M. Tsukada, F. Cuiulinao, M. Norihiko, A. Ciulia, Preparation and Application of Porous Silk Fibroin Materials, *Journal of Applied Polymer Science* 54 (1994) 507-514.
 24. R. Nazarov, H.J. Jin, D.L. Kaplan, Porous 3-D scaffolds from regenerated silk fibroin, *Biomacromolecules* 5 (3) (2004) 718-26.

25. U.J. Kim, J. Park, H.J. Kim, M. Wada, D.L. Kaplan, Three-dimensional aqueous-derived biomaterial scaffolds from silk fibroin, *Biomaterials* 26 (15) (2005) 2775-85.
26. H.J. Kim, U.J. Kim, G. Vunjak-Novakovic, B.H. Min, D.L. Kaplan, Influence of macroporous protein scaffolds on bone tissue engineering from bone marrow stem cells, *Biomaterials* 26 (21) (2005) 4442-52.
27. L. Meinel, O.E. Illi, J. Zapf, M. Malfanti, H. Peter Merkle, B. Gander, Stabilizing insulin-like growth factor-I in poly(D,L-lactide-co-glycolide) microspheres, *J Control Release* 70 (1-2) (2001) 193-202.
28. ICH, *Q3C(R3) - Guidelines for residual solvents*.
29. Z. Ma, C. Gao, Y. Gong, J. Shen, Paraffin spheres as porogen to fabricate poly(L-lactic acid) scaffolds with improved cytocompatibility for cartilage tissue engineering, *J Biomed Mater Res B Appl Biomater* 67 (1) (2003) 610-7.
30. V.J. Chen, P.X. Ma, Nano-fibrous poly(L-lactic acid) scaffolds with interconnected spherical macropores, *Biomaterials* 25 (11) (2004) 2065-73.
31. J. Magoshi, Y. Magoshi, Physical Properties and Structure of Silk. The Glass Transition and Conformational Changes of Tussah Silk Fibroin., *J. Appl Polym. Sci.:* (1977) 2405-2407.
32. U.S. Pharmacopeia, *Chapter (467): Organic volatile impurities - Residual solvents*, in *USP XXVIII*. 2006, The United States Pharmacopeia Convention, Inc.
33. P. Ruegsegger, B. Koller, R. Muller, A microtomographic system for the nondestructive evaluation of bone architecture, *Calcif Tissue Int* 58 (1) (1996) 24-9.
34. T. Hildebrand, A. Laib, R. Muller, J. Dequeker, P. Ruegsegger, Direct three-dimensional morphometric analysis of human cancellous bone: microstructural data from spine, femur, iliac crest, and calcaneus, *J Bone Miner Res* 14 (7) (1999) 1167-74.
35. R. Muller, T. Hildebrand, P. Ruegsegger, Non-invasive bone biopsy: a new method to analyse and display the three-dimensional structure of trabecular bone, *Phys Med Biol* 39 (1) (1994) 145-64.
36. N.V. Bhat, G.S. Nadiger, Crystallinity in Silk Fibers: Partial Acid Hydrolysis and Related Studies., *J. Appl. Polym. Sci.* 25 (1979) 921-932.
37. R.B. Martin, D.B. Burr, N.A. Sharkey, *Skeletal tissue mechanics*. 1998: Springer-Verlag New York, Inc.

38. A. Bigi, G. Cojazzi, S. Panzavolta, A. Ripamonti, N. Roveri, M. Romanello, K. Noris Suarez, L. Moro, Chemical and structural characterization of the mineral phase from cortical and trabecular bone, *J Inorg Biochem* 68 (1) (1997) 45-51.
39. M.J. van Luyn, P.B. van Wachem, L.H. Olde Damink, P.J. Dijkstra, J. Feijen, P. Nieuwenhuis, Secondary cytotoxicity of cross-linked dermal sheep collagens during repeated exposure to human fibroblasts, *Biomaterials* 13 (14) (1992) 1017-24.
40. M. van Luyn, P. van Wachem, O. Damink L, J. Dijkstra P, J. Feijen, P. Nieuwenhuis, Relations between *in vitro* cytotoxicity and crosslinked dermal sheep collagens., *J Biomed Mater Res* 26 (1992) 1091-1110.
41. T. Asakura, A. Kuzuhara, Conformation Characterization of Bombyx mori Silk Fibroin in the Solid State by High-Frequency ¹³C Cross Polarization-Magic Angle Spinning NMR, X-ray Diffraction, and Infrared Spectroscopy, *Macromolecules* 18 (1984) 1841-1845.
42. L. Mingzhong, L. Shenzhou, W. Zhengyu, Y. Haojing, M. Jingyu, W. Lihong, Studies on porous silk fibrion materials. I. Fine structure of freeze dried silk fibrion, *Journal of Applied Polymer Science* 79 (1999) 2185-2191.
43. R. Valluzzi, S.P. Gido, W. Muller, D.L. Kaplan, Orientation of silk III at the air-water interface, *Int J Biol Macromol* 24 (2-3) (1999) 237-42.
44. R. Valluzzi, S. Winkler, D. Wilson, D.L. Kaplan, Silk: molecular organization and control of assembly, *Philos Trans R Soc Lond B Biol Sci* 357 (1418) (2002) 165-7.
45. A.S. Lin, T.H. Barrows, S.H. Cartmell, R.E. Guldberg, Microarchitectural and mechanical characterization of oriented porous polymer scaffolds, *Biomaterials* 24 (3) (2003) 481-9.
46. L. Moroni, J.R. de Wijn, C.A. van Blitterswijk, 3D fiber-deposited scaffolds for tissue engineering: Influence of pores geometry and architecture on dynamic mechanical properties, *Biomaterials* 27 (7) (2006) 974-85.
47. J.C. Le Huec, T. Schaefferbeke, D. Clement, J. Faber, A. Le Rebeller, Influence of porosity on the mechanical resistance of hydroxyapatite ceramics under compressive stress, *Biomaterials* 16 (2) (1995) 113-8.
48. D.F. Meaney, Mechanical properties of implantable biomaterials, *Clin Podiatr Med Surg* 12 (3) (1995) 363-84.
49. F.P. Barry, R.E. Boynton, S. Haynesworth, J.M. Murphy, J. Zaia, The monoclonal antibody SH-2, raised against human mesenchymal stem cells, recognizes an epitope on endoglin (CD105), *Biochem Biophys Res Commun* 265 (1) (1999) 134-9.

50. M.K. Majumdar, V. Banks, D.P. Peluso, E.A. Morris, Isolation, characterization, and chondrogenic potential of human bone marrow-derived multipotential stromal cells, *J Cell Physiol* 185 (1) (2000) 98-106.
51. W. Judd, C.A. Poodry, J.L. Strominger, Novel surface antigen expressed on dividing cells but absent from nondividing cells, *J Exp Med* 152 (5) (1980) 1430-5.
52. L.C. Kuhn, A. McClelland, F.H. Ruddle, Gene transfer, expression, and molecular cloning of the human transferrin receptor gene, *Cell* 37 (1) (1984) 95-103.
53. H.M. DeLisser, P.J. Newman, S.M. Albelda, Platelet endothelial cell adhesion molecule (CD31), *Curr Top Microbiol Immunol* 184 (1993) 37-45.
54. R.S. Negrin, K. Atkinson, T. Leemhuis, E. Hanania, C. Juttner, K. Tierney, W.W. Hu, L.J. Johnston, J.A. Shizurn, K.E. Stockerl-Goldstein, K.G. Blume, I.L. Weissman, S. Bower, R. Baynes, R. Dansey, C. Karanes, W. Peters, J. Klein, Transplantation of highly purified CD34+Thy-1+ hematopoietic stem cells in patients with metastatic breast cancer, *Biol Blood Marrow Transplant* 6 (3) (2000) 262-71.
55. G.J. Spangrude, S. Heimfeld, I.L. Weissman, Purification and characterization of mouse hematopoietic stem cells, *Science* 241 (4861) (1988) 58-62.
56. S.L. Ishaug, G.M. Crane, M.J. Miller, A.W. Yasko, M.J. Yaszemski, A.G. Mikos, Bone formation by three-dimensional stromal osteoblast culture in biodegradable polymer scaffolds, *J Biomed Mater Res* 36 (1) (1997) 17-28.
57. I. Martin, V.P. Shastri, R.F. Padera, J. Yang, A.J. Mackay, R. Langer, G. Vunjak-Novakovic, L.E. Freed, Selective differentiation of mammalian bone marrow stromal cells cultured on three-dimensional polymer foams, *J Biomed Mater Res* 55 (2) (2001) 229-35.
58. G. Vunjak-Novakovic, B. Obradovic, I. Martin, P.M. Bursac, R. Langer, L.E. Freed, Dynamic cell seeding of polymer scaffolds for cartilage tissue engineering, *Biotechnol Prog* 14 (2) (1998) 193-202.
59. S.J. Lee, Cytokine delivery and tissue engineering, *Yonsei Med J* 41 (6) (2000) 704-19.
60. W.L. Murphy, M.C. Peters, D.H. Kohn, D.J. Mooney, Sustained release of vascular endothelial growth factor from mineralized poly(lactide-co-glycolide) scaffolds for tissue engineering, *Biomaterials* 21 (24) (2000) 2521-7.
61. M.J. Whitaker, R.A. Quirk, S.M. Howdle, K.M. Shakesheff, Growth factor release from tissue engineering scaffolds, *J Pharm Pharmacol* 53 (11) (2001) 1427-37.

62. T.A. Holland, Y. Tabata, A.G. Mikos, Dual growth factor delivery from degradable oligo(poly(ethylene glycol fumarate)) hydrogel scaffolds for cartilage tissue engineering, *J Control Release* 101 (1-3) (2005) 111-25.
63. D.D. Hile, M.L. Amirpour, A. Akgerman, M.V. Pishko, Active growth factor delivery from poly(D,L-lactide-co-glycolide) foams prepared in supercritical CO₂, *J Control Release* 66 (2-3) (2000) 177-85.

CHAPTER III

Biocompatibility and osteoconduction of macroporous silk fibroin implants in cortical defects in sheep

Lorenz Uebersax¹, Tanja Apfel², Katja M. R. Nuss², Rainer Vogt², Hyoen Yoo Kim³, Lorenz Meinel^{1,3}, David L. Kaplan³, Joerg A Auer², Hans P. Merkle¹, and Brigitte von Rechenberg²

¹*Institute of Pharmaceutical Sciences, ETH Zurich, Zurich, Switzerland*

²*Musculoskeletal Research Unit (MSRU), Equine Hospital, Vetsuisse Faculty, Zurich, Switzerland*

³*Department of Biomedical Engineering, Tufts University, Medford, MA, USA*

ABSTRACT

The goal of the presented study was to compare the biocompatibility and cellular responses to porous silk fibroin (SF) scaffolds produced in a water-based (UPW) or a solvent based process (HFIP) using two different SF sources. For that reason, four different SF scaffolds were implanted (n=6) into drill-hole defects in the cancellous bone of sheep femura and humeri. The scaffolds were evaluated histologically for biocompatibility, cell-material interaction and cellular ingrowth. New bone formation was observed macroscopically and histologically at 8 weeks after implantation. For semiquantitative evaluation, the investigated parameters were scored and subjected to a statistical analysis (factorial ANOVA). All implants showed good biocompatibility as evident by low infiltration of inflammatory cells and the absence of encapsulation of the scaffolds in connective tissue. Multinuclear foreign body giant cells (GCs) and macrophages were present in all parts of the scaffold at the material surface indicating their active degradation of the SF material. Cell ingrowth and vascularization of the scaffold were very uniform. However, in HFIP scaffolds local regions of empty pores were present throughout the scaffold, probably due to the low pore interconnectivity in this scaffold type in contrast to UPW scaffolds. The amount of newly formed bone was very low in both scaffold types but was more abundant in the periphery than in the center of the scaffolds.

INTRODUCTION

Bone grafts or bone substitutes are indicated when the physiologic healing process fails or is delayed, e.g., due to complicated fractures, age of the patient, long term use of nicotine, in the presence of diabetes or autoimmune diseases, or in case of non-bridging defects after surgical removal of large masses of bone [1, 2]. For orthopaedic applications, 500,000 to 600,000 interventions involving bone grafting are conducted every year in the US [3]. Although autografts or allografts are still considered the clinical gold standard for bone replacement, they have been associated with significant drawbacks, the most important one being their often largely restricted availability. Moreover, complications such as pain, patient morbidity, and failure of bone regeneration at the harvest-site have been reported as well as necrosis of the grafted material and failure of its integration into the defect after implantation [4-7]. Such severe drawbacks may result in prolonged hospitalization and negatively affect patients' compliance, raising the quest for alternatives. Artificial porous bone substitutes share numerous advantages over autografts and allografts including their practically unlimited supply, straightforward sterilization and storage. Such implants provide well defined physical properties and may accommodate signalling molecules to improve or control the repair process. Despite the numerous advantages, synthetic bone graft substitutes - mostly ceramics and polyesters - currently represent only 10% of the bone substitutes on the market [8]. Disadvantages of ceramic implants include high brittleness, variable rates of resorption, and potentially adverse effects on normal bone remodeling [3]. New generations of substitutes, based on biopolymers such as proteins or polysaccharides, could provide an ideal microenvironment for cells, wherein they can thrive and foster the natural regeneration process. However, collagen-based bone substitutes, the most abundant ECM protein in bone, exert only low mechanical strength and undergo rapid degradation. Therefore, collagens perform poorly when it comes to provide

the necessary mechanical support and spatial guidance during bone regeneration. Accordingly, their application potential is limited [9].

Silk fibroin (SF) can be harvested in relevant amounts from cocoons of the silkworm *Bombyx mori* and represents one of nature's toughest fibers, able to absorb more energy than synthetic fibers such as Kevlar [9]. Previously reported problems regarding the biocompatibility of this material could be resolved by separating the immunogenic glycoprotein sericin from the pure SF proteins [10, 11]. Various scaffolding technologies have been developed to produce 3-dimensional porous SF constructs from either organic solvent or water based systems, benefiting from its versatile processability [12-15]. Since then, numerous examples have demonstrated how SF can be applied as a substrate for *in vitro* tissue engineering. When implanted in rodents, SF revealed only moderate inflammatory potential, comparable or lower than that observed with collagen or biodegradable polyesters [11, 16-20]. Moreover, SF has been suggested as a carrier for growth factors, fabricated either by an organic solvent based process using hexafluoro-isopropanol (HFIP) such as with BMP-2 loaded SF scaffolds [21], or through an ultra purified water (UPW) based freeze-drying protocol using aqueous SF solutions containing IGF-I [22]. Both approaches showed promising results for future applications of SF as bioactive implant material. Despite the promising record of SF as to its biocompatibility, the final performance of an SF implant under physiological conditions *in vivo* still awaits testing. In particular, the influence of different scaffolding techniques, e.g., in terms of process parameters and residual solvents, on the *in vivo* performance and biocompatibility of the resulting implants, is difficult to predict from *in vitro* cell culture studies and calls for further experimental confirmation.

Typically, rats, mice and other rodents are the preferred animal models for testing biomaterial implants. They allow for a large number of parallel experiments under similar condition and time, and are likely to be justified from both ethical and economical points of view. However, the morphology and mechanical properties of rodent bones are quite different from humans [23]. Unlike rodent models the sheep model benefits from large similarities with

humans in weight, bone and joint structure, as well as in general bone metabolism endorsing the use of sheep for orthopaedic research [24-26]. Recently, an animal model has been developed that allows for the intraosseous implantation of eight different samples per sheep in long bones, which makes it ideally suited for standardized testing of biodegradable materials for use in orthopaedics and for maxillofacial and dental surgery [27-29]. In fact, the sheep drill hole model - as used in this study - largely facilitates the testing of inter- and intra-individual differences among various types of materials, while at the same time overall suffering of animals can be reduced and the necessary numbers of animals minimized to satisfy statistical requirements.

In the present study the sheep drill hole model was employed to evaluate biocompatibility, integrity and osteoconductivity of various SF implants, mainly in the context of identifying a reliable source of SF and a suitable scaffolding process. In particular, we elucidated the suitability of porous SF implants in light of their future application as scaffolds for bone repair.

MATERIALS AND METHODS

Materials and Instruments

In addition to routine surgical instruments, Weitlaner- and Gelpi-retractors, a periosteal elevator, a pneumatic drill (Synthes, Waldenburg, Switzerland) with an 8 mm, slightly modified drill bit (KaVo INTrASurg 500®, KaVoDental AG Biberach, Germany, modified by Synthes, Waldenburg, Switzerland) and a corresponding drill guide were used. The drill bit was modified with a special depth-regulating device and the tip was flattened while still having good cutting characteristics. n-Hexane for paraffin extraction and gas chromatography was from Scharlau-Chemie S.A. (Sentmenat, Barcelona, Spain), and gelatine (Golddruck) was purchased from Hänseler AG (Herisau, Switzerland). Paraffin with a melting temperature of 54–56 °C, hexafluoro-isopropanol (HFIP), and lithium bromide were from Sigma-Aldrich (Fluka, St. Louis, MO).

Silk preparation

Silk fibroin solution was prepared as described previously [14]. Briefly, cocoons from *Bombyx mori* were obtained from either M. Tsukada, Institute of Sericulture, Tsukuba, Japan (silk source 1) or Trudel, Zurich, Switzerland (silk source 2) and boiled in 0.02 M Na₂CO₃ solution, rinsed and dissolved in 9M LiBr for 3 h at 58 °C to generate a 10% (w/v) solution. The solution was dialyzed (Pierce, Rockford, IL; molecular weight cutoff 3'500 Da) in 1.5 l of ultra purified water (UPW; NANOpure Diamond, Barnstead International, IA, USA). UPW was exchanged 5 times in 72 h resulting in a purified silk fibroin concentration of 3% (w/v).

HFIP scaffolding protocol

HFIP type SF scaffold were prepared as previously described [12]. 3% dialyzed silk fibroin (w/w) was lyophilized, and resolved in 17% hexafluoro-2-propanol (HFIP, w/v). A given amount of granular NaCl (200-300 µm) as porogen was accurately weighed in a Teflon container and silk solution was added at a ratio of 20:1 (NaCl/silk). HFIP was allowed to evaporate for 2 days and, for hardening, NaCl/SF blocks were immersed in 90% (v/v) methanol for 30 min. Blocks were removed, dried, and NaCl was washed out with water for 2 days. Porous scaffolds were cut into cylinders of 8 mm diameter and packed in aluminium foil before they were steam autoclaved at 121 °C for 20 minutes.

UPW scaffolding protocol

Instead of using granular NaCl, paraffin spheres served as porogen. Their preparation followed an emulsion process using water, gelatin and solid paraffin as described before [14]. Solidified paraffin spheres were harvested and washed with UPW. The spheres were filtered through 12-25 µm pore filter paper (Schleicher & Schuell, Switzerland), dried at room temperature and classified with standard sieves (Retsch, Haan, Germany). Fractions of >500 µm, 400-500 µm,

300-400 μm , 200-300 μm , 100-200 μm were collected and stored at 4 °C. For scaffolding, heat induced sintering of paraffin globules (200-300 μm) in a cylindrical mold was performed as described previously [14]. Briefly, 1.2 g of paraffin porogen was loaded into 20 ml falcon syringes (BD Bioscience, Maryland, MD). The surface was evened by the use of a pistil, followed by controlled sintering at 37 °C to assure pore interconnectivity (Thermocenter, Salvis OAKTON Instruments, Vernon Hills, NY) for 50 min. After sintering, the tubular mold was left to cool to room temperature and stored for later use. Freshly prepared silk solution in UPW was transferred to a dialysis chamber and further dialyzed against a 13.3% (w/v) PEG 6000 solution in UPW overnight resulting in a 20% (w/v) SF solution. One ml of this solution was soaked into the prepared tubular mold (d = 8 mm, height = 20 mm) consisting of sintered paraffin spheres, so that SF solution filled all pores throughout the mold. The mold was then shock frozen in liquid nitrogen for 1 min and freeze dried at -30 °C under temperature control for 48 h (Lyovac GT2, Finn-Aqua, Hurth, Germany). For hardening, the scaffolds featuring highly interconnective pores were immersed in 90% (v/v) methanol for 30 minutes and then air dried. As validated, exhaustive extraction of paraffin was achieved by complete exchange of hexane every 12 hours for a total of 4 exchanges (see below). The porous silk scaffolds were air-dried and then placed in a vacuum-dryer for 24 h. The dried scaffolds were packed in aluminium foil and autoclaved at 121 °C for 20 min.

Gravimetric and gas chromatographical analysis of paraffin leaching procedure

Extraction of paraffin spheres from scaffolds was by leaching with n-hexane (n=4) at a ratio of 27 ml n-hexane per g of paraffin. Hexane was completely replaced every 12 hours for a total of 6 changes. The paraffin content in 1.0 ml of solvent was assessed and the percentage of leached paraffin was calculated. Batches 4 to 6 were analyzed by gas chromatography for residual paraffin in the hexane using a Trace MC (Thermo Electron corporation, US) equipped with a quadrupol mass spectrometer and a Factorfour Vf-5MS column

(Variant, US). Helium flow rate was set to 6 ml/min, inlet temperature was 180 °C and split-less time 1 min with a split ratio of 1:6. The oven temperature was increased from 40 °C to 45 °C at 2 °C/min and from 45 °C to 250 °C at 30 °C/min.

Sheep

Three adult Swiss Alpine sheep, all castrated male of 2 years of age, with a body weight ranging from 53–70 kg were used for the study, which was approved by the local Ethical Committee and veterinary authorities (application number 188/2004). The sheep were examined for their state of health both clinically and haematologically. Tetanus vaccine and an anthelmintic were administered. The animals were acclimatized to their new housing facilities for 2 weeks before surgery.

Scaffold location

Porous SF cylinders of the four groups (**Table 1**) were distributed randomly to eight predefined metaphyseal or epiphyseal locations in long bones of the sheep: namely left and right proximal humerus, proximal femur, proximal tibia, and distal femur [27, 29]. A total of 8 samples were implanted in each sheep.

Table 1: Description of the scaffold types

SF source	Scaffolding protocol	
	HFIP process	UPW process
SF source 1	HFIP1	UPW1
SF source 2	HFIP2	UPW2

Anaesthesia

Anaesthesia was performed as previously described [27, 29]. Briefly, sheep were sedated with medetomidine (5 µg/kg i.m., Domitor, Orion Animal Health, Finland) and anaesthesia was induced with diazepam (0.1 mg/kg, Valium, Roche Pharama, Switzerland) and ketamin (2 mg/kg, Narketan 10, Chassot GmbH, Germany). Anaesthesia was maintained by isoflurane–oxygen inhalation (FORENE, Abbot AG, Switzerland).

Medication

Prior to anaesthesia 30'000 IU/kg aqueous penicillin G (Grünenthal 10 Mega, Grünenthal GmbH, Aachen, Germany) and 6 mg gentamicin sulfate (G. Streuli Ag, Uznach, Switzerland) were administered via a jugular catheter. Perioperative analgesic and anti-inflammatory therapy was provided with 0.01 mg/kg buprenorphine (Temgesic, Essex Chemie AG, Luzern, Switzerland) intramuscularly and 4 mg/kg carprofene (Rimadyl, Pfizer AG, Zurich, Switzerland) intravenously. Anti-inflammatory and antibiotic medication was maintained for 4 days after surgery.

Surgery

The sheep were placed in lateral recumbency. Aseptic preparation of the surgical site was performed routinely as previously described [27]. After implanting all samples from one side the animals were rotated onto the other side for the same procedure. A small lateral approach with stab incision was made directly over the location. The fascia was incised and a blunt dissection was performed down to the bone. The drill holes were created with an 8 mm drill with a stop at 13 mm length (KaVo INTrASurg 500, KaVo Dental AG Biberach, Germany). After drilling, the holes were flushed and cleaned with saline (0.9%) and a sterile swab. Porous SF scaffolds were soaked in PBS and subsequently in blood supplied by the same sheep. Blood infiltration was achieved by creating a

vacuum within the syringe cylinder and the cylinders were carefully inserted into the drill holes manually. Overlying soft tissue was closed in layers with resorbable suture (Vicryl 2/0 Johnson & Johnson, Brussels, Belgium) and skin staples were used to close the skin (Davis and Geck Appose ULCr, B. Braun Aesculap AG, Tuttlingen, Germany). The staples were removed 10 days after surgery. Subsequently, the animals were allowed to roam freely on the pasture until slaughter.

Macroscopic and microscopic evaluation

The bones were harvested immediately after slaughter and the macroscopic appearance was assessed with regard to inflammatory reaction, overgrowth of neighboring tissue and by the coloration of the tissue at the implant site. All specimens were prepared as reported before [29]. A band saw (Exakt band system, Apparatebau Norderstedt, Germany) was used to prepare the bone samples. The specimens including a segment of adjacent bone (0.3 - 0.5 cm) were sawed at a 90° angle to the longitudinal axis of the bone. For this purpose, they were fixed in 4% formalin for 4 days before being dehydrated in an ascending series of ethanol (50–100%) and defatted with xylene. After infiltration of the samples with a mix of methacrylic acid methylester, dibutylphthalate and perkadox as peroxide in a proportion of 89.5:10:0.5 in an air-evacuated container at 41 °C for 14 days, they were polymerized with PMMA into ready-to-cut sample blocks [35,36]. According to the size of the blocks, a saw microtome (Leica SP1600, Leica Instruments GmbH, Germany) was used to cut 200 µm thick sections.

Histology

Sections were then ground to a thickness of 30 - 40 µm and used for histological and histomorphometric evaluations as described earlier [29]. Basically, all radial sections were cut in the centre of the cylinder. The ground sections were surface stained with toluidine blue, whereas the thin sections were

deplastified and stained with toluidine blue and von Kossa/Mc Neal's Tetrachrome.

Semiquantitative evaluation and scoring system

The thick sections were evaluated for new bone, scaffold remnants and formation of fibrous tissue. However, since new bone formation was scarce within the given time period, histomorphometry was not considered a valuable tool for evaluation. Thin sections were used for the qualitative and semiquantitative evaluation. The quality of new bone formation, scaffold integrity, vascularization and occurrence of fibrous infiltration and inflammatory cells was described. The character and amount of the cells found in three fields of vision of the whole implant area of each section were evaluated, supported by a specifically developed scoring system (Leica DMR; Leica Microsystems Wetzlar GmbH, Wetzlar, Germany). For semiquantitative analysis, histology sections were divided into periphery, middle part, and central part (**Fig. 1**) and the parameters were scored for each part and group according to **Table 2**.

Table 2: Overview of scores for evaluation of histology

Scoring parameter	Magnification	Scoring
Multinuclear foreign body giant cells (GCs)	10	0 = none; 1 < 25%; 2 < 50%; 3 > 50%
Lymphocytes and plasma cells	5	0 = low; 1 = moderate; 2 = strong
Bone in scaffold	20	0 = none; 1 = low; 2 = moderate
Bone islands in pores	10	0 = none; 1 = moderate; 2 = many
Scaffold resorption	10	0 = weak; 1 = moderate; 2 = strong
Osteoid	20	0 = none; 1 < 10%; 2 < 25%; 3 > 25%
Vascularization	20	0 = none vessels; 1 = 5-10 vessels; 2 = 10-15 vessels; 3 = 15-20 vessels
Fibrous tissue	20	0 = none; 1 = loose; 2 = mature

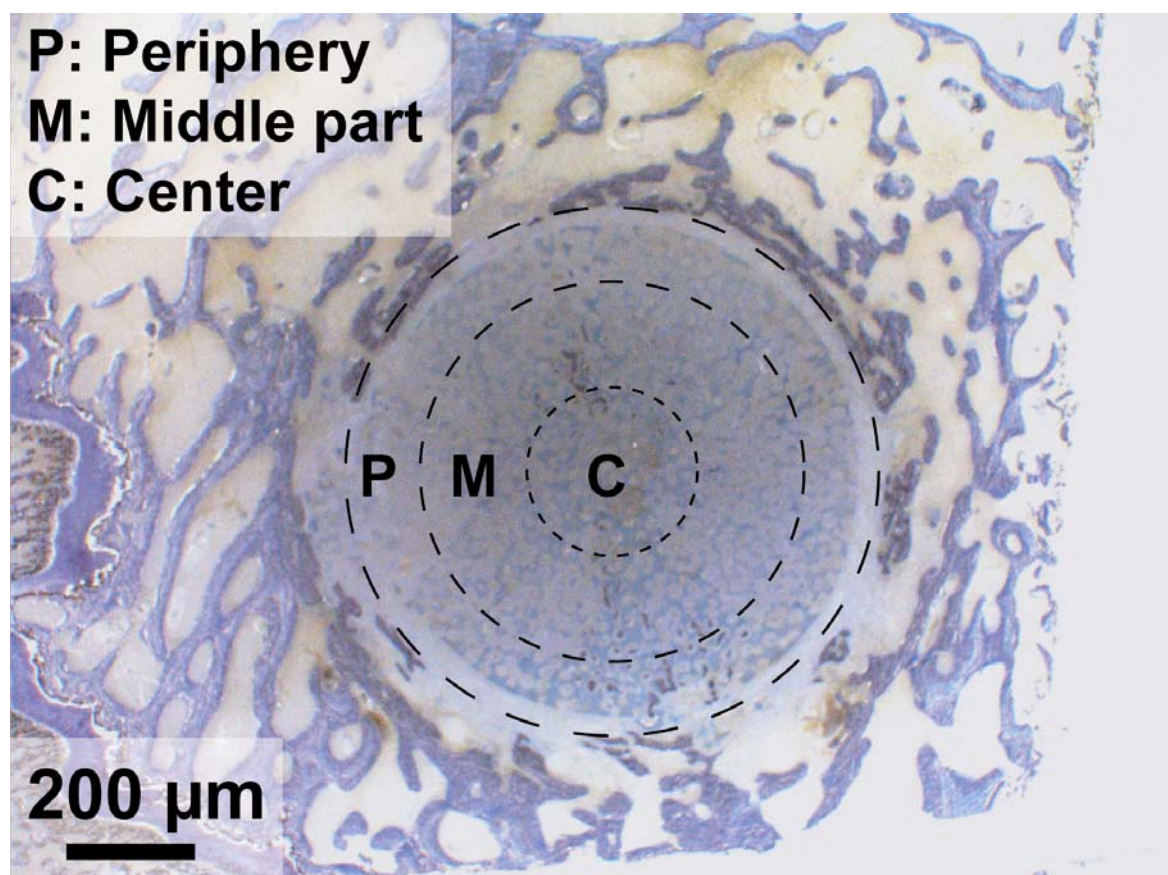


Fig. 1: Defect area including SF implant subdivided into axial areas: periphery (P), middle part (M) and center (C).

Statistics

An univariate analysis of variance (ANOVA) and a Scheffe Post-Hoc test (SPSS 14.0 for Windows, SPSS Inc, Chicago, Ill) were carried out for the semiquantitative results obtained by the scoring of individual parameter. A Student t-test was also applied to assess (i) the effect of the silk source, (ii) the effect of the scaffolding process, and (iii) the location within the scaffold (C, M and P). Results were considered to be significant at $p < 0.05$.

RESULTS

Gravimetric and gas chromatographic analysis of paraffin leaching procedure

To eliminate any possibility of an interference of paraffin residuals with the biocompatibility of the SF material, the paraffin content in the hexane extractions was assessed by gravimetry and gas chromatography to assure the completion of the leaching process. After 3 exchanges of hexane no further extraction of paraffin could be achieved as assessed by gravimetry (**Fig. 2**). Paraffin traces in the subsequent extraction were below the background and could not be detected by MS coupled gas chromatography. The residual hexane concentration was below official limits as previously reported [14].

Surgery

Surgery was performed without complications. SF scaffolds exhibited stiff and brittle properties in dry state and were pre-swollen before the introduction into the defect. The samples could be easily infiltrated with blood using the vacuum system. Swollen scaffolds showed good compressibility and elastic, sponge-like properties, and could be easily inserted into the defects. All samples, except for the UPW1 group, could be introduced without damage into the defects. Because of their enlarged brittleness, scaffolds of the UPW1 group were partially broken upon sterilization and were introduced in 2 to 3 fragments into the defect. All sheep recovered well and showed no signs of lameness within the following 10 days, with the exception of one sheep 3102 that showed slight signs of swelling and associated lameness of the distal right femur. Analgesia was maintained by subcutaneous injection of 5 ml carprofen (Rimadyl, Pfizer, Dr. E. Gräub AG; Bern, Schweiz) per day over a total period of 5 days. The presence of a fracture could be excluded after X-ray images were taken. All sheep returned healthy before slaughter after 8 weeks.

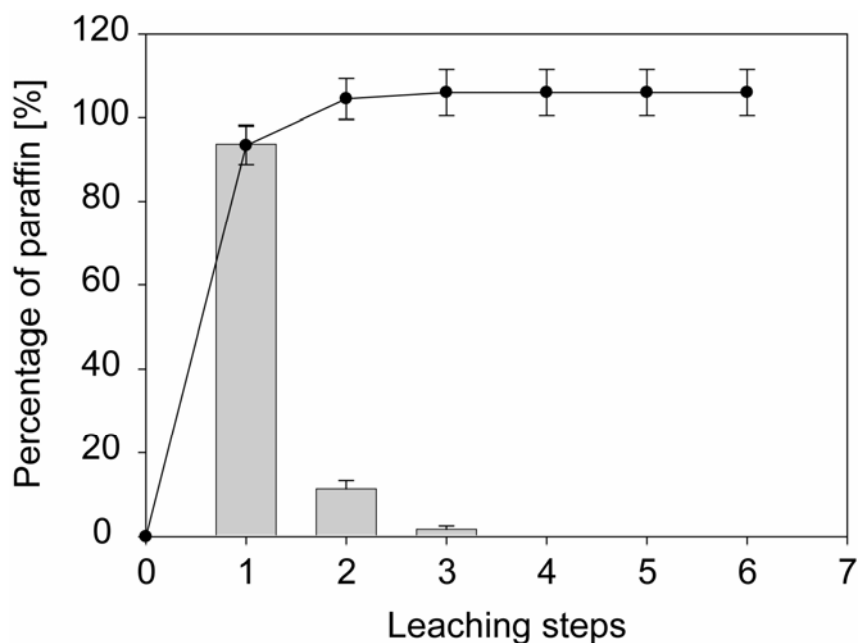


Fig. 2: Gravimetric analysis of paraffin content in hexane during the leaching process. Bars: percentage of residual paraffin extracted from the hexane of one leaching step (12h). (●) Percentage of cumulatively leached paraffin; histograms indicating percentage of leached paraffin per leaching step.

Macroscopic and microscopic evaluation

The locations of the defects and the SF implants were still visible after 8 weeks and no notable macroscopic differences were observed between the different scaffold types (HFIP1, HFIP2, UPW1, UPW2) (**Fig. 3**). All SF implants were found to be readily introduced into the defect and interlocked with adjacent bone. However, the dimensions of the implants did not always fill the whole defect resulting in void spaces between bone and implant, which were filled with ingrowing tissue. The ingrowth of soft tissue emerged throughout the porous structure of the SF implant as irregular patches (**Fig. 3, 4**). The macroporous structure of the SF implants contained loose connective tissue with spindle-shaped cells becoming less organized from the periphery to the center of the scaffold.

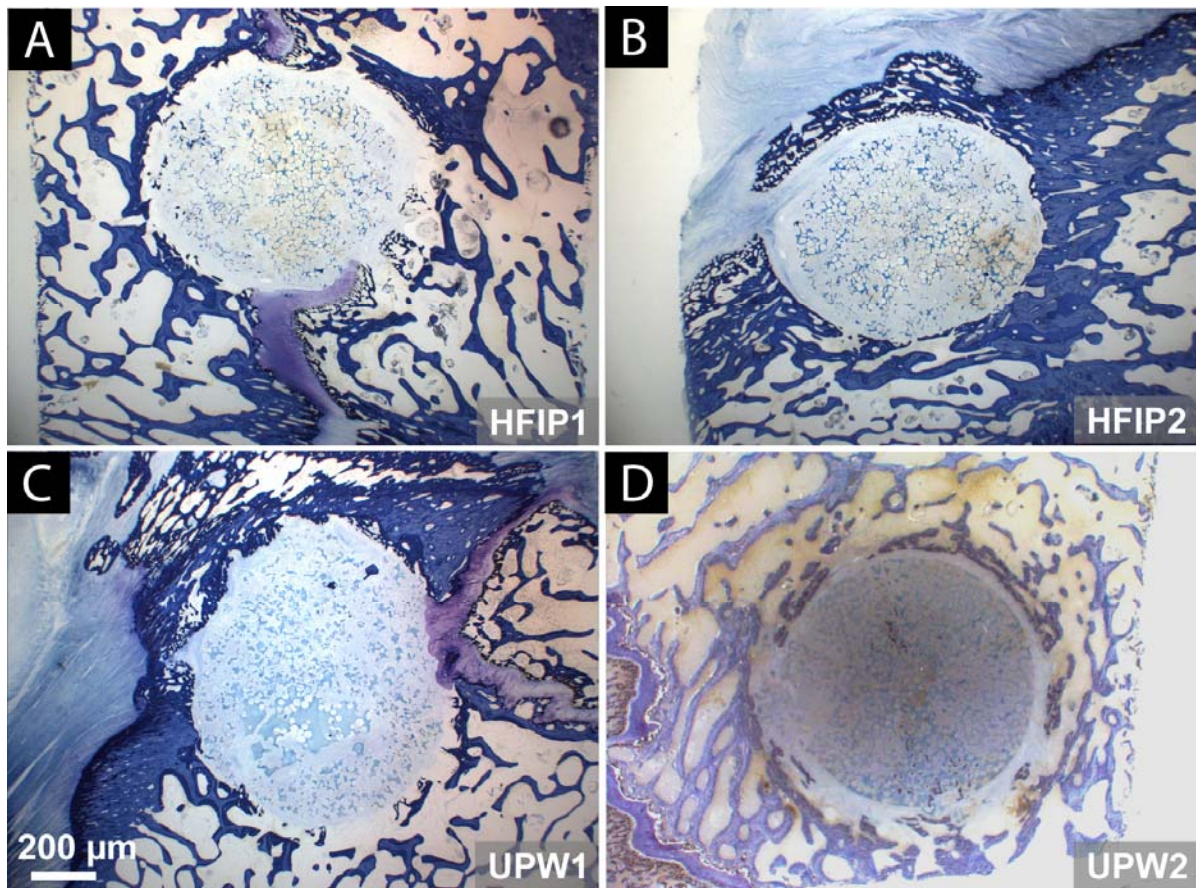


Fig. 3: Histological appearance of the ground sections after toluidine blue staining. Overview of the defect area including four different implant types: HFIP1, HFIP2, UPW1, UPW2

In general, the SF implants' degradation was slight, but stronger at the periphery than in the center of the scaffold (**Fig. 4**). Degradation could be microscopically visualized through loss of homogenous appearance of the implant matrix and when individual fibres could be recognized. The interconnective macroporosity of the SF implants remained well intact during the entire 8 weeks and led to sustained ingrowth of tissue. New bone formation at the periphery was minor and restricted to areas of direct contact between implant and the bone. However, throughout the different sections of the implant (periphery, middle part, center), formation of new bone was detected as small insular-like patches of dense deep blue matrix (von Kossa staining) with osteocyte-like cells trapped within their lacunae. Bone islands were more frequent towards the centre of the porous implants, and seamed with dense osteoid visible as a light blue matrix.

Foreign body granuloma (giant cells, plasma cells and lymphocytes infiltration)

Inflammatory cells were still visible in the macroporous structure of the implant at 8 weeks after implantation. The infiltration of the implant by lymphocytes and plasma cells as well as macrophages and multinuclear foreign body giant cells (GCs) was less dominant towards the centre of the implant (**Fig. 4, 5**). In general, clusters of dense proliferation were more present in the periphery of the scaffold than in the middle or central sections. Noteworthy, there was no appearance of neutrophils that usually represent the first line of defense after injuries and/or infections. Overall, the presence of lymphocytes and plasma cells was moderate. The presence of a large number of these cell types are typically implicated in the pathology of many chronic inflammations.

Bone formation and scaffold bone interaction

In all scaffold types and regions, bone was produced by intramembranous bone formation as indicated by the presence of congregated mesenchymal cells and numerous small blood vessels. The cells condensed, aligned and started to produce the organic matrix of the osteoid (OS) with osteocytes (OC) entrapped in their lacunae (OS, light blue; **Fig. 5**). Osteoblasts started to line the OS and deposit calcium salts producing the calcified bone matrix (CB). Signs of endochondral bone formation, such as the presence of chondrocytes, hypertrophic chondrocytes or glycosaminoglycan deposition, were absent.

In regions of direct contact between the implant material and the bone, moderate bone ingrowth could be observed, independent of implant type. Spontaneous bone formation took place within different regions of the porous structure of the implants (periphery, middle and central part) resulting in regional clusters of new bone. However, the total amount of new bone was low and osteoinductivity of the SF material was absent, as expected. The interface between the SF implants and the surrounding bone was further evaluated using ground and thin histology sections.

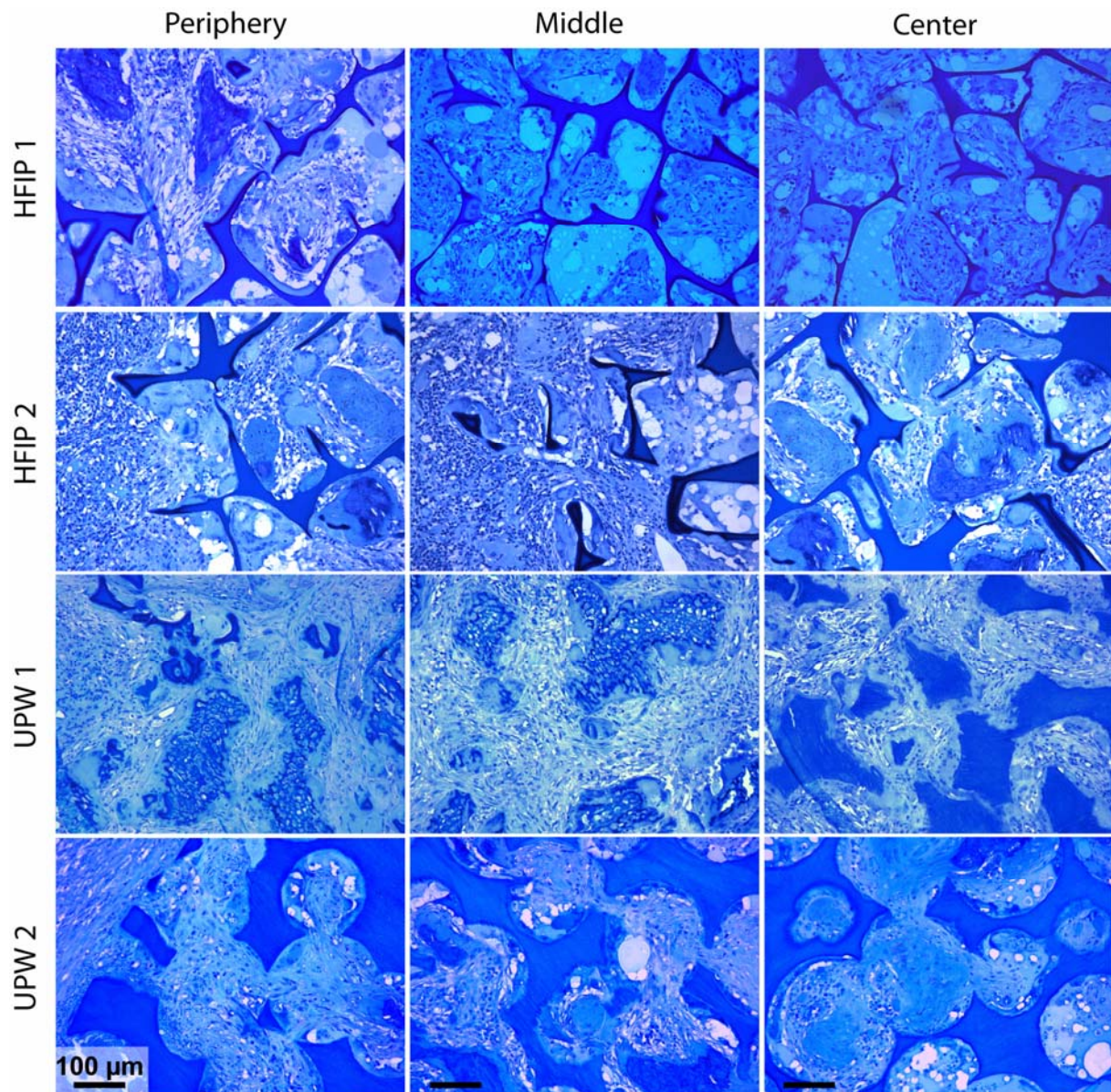


Fig. 4: Cell infiltration and inflammatory cells in the four different implant types and the axial section (P, M, C). Histological appearance of the thin sections after staining with toluidine blue. Clusters of proliferating lymphocytes are visible as dark blue dots. Image magnification: 10 x. Scale bar = 100 μm.

The empty transition zone between the scaffold and the old bone was filled with ingrowing tissue. Bone ingrowth from the periphery could be observed in the case of direct scaffold to bone contact.

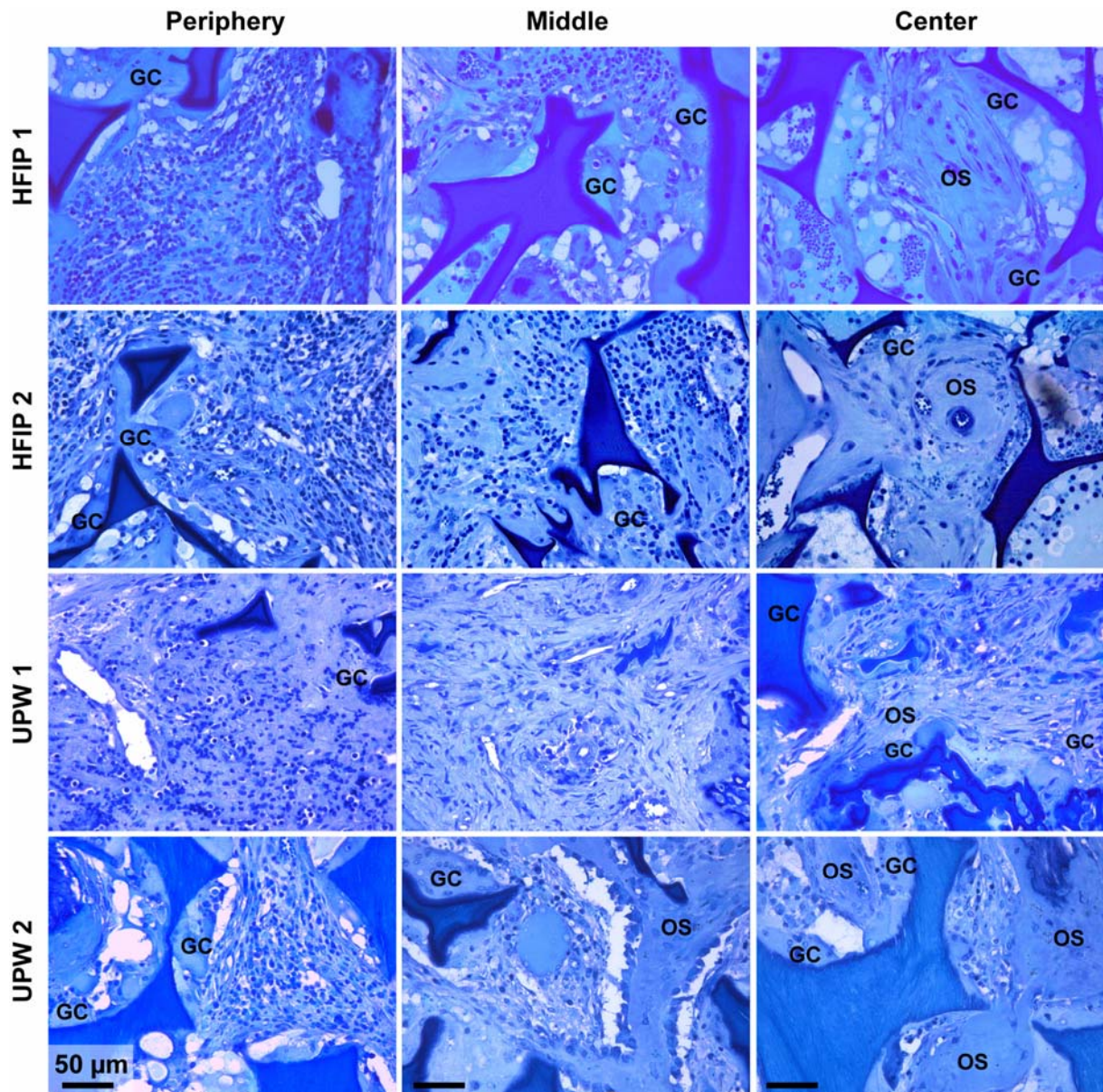


Fig. 5: Infiltration of (GCs) and formation of osteoid (OS) in the four different implant types and the axial section (periphery, middle, center). Histological appearance of thin sections after toluidine blue staining. Magnification of the image: 20 x; Scale bar = 50 μm.

The size of the transition zone varied between the individual implants independent of scaffold type. However, the formation of a fibrous capsule of connective tissue around the implant was not observed (**Fig. 6**). Osteoblasts started to fill out single pores with OS, which was further calcified from the center resulting in a dark calcified bone surrounded by the OS (Von Kossa, CB, dark blue-black; **Fig. 6**).

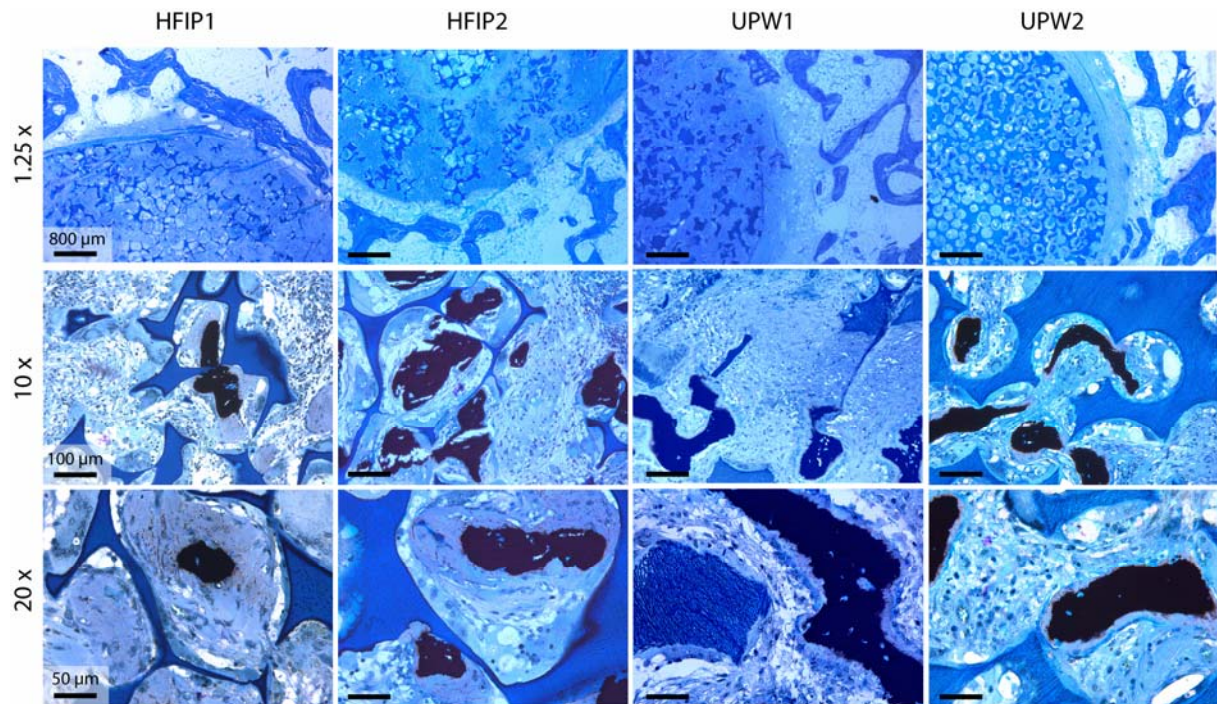


Fig. 6: Bone-implant transition zone and new bone formation in the four different scaffold types. Appearance of thin histology sections after von Kossa/Mc Neal staining. Osteoid is visible as blue light matrix and calcified bone is visualized in dark blue to black.

Co-existence of multinuclear foreign body GCs, scaffold degradation and bone formation

A relationship between GCs, scaffold degradation (SD) and new bone formation was obvious in all of the four different implant types. GCs did not inhibit the formation of new osteoid and calcified bone (CB) in its close proximity. Local SD by GCs was followed by the production of extracellular matrix and the calcification of the OS. The degradation of SF by GCs seemed to foster the direct contact between SF and OS or CB (**Fig. 7**). In this context, bone formation – after GCs mediated SD - followed a similar pattern as observed during bone remodeling in healthy bone.

Scaffold design and tissue morphology

The interconnectivity of the pores - as controlled by the scaffolding process (UPW or HFIP) - had a large effect on the localization of the newly formed bone in the porous structure. In the HFIP scaffolds, bone formation was mainly restricted to single pores forming single bone islands. In contrast, osteoid and calcified tissue in the pores of the UPW scaffolds started to fuse and fill the interconnected voids of the porous structures resulting in a trabecular-like morphology of the new bone. Moreover, the UPW scaffolds were able to conduct bone ingrowth from the periphery (**Fig. 7A**) and localize and guide new bone in the inner part (middle part, center) of the scaffold (**Fig. 7B, C**). Implants produced by the HFIP process using salt crystals as porogen exerted porous regions with low interconnectivity and small interconnective pore diameter (**Fig. 4, 8**).

Semi-quantitative histology and statistical analysis

Semiquantitative histology, based on a scoring system of the individual parameters (**Table 2**), did not reveal any fundamental difference between the four different scaffold types (**Table 3**). Throughout all types of scaffolds the presence of inflammatory cells such as GCs, lymphocytes and plasma cells tended to decrease towards the center of the scaffolds, correlating with the stage of SF resorption and formation of new bone or ingrowth of cells from the periphery towards the center. Vascularization alone did not follow this trend showing very similar results throughout the various implants. To statistically assess the effects of the different silk sources and scaffolding protocols on the investigated parameters, a post-hoc test analysis was performed (Scheffe) on the results obtained by semiquantitative scoring of the investigated parameter. Implants produced by UPW process showed significantly ($p < 0.05$) lower infiltration with lymphocytes and plasma cells (score mean \pm CI; 0.88 ± 0.25) than HFIP scaffolds (score mean \pm CI; 1.60 ± 0.24).

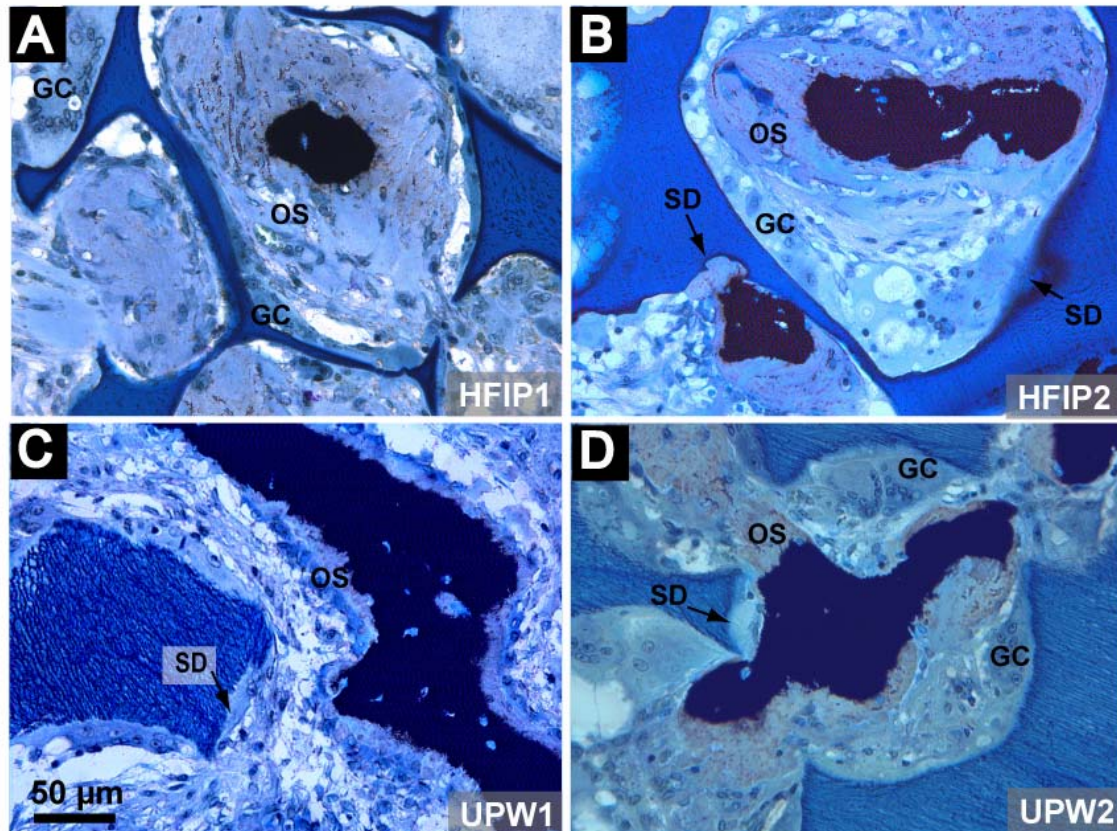


Fig. 7: Multinuclear foreign body GCs mediated scaffold degradation (SD) and formation of new bone. Appearance of thin histology sections after von Kossa/Mc Neal staining. Osteoid (OS) is visible as light blue matrix and calcified bone (CB) is visualized in dark blue to black. GCs and bone formation co-exist in close proximity and SD by FGC is followed by the deposition of OS and calcification of the bone. Magnification of the image from top to bottom: 20 x.

SF scaffolds produced with SF from source 2 (score mean \pm CI; 0.97 ± 0.23) attracted significantly less lymphocytes and plasma cells than SF from source 1 (score mean \pm CI; 1.50 ± 0.26). Furthermore, scaffolds produced by the UPW process using SF from source 2 (UPW2) showed significantly lower scaffold resorption and infiltration (score mean \pm CI; 0.51 ± 0.16) than HFIP scaffold produced using SF from source 1 (HFIP1; score mean \pm CI; 1.17 ± 0.16). The lower resorption of the scaffold coincided with significantly lower numbers of GCs found in this scaffold type ($p=0.00$).

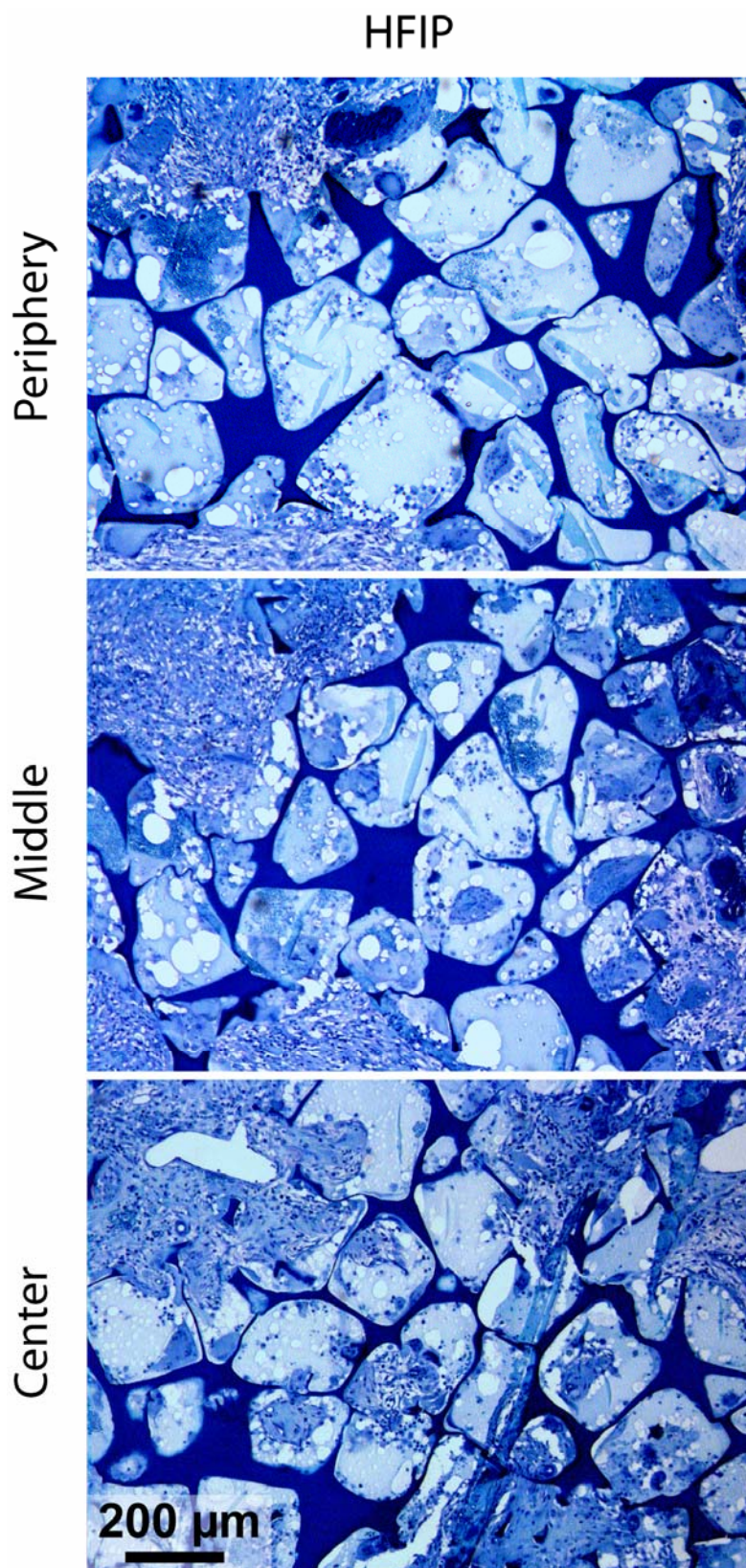


Fig. 8: Local clusters of empty pores with low pore interconnectivity and poor cell infiltration in the axial sections (Periphery, Middle, Center) of HFIP scaffolds. Appearance of the thin histology sections after toluidine blue staining. Magnification of the image: 5 x.

The presence of lymphocytes and plasma cells in UPW2 scaffolds was in general lower than in all the other scaffold types (UPW2, HFIP1, HFIP2). The choice of a specific scaffolding protocol or SF source did not significantly influence the outcomes of the other scored parameters (**Table 3**).

Table 3: Semi-quantitative analysis of scoring parameters (scoring levels *see* Table 2)

Parameter & Sections		Scores (means \pm SD)				
		Average	HFIP 1	HFIP 2	UPW 1	UPW 2
Giant cells	average		2.00 \pm 0.75	2.20 \pm 0.68	2.00 \pm 0.43	1.50 \pm 0.62
	central	1.68 \pm 0.6	1.6 \pm 0.9	1.6 \pm 0.9	2.0 \pm 0.0	1.5 \pm 0.0
	middle	1.92 \pm 0.6	1.6 \pm 0.5	1.8 \pm 0.5	2.0 \pm 0.0	1.7 \pm 0.0
	periphery	2.18 \pm 0.8	2.6 \pm 0.6	2.6 \pm 0.6	2.0 \pm 0.8	1.4 \pm 0.8
Lymphocytes and plasma cells	average		1.60 \pm 0.63	1.60 \pm 0.74	1.42 \pm 0.80	0.33 \pm 0.50
	central	0.90 \pm 0.7	1.0 \pm 0.7	1.2 \pm 1.0	1.3 \pm 1.0	0.2 \pm 0.4
	middle	1.20 \pm 0.8	1.8 \pm 0.4	1.8 \pm 0.4	1.3 \pm 1.0	0.2 \pm 0.4
	periphery	1.60 \pm 0.9	2.0 \pm 0.0	2.0 \pm 0.0	1.8 \pm 0.5	0.7 \pm 0.5
Bone in scaffold	average		1.00 \pm 0.65	1.27 \pm 0.79	0.58 \pm 0.66	1.00 \pm 0.69
	central	0.63 \pm 0.7	0.6 \pm 0.5	1.0 \pm 1.0	0.3 \pm 0.5	0.7 \pm 0.8
	middle	1.17 \pm 0.8	1.0 \pm 0.7	1.6 \pm 0.5	0.8 \pm 1.0	1.3 \pm 0.8
	periphery	1.09 \pm 0.6	1.4 \pm 0.5	1.2 \pm 0.83	0.8 \pm 0.5	1.0 \pm 0.0
Bone islands in pores	average		0.20 \pm 0.35	0.53 \pm 0.41	0.42 \pm 0.66	0.33 \pm 0.32
	central	0.14 \pm 0.4	0.0 \pm 0.0	0.4 \pm 0.54	0.0 \pm 0.0	0.2 \pm 0.4
	middle	0.46 \pm 0.7	0.2 \pm 0.4	0.8 \pm 0.83	0.5 \pm 1.0	0.3 \pm 0.5
	periphery	0.51 \pm 0.7	0.4 \pm 0.5	0.4 \pm 0.54	0.8 \pm 0.9	0.5 \pm 0.8
Scaffold resorption	average		1.13 \pm 0.35	1.20 \pm 0.41	0.92 \pm 0.66	0.11 \pm 0.32
	central	0.69 \pm 0.5	1.0 \pm 0.0	1.0 \pm 0.0	0.8 \pm 0.5	0.0 \pm 0.0
	middle	0.78 \pm 0.6	1.0 \pm 0.0	1.2 \pm 0.5	0.8 \pm 0.5	0.2 \pm 0.4
	periphery	1.05 \pm 0.8	1.4 \pm 0.5	1.4 \pm 0.5	1.25 \pm 1.0	0.2 \pm 0.4
Osteoid	average		0.67 \pm 0.81	0.53 \pm 0.63	0.50 \pm 0.91	0.78 \pm 1.0
	central	0.35 \pm 0.6	0.4 \pm 0.9	0.4 \pm 0.5	0.3 \pm 0.5	0.3 \pm 0.5
	middle	0.59 \pm 0.8	0.6 \pm 0.9	0.6 \pm 0.5	0.5 \pm 1.0	0.6 \pm 0.5
	periphery	0.92 \pm 1.0	1.0 \pm 0.7	0.6 \pm 0.9	0.8 \pm 0.5	1.3 \pm 1.3
Vascularization	average		2.00 \pm 0.92	1.33 \pm 0.61	1.58 \pm 0.74	2.00 \pm 0.84
	central	1.65 \pm 0.9	2.2 \pm 0.8	1.4 \pm 0.9	1.0 \pm 0.0	2.0 \pm 0.9
	middle	1.73 \pm 0.9	1.8 \pm 1.0	1.2 \pm 0.4	1.8 \pm 0.9	2.2 \pm 0.8
	periphery	1.81 \pm 0.6	2.0 \pm 1.0	1.4 \pm 0.5	2.0 \pm 0.8	1.8 \pm 0.9
Fibrous tissue	average		1.35 \pm 0.50	1.07 \pm 0.25	1.42 \pm 0.51	1.28 \pm 0.46
	central	1.17 \pm 0.4	1.4 \pm 0.5	1.0 \pm 0.0	1.3 \pm 0.5	1.2 \pm 0.4
	middle	1.26 \pm 0.54	1.2 \pm 0.4	1.0 \pm 0.0	1.5 \pm 0.6	1.3 \pm 0.5
	periphery	1.41 \pm 0.	1.6 \pm 0.5	1.2 \pm 0.4	1.5 \pm 0.6	1.3 \pm 0.5

DISCUSSION

The specific aims of this study were twofold: (i) to evaluate the effect of different silk sources, and (ii) to assess the effect of different scaffolding protocols used to produce macroporous SF scaffolds [12, 14, 30] on several cellular response indicators such as inflammation, bone formation and osteoconductivity at the implantation site. For these purposes, porous SF cylinders of 13 mm length and 8 mm in diameter were implanted into drill hole defects in cancellous bone of sheep. The respective tissue was harvested after 8 weeks and evaluated macroscopically and histologically. Histological evaluations were performed qualitatively and semiquantitatively.

Animal model

In light of the subject of this article, i.e. a biocompatibility testing of various SF scaffolds in parallel, the drill hole defect model in sheep was chosen because of three reasons: (i) its relevance for a prospective human use [27], (ii) its potential to minimize the number of test animals while still yielding sufficient data for statistical evaluation, and finally (iii) its comparably low impact on the animals using standardized defect locations with direct accessibility. From both ethical and financial points of view, small experimental animals such as mice, rats or rabbits could be preferred animal models to test biomaterials for their use as bone substitutes [27]. However, the large divergence between rodents and humans in size, weight and bone metabolism may compromise the relevance of rodent models for an extrapolation to humans. In contrast, sheep dispose of similar weight and bone metabolism as humans, are of similar size and calm character, and can be cost efficiently accommodated under appropriate conditions. In this study, exclusively two year old sheep were used to assure comparable bone physiology and weight [24]. Sheep were operated bilaterally at the proximal and distal humerus and femur as described previously [27]. The preoperative positioning of the extremities to ensure an optimal placement of the drill hole was

challenging. During surgery, this was of particular importance for the condyles of the distal humerus, as the drill could easily slip and harm the elbow joint. Unfortunately, the surrounding structure did not allow for an application of a drill template at the described location. By an appropriate surgical technique and the use of anatomical landmarks this problem could be overcome. From earlier experience we knew that the cortical drill hole model allowed the operated sheep to move their limbs shortly after surgery, therefore reducing post-operational local pain to a minimum [27-29]. These findings were further corroborated in the present study. Moreover, we abstained from using empty control defects, as previous experiments conducted in our group revealed that empty defects were generally filled with fibrous tissue within the given experimental time span (Nuss et al., unpublished data). This measure further helped to reduce the number of animals to a minimum still satisfying the requirements for statistical analysis. Neither the macroscopic evaluation of the defect during surgery nor after slaughter of the animal could clarify any reason(s) for the transient lameness of sheep number 3102 at the distal right femur and the associated swelling of the adjacent soft parts. The most likely cause was bleeding of a small vessel after surgery and subsequent seroma formation that was almost subsided at the time of sacrifice.

Sample extraction for histology

After sacrifice, cuboid samples were cut out from both humerus and femur containing the SF scaffolds and adjacent bone. Four out of 24 bone cuboids did not or only partly contain the respective defects with the implanted SF scaffold. As a consequence, only 20 explants were subjected to histological analysis. For histological assessment, sections were cut out from the centre of the cylinder. The centre section was chosen because it was expected to show the least bone ingrowth or scaffold resorption. Generally, resorption of a biomaterial as well as cell ingrowth proceed from the periphery to the center [29]. Moreover, the fact that all sections stemmed from the same location of the implant was assumed to standardize the histological evaluation.

Histology and statistical analysis

All SF scaffolds were found to be biocompatible, and there were no excessive foreign body reactions. The macroscopic evaluation of the defects right after sacrifice did not reveal any encapsulation of the implant by a fibrous capsule of connective tissue or a hyperemia of adjacent bone or soft tissue (**Fig. 3, 6**). The thickness of the transition zone between the adjacent bone and the SF scaffold showed large variations between different defects and even between different locations at the bone-scaffold interface of a single defect. These differences probably stemmed from small geometrical variations of each individual defect resulting in some local lack of fit that could have caused micro-movements of the implant in the defect. To improve the fit the use of slightly larger SF scaffolds should be considered for future studies. In principle, SF scaffolds, when in a swollen state, exert a sponge-like character that should allow an insertion of slightly larger scaffolds into the defects.

The previously observed slow biodegradation of SF materials *in vivo* [10, 14, 16, 18] was further corroborated in the present study. The different scaffold types largely maintained their initial morphology throughout the 8 weeks of the test and provided sufficiently stable mechanical support and conduction for ingrowing tissue and vascularization (**Fig. 3, 4**). Nevertheless, we observed initial indications for SF biodegradation in the periphery of all scaffold types. The initially smooth SF scaffolds appeared to be roughened and single SF fibers became visible. The presence of small particulates of SF within the vacuoles of local macrophages and GCs suggested cellular biodegradation following phagocytosis, as generally observed when biodegradable biomaterials were implanted in bone [29]. The foreign body reactions were moderate and generally more distinct in the periphery and the middle section than in the center of the scaffold. However, large accumulations of GCs were absent in any part of the scaffolds. While the presence of macrophages during the degradation of biomaterials in bone could be classified as physiological [29, 31], the presence of GCs remains ambiguous in this context. Generally, biomaterials from non-

autologous origin are likely to induce a moderate foreign body reaction, and the response to SF was comparable to most commonly used synthetic materials [28, 31]. GCs result from fusion of macrophages in order to digest larger amount of foreign body material. Previous studies in our group suggested that the presence of GCs in direct contact with osteoblasts and their progenitor cells (**Fig. 7**) could be classified as biocompatible, if indications for a large accumulation of lymphocytes, plasma cells or a fibrous capsule of connective tissue were absent (Nuss et al., unpublished data). In the present study, we observed no indications for massive inflammation. Therefore, we propose a physiological and non-inflammatory degradation of the SF. GCs were always observed in close proximity to osteoblasts and progenitor cells, and SD by GCs was followed by deposition of OS and subsequent calcification of the matrix in the same location (**Fig. 7**). The processing of SF by GCs seemed to foster the deposition of the newly formed bone in close contact with the SF scaffold.

Our observations resembled physiological processes during bone remodeling, such as the attraction of osteoblasts and bone formation following bone resorption by multinuclear osteoclast. It is still elusive, whether the observed coexistence of GCs and osteoblasts during SF degradation is a coincidence and based on biomaterial degradation that may have triggered the fusion of macrophages to become GCs or triggered by cellular cross-talk between GCs and osteoblasts. Further studies with a specific focus on this subject will be necessary to elucidate this relationship. In general, the amount of new bone was very low in all scaffold types and could not be quantified using radiological images taken from the defect.

Both SF scaffolding processes (HFIP and UPW) produced macroporous implants that supported tissue infiltration and sufficient vascularization of the defect. However, HFIP scaffolds displayed local clusters of empty, unfilled pores throughout the sections of the defect (periphery, middle part, center – **Fig. 8**). This was probably due to inferior pore interconnectivity and locally insufficient interconnective pore diameters in this scaffold type in contrast to UPW scaffolds (**Fig. 8**). The visibly increased pore interconnectivity and interconnective pore

diameters in UPW scaffolds was achieved through sintering of paraffin microspheres and has been reported earlier [14]. The beneficial effects of an elevated interconnectivity in combination with enlarged interconnective pore diameters on the homogenous distribution of *in vitro* tissue engineered bone-like tissue on UPW scaffolds, using hMSC under osteogenic conditions, has already been demonstrated [14]. In the present study, the improved design of the porous structure in this scaffold type allowed for a uniform ingrowth of tissue and the fusion of single bone islands into local, trabecular-like clusters of bone (**Fig. 6, 7, 9**). Moreover, osteoconduction over a distance of more than one pore diameter was exclusively observed in this scaffold type (**Fig. 7, 9**). Other authors reported that the interconnective pore diameter must exceed 50 μm to allow the growth of new bone into the porous structure of an artificial implant *in vivo* [32-34]. Our evidence supports these findings and suggests that in porous implants a minimal interconnective pore diameter is pivotal for successful bone growth rather than the overall pore diameter itself [35, 36]. For an improvement in HFIP based scaffolding we recommend to further increase the interconnective diameter. For this aim we suggest the salt crystal matrix used as porogen be exposed to a high relative humidity (95%) environment before filling the void space with the solution of SF in HFIP. The controlled high humidity treatment is likely to fuse the contact sites between the salt crystals and thus allows SF scaffolding with improved pore interconnectivity and pore sizes after leaching the porogen [37].

The statistical analysis of the semiquantitative results obtained from the scored parameters (**Table 2**) revealed significantly ($p < 0.05$) lower infiltration of the UPW scaffold with inflammatory cells, such as lymphocytes and plasma cells, which further coincided with a significantly lower ($p < 0.05$) scaffold resorption. The differences were most prominent in the periphery of the scaffolds (**Table 3**). As a consequence of the modifications of the scaffolding process the used UPW protocol, in contrast to the HFIP protocol, led to scaffolds which more exactly fitted the defect (diameter = 8 mm; length 13 mm) and, exhibited a smoother surface. Because of the need to cut HFIP scaffolds out of bigger specimens, their

surface to the adjacent bone was rougher. Increased scaffold surface and the presence of small fragments of SF material are likely to attract increased numbers of inflammatory cells. The fact that both scaffold resorption and infiltration with lymphocytes and plasma cells were significantly lowered with the UPW2 scaffold as compared to the other scaffold types further corroborated this relationship. Significantly increased infiltration of lymphocytes and plasma cells was also observed in scaffolds produced with SF from silk source 1.

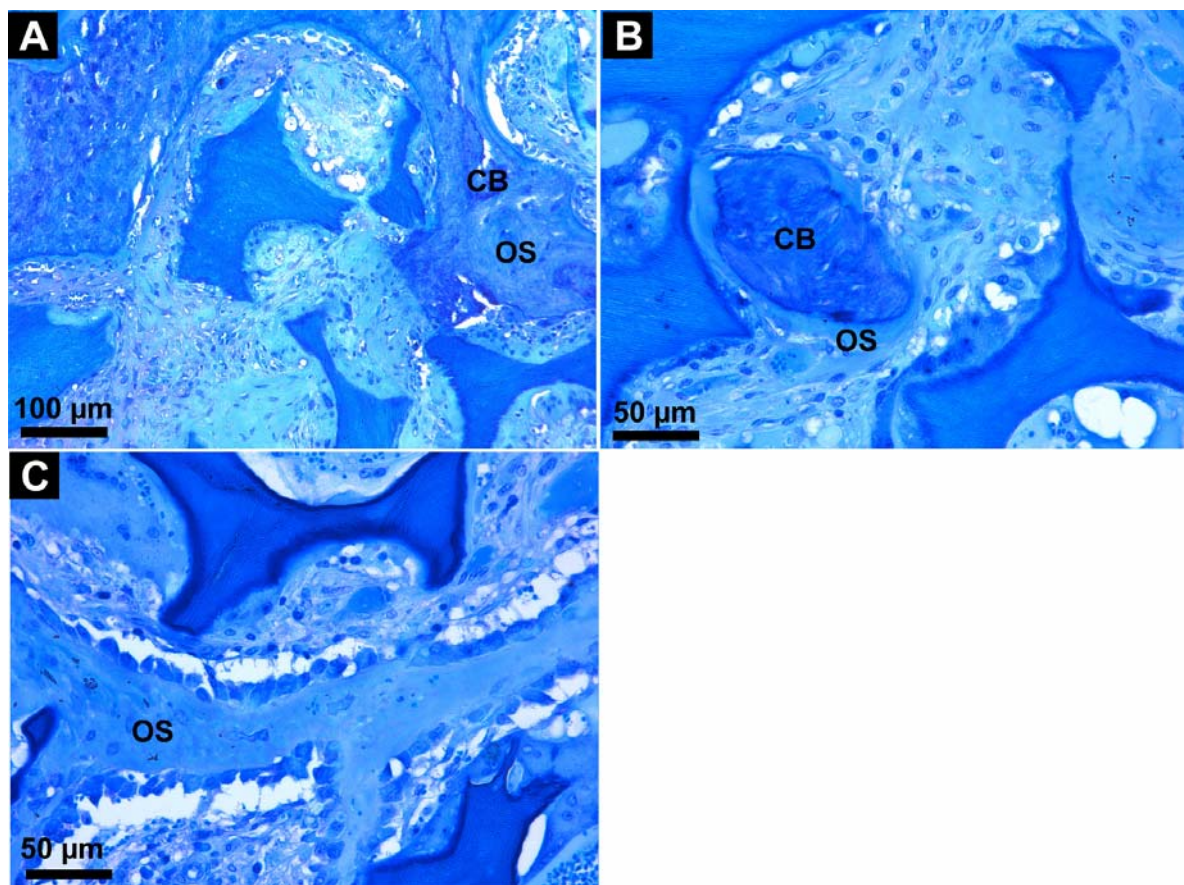


Fig. 9: Guidance of new bone formation in UPW scaffolds. Appearance of thin histology sections after von Kossa/Mc Neal staining. Osteoid (OS) is visible as light blue matrix and calcified bone (CB) is visualized in dark blue to black. (A) Bone ingrowth from the periphery. Deposition of OS is followed by the calcification of the matrix (CB). (B) New bone formation in a single pore at the interface to the SF. (C) Conduction of newly formed bone in the interconnected porous voids of UPW scaffolds. Osteoblasts are lining the OS. Magnification of the image A = 10 x; B, C = 20 x.

However, these differences were only observed between UPW scaffolds produced from different SF sources. HFIP scaffolds, in contrast, led to identical frequencies in lymphocytes and plasma cells independent of the two SF sources used (**Table 3**).

Therefore, the observed differences are not likely to stem from diverse qualities of the two raw materials. As mentioned above, UPW1 scaffolds were partly cracked and thus had to be inserted in several fragments into the defects. The lower physical integrity of the scaffold may have as well contributed to the higher infiltration of lymphocytes and plasma cells into this scaffold type. Nevertheless, variations in the purification protocol as well as contamination from parasites, nutrition or inappropriate breeding of the silk worms may have also affected the composition and purity of SF and consequently influenced the mechanical properties as well as the biocompatibility of regenerated SF. For future applications of SF as biomedical implants, rigorously standardized analytical methods will be pivotal to assure purity and quality of SF extracted from different batches of silk cocoons.

CONCLUSION

In general, SF scaffolds did not exert measurable osteoinductive properties as clearly indicated by the low amounts of new bone found in the defects. Further measures would be necessary to improve SF scaffolds in this respect, such as loading with growth factors for pulsed and/or sustained release. A most important finding was that neither the scaffolding protocols (HFIP, UPW) nor the two different SF sources negatively affected the generally favorable biocompatibility of the SF scaffolds. Scaffold design with large interconnective pore diameter allowed the fusion of bone islands, which formed in different pores of the scaffold. The local network of trabecular-like bone was comparable to that in cancellous bone. Improvements in the osteoinductive properties of SF scaffolds, e.g., by accommodation of growth factors for sustained release, are subject of

ongoing studies and should further improve regeneration time and quality of regenerated bone.

ACKNOWLEDGEMENTS

We thank Trudel (Zurich, Switzerland) and M. Tsukada, Institute of Sericulture, Tsukuba, Japan for silk cocoons. Financial support was from AO (AO Biotechnology Research Grant 2003), the Association for Orthopaedic Research and ETH Zurich (TH-Gesuch 26.04-1). We also thank the NIH (NIBIB) for support through the Tissue Engineering Resource Center (TERC).

REFERENCES

1. L. Ma, L.W. Zheng, L.K. Cheung, Inhibitory effect of nicotine on bone regeneration in mandibular distraction osteogenesis, *Front Biosci* 12 (2007) 3256-62.
2. N. Chbinou, J. Frenette, Insulin-dependent diabetes impairs the inflammatory response and delays angiogenesis following Achilles tendon injury, *Am J Physiol Regul Integr Comp Physiol* 286 (5) (2004) R952-7.
3. R.W. Bucholz, Nonallograft osteoconductive bone graft substitutes, *Clin Orthop Relat Res* (395) (2002) 44-52.
4. A.N. Kager, M. Marks, T. Bastrom, P.O. Newton, Morbidity of iliac crest bone graft harvesting in adolescent deformity surgery, *J Pediatr Orthop* 26 (1) (2006) 132-4.
5. S.N. Parikh, Bone graft substitutes: past, present, future, *J Postgrad Med* 48 (2) (2002) 142-8.
6. D. Bettin, H. Bohm, M. Clatworthy, D. Zurakowski, T.M. Link, Regeneration of the donor side after autogenous fibula transplantation in 53 patients: evaluation by dual x-ray absorptiometry, *Acta Orthop Scand* 74 (3) (2003) 332-6.
7. D.C. Rees, F.S. Haddad, Bone transplantation, *Hosp Med* 64 (4) (2003) 205-9.
8. J.O. Hollinger, J. Brekke, E. Gruskin, D. Lee, Role of bone substitutes, *Clin Orthop Relat Res* (324) (1996) 55-65.
9. P.M. Cunniff, S.A. Fossey, M.A. Auerbach, J.W. Song, D.L. Kaplan, W. Adams, R.K. Eby, D. Mahoney, D. Deborah, D.L. Vezie, Mechanical and thermal properties of Dragline Silk from the Spider *Nephila cavipes*, *Polymers for Advanced Technologies* 5 (1994) 401-410.
10. G.H. Altman, F. Diaz, C. Jakuba, T. Calabro, R.L. Horan, J. Chen, H. Lu, J. Richmond, D.L. Kaplan, Silk-based biomaterials, *Biomaterials* 24 (3) (2003) 401-16.
11. L. Meinel, S. Hofmann, V. Karageorgiou, C. Kirker-Head, J. McCool, G. Gronowicz, L. Zichner, R. Langer, G. Vunjak-Novakovic, D.L. Kaplan, The inflammatory responses to silk films in vitro and in vivo, *Biomaterials* 26 (2) (2005) 147-55.
12. R. Nazarov, H.J. Jin, D.L. Kaplan, Porous 3-D scaffolds from regenerated silk fibroin, *Biomacromolecules* 5 (3) (2004) 718-26.
13. U.J. Kim, J. Park, H.J. Kim, M. Wada, D.L. Kaplan, Three-dimensional aqueous-derived biomaterial scaffolds from silk fibroin, *Biomaterials* 26 (15) (2005) 2775-85.

14. L. Uebersax, H. Hagenmuller, S. Hofmann, E. Gruenblatt, R. Muller, G. Vunjaknovakovic, D.L. Kaplan, H.P. Merkle, L. Meinel, Effect of Scaffold Design on Bone Morphology in Vitro, *Tissue Eng* 12 (12) (2006) 3417-29.
15. H.J. Jin, S.V. Fridrikh, G.C. Rutledge, D.L. Kaplan, Electrospinning Bombyx mori silk with poly(ethylene oxide), *Biomacromolecules* 3 (6) (2002) 1233-9.
16. L. Meinel, V. Karageorgiou, R. Fajardo, B. Snyder, V. Shinde-Patil, L. Zichner, D. Kaplan, R. Langer, G. Vunjak-Novakovic, Bone tissue engineering using human mesenchymal stem cells: effects of scaffold material and medium flow, *Ann Biomed Eng* 32 (1) (2004) 112-22.
17. L. Meinel, O. Betz, R. Fajardo, S. Hofmann, A. Nazarian, E. Cory, M. Hilbe, J. McCool, R. Langer, G. Vunjak-Novakovic, H.P. Merkle, B. Rechenberg, D.L. Kaplan, C. Kirker-Head, Silk based biomaterials to heal critical sized femur defects, *Bone* 39 (4) (2006) 922-31.
18. L. Meinel, R. Fajardo, S. Hofmann, R. Langer, J. Chen, B. Snyder, G. Vunjak-Novakovic, D. Kaplan, Silk implants for the healing of critical size bone defects, *Bone* 37 (5) (2005) 688-98.
19. S. Hofmann, H. Hagenmuller, A.M. Koch, R. Muller, G. Vunjak-Novakovic, D.L. Kaplan, H.P. Merkle, L. Meinel, Control of in vitro tissue-engineered bone-like structures using human mesenchymal stem cells and porous silk scaffolds, *Biomaterials* 28 (6) (2007) 1152-62.
20. J. Chen, R.L. Horan, D. Bramono, J.E. Moreau, Y. Wang, L.R. Geuss, A.L. Collette, V. Volloch, G.H. Altman, Monitoring Mesenchymal Stromal Cell Developmental Stage to Apply On-Time Mechanical Stimulation for Ligament Tissue Engineering, *Tissue Eng* 12 (11) (2006) 3085-95.
21. V. Karageorgiou, M. Tomkins, R. Fajardo, L. Meinel, B. Snyder, K. Wade, J. Chen, G. Vunjak-Novakovic, D.L. Kaplan, Porous silk fibroin 3-D scaffolds for delivery of bone morphogenetic protein-2 in vitro and in vivo, *J Biomed Mater Res A* 78 (2) (2006) 324-34.
22. L. Uebersax, H.P. Merkle, L. Meinel, Insulin-like growth factor I releasing silk fibroin scaffolds induce chondrogenic differentiation of human mesenchymal stem cells, *J Control Release* 127 (1) (2008) 12-21.
23. J.L. Kuhn, S.A. Goldstein, M.J. Ciarelli, L.S. Matthews, The limitations of canine trabecular bone as a model for human: a biomechanical study, *J Biomech* 22 (2) (1989) 95-107.

24. D.M. Nunamaker, Experimental models of fracture repair, *Clin Orthop Relat Res* (355 Suppl) (1998) S56-65.
25. P. Augat, K. Margevicius, J. Simon, S. Wolf, G. Suger, L. Claes, Local tissue properties in bone healing: influence of size and stability of the osteotomy gap, *J Orthop Res* 16 (4) (1998) 475-81.
26. A.G. Bosanquet, A.N. Goss, The sheep as a model for temporomandibular joint surgery, *Int J Oral Maxillofac Surg* 16 (5) (1987) 600-3.
27. K.M. Nuss, J.A. Auer, A. Boos, B. von Rechenberg, An animal model in sheep for biocompatibility testing of biomaterials in cancellous bones, *BMC Musculoskelet Disord* 7 (2006) 67.
28. M.C. von Doernberg, B. von Rechenberg, M. Bohner, S. Grunenfelder, G.H. van Lenthe, R. Muller, B. Gasser, R. Mathys, G. Baroud, J. Auer, In vivo behavior of calcium phosphate scaffolds with four different pore sizes, *Biomaterials* 27 (30) (2006) 5186-98.
29. A. Oberle, F. Theiss, M. Bohner, J. Muller, S.B. Kastner, C. Frei, I. Boecken, K. Zlinszky, S. Wunderlin, J.A. Auer, B. von Rechenberg, [Investigation about the clinical use of brushite- and hydroxylapatite-cement in sheep], *Schweiz Arch Tierheilkd* 147 (11) (2005) 482-90.
30. L. Meinel, V. Karageorgiou, S. Hofmann, R. Fajardo, B. Snyder, C. Li, L. Zichner, R. Langer, G. Vunjak-Novakovic, D.L. Kaplan, Engineering bone-like tissue in vitro using human bone marrow stem cells and silk scaffolds, *J Biomed Mater Res A* 71 (1) (2004) 25-34.
31. D. Apelt, F. Theiss, A.O. El-Warrak, K. Zlinszky, R. Bettschart-Wolfisberger, M. Bohner, S. Matter, J.A. Auer, B. von Rechenberg, In vivo behavior of three different injectable hydraulic calcium phosphate cements, *Biomaterials* 25 (7-8) (2004) 1439-51.
32. B. Flautre, M. Descamps, C. Delecourt, M.C. Blary, P. Hardouin, Porous HA ceramic for bone replacement: role of the pores and interconnections - experimental study in the rabbit, *J Mater Sci Mater Med* 12 (8) (2001) 679-82.
33. F.R. Rose, L.A. Cyster, D.M. Grant, C.A. Scotchford, S.M. Howdle, K.M. Shakesheff, In vitro assessment of cell penetration into porous hydroxyapatite scaffolds with a central aligned channel, *Biomaterials* 25 (24) (2004) 5507-14.

34. J.X. Lu, B. Flautre, K. Anselme, P. Hardouin, A. Gallur, M. Descamps, B. Thierry, Role of interconnections in porous bioceramics on bone recolonization in vitro and in vivo, *J Mater Sci Mater Med* 10 (2) (1999) 111-20.
35. A.I. Itala, H.O. Ylanen, C. Ekholm, K.H. Karlsson, H.T. Aro, Pore diameter of more than 100 microm is not requisite for bone ingrowth in rabbits, *J Biomed Mater Res* 58 (6) (2001) 679-83.
36. V. Karageorgiou, D. Kaplan, Porosity of 3D biomaterial scaffolds and osteogenesis, *Biomaterials* 26 (27) (2005) 5474-91.
37. W.L. Murphy, R.G. Dennis, J.L. Kileny, D.J. Mooney, Salt fusion: an approach to improve pore interconnectivity within tissue engineering scaffolds, *Tissue Eng* 8 (1) (2002) 43-52.

CHAPTER IV

Insulin-like growth factor I releasing silk fibroin scaffolds induce chondrogenic differentiation of human mesenchymal stem cells

Lorenz Uebersax, Hans P. Merkle, Lorenz Meinel

Institute of Pharmaceutical Sciences, ETH Zurich, Zurich, Switzerland

Slightly shortened version of this chapter is published in:

J Control Release 127 (1) (2007) 12-21

ABSTRACT

Growth factor releasing scaffolds are an emerging alternative to autologous or allogeneous implants, providing a biologically active template for tissue (re)generation. The goal of this study is to evaluate the feasibility of controlled insulin-like growth factor I (IGF-I) releasing silk fibroin (SF) scaffolds in the context of cartilage repair. The impact of manufacturing parameters (pH, methanol treatment and drug load) was correlated with IGF-I release kinetics using ELISA and potency tests. Methanol treatment induced water insolubility of SF scaffolds, allowed the control of bioactive IGF-I delivery and did not affect IGF-I potency. The cumulative drug release correlated linearly with the IGF-I load. To evaluate the chondrogenic potential of the scaffolds, hMSC were seeded on unloaded and IGF-I loaded scaffolds in TGF- β supplemented medium. Chondrogenic differentiation of hMSC was observed on IGF-I loaded scaffolds, starting after 2 weeks and more strongly after 3 weeks, whereas no chondrogenic responses were observed on unloaded control scaffolds. IGF-I loaded porous SF scaffolds have the potential to provide chondrogenic stimuli to hMSC. Evidence for *in vivo* cartilage (re)generation must be demonstrated by future, pre-clinical proof of concept studies.

INTRODUCTION

Biomaterials used for tissue engineering should assist in local support and formation of functional tissue during *in vitro* culture of cellular constructs or *in vivo* repair of defects, with the aim to restore the morphological and physiological archetype of the desired tissue. Although a large number of materials feature biocompatible and conductive properties, their functional outcomes are often limited by insufficient mediation of stimuli that are needed to induce tissue specific self regulation upon injury or disease. Physiologically, tissue repair is partly guided by the production of local regulatory factors such as growth factors (GF). GF are produced by specialized cells and act in an autocrine or paracrine manner, or they are bound to components of the extra-cellular matrix, e.g., to binding proteins, negatively charged heparin sulfates or matrix proteins such as collagens [1]. Insulin-like growth factor I (IGF-I) is entrapped in the mineralized matrix of bone during formation [2, 3]. Following osteoclastic resorption, IGF-I is actively released during bone remodeling and supports the induction of new bone through activation of osteoblasts [4, 5]. Moreover, IGF-I was reported to affect cell proliferation, by stimulating growth in various progenitor cell types and by blocking apoptosis [6]. Furthermore, IGF-I modulated chondrogenesis in hMSC induced the expression of chondrocyte markers, and, together with TGF- β 1, showed additive effects on chondrogenesis [7, 8].

In order to reduce the regeneration time and quality of successful tissue repair the use of drug loaded biomaterials has found increasing interest [9, 10], but so far with rather limited market entry. Since 2001 health authorities approved a collagen carrier delivery system (OP-1; from Stryker Biotech) loaded with recombinant human bone morphogenetic protein 7 (BMP-7), to aid in recalcitrant long bone nonunion where autografts are unfeasible and alternative treatments failed. INFUSE® Bone Graft (from Medtronic Inc.) is another absorbable collagen sponge (ACS) carrier that delivers recombinant human bone morphogenetic protein-2 (BMP-2), and is clinically used in combination with a

metal based device for spinal fusion in skeletally mature patients with degenerative disc disease. Further approaches for growth factor delivery in skeletal tissue engineering included the adsorption of BMP-2 on various biomaterials such as natural or synthetic collagen matrices [11], a hyaluronic acid-based scaffold [12], titanium fiber meshes and porous calcium phosphates [13]. Other strategies were aimed at the direct encapsulation of IGF-I in poly(D,L-lactide-co-glycolide) microparticles, supporting the bridging of drill hole defects in a sheep tibia model [5].

Manufacturing processes of drug loaded scaffolds are challenging [14]. In fact, most synthetic degradable polymers used to prepare load-bearing scaffolds do not allow for a direct embedding of growth factors, because the manufacturing conditions needed for scaffolding - such as shear, heat, use of organic solvents, high ionic strengths or extreme pH during processing – are likely to compromise the biological activity of the GF. SF scaffolds have potential to overcome such limitations, as they allow mild manufacturing conditions. SF from *Bombyx mori* is a protein soluble in organic solvents as well as in water, and, when processed into scaffolds, results a biomaterial with excellent mechanical properties, slow biodegradation and well established biocompatibility [15]. SF has been used for a wide range of potential biomedical applications [15-24]. Furthermore, SF has been suggested as a platform for drug delivery either in the form of films [25] or as genetically engineered silk-elastine hydrogels [26, 27]. However, the currently available protocols for the preparation of porous 3D scaffolds of SF require organic solvents such as hexafluoroisopropanol (HFIP) or high salt concentrations which frequently have a negative impact on GF integrity and bioactivity. Here we report on a protocol for the direct embedding of IGF-I in a SF scaffold under mild conditions that sustain its activity. We investigated in detail the impact of manufacturing parameters such as pH, methanol treatment to induce SF water insolubility, and drug loading with respect to IGF-I potency, and release kinetics. Cellular response was tested with hMSC which were cultured in minimal chondrogenic medium containing TGF- β 1 to assess the impact of IGF-I release on the chondrogenic differentiation of hMSC when seeded onto the scaffold.

MATERIALS AND METHODS

Materials

Paraffin with a melting temperature of 54 - 56 °C, lithium bromide, Na₂CO₃, poly(ethylene glycol) (PEG) (MW 6000), gelatin, sodium azide, Tween 40, sodium acetate, formalin, ascorbic acid, dexamethasone, selenious acid, lineolic acid and transferrin were purchased from Sigma-Aldrich (St. Louis, MO). Potassium bromide was from Merck (Darmstadt, Germany). All antibodies, CD44 (endothelial cells), CD34 (sialomucin/hematopoietic progenitors), CD71 (transferring receptor/proliferating cells), as well as CD105 (endoglin), anti-CD44, anti-CD14 conjugated with fluoresceine isothiocyanate (CD44-FITC, CD14-FITC), anti-CD31 conjugated with phycoerythrin (CD31-PE), anti-CD34 conjugated with allophycocyanine (CD34-APC), anti-CD71-APC and anti-CD105 with the exception of secondary rat-antimouse IgG-FITC antibody (Neomarkers, Fremont, CA) were purchased from BD Bioscience (Maryland, MD). RPMI1640, Dulbecco's modified eagle medium (DMEM), fetal bovine serum (FBS), bFGF, penicillin-streptomycin, fungizone, insulin and TGF-β1 were from Gibco (Palo Alto, CA). Papain solution was from BD Bioscience (Maryland, MD). Osteosarcoma cell line MG63 was purchased from ATCC (Manassas, VA). Insulin-like growth factor was kindly provided by Genentech (South San Francisco, CA).

Preparation of aqueous SF solution from Bombyx mori cocoons

SF solution was prepared as described previously [22]. Briefly, cocoons from *Bombyx mori* (Trudel, Zurich, Switzerland), were boiled in 0.02 M Na₂CO₃ solution, rinsed and dissolved in 9M LiBr for 3 h at 55 °C to generate a 10% (w/v) solution. The solution was dialyzed (Pierce, molecular weight cut-off 3,500 Da) in 1.5 l of ultra purified water (UPW). UPW was exchanged 5 times in 72 h resulting in a 3% (w/v) SF solution.

Preparation of paraffin globules

Paraffin globules were used as porogen for SF scaffolding. They were prepared in an emulsion process using water, gelatin and paraffin as described before [14]. Briefly, gelatin was dissolved at 80 °C in hot UPW at a concentration of 30 g/l, and carefully mixed with paraffin ($T_m = 54-56$ °C) upon melting at a final concentration of 200 g/l. Phases were emulsified by stirring at 9,000 min⁻¹ for 10 minutes and the emulsion poured into ice-cold water. The solidified paraffin globules were harvested and washed with UPW. After filtering through 12-25 µm pore filter paper (Schleicher & Schuell, Switzerland) and drying, the globules were classified with standard sieves (Retsch, Haan, Germany). Fractions of >500 µm, 400-500 µm, 300-400 µm, 200-300 µm, 100-200 µm were collected and stored at 4 °C.

Sintering of paraffin globules

Heat induced sintering of paraffin globules (200-300 µm) in a cylindrical mold was performed as described previously [14]. Briefly, 1.2 g of porogen was loaded into 20 ml falcon syringes (BD Bioscience, Maryland, MD). The surface was evened by the use of a pistil, followed by controlled sintering at 37 °C (Thermocenter, Salvis OAKTON Instruments, Vernon Hills, NY) for 50 min. After the heat treatment the mold was left to cool to RT.

Preparation and freeze drying of IGF-I loaded SF scaffolds

Freshly prepared silk solution in UPW was transferred to a dialysis chamber and further dialyzed against a 13.3% (w/v) PEG 6000 solution in UPW overnight, resulting in a 20% (w/v) silk fibroin solution. 5, 10, 20, 40 µg of IGF-I were added per ml of silk solution and mixed for 10 min at 4 °C. Soaking of 1.0 ml of this solution into the previously prepared paraffin mold was to fill the interspace between the porogen spheres. To check for potential effects of electrostatic interactions between IGF-I and SF the pH of the formulations was

either left at 7 or set to 4, by adding 40 μ l of 100% acetic acid per ml, in order to promote the interference of negative charges on silk fibroin (pI = 4.3; Cheng, Peng et al. 2005) with the positively charged IGF-I (pI = 8.3). The preparations were then flash frozen in liquid nitrogen for 1 min, and freeze dried at -30 °C under temperature control for 48 h (Lyovac GT2, Finn-Aqua, Hurth, Germany). Scaffolds were immersed in 90% (v/v) methanol for 30 minutes and then air dried. The paraffin was extracted in hexane. Hexane was replaced after 12 and 24 h and the leached scaffolds were dried under vacuum for 12 h to minimize residual hexane as previously reported [14].

Characterization of freeze dried SF scaffolds by Fourier-transformed infrared spectroscopy (FTIR)

To prepare for FTIR, 5 mg of SF scaffold material were ground using mortar and pestle, then mixed with 300 mg potassium bromide, and compressed to a pellet with 10 tons (13 mm diameter) under vacuum for one minute. A 2000 FT-IR Spectrum V3,01 (Perkin Elmer, Boston, MA) was used to analyze the pellet.

Assessment of IGF-I release profiles from freeze dried SF scaffolds by ELISA

Specimens of approx. 10 mg scaffold material were cut out and immersed in 1 ml of 50 mM acetate buffer containing 100 mM NaCl, 0.02% Tween 40 and 0.12% sodium azide. Samples were collected by complete exchange of the buffer twice a day in the first week, and every second or third day in the following weeks. The samples were analyzed for IGF-I by ELISA (DuoSet Human, R&D Systems, Minneapolis, MN) according to the manufacturer's protocol (n = 4).

IGF-I potency assay using MG63 cells

The potency of released IGF-I was assessed by an MTT bioassay using quiescent MG-63 cells showing a mitogenic response to added IGF-I [28-30].

Briefly, MG63 cells were cultured in a medium consisting of minimum essential medium (MEM) containing 8.9% FBS, 1.79 mM L-glutamine, 89 U/ml penicillin, and 89 $\mu\text{g/ml}$ streptomycin. Cells were trypsinized and resuspended in assay medium (MEM, 0.452% BSA, 1.82 mM L-glutamine, 89 U/ml penicillin, and 89 $\mu\text{g/ml}$ streptomycin) and diluted to a concentration of 2×10^6 cells per ml. 100 μl of cell suspension (2×10^5 cells) were then plated in each well of a tissue culture treated 96 well plate. After one day of pre-incubation, the medium was exchanged with 100 μl of the same medium. 10 μl of the collected sample containing the released IGF-I and cells were further incubated for another two days. After incubation excess medium was soaked off and the cells were stained with MTT solution (2% MTT in PBS) for 4 h. Again, excess solution was soaked off and the cells were incubated in 3% SDS and 0.04 M HCl in 2-propanol for 1.5 h at RT in the dark in order to solubilize the formed formazan crystals in the cells. Using a Thermomax microplate reader (Molecular Devices Corporation, Sunnyvale, CA) the absorbance was read at 570 nm and subtracted from the background (630 nm).

Isolation and expansion of hMSC

hMSC were isolated from samples of bone marrow, obtained from a single donor (Cambrex Corporation, Lonza Group Ltd, Basel, Switzerland), as previously described and characterized with respect to the expression of surface antigens and their ability to selectively differentiate along the chondrogenic or osteogenic lineages [14, 22, 31].

Tissue engineering of cartilage using hMSC and IGF-I loaded SF scaffolds

Methanol treated scaffolds, prepared with porogen and treated at 37 °C, were cut into slices of 1-2 mm thickness. From this material, disc-shaped scaffolds of 5 mm diameter were punched out having final scaffold dry weights between 2.5–3 mg. hMSC suspensions as obtained by the above described protocol were trypsinized and cell numbers were assessed using a Neubauer hemocytometer

(Brand GmbH, Wertheim, Germany). Per well three scaffolds of the same composition were pinned down in Falcon non-tissue culture treated 6 well plates (BD Bioscience, Maryland, MD). 20 μ l of cell suspension, containing about 10^6 hMSC, was seeded on the scaffolds. The plates were then incubated at 37 °C and 5% CO₂ for 90 min until the cells adhered to the SF. Then 5 ml of medium was added to each well. In order to investigate the effects of IGF-I on the deposition of GAG by hMSC, IGF-I loaded (IGF40; see **Table 1**) and control scaffolds (IGF0; see **Table 1**) were cultured in TS+ medium (without insulin) containing DMEM supplemented with 100 U/mL penicillin, 1000 U/mL streptomycin, 0.2% fungizone, 0.1 mM non-essential amino acids, 50 μ g/ml ascorbic acid, 10 nM dexamethasone, 5.5 μ g/ml human transferrin, 5 ng/ml selenous acid, 1.75 mg/ml BSA, 4.7 μ g/ml linoleic acid and 5 ng/ml TGF- β 1. As a positive control for chondrogenesis we cultured control scaffolds (IGF0) in ITS+ medium consisting of TS+ medium additionally supplemented with 1 μ g/ml of human insulin (IGF0/ITS). Total culture time was 3 weeks. After cultivation, the constructs were harvested to assess the wet weights (Mettler-Toledo AX205 Deltarange, Greifensee, Switzerland) and transferred into 2 ml screw cap tubes (Fisher Scientific, Pittsburgh, PA) for analytical evaluation.

Table 1. Experimental groups for cartilage tissue engineering

Culture condition	IGF-I loading	Medium	Insulin
IGF0/TS	0	TS+ 5 ng/ml TGF- β 1	0
IGF40/TS	40 μ g	TS+ 5 ng/ml TGF- β 1	0
IGF0/ITS	0	ITS+ 5 ng/ml TGF- β 1	1 μ g/ml

DNA assay

Scaffolds (n=4) were immersed in 1 ml 0.2% (v/v) Triton X100 and 5 mM MgCl₂, disintegrated using steel balls and a Minibead-beater (Biospec, Bartlesville, OK), and incubated at RT for 48 h. The samples were centrifuged at 300 g for 10 minutes at 4 °C, and the supernatant analyzed using the PicoGreen assay (Molecular Probes, Eugene, OR), according to the protocols of the manufacturer. Fluorometric analysis of the samples was at an excitation wavelength of 480 nm and an emission wavelength of 528 nm (Packard instrument, Downes Gore, IL).

GAG assay

To measure the GAG content of the cell cultures, four samples per group and time point were frozen, freeze dried, and then digested for 15 h at 60 °C with 1 mg/cm³ papain solution in buffer (0.1 M disodiumhydrogenphosphate, 0.01 M EDTA at pH 6.5). GAG content was determined spectrophotometrically (Perkin Elmer, Oak BridgeIL) at 525 nm upon binding to the dimethylmethylene blue dye [32] and normalized to a standard of chondroitin sulfate.

Stability of insulin and IGF-I under physiological conditions in cell culture medium by RP-HPLC

To assess the stability of IGF-I and insulin for up to three days under cell culture condition, 75 µg/ml of each protein was incubated in DMEM containing BSA and 1% penicillin/streptomycin solution at 37 °C and assayed by RP-HPLC. A Hitachi LaChrom HPLC, equipped with a L-7100 pump and a L-7485 fluorescence detector (Hitachi Ltd, Tokyo, Japan) was used with a Zorbax® 300SB CN column (150 x 4.6 mm) under gradient conditions at a flow rate of 0.8 ml/min. Two eluents were used, (A) consisting of 5% acetonitrile and 0.2% trifluoroacetic acid (TFA) in water and (B) 80% acetonitrile and 0.2% TFA in water. The solvent was initially composed of 74% (v/v) eluent A and changed linearly over 30 minutes to eluent B. IGF-I and insulin were detected measuring

the fluorescence at 280 nm.

Histology

For histology, specimens (n=4) were fixed in 10% (v/v) neutral-buffered formaldehyde (24 h at 4 °C), dehydrated in graded ethanol solutions, embedded in paraffin, bisected through the center, and cut into 5 µm thick sections. In order to visualize hMSCs in the scaffold cross sections, H&E staining was carried out after deparaffinization through graded ethanol. To stain for GAG, sections were treated with eosin for 1 min and 0.2% aqueous safranin-O solution for 5 min, rinsed with distilled water, dehydrated through xylene, mounted, and placed under a coverslip.

Statistics

Statistical data analysis was performed by using a general linear model for univariate analysis of variance and Tukey-HST test for post hoc pair-wise comparison using SPSS 14.0 software for Windows (SPSS Inc., Zurich, Switzerland); $p < 0.05$ was considered statistically significant. The 95% confidence interval was calculated as previously described [33].

RESULTS

Morphological characterization of freeze dried scaffolds

Scanning electron microscope images were taken from scaffolds prepared with pore sizes of 200-300 µm. As previously described, leaching of the paraffin from IGF-I loaded SF matrices with hexane resulted in porous scaffolds of high interconnectivity [14]. The SF matrix between the large interconnecting pores (**Fig. 1A, B, C**) consisted of a network of small pores. The small pores were parallel organized, tubular structured with pore diameters between 5 and 10 µm. The inner surface of the porous structure was closed with some randomly distributed pores as qualitatively assessed (**Fig. 1D**).

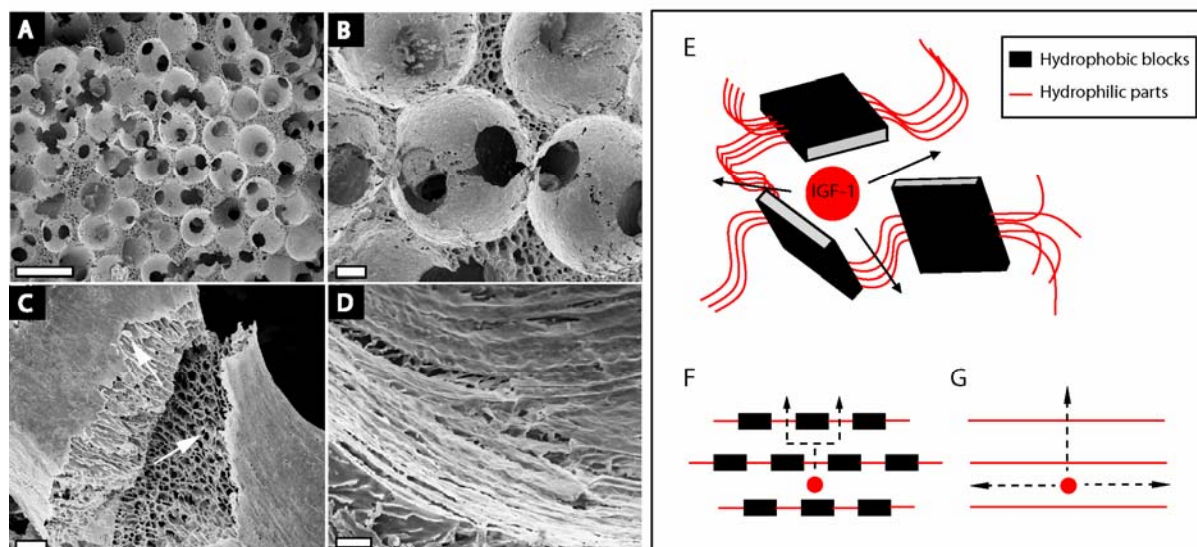


Fig. 1: Scaffold morphology and schematic description of the hypothesis for IGF-I retention in SF scaffolds. (A-D) SEM images of porous SF scaffolds. Scale bars (A) 500 μm, (B) 50 μm, (C, D) 10 μm. (E) Growth factor entrapment in SF structure. (F, G) Cartoon demonstrating a possible mechanisms of IGF-I retention in SF scaffolds, based on observations within this study.

Effect of pH and methanol treatment of SF scaffolds on IGF-I release kinetics and potency

IGF-I release kinetics were evaluated for 25 days *in vitro* from SF scaffolds prepared from 20% (w/w) aqueous SF solution at a pH of either 4 or 7, containing 5 μg/ml IGF-I (**Fig. 2**). SF scaffolds formulated without additional methanol treatment showed a large and variable initial burst within the first day of release (mean ± SD; pH 7: 12.62 ± 5.44 ng mg⁻¹ d⁻¹; pH 4: 13.63 ± 0.64 ng mg⁻¹ d⁻¹) (**Fig. 2A, B**). The burst was significantly ($p < 0.01$) smaller for methanol treated scaffolds (pH 7: 6.93 ± 0.92 ng mg⁻¹ d⁻¹; pH 4: 6.00 ± 0.36 ng mg⁻¹ d⁻¹). IGF-I release from untreated scaffolds decreased after 1 day and further after 5 days and was completed after 11 days for formulations made at pH 7, and after 9 days for pH 4 formulations, respectively. Daily IGF-I release was significantly lower for untreated formulations when compared to methanol treated scaffolds. The release

from methanol treated scaffolds increased slowly during the first 3 days, peaking at day 4 (pH 7: $12.79 \pm 3.31 \text{ ng mg}^{-1} \text{ d}^{-1}$; pH 4: $9.51 \pm 0.61 \text{ ng mg}^{-1} \text{ d}^{-1}$) and decreased between days 5 and 9 until completion after 24 days (**Fig. 2A, B**). These findings were further reflected by the total cumulative release after 25 days (**Fig. 2C**). The total cumulative release from methanol treated scaffolds given as means \pm SD (pH 7: $5.99 \pm 1.06 \text{ ng}$; pH 4: $5.88 \text{ g} \pm 0.29 \text{ ng}$) exceeded significantly ($p < 0.01$) the release from untreated scaffolds (pH 7: $3.82 \pm 0.76 \text{ ng}$; pH 4: $2.42 \pm 0.41 \text{ ng}$) by the factor of 1.5 for pH 7 and 2.5 for pH 4, respectively. IGF-I was assessed for pooled samples at different release time points (0.75 - 1, 2.75 - 3, 4 - 7 and 17.5 - 25 days) using IGF-I responsive MG63 cells.

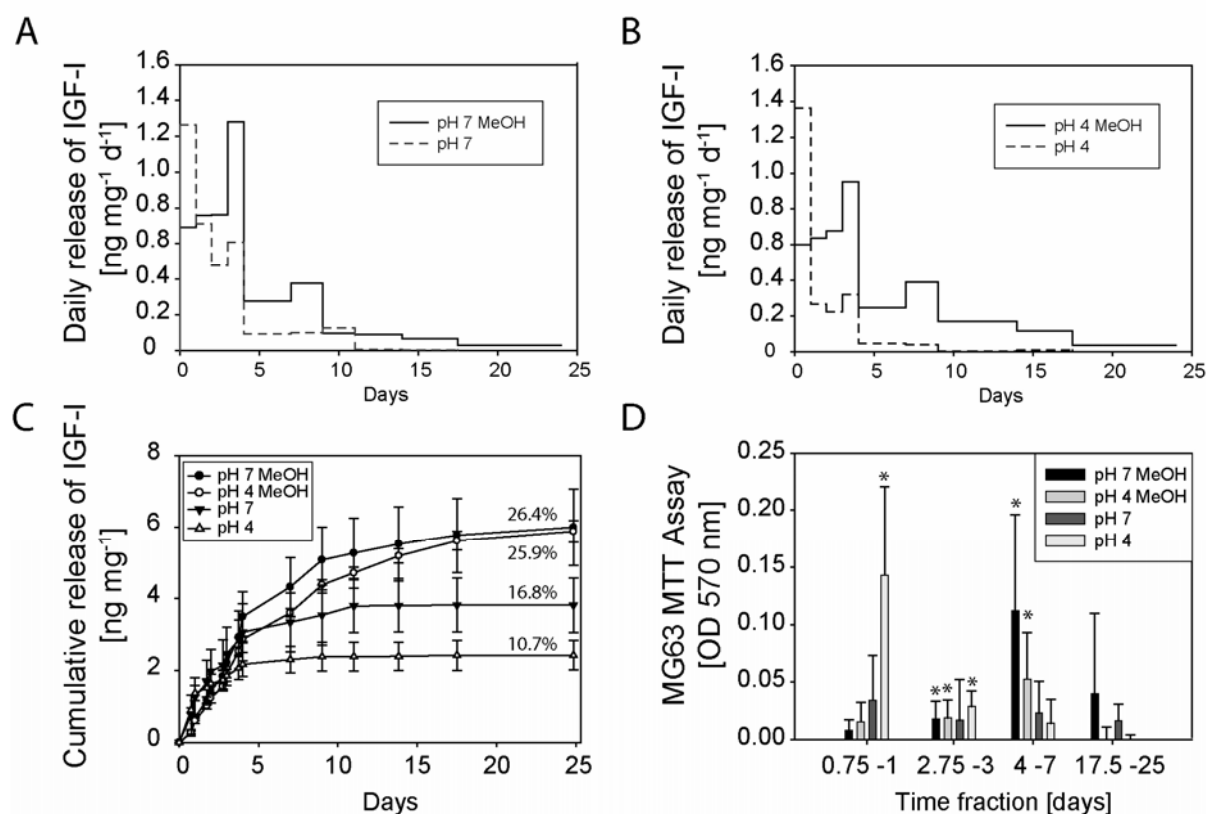


Fig. 2: IGF-I release profiles from SF scaffolds and potency of released growth factor, which were formulated at different pH values and with and without methanol treatment. Daily release from untreated and methanol treated scaffolds at pH 7 (A) and pH 4 (B). (C) Cumulative release of all formulations and percentages of initial loading released within 24 days. (D) Potency of IGF-I release fractions on MG63 proliferation ($p < 0.05$).*

All pooled samples collected in the period between 2.75 - 3 days induced significant ($p < 0.05$) MG63 proliferation (**Fig. 2D**) as well as samples from untreated scaffolds prepared at pH 7 and collected in the period of 0.75 – 1 days. Samples taken from methanol treated scaffolds (pH 7 and pH 4) between days 4 - 7 induced MG63 proliferation in contrast to samples from untreated scaffolds. Samples taken between 17.5 - 25 days from any of the formulations did not significantly induce proliferation of the cells, indicating insufficient IGF-I activities after this time.

Effect of pH and methanol treatment on SF scaffold integrity

To correlate the drug release profiles with conformational changes and the scaffold integrity, the structural state of different SF formulations was assessed by FTIR. Also we investigated the mass loss of SF matrices after incubation in release medium. Neither the presence of IGF-I nor the formulation at lower pH (pH 4) induced structural changes in the SF as assessed by FTIR (**Fig. 3B**). In contrast, the treatment with 90% methanol for 30 min induced amide band shifts from 1232 to 1262 cm^{-1} (amide III) and 1660 to 1627 cm^{-1} (amide I) in all formulations, previously attributed to β -sheet conformation of SF [34].

Conformational changes correlated with insolubility of the matrices at both pH values when treated with methanol. No loss was observed for methanol treated matrices at pH 7, and $2.2 \pm 6.7\%$ of the initial mass (mean \pm SD) was lost at pH 4 after 25 days. Untreated scaffolds disintegrated almost completely within 25 days losing 79% (pH 7) and 95% (pH 4) of their initial mass (**Fig. 3A**).

Effect of drug load on IGF-I release kinetics and IGF-I activity

To investigate the effect of IGF-I loading on the release kinetics, drug loaded scaffolds were prepared at pH 7 and treated with methanol. For the preparation of the scaffolds, 20% (w/w) SF solution containing 5, 10, 20 and 40 $\mu\text{g/ml}$ IGF-I were used (IGF5, IGF10, IGF20, IGF40). IGF-I release from scaffold specimens of 10 mg was investigated by ELISA over a period of 29 days.

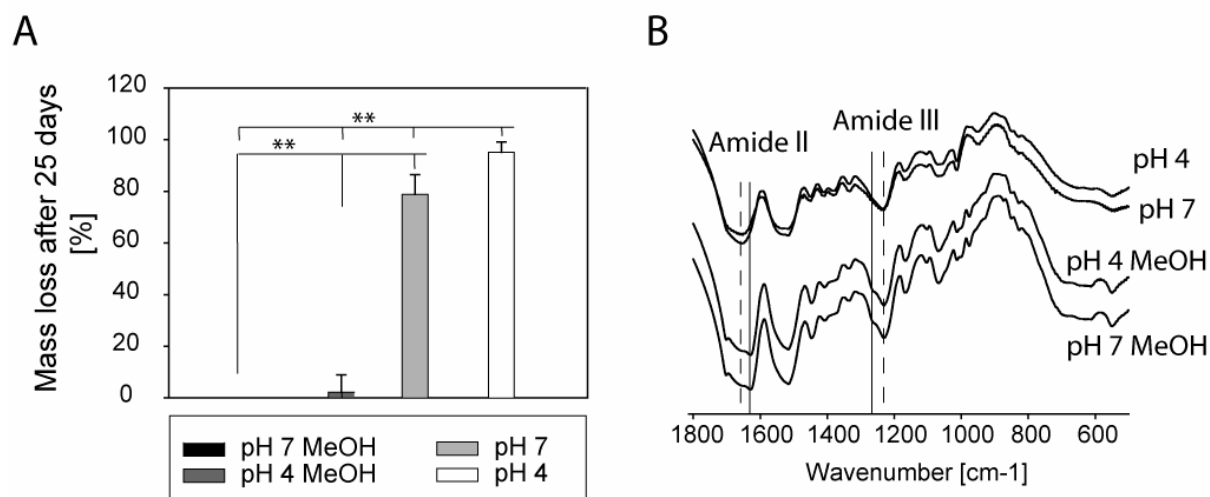


Fig. 3: Mass loss and FTIR of SF scaffolds. (A) Percentage of mass loss after 25 days in acetate buffer (** $p < 0.01$). (B) FTIR spectra of SF scaffold. Dotted line: random coil amide bands; straight line: β -sheet amide bands.

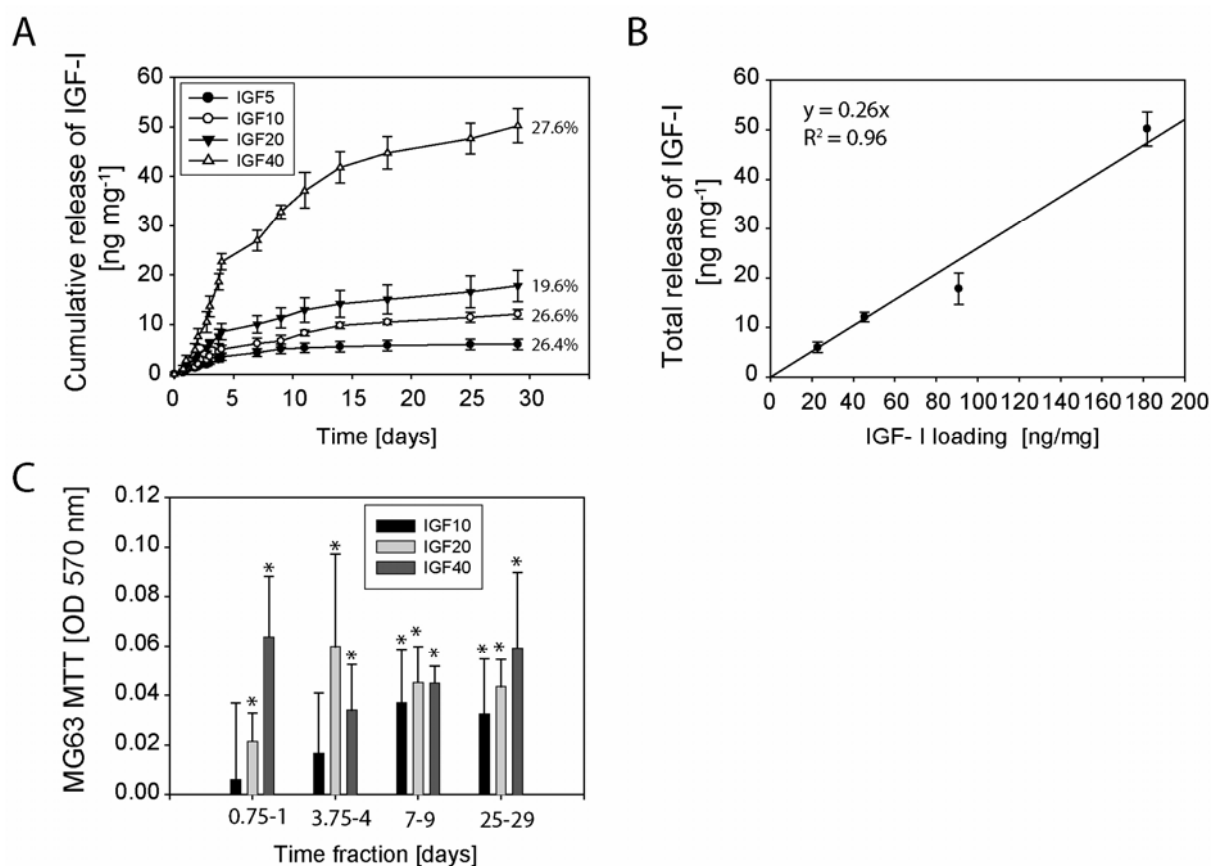


Fig. 4: IGF-I release profiles and potency from SF scaffold loaded with different IGF-I amounts. (A) Cumulative release and percentage of initial IGF-I after 29 days. (B) Linear correlation of IGF-I loading and total cumulative release after 29 days. (C) Potency of IGF-I release fractions on MG63 proliferation ($*p < 0.05$).

Table 2: Summary of formulations, IGF-I loading and total release (29 days)

	Formulations						
	pH7 MeOH / IGF5	pH4 MeOH	pH7	pH4	IGF10	IGF20	IGF40
Methanol treatment	+	+	-	-	+	+	+
pH	7	4	7	4	7	7	7
IGF-1 load per SF solution [$\mu\text{g}/\text{ml}$]	5	5	5	5	10	20	40
IGF-1 load per SF dry weight [ng/mg]	22.7	22.7	22.7	22.7	45.4	90.8	181.6
Total IGF-1 release [ng/mg]	5.99 \pm 1.06	5.87 \pm 0.29	38.15 \pm 7.57	24.17 \pm 4.11	12.09 \pm 0.97	17.83 \pm 3.17	50.21 \pm 3.44
Total IGF-1 release [%]	26.39 \pm 4.7	25.88 \pm 1.31	16.8 \pm 3.33	10.65 \pm 1.81	26.64 \pm 1.9	19.62 \pm 3.48	27.64 \pm 1.89

Total cumulative IGF-I release after 29 days but not the kinetics of the release was affected by the initial loading (**Fig. 4A, B - Table 2**). IGF-I release per mg scaffold after 29 days was linearly correlated to the initial load (y [ng mg^{-1}] = $0.26 \times [\text{ng}^{-1} \text{mg}]$; with y representing the total release per mg of scaffold after 29 days, and x the IGF-I loading per mg of scaffold; see **Fig. 4A**).

Chondrogenic differentiation of human mesenchymal stem cells on IGF-I loaded SF scaffold

The impact of released IGF-I in TGF- β 1 supplemented media on the chondrogenesis of hMSC *in vitro* was assessed. SF scaffolds were formulated without IGF-I (IGF0) or with 40 μg IGF-I per ml of SF solution (IGF40) and cultured for 3 weeks in insulin free minimal TS+ medium supplemented with 5 ng/ml TGF- β 1 (IGF0/TS; IGF40/TS). The drug load of 40 μg per ml of SF was used due to the significant effect on MG63 proliferation. Insulin, frequently used

in many chondrogenic media, was excluded to avoid the interference of insulin with the IGF-I receptor [7]. As a positive control for chondrogenesis, hMSC were cultured on IGF0 scaffolds in ITS+ medium (IGF0/ITS) containing 1 $\mu\text{g/ml}$ insulin and was otherwise identical (**Table 1**).

IGF-I and insulin stability in culture media without growth factors was assayed by HPLC (**Fig. 5**). Main peaks were detected for IGF-I and insulin at 12.2 and at 14.5 minutes, respectively. Under these conditions protein conformation was largely retained with IGF-I being more affected by the unfolding of the native structure during the three days of observation, as indicated by increasing peaks (indicated by arrows), in particular one prior to the main peak [35]. Byproducts of IGF-I were observed after 12 hours and increased further with time, whereas insulin was more stable (**Fig. 5**). The scaffolds released between 1 to 8 $\text{ng mg}^{-1} \text{day}^{-1}$ IGF-I within the first 14 days before the release dropped for the next 15 days (**Fig. 6A**). Scaffold dry weights were between 2.5 - 3 mg. Time had a significant effect on the general DNA content (**Fig. 6B**), indicated by significantly lower contents at week 3 as compared to weeks 1 and 2. At the different time points no significant difference was observed between the DNA contents of the different culture conditions (IGF0/TS, IGF40/TS, and IGF0/ITS). However, after 3 weeks of culture, an insignificant decrease in the DNA content of the cultures was observed when scaffolds were loaded with IGF-I or when supplemented with insulin (IGF40/TS and IGF0/ITS) as compared to cultures with unloaded scaffolds and without insulin (IGF0/TS).

Statistical analysis of overall glycosaminoglycan (GAG) deposition revealed a significant effect ($p < 0.01$) of the IGF-I loaded scaffolds (40/TS) on GAG deposition as compared to unloaded scaffolds (IGF0/TS). Unloaded scaffolds cultured in medium supplemented with insulin (IGF0/ITS) performed significantly ($p < 0.01$) better than all other conditions (IGF0/TS, IGF40/TS; **Fig. 6C**). However, at the individual time points of the study (1, 2, 3 weeks), no significant difference between GAG contents in cultures with unloaded scaffolds (IGF0/TS) and cultures with loaded scaffolds (IGF40/TS) was observed.

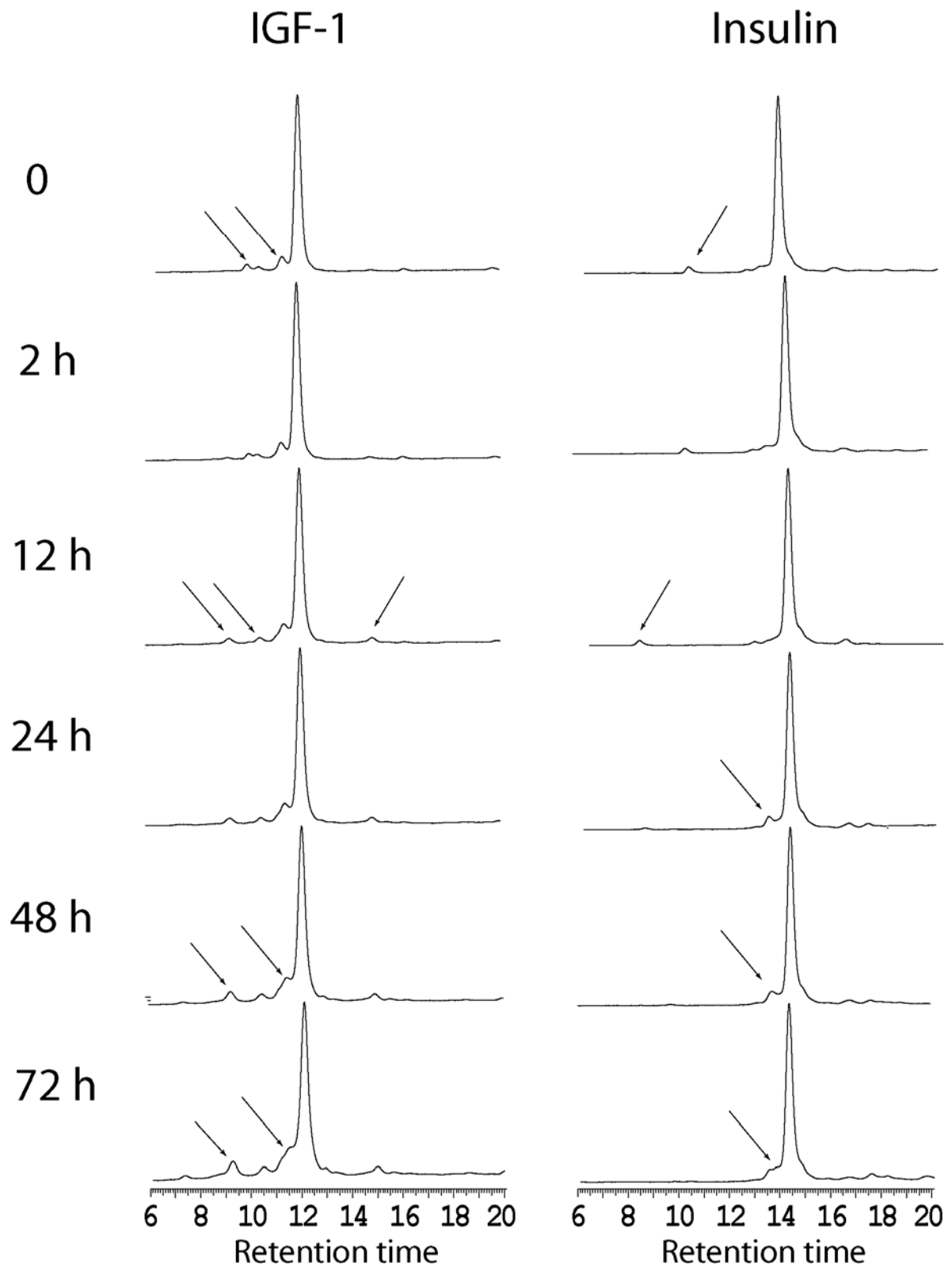


Fig. 5: IGF-I and insulin stability in cell culture media at 37 °C measured by RP-HPLC. Degradation peaks are indicated by arrows.

GAG contents in cultures containing insulin as supplement (IGF0/ITS) were significantly higher than in the other cultures (IGF0/TS, IGF40/TS) at each time point, except for IGF-I loaded scaffold after 2 weeks of culture (IGF40/TS, 2 weeks). For each time point, the GAG content was normalized by the DNA content (GAG/DNA) and the standard deviation (SD) was calculated when using standard error propagation rules (**Fig. 6D**). For the statistical comparison of the GAG content normalized by DNA in different cultures and at individual time points, the 95% confidence interval (CI₉₅) was calculated for each mean of the ratio [33]. The GAG/DNA ratio was significantly (CI₉₅) increased for IGF0/ITS cultures as compared to IGF0/TS at each time point, whereas no significant increase was observed when compared to IGF-I loaded scaffolds (IGF40/TS). GAG content per DNA was significantly increased (CI₉₅) in cultures with IGF-I loaded scaffolds (IGF40/TS) as compared to unloaded scaffolds (IGF0/TS) after 3 weeks of culture (**Fig. 6D**). The wet weights of the cultured scaffolds did not significantly differ between the culture conditions at the individual time points but in general insignificantly increased during the culture (**Table 3**).

Table 3: Wet weights of cultured SF scaffolds

Culture time	Average wet weights of cultured scaffolds (mg)		
	IGF0/TS	IGF40/TS	IGF0/ITS
1 week	14.3 ± 4.4	14.3 ± 2.8	17.1 ± 3.7
2 weeks	12.3 ± 3.1	13.8 ± 2.8	16.25 ± 4.7
3 weeks	14.8 ± 2.8	16.5 ± 2.8	19.2 ± 3.9

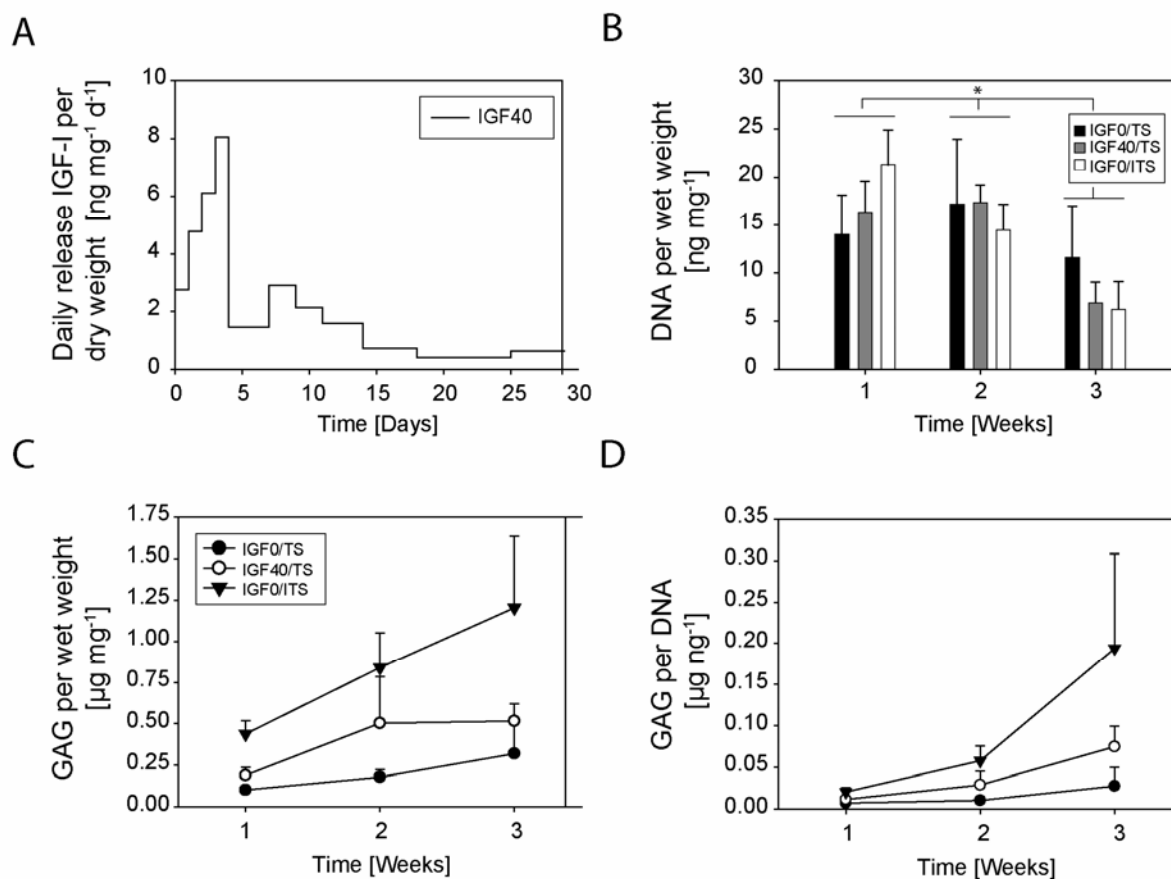


Fig. 6: Impact of IGF-I release from SF scaffolds on chondrogenesis of hMSC during 3 weeks of culture in TGF-β1 supplemented medium. (A) Daily IGF-I release from scaffold loaded with 40 μg IGF-I per ml SF solution. (B) DNA content per scaffold wet weight, (C) GAG per scaffold wet weight and (D) GAG per DNA content of constructs after 1, 2 and 3 weeks of cultivation. GAG content was normalized to a standard of chondroitin sulfate (CS).

Histology

Released IGF-I as well as insulin supplements in combination with TGF-β1 had substantial effects on the type of tissue formed by hMSC, as observed by hematoxylin staining of the scaffolds (**Fig. 7**). hMSC grown on unloaded scaffolds retained a fibroblast-like morphology during the 3 weeks culture period, and formed dense fibrous cell clusters after 2 weeks of culture. No cartilage-like matrix was detected. hMSC cultured on the IGF-I loaded scaffold (IGF40/TS) organized in a regular structure within the first week; chondrogenic condensation was observed after week 2 and resulted in cartilage-like tissue from week 2 to

week 3. The positive control resulted in cartilage-like morphologies after 2 weeks in culture. The findings were corroborated by Safranin-O staining of cartilage matrix components (**Fig. 8**). hMSC grown under IGF0/TS conditions did not specifically stain for cartilage-like tissue with Safranin-O, however deposition of other matrix components was apparent (violet staining).

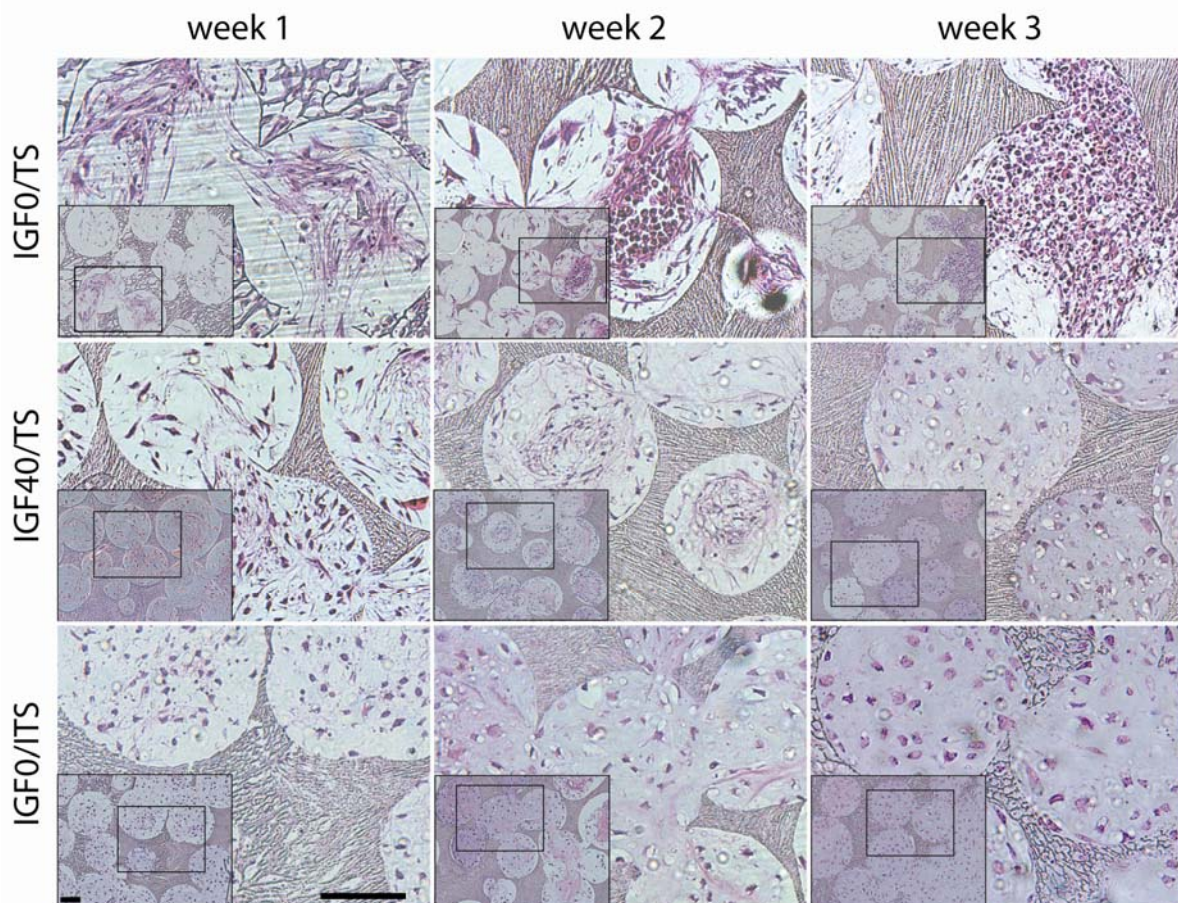


Fig. 7: Histological analysis of SF scaffolds sections after 1, 2 and 3 weeks of culture. Hematoxylin/Eosin staining (H&E). Frames in the inserts correspond to the magnified section. Scale bar: 100 μ m

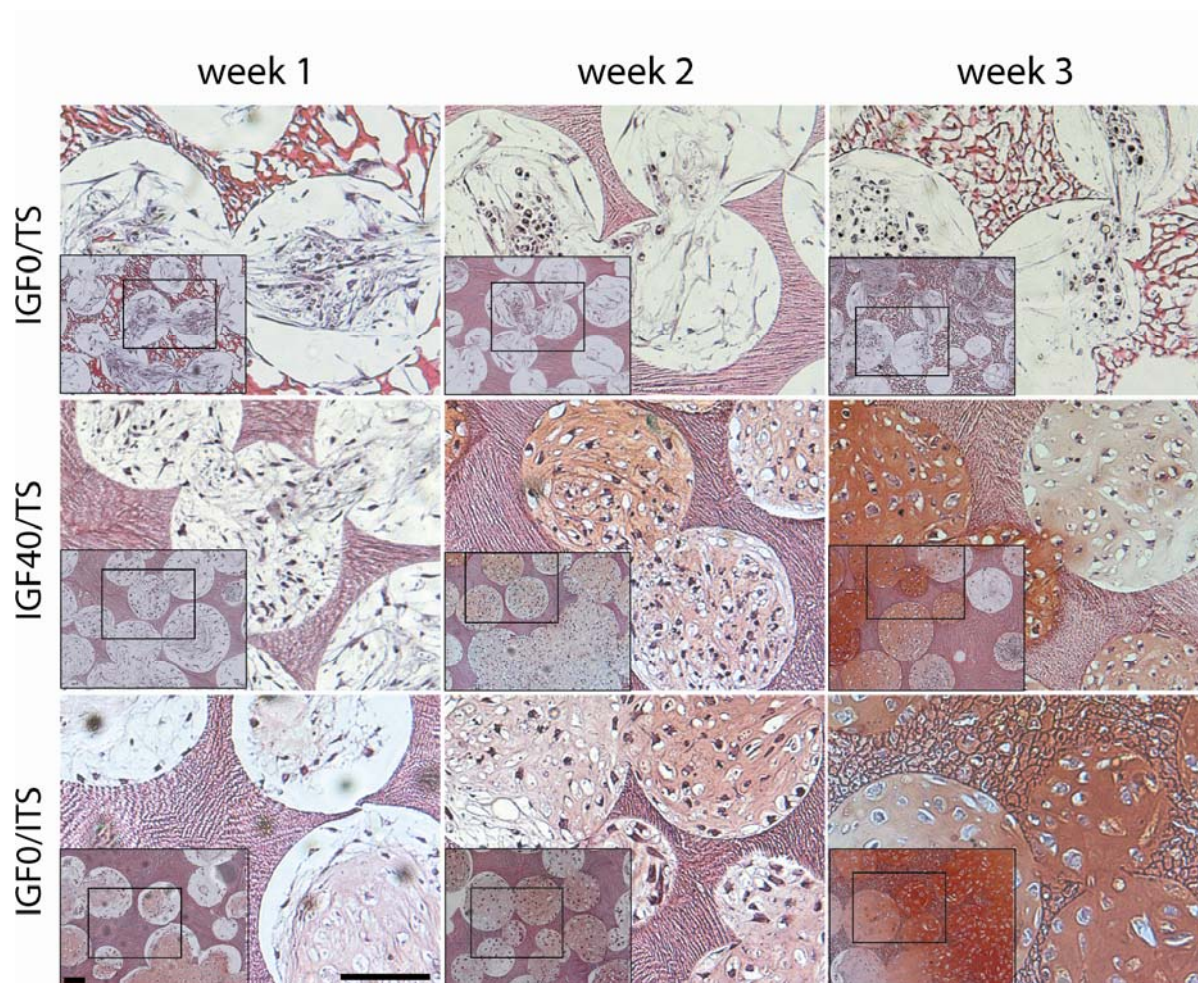


Fig. 8: Histological analysis of SF scaffold sections after 1, 2 and 3 weeks of culture and Safranin-O staining. Frames in the inserts correspond to the magnified section. Scale bar: 100 μ m

DISCUSSION

Since the early discovery of the auto-inductive properties of bone matrix [36], the involved GFs as key mediators for self repair were isolated and characterized [3, 4, 37], and substantial insights into their chondro- and osteogenic potential have been described [5, 13, 38-40]. The delivery of such growth factors can support the (re)generation of skeletal tissue, e.g. after trauma, resection of bone tumors, joint replacement or after pannus formation in joints [41]. Controlled release of the growth factor can avoid potential toxicity

associated with bolus administration and deliver optimum doses for tissue (re)generation [5, 30, 41-43]. In this study, IGF-I was formulated under aqueous conditions into a 3-dimensional, mechanically stable, highly porous and interconnected implant, as previously described [14]. IGF-I potency was preserved. This is in contrast to previous, harsher protocols including fluorinated solvents, in which protein folding was affected and followed by aggregation. This has been previously reported for fibroblast growth factor 1 (FGF-1) when exposed to trifluoroethanol [44, 45].

Subsequent methanol treatments after freeze drying of IGF-I loaded SF scaffolds induced the formation of β -sheet blocks in SF, reduced the initial burst (18 hours), and resulted in more sustained IGF-I release as compared to untreated scaffolds of amorphous SF (**Fig. 2, 3**). The improved sustainment of IGF-I release is supposed to be the result of β -sheet formation which may hinder the diffusion of IGF-I within the SF structure (**Fig. 1**) [25]. Moreover the total release of IGF-I was significantly higher for methanol treated scaffolds as compared to untreated amorphous scaffolds, which degraded quickly into small particulate debris. The overall reduction of total IGF-I release in untreated scaffolds may be a result of (IGF-I loaded) debris aspiration upon buffer exchange in the quicker degrading, untreated scaffolds. A MG63 proliferation assay [28, 46-48] was used to investigate if the bioactivity of released IGF-I was preserved over time (4 weeks) or impacted by methanol treatment. IGF-I released from methanol treated scaffolds did not show any decreased potency as compared to IGF-I released from untreated scaffolds over the full time period. Apparently SF was able to preserve the potency of IGF-I during methanol treatment and hexane leaching (**Fig. 2**). The *in vivo* degradation of methanol treated SF matrices by cells and proteases is slow (6 - 12 months) and GF release is not a result of scaffold degradation (**Table 1**). GF release from SF scaffolds is mainly diffusion driven and supposed to be either a result of GF-SF interaction and/or physical engravment and diffusional hindrance by hydrophobic blocks in the SF matrix (**Fig. 1E, F, G**). To investigate the impact of GF-SF interaction during manufacture, scaffold preparation was either performed at neutral pH, or at pH 4, with lowering the negative charges of

SF at pH 4 ($pI_{[SF]} = 4.3$) [49] and thus its ionic interference with the positively charged IGF-I ($pI_{[IGF-I]} = 8.3$). Differences in IGF-I release were not observed for methanol treated (β -sheet conformational change) scaffolds, suggesting that differences in ionic interaction during manufacture do not translate into changes in drug delivery kinetics (measured at pH 7). Drug delivery at different pH in the release buffer was not tested due to the physiologic irrelevance. This data suggests that β -sheet induction of crystalline blocks during manufacture plays a more important role to control drug delivery by processing parameters as compared to ionic interactions as previously reported [25, 50].

To assess the effect of IGF-I on hMSC differentiation under chondrogenic conditions, culture medium providing minimal amounts of TGF- β 1 (5 ng/ml) was used. IGF-I or insulin in combination with TGF- β 1 did not significantly stimulate the proliferation of hMSC, as compared to TGF- β 1 alone. This is consistent with work published by other authors [8, 51-54]. Yet, it has been described for progenitor cells that progression towards the ultimate phenotype can be correlated with a decrease in proliferation rates [55]. Therefore, the insignificant decrease of DNA content in cultures with IGF-I releasing scaffolds or insulin supplementation compared to unloaded scaffolds might reflect an advanced differentiation of hMSC under these conditions which is further reflected by the histological staining (**Fig. 7**). hMSC cultures containing low concentrations of TGF- β 1 (5 ng/ml) without the presence of IGF-I or insulin did not result in the formation of cartilage-like tissue suggesting an insufficient differentiation of hMSC under these conditions. IGF-I supported the propagation of hMSC chondrogenesis in this study as previously reported [56-58] and synergistically interacted with TGF- β 1 on the engineering of cartilage-like tissue *in vitro* [7, 8, 59]. Future, preclinical studies are needed to assess the performance of IGF-I loaded scaffolds on chondrogenesis *in vivo*, as *in vitro* systems at best in part reflect *in vivo* conditions [60].

CONCLUSION

This study demonstrated that IGF-I can be processed into SF implants, while controlling release rates as a function of SF β -sheet formation as indicated by a decreased initial burst and a more sustained release after methanol treatment. The total cumulative IGF-I release obtained from SF implants followed a dose-dependent pattern that was correlated to the initial loading of 5 to 40 μg per ml SF solution. MSC cultured on IGF-I releasing implants deposited cartilage-like tissue after 3 weeks in contrast to unloaded scaffolds. These results suggest that IGF-I loaded SF implants have the potential to support chondrogenesis in the presence of hMSC. Pre-clinical proof of concept studies will be needed to validate this *in vitro* evidence.

ACKNOWLEDGEMENT

We thank Trudel (Zurich, Switzerland) for silk cocoons, Genentech (South San Francisco, CA) for IGF-I. Financial support was from AO (AO Biotechnology Research Grant 2003), the Association for Orthopedic Research and ETH Zurich (TH 26.04-1).

REFERENCES

1. T. Aigner, J. Stove, Collagens--major component of the physiological cartilage matrix, major target of cartilage degeneration, major tool in cartilage repair, *Adv Drug Deliv Rev* 55 (12) (2003) 1569-93.
2. C.M. Bautista, S. Mohan, D.J. Baylink, Insulin-like growth factors I and II are present in the skeletal tissues of ten vertebrates, *Metabolism* 39 (1) (1990) 96-100.
3. E. Solheim, Growth factors in bone, *Int Orthop* 22 (6) (1998) 410-6.
4. S. Mohan, D.J. Baylink, Bone growth factors, *Clin Orthop Relat Res* (263) (1991) 30-48.
5. L. Meinel, E. Zoidis, J. Zapf, P. Hassa, M.O. Hottiger, J.A. Auer, R. Schneider, B. Gander, V. Luginbuehl, R. Bettschart-Wolfisberger, O.E. Illi, H.P. Merkle, B. von Rechenberg, Localized insulin-like growth factor I delivery to enhance new bone formation, *Bone* 33 (4) (2003) 660-72.
6. S. Yakar, P. Pennisi, Y. Wu, H. Zhao, D. LeRoith, Clinical relevance of systemic and local IGF-I, *Endocr Dev* 9 (2005) 11-6.
7. L. Longobardi, L. O'Rear, S. Aakula, B. Johnstone, K. Shimer, A. Chytil, W.A. Horton, H.L. Moses, A. Spagnoli, Effect of IGF-I in the chondrogenesis of bone marrow mesenchymal stem cells in the presence or absence of TGF-beta signaling, *J Bone Miner Res* 21 (4) (2006) 626-36.
8. N. Indrawattana, G. Chen, M. Tadokoro, L.H. Shann, H. Ohgushi, T. Tateishi, J. Tanaka, A. Bunyaratvej, Growth factor combination for chondrogenic induction from human mesenchymal stem cell, *Biochem Biophys Res Commun* 320 (3) (2004) 914-9.
9. M.J. Whitaker, R.A. Quirk, S.M. Howdle, K.M. Shakesheff, Growth factor release from tissue engineering scaffolds, *J Pharm Pharmacol* 53 (11) (2001) 1427-37.
10. S.J. Lee, Cytokine delivery and tissue engineering, *Yonsei Med J* 41 (6) (2000) 704-19.
11. A. Kanematsu, S. Yamamoto, M. Ozeki, T. Noguchi, I. Kanatani, O. Ogawa, Y. Tabata, Collagenous matrices as release carriers of exogenous growth factors, *Biomaterials* 25 (18) (2004) 4513-20.
12. H.D. Kim, R.F. Valentini, Retention and activity of BMP-2 in hyaluronic acid-based scaffolds in vitro, *J Biomed Mater Res* 59 (3) (2002) 573-84.

13. J.A. Jansen, J.W. Vehof, P.Q. Ruhe, H. Kroeze-Deutman, Y. Kuboki, H. Takita, E.L. Hedberg, A.G. Mikos, Growth factor-loaded scaffolds for bone engineering, *J Control Release* 101 (1-3) (2005) 127-36.
14. L. Uebersax, H. Hagenmuller, S. Hofmann, E. Gruenblatt, R. Muller, G. Vunjaknovakovic, D.L. Kaplan, H.P. Merkle, L. Meinel, Effect of Scaffold Design on Bone Morphology in Vitro, *Tissue Eng* 12 (12) (2006) 3417-29.
15. L. Meinel, S. Hofmann, V. Karageorgiou, C. Kirker-Head, J. McCool, G. Gronowicz, L. Zichner, R. Langer, G. Vunjak-Novakovic, D.L. Kaplan, The inflammatory responses to silk films in vitro and in vivo, *Biomaterials* 26 (2) (2005) 147-55.
16. P.M. Cunniff, S.A. Fossey, M.A. Auerbach, J.W. Song, D.L. Kaplan, W. Adams, R.K. Eby, D. Mahoney, D. Deborah, D.L. Vezie, Mechanical and thermal properties of Dragline Silk from the Spider *Nephila cavipes*, *Polymers for Advanced Technologies* 5 (1994) 401-410.
17. S. Sofia, M.B. McCarthy, G. Gronowicz, D.L. Kaplan, Functionalized silk-based biomaterials for bone formation, *J Biomed Mater Res* 54 (1) (2001) 139-48.
18. B. Panilaitis, G.H. Altman, J. Chen, H.J. Jin, V. Karageorgiou, D.L. Kaplan, Macrophage responses to silk, *Biomaterials* 24 (18) (2003) 3079-85.
19. G.H. Altman, F. Diaz, C. Jakuba, T. Calabro, R.L. Horan, J. Chen, H. Lu, J. Richmond, D.L. Kaplan, Silk-based biomaterials, *Biomaterials* 24 (3) (2003) 401-16.
20. L. Meinel, S. Hofmann, V. Karageorgiou, L. Zichner, R. Langer, D. Kaplan, G. Vunjak-Novakovic, Engineering cartilage-like tissue using human mesenchymal stem cells and silk protein scaffolds, *Biotechnol Bioeng* 88 (3) (2004) 379-91.
21. L. Meinel, V. Karageorgiou, R. Fajardo, B. Snyder, V. Shinde-Patil, L. Zichner, D. Kaplan, R. Langer, G. Vunjak-Novakovic, Bone tissue engineering using human mesenchymal stem cells: effects of scaffold material and medium flow, *Ann Biomed Eng* 32 (1) (2004) 112-22.
22. L. Meinel, V. Karageorgiou, S. Hofmann, R. Fajardo, B. Snyder, C. Li, L. Zichner, R. Langer, G. Vunjak-Novakovic, D.L. Kaplan, Engineering bone-like tissue in vitro using human bone marrow stem cells and silk scaffolds, *J Biomed Mater Res A* 71 (1) (2004) 25-34.
23. N. Minoura, S. Aiba, M. Higuchi, Y. Gotoh, M. Tsukada, Y. Imai, Attachment and growth of fibroblast cells on silk fibroin, *Biochem Biophys Res Commun* 208 (2) (1995) 511-6.

24. L. Uebersax, D.E. Fedele, C. Schumacher, D.L. Kaplan, H.P. Merkle, D. Boison, L. Meinel, The support of adenosine release from adenosine kinase deficient ES cells by silk substrates, *Biomaterials* 27 (26) (2006) 4599-607.
25. S. Hofmann, C.T. Wong Po Foo, F. Rossetti, M. Textor, G. Vunjak-Novakovic, D.L. Kaplan, H.P. Merkle, L. Meinel, Silk fibroin as an organic polymer for controlled drug delivery, *J Control Release* 111 (1-2) (2006) 219-27.
26. Z. Megeed, J. Cappello, H. Ghandehari, Controlled release of plasmid DNA from a genetically engineered silk-elastinlike hydrogel, *Pharm Res* 19 (7) (2002) 954-9.
27. Z. Megeed, M. Haider, D. Li, B.W. O'Malley, Jr., J. Cappello, H. Ghandehari, In vitro and in vivo evaluation of recombinant silk-elastinlike hydrogels for cancer gene therapy, *J Control Release* 94 (2-3) (2004) 433-45.
28. K. Raile, R. Hille, S. Laue, A. Schulz, G. Pfeifer, F. Horn, W. Kiess, Insulin-like growth factor I (IGF-I) stimulates proliferation but also increases caspase-3 activity, Annexin-V binding, and DNA-fragmentation in human MG63 osteosarcoma cells: co-activation of pro- and anti-apoptotic pathways by IGF-I, *Horm Metab Res* 35 (11-12) (2003) 786-93.
29. W. Lopaczynski, S. Harris, P. Nissley, Insulin-like growth factor-I (IGF-I) dependent phosphorylation of the IGF-I receptor in MG-63 cells, *Regul Pept* 48 (1-2) (1993) 207-16.
30. V. Luginbuehl, E. Wenk, A. Koch, B. Gander, H.P. Merkle, L. Meinel, Insulin-like growth factor I-releasing alginate-tricalciumphosphate composites for bone regeneration, *Pharm Res* 22 (6) (2005) 940-50.
31. S. Hofmann, D. Kaplan, G. Vunjak-Novakovic, L. Meinel, *Tissue Engineering of Bone*, in *Culture of Cells for Tissue Engineering*, G. Vunjak-Novakovic, R.I. Freshney, Editors. 2006, John Wiley & Sons Inc.: Hoboken, New Jersey (published simultaneously in Canada) p. 323 - 373.
32. R.W. Farndale, C.A. Sayers, A.J. Barrett, A direct spectrophotometric microassay for sulfated glycosaminoglycans in cartilage cultures, *Connect Tissue Res* 9 (4) (1982) 247-8.
33. D.L. Streiner, Maintaining standards: differences between the standard deviation and standard error, and when to use each, *Can J Psychiatry* 41 (8) (1996) 498-502.
34. N.V. Bhat, G.S. Nadiger, Crystallinity in Silk Fibers: Partial Acid Hydrolysis and Related Studies., *J. Appl. Polym. Sci.* 25 (1979) 921-932.

35. S.J. Milner, G.L. Francis, J.C. Wallace, B.A. Magee, F.J. Ballard, Mutations in the B-domain of insulin-like growth factor-I influence the oxidative folding to yield products with modified biological properties, *Biochem J* 308 (Pt 3) (1995) 865-71.
36. M.R. Urist, Bone: formation by autoinduction, *Science* 150 (698) (1965) 893-9.
37. J.M. Wozney, V. Rosen, A.J. Celeste, L.M. Mitsock, M.J. Whitters, R.W. Kriz, R.M. Hewick, E.A. Wang, Novel regulators of bone formation: molecular clones and activities, *Science* 242 (4885) (1988) 1528-34.
38. J.M. Wozney, The bone morphogenetic protein family and osteogenesis, *Mol Reprod Dev* 32 (2) (1992) 160-7.
39. F. Kandziora, G. Schmidmaier, G. Schollmeier, H. Bail, R. Pflugmacher, T. Gorke, M. Wagner, M. Raschke, T. Mittlmeier, N.P. Haas, IGF-I and TGF-beta1 application by a poly-(D,L-lactide)-coated cage promotes intervertebral bone matrix formation in the sheep cervical spine, *Spine* 27 (16) (2002) 1710-23.
40. V. Karageorgiou, M. Tomkins, R. Fajardo, L. Meinel, B. Snyder, K. Wade, J. Chen, G. Vunjak-Novakovic, D.L. Kaplan, Porous silk fibroin 3-D scaffolds for delivery of bone morphogenetic protein-2 in vitro and in vivo, *J Biomed Mater Res A* 78 (2) (2006) 324-34.
41. F.R. Rose, Q. Hou, R.O. Oreffo, Delivery systems for bone growth factors - the new players in skeletal regeneration, *J Pharm Pharmacol* 56 (4) (2004) 415-27.
42. L. Meinel, O.E. Illi, J. Zapf, M. Malfanti, H. Peter Merkle, B. Gander, Stabilizing insulin-like growth factor-I in poly(D,L-lactide-co-glycolide) microspheres, *J Control Release* 70 (1-2) (2001) 193-202.
43. V. Luginbuehl, L. Meinel, H.P. Merkle, B. Gander, Localized delivery of growth factors for bone repair, *Eur J Pharm Biopharm* 58 (2) (2004) 197-208.
44. S. Srisailam, T.K. Kumar, T. Srimathi, C. Yu, Influence of backbone conformation on protein aggregation, *J Am Chem Soc* 124 (9) (2002) 1884-8.
45. Q. Xu, T.A. Keiderling, Trifluoroethanol-induced unfolding of concanavalin A: equilibrium and time-resolved optical spectroscopic studies, *Biochemistry* 44 (22) (2005) 7976-87.
46. M.N. Pollak, C. Polychronakos, M. Richard, Insulinlike growth factor I: a potent mitogen for human osteogenic sarcoma, *J Natl Cancer Inst* 82 (4) (1990) 301-5.
47. L. Franklin, L. Haynie, J. Davis, M. Tucci, H. Benghuzzi, G. Russell, A. Ragab, Evaluation of insulin-like growth factor-1 and parathyroid hormone on growth characteristics of MG-63 cells, *Biomed Sci Instrum* 41 (2005) 217-22.

48. H. Madry, D. Zurakowski, S.B. Trippel, Overexpression of human insulin-like growth factor-I promotes new tissue formation in an ex vivo model of articular chondrocyte transplantation, *Gene Ther* 8 (19) (2001) 1443-9.
49. Q. Cheng, T.Z. Peng, X.B. Hu, C.F. Yang, Charge-selective recognition at fibroin-modified electrodes for analytical application, *Anal Bioanal Chem* 382 (1) (2005) 80-4.
50. X. Wang, E. Wenk, A. Matsumoto, L. Meinel, C. Li, D.L. Kaplan, Silk microspheres for encapsulation and controlled release, *J Control Release* 117 (3) (2007) 360-70.
51. S. Walsh, C.M. Jefferiss, K. Stewart, J.N. Beresford, IGF-I does not affect the proliferation or early osteogenic differentiation of human marrow stromal cells, *Bone* 33 (1) (2003) 80-9.
52. M. Baddoo, K. Hill, R. Wilkinson, D. Gaupp, C. Hughes, G.C. Kopen, D.G. Phinney, Characterization of mesenchymal stem cells isolated from murine bone marrow by negative selection, *J Cell Biochem* 89 (6) (2003) 1235-49.
53. M. Milne, J.M. Quail, C.J. Rosen, D.T. Baran, Insulin-like growth factor binding proteins in femoral and vertebral bone marrow stromal cells: expression and regulation by thyroid hormone and dexamethasone, *J Cell Biochem* 81 (2) (2001) 229-40.
54. M. Mastrogiacomo, R. Cancedda, R. Quarto, Effect of different growth factors on the chondrogenic potential of human bone marrow stromal cells, *Osteoarthritis Cartilage* 9 Suppl A (2001) 36-40.
55. P.A. Conget, J.J. Minguell, Phenotypical and functional properties of human bone marrow mesenchymal progenitor cells, *J Cell Physiol* 181 (1) (1999) 67-73.
56. G. Maor, M. Silbermann, K. von der Mark, D. Heingard, Z. Laron, Insulin enhances the growth of cartilage in organ and tissue cultures of mouse neonatal mandibular condyle, *Calcif Tissue Int* 52 (4) (1993) 291-9.
57. G. Maor, Z. Hochberg, M. Silbermann, Insulin-like growth factor I accelerates proliferation and differentiation of cartilage progenitor cells in cultures of neonatal mandibular condyles, *Acta Endocrinol (Copenh)* 128 (1) (1993) 56-64.
58. K. Kellner, M.B. Schulz, A. Gopferich, T. Blunk, Insulin in tissue engineering of cartilage: a potential model system for growth factor application, *J Drug Target* 9 (6) (2001) 439-48.

-
59. J. Elisseeff, W. McIntosh, K. Fu, B.T. Blunk, R. Langer, Controlled-release of IGF-I and TGF-beta1 in a photopolymerizing hydrogel for cartilage tissue engineering, *J Orthop Res* 19 (6) (2001) 1098-104.
 60. T.A. Holland, E.W. Bodde, V.M. Cuijpers, L.S. Baggett, Y. Tabata, A.G. Mikos, J.A. Jansen, Degradable hydrogel scaffolds for in vivo delivery of single and dual growth factors in cartilage repair, *Osteoarthritis Cartilage* 15 (2) (2007) 187-9.

CHAPTER V

Silk fibroin matrices for the controlled release of nerve growth factor (NGF)

*Lorenz Uebersax¹, Marta Mattotti¹, Michaël Papaloïzos², Hans P. Merkle¹,
Bruno Gander¹, Lorenz Meinel¹*

¹Institute of Pharmaceutical Sciences, ETH Zurich, Zurich, Switzerland

*²Center for Hand Surgery and Therapy, CH8, Rue Charles-Humbert 8, 1205
Geneva, Switzerland*

ABSTRACT

Nerve conduits (NC) for peripheral nerve repair should guide the sprouting axons and physically protect the axonal cone from any damage. The NC should also degrade after completion of its function to obviate the need of subsequent explantation and should optionally be suitable for controlled drug release of embedded growth factors to enhance nerve regeneration. SF is a biocompatible and slowly biodegradable biomaterial with excellent mechanical properties that could meet the above stated requirements. SF material (films) supported the adherence and metabolic activity of PC12 cells, and, in combination with NGF, supported neurite outgrowth during PC12 cell differentiation. NGF-loaded SF-NC were prepared from aqueous solutions of NGF and SF (20%, w/w), which were air-dried or freeze-dried (freezing at -20 °C or -196 °C) in suitable molds. NGF release from the three differently prepared SF-NC was prolonged over at least three weeks, but the total amount released depended on the drying procedure of the NC. The potency of released NGF was retained within all formulations. Control experiments with differently dried NGF-lactose solutions did not evidence marked protein aggregation (SEC, HPLC), loss of ELISA-reactivity or PC12 cell bioactivity. This study encourages the further exploitation of SF-NC for growth factor delivery and evaluation in peripheral nerve repair.

INTRODUCTION

Peripheral nerve injury is a serious issue affecting 2.8% of trauma patients, many of whom will be subjected to life-long disability [1]. For successful nerve regeneration, axons from the proximal stump of a severed nerve have to bridge the gap towards the distal stump, where they should follow the idiosyncratic Schwann cell tubes, replicating the original receptor innervation pattern and finally leading to restoration of function of sensory and/or motor targets [2]. Throughout this critical process, the axons are supported by neurotropic factors, such as the nerve growth factor (NGF), which are released from in-growing Schwann cells or cells from the distal stump [3, 4]. Axonal growth is guided through physical (contact guidance) and chemotactical (neurotropism) mechanisms. For the bridging of small nerve gaps, microsurgical end-to-end sutures of the nerve stumps are often used [5, 6]; for longer gaps, autologous nerve grafts [5] have to be implanted. Despite the well developed microsurgical techniques used, the functional motor and sensory regeneration is often unsatisfactory because of neuroma and scar formation at the suture site, axonal loss, or failure of target reinnervation.

The limited availability of donor tissue for nerve autografts with the related morbidity at the donor site motivated the use of synthetic nerve conduits (NC) [7]. NC made of non-bioresorbable materials [8, 9] such as S-hydrophilic nitrocellulose (ShNC), S-hydrophobic poly(vinylidene fluoride) (PVDF) [10], or silicone showed promising results, but caused sometimes inflammation or compression of the nerve [11]. NC made of bioresorbable materials such as bioglass [12, 13], poly(L-lactide-co-ethylene oxide) (p(LA-co-EO)) [14, 15], poly(2-hydroxyethyl methacrylate-co-methyl methacrylate) (p(HEMA-co-MMA)) [16], and poly(glycolic acid) (PGA) [17, 18] have been successfully used in small gaps. However, the outgrowth of sensory axons after nerve transection was compromised in the case of a synthetic PGA NC [11]. NC have also been successfully produced from natural materials such as collagen and collagen/agarose blends [19, 20], although the physical stability of pure collagen

NC was increased by cross-linking [21]. Cross-linked collagen NC has produced inflammatory reactions and shown complete bioerosion within two months after implantation [22].

To promote the bridging of gaps exceeding the critical size of 10 mm, NC have been combined with neurotrophic factors [23]. Such NC drug delivery systems promoted efficaciously nerve guidance and target reinnervation [24, 25] both *in vitro* and *in vivo* [26-28]. The sustained delivery of GDNF or NGF from NC enhanced nerve regeneration over long gaps *in vivo* [29]. A general problem in using growth factors in combination with drug delivery systems resides in the inherent instability of such proteins, which tend to degrade or aggregate in solution or during processing [30]. The stability of neuronal factors during processing and formulation might be reduced when using mild processing conditions, e.g. through avoiding organic solvents, aqueous/organic interfaces, or chemical reagents. Indeed, the fabrication of parenteral delivery systems frequently requires one or several of these stress factors either for dissolving or shaping the matrix materials or for rendering water-soluble matrix materials insoluble by cross-linking. The latter point is of particular interest for silk fibroin (SF). Thanks to its solubility in water, SF can be processed in aqueous media by freeze-drying [31, 32] or air-drying, and subsequently be rendered insoluble by physical induction of β -sheet formation. This qualifies SF as a promising biomaterial for the fabrication of protein delivery systems, in particular long nerve guidance conduits, as it is biocompatible, of high resilience, and slowly biodegrading [33-36]. Silk has been used for decades as suture material and has a long standing clinical history [37, 38]. Moreover, silk fibers are mechanically strong and can absorb high amounts of energy before break [36]. These properties are important for NC materials. The use of SF as a substrate for neuronal cells [39] as well as a biomaterial for the delivery of proteins [40] has been well documented by our group as well as their biocompatibility *in vitro* and *in vivo* [34, 35].

The present study investigated SF derived from the silk worm *Bombyx mori* as a biomaterial for the preparation of NGF-loaded NC. The NGF-loaded SF-NC were prepared from aqueous solutions of NGF and SF and subsequent drying of

this solution in suitable molds according to three different protocols (air-drying, freeze-drying after freezing at $-20\text{ }^{\circ}\text{C}$ or $-196\text{ }^{\circ}\text{C}$). An initial experiment revealed that PC12 cells adhered well to SF, remained metabolically active, and showed neurite outgrowth during cell differentiation when NGF was supplemented, which is in agreement with findings in the literature [41-43]. The different processing conditions used for preparing NGF-loaded SF NC did not destroy the NGF bioactivity. The release of bioactive NGF over 4 weeks from both freeze-dried and air-dried formulations substantiated the potential of NGF-loaded SF materials for use in peripheral nerve defects.

MATERIALS AND METHODS

Materials

Cocoons from *Bombyx mori* were obtained from Trudel, Zurich, Switzerland, and processed in-house to obtain silk fibroin (SF), as described below. Collagen 1 (Calf Skin) and laminin (natural mouse) were purchased from Invitrogen (Carlsbad, CA, USA). Recombinant human beta-NGF (NGF) was kindly provided by Genentech (South San Francisco, CA). All cell culture materials including the medium and medium supplements were purchased from Invitrogen (Carlsbad, CA, USA), unless otherwise stated. The ATP bioluminescent assay kit, MTT assay kit, Triton-X, paraformaldehyde, and EDTA were from Sigma-Aldrich (St. Louis, MO, USA), and the Pico green assay kit from Molecular Probes Europe BV (Leiden, The Netherlands). The duo-set ELISA kit for NGF was from R&D systems (Minneapolis, MN).

Purification of silk fibroin (SF)

Silk fibroin (SF) was prepared as described previously [44]. Briefly, cocoons from *Bombyx mori* were boiled in ultra purified water (UPW) containing $0.02\text{ M Na}_2\text{CO}_3$, rinsed with water, and dissolved in 9 M LiBr at $55\text{ }^{\circ}\text{C}$ to obtain a

10% SF (w/v) solution. This solution was dialyzed (Pierce, MWCO 2000 g/mol) against UPW for 3 days to obtain a 4% (w/v) SF solution.

Preparation of SF films, collagen 1 films and laminin coatings for PC12 cell assays

SF films

SF films were prepared from 2 ml of sterile filtered (0.2 μm pore size filter) aqueous SF solution (3%, w/w) that was filled into 22 mm diameter flat Teflon molds. SF films were obtained upon evaporation under laminar airflow overnight and subsequently treated with 90% methanol (v/v) for 30 min to induce insolubility in aqueous media.

Collagen (Col-1) films

Calf skin Col-1 films were prepared in 12-well non-tissue culture polystyrene plates (Techno Plastic Products, TPP, Trasadingen, Switzerland) by pipetting 1 ml of a collagen solution (0.5 g/l in 0.1% (v/v) acetic acid) into each well. Col-1 films were obtained upon drying overnight, neutralizing with 2 ml of 0.1 M Na_2HPO_4 for 1 h, and washing twice with PBS.

Laminin (LN) coating

LN coating was applied to 12-well non-tissue culture polystyrene plates (TPP) by pipetting 640 μl of a laminin solution (1 $\mu\text{g}/\text{ml}$ in PBS of pH 7.4) into each well. After 2 h, the solution was withdrawn, and the wells were washed twice with 1 ml of PBS of pH 7.4.

Preparation of NGF-loaded SF films and SF tubes

SF films were prepared as described above; NGF was embedded by adding 16 µg NGF to 2 ml of 4% (w/w) SF solution, which was then poured into Teflon molds for evaporation of water. Films were then dried under laminar airflow. SF tubes were prepared as follows. The 3% (w/v) SF solution as prepared above was dialyzed against PEG 6000 (Pierce, MWCO 2000 g/mol) to yield a viscous solution with a final concentration of 20% (w/w) SF. Then, 40 µg NGF was added to 1 ml of the 20% SF solution, which was shaken for 10 min at 4 °C to achieve homogeneity. This resulting solution was poured into tubular molds designed to obtain SF tubes with an outer and inner diameter of 3 and 1 mm, respectively. The filled molds were deep frozen at -20 °C during 1 h (Lyo-20) or shock-frozen at -196 °C in liquid nitrogen (Lyo-196) before they were freeze-dried at -30 °C during 36 h (LYOVAC GT2, FINN-AQUA, Hurth, Germany). Dried films and tubes were treated with 90% (v/v) methanol in UPW for 30 min to induce insolubility of the SF matrices in aqueous media.

Scanning electron microscopy (SEM)

SF films and SF tubes were cut into slices of 1 - 2 mm thickness, dried, platinum-coated and analyzed by scanning electron microscopy (SEM; Leo 1530, Carl Zeiss, Trasadingen, Germany).

Fourier transformed infrared spectroscopy (FTIR)

For FTIR, 5 mg of SF film or SF tube were ground with mortar and pestle, mixed with 300 mg KBr, and compressed with 10 tons (diameter of compact = 13 mm) under vacuum during one min before analysis (2000 FT-IR Spectrometer, V3,01, Perkin Elmer, Boston, MA).

Differential scanning calorimetry (DSC)

DSC was performed with 3 mg of SF film or SF tube at a heating rate of 10 °C/min and nitrogen flushing at 100 ml/min in two subsequent scans from 25 to 200 °C, and 25 to 260 °C, respectively (DSC822, Mettler Toledo, Greifensee, Switzerland). The thermal transitions of SF were determined from the second scan, after evaporation of the initial moisture.

Size exclusion chromatography (SEC) of processed NGF

The effect of the processing (air-drying, freeze-drying) on the stability of NGF was examined by SEC to detect high molecular weight aggregates. To exclude potential effects of SF, lactose was used as a surrogate excipient for SF, at a NGF : lactose ratio of 1 : 5'500. Aqueous lactose solutions (20%, w/v, for mimicking the SF freeze-drying; 3%, w/v, for mimicking the SF air-drying) were mixed with a NGF solution (3.16 mg/ml) to obtain a final NGF concentration of 40 µg/ml. The lactose-NGF solutions were freeze-dried after initial freezing at -20 °C or -196 °C, or air-dried at room temperature under laminar air flow. NGF in acetate buffer (40 µg/ml; pH 5.5) containing the same NGF: lactose ratio was used as control. The freeze-dried and air-dried materials were re-suspended in acetate buffer (pH 5.5) to obtain a NGF concentration of 100 µg/ml. Then, 50 µl (2.5 µg NGF) of the solution were injected in a Tosohas TSK G2000 SW (7.5 mm x 300 mm, 10 µm) size exclusion column installed in a Hitachi LaChrom HPLC, equipped with a L-7100 pump and a L-7485 fluorescence detector (Hitachi, Tokyo, Japan). Elution was done at 1 ml/min using a mobile phase of 0.2 M potassium phosphate and 0.45 M potassium chloride of pH 7.0. All solutions were filtered through a cellulose acetate membrane (0.45 µm; Sartorius, Goettingen, Germany) and degassed by ultrasonication. Insulin (5.77 kDa), myoglobin (18 kDa) and ovalbumin (44.3 kDa) were used as reference proteins.

RP-HPLC of processed NGF

The samples that had been used in SEC were also analyzed for chemical degradation by reverse phase HPLC (RP-HPLC) using a C4 RP-HPLC column (Symmetry 300™ C4, 2.1 mm x 150 mm, 3.5 μm; Waters Corporation, Milford, MA). NGF was eluted at 0.5 ml/min using eluent A (5% acetonitril and 0.2% TFA in water) and eluent B (80% acetonitril, 0.2% TFA) under the following gradient: 74% A from 0 to 1 min, 40% A from 1 to 25 min, 100% A from 25 to 29 min, and 26% A from 30 to 40 min.

NGF in vitro release and quantification by ELISA

Pieces of tubes or films (~10 mg, n=6) were immersed in 50 mM acetate buffer of pH 5.0 containing 0.02% Tween 40 and 0.05% sodium azide. Samples were taken at regular intervals during 4 weeks, and the liquid was replaced with fresh buffer. NGF concentration was assayed by a duo-set ELISA kit for NGF following the manufacturer's protocol. Briefly, flat-bottom 96-well polystyrene plates (Nalge Nunc, Roskilde, Denmark) were washed with a 0.05% Tween 20-PBS solution of pH 7.4 between every step of the assay and 3 times at each step (300 μl/well). Microplates were initially coated overnight with a purified mouse monoclonal IgG1 anti hβ-NGF in PBS (100 μl/well), and non specific sites were blocked for 1 h using a solution of 1% BSA (w/v), 5% sucrose, 0.05% NaN₃ in PBS (300 μl/well). The samples and the biotinylated antibody, appropriately diluted in a 1% BSA-TBST solution were sequentially added and incubated for 2 h each. The streptavidin-HRP was diluted in a 5% BSA (w/v) PBS solution and added and incubated for 20 min. Reactant volumes were 100 μl/well. A tablet of TMB (Sigma-Aldrich, St. Louis, MO, USA) was dissolved in 0.05 M phosphate-citrate buffer of pH 5.0 containing 0.02% hydrogen peroxide 30% and placed in the wells for 20 min. The reaction was stopped by the addition of 50 μl of 1 M H₂SO₄. Absorbance was read at 450-570 nm using a microplate reader (Molecular Devices, Bucher Biotec, Basel, Switzerland).

Expansion and differentiation of PC12 cells

PC12 cells were cultured on Petri dishes for tissue culture (TPP) using DMEM containing 10% fetal calf serum (FCS) and 1% penicillin/streptomycin (P/S) solution. The cells were split every 2 to 3 days. For assessing PC12 proliferation and differentiation on different substrates (see below), 5×10^4 cells/well were seeded in a 12-well plate in DMEM containing 1% FCS and 1% P/S.

Proliferation and differentiation of PC12 on LN, Col-1 and SF substrates

PC12 cell proliferation on the various substrates was assessed by total DNA quantification and a MTT assay. For the DNA assay, cells were seeded in quintuplicate at 5×10^4 cells/well on the different substrates inserted into the wells of 12-well plates and incubated at 37 °C and 5% CO₂. After 24 h, the DNA content in each well was assessed by the PicoGreen assay according to the manufacturer's protocol. Supernatant was soaked off, and the cells were disrupted by adding 1 ml of lysis buffer (0.2% Triton-X and 5 mM MgCl₂) to each well and incubated in the dark for 48 h. The lysates were transferred into tubes and centrifuged at 3000 g and RT for 10 min. Then, 41 µl of supernatant were transferred into a new tube and complemented with 166.6 µl of diluted PicoGreen solution (PicoGreen dimethylsulfoxide stock solution diluted 200 times in TE assay buffer). After vortexing for 3 min, 100 µl of the solution were transferred to a 96-well plate and incubated for 5 min in the dark. The fluorescence of the standard and sample solutions was measured in a FluoroCount plate reader with λ_{ex} and λ_{em} of 485 and 530 nm, respectively (Packard Instrument, Downes Gore, IL).

For the MTT-assay, PC12 cells were seeded on the different substrates and incubated for 24 h as described above. MTT dissolved in PBS (5 mg/ml) was sterile filtered and diluted 10 times with DMEM before use. For the assay, the cell medium was soaked off, and 2.0 ml of the MTT solution was added to the cells, which were then incubated at 37 °C and 5% CO₂ for 2 h. Then, the solution was

soaked off, and 1 ml of acidic isopropyllic acid (500 ml isopropyllic acid + 3.5 ml 6 M HCl) was added to dissolve the formed crystals. After 10 minutes incubation at RT, the tubes were centrifuged (300 g, 1 min, 4 °C), and 100 µl of the supernatant were transferred to a 96 well plate. The absorbance was measured at 570 nm and the background (630 nm) subtracted using a Thermomax microplate reader (Molecular Devices Corporation, Sunnyvale, CA).

For assessing the differentiation of PC12 cells, 5×10^4 cells per well were seeded in triplicate on the different substrates (SF, Col-1, LN) and incubated for 24 h as described above. Then, the medium was replaced by DMEM containing 1% FCS and 100 ng/ml of NGF. Neurite outgrowth from PC12 cells was subsequently monitored during three days. Cells exposing neurites exceeding double the length of their cellular body were considered as fully differentiated. The extent of differentiation was quantified on the basis of 100 cells per specimen.

Assessment of bioactivity of released NGF from SF matrices

For assessing the bioactivity of released NGF, pieces of 10 mg of films or freeze-dried tubes were incubated in triplicate in acetate buffer at 37 °C on an orbital shaker (80 rpm). After 0, 1, 2, 3 and 4 weeks of incubation, the SF matrices were taken out and rinsed with PBS before they were added ($n = 3$) to plated PC12 cells (5×10^4 cell per well) in DMEM containing 1% FCS on LN-coated 12-well plates (TPP). DMEM containing 1% FCS and 100 ng/ml of NGF was used as control for all experiments. Pictures of PC12 cells were taken after 4 days of culture using an Axiovert 35 microscope equipped with an Axio Cam MRc5 digital camera (Carl Zeiss, Jena, Germany). For quantification, cells were considered fully differentiated when the outgrowth of the exposed neurites exceeded double the size of their cellular body; average and standard deviation of 100 differentiated cells per specimen were calculated.

Statistical analysis

Statistical data analysis was performed by one-way analysis of variance (ANOVA) and Tukey-HST procedure for *post hoc* comparison using Minitab® Release 14 for Windows. Values with $p < 0.05$ were considered statistically significant.

RESULTS

Proliferation and differentiation of PC12 cells on LN, SF and Col-1 substrates

Prior to the seeding of PC12 cells on the three substrates SF, Col-1 and LN, the static contact angle (θ) of purified water on the materials and the tissue culture plates (TCP) was assessed at 22 °C using a goniometer (NRL C, Ramé-Hart, Mountain Lakes, NJ, USA). All three substrates were more hydrophilic than the TCP, with SF being the most hydrophilic followed by Col-1 and LN ($\theta_{\text{SF}} = 43.0 \pm 1.4^\circ$; $\theta_{\text{Col-1}} = 58.3 \pm 0.7^\circ$; $\theta_{\text{LN}} = 62.1 \pm 0.4^\circ$; $\theta_{\text{TCP}} = 77.2 \pm 0.8^\circ$).

The metabolic activity (MTT assay; Fig. 1A) and proliferation (DNA content) of adherent PC12 cells did not reveal any significant differences between the cells grown on SF, Col-1, and LN ($n=5$) after a cultivation time of 24 h. Hence, the metabolic cell activity normalized to the DNA content of the cultures ($\text{OD}_{\text{MTT}}/\text{DNA}$) was also comparable between the cells grown on the different substrates (**Fig. 1B**).

The differentiation of adherent PC12 cells grown on the various substrates was assessed after addition of 100 ng/ml NGF in terms of neurite outgrowth (**Fig. 2**). Microscope images demonstrated that all substrates supported the outgrowth of neurites from differentiated PC12 cells (**Fig. 2A**). The percentage of differentiated cells increased gradually on all the three substrates during the 3 days of incubation (**Fig. 2B**). Statistical differences in the numbers of differentiated cells grown on the three substrates were observed only at day 2, whereas the percentage of differentiated PC12 cells was comparable on all substrates at days 1 and 3 of culture.

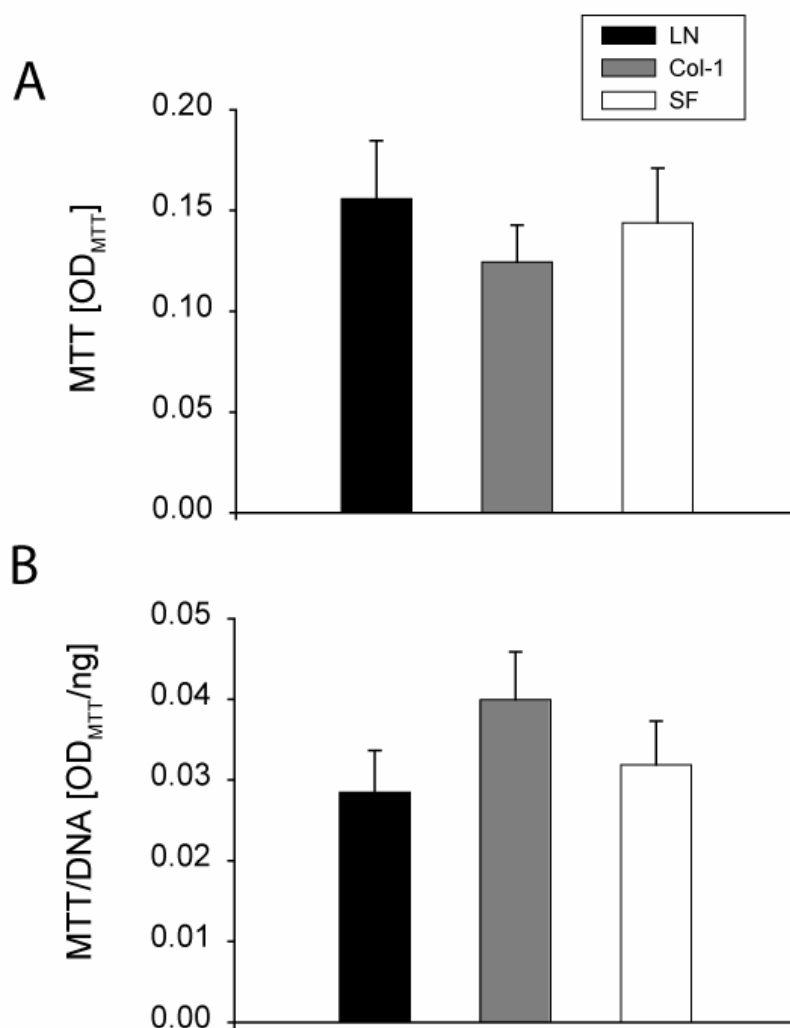


Fig. 1: Proliferation of PC12 cells grown on laminin (LN), collagen 1 (Col-1) and silk fibroin (SF) after 24 h ($n=5$). (A) Optical density (OD_{MTT}) of the converted MTT. (B) MTT conversion normalized to DNA content of the cells (OD_{MTT}/ng DNA).

Porosity and crystallinity of air-dried and freeze-dried SF matrices

Scanning electron microscopy (SEM) revealed a porous morphology of freeze-dried SF tubes and an essentially non-porous structure of air-dried SF films (**Fig. 3, column 3-5**). SF solutions slowly frozen at -20 °C (Lyo-20) prior to freeze-drying at -30 °C yielded a porous matrix exposing a connected meshwork of unordered lamellar-like pores of sizes between 20 and 100 μm (**Fig. 3, Lyo-20, row 1**); the inner wall of the tube (**Fig. 3, column**) was smooth and also porous. In contrast, SF solutions shock-frozen at -196 °C (**Fig. 3, Lyo-196, row 2**) prior to

freeze-drying at $-30\text{ }^{\circ}\text{C}$ yielded matrices with smaller pores of about $5\text{-}20\text{ }\mu\text{m}$ in diameter; the inner wall of the tube was smooth and displayed few small pores.

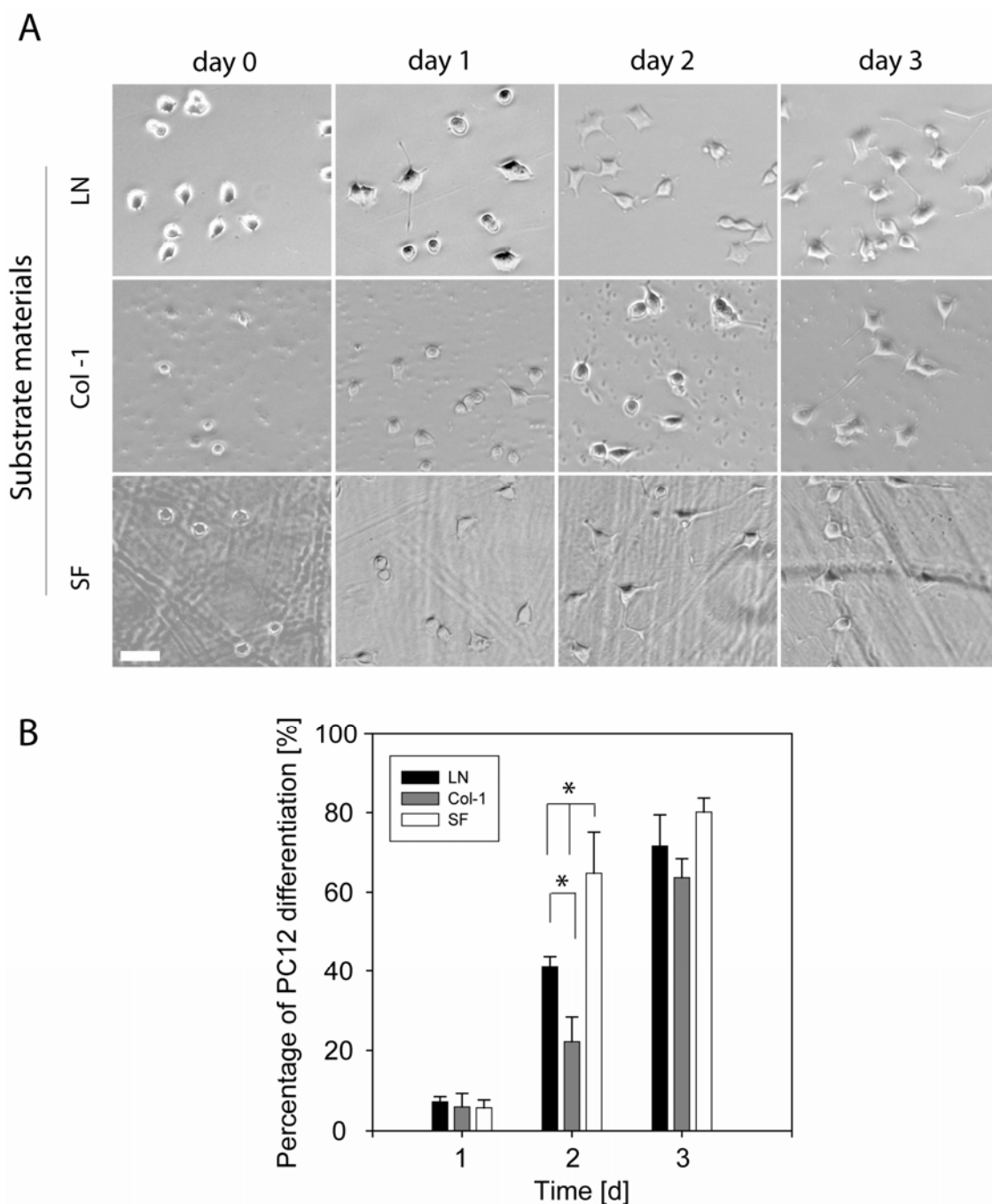


Fig. 2: Neurite outgrowth of PC12 cells grown on laminin (LN), collagen 1 (Col-1) and silk fibroin (SF). Neurite outgrowth was induced by addition of 100 ng/ml of nerve growth factor (NGF). (A) Phase contrast micrographs of adherent PC12 cells at different days after addition of NGF; scale bar = $20\text{ }\mu\text{m}$. (B) Percentage of differentiated PC12 cells showing neurite outgrowth at different days after addition of NGF.

Finally, the air-drying of SF solutions at ambient temperature and pressure resulted in 20-40 μm thick films that were even and smooth (**Fig. 3, films, row 3**). The measurement of total porosity, ϵ , by helium pycnometry ($n=5$; Accupyc 1330, Micromeritics, Moenchengladbach, Germany) corroborated the SEM observations in that the air-dried SF-films were essentially non-porous, whereas the freeze-dried SF tubes featured a high porosity, which was essentially independent of the mode of initial freezing temperature and rate: $\epsilon = 84.03 \pm 1.98\%$ for Lyo-196; $\epsilon = 87.39 \pm 2.69\%$ for Lyo-20).

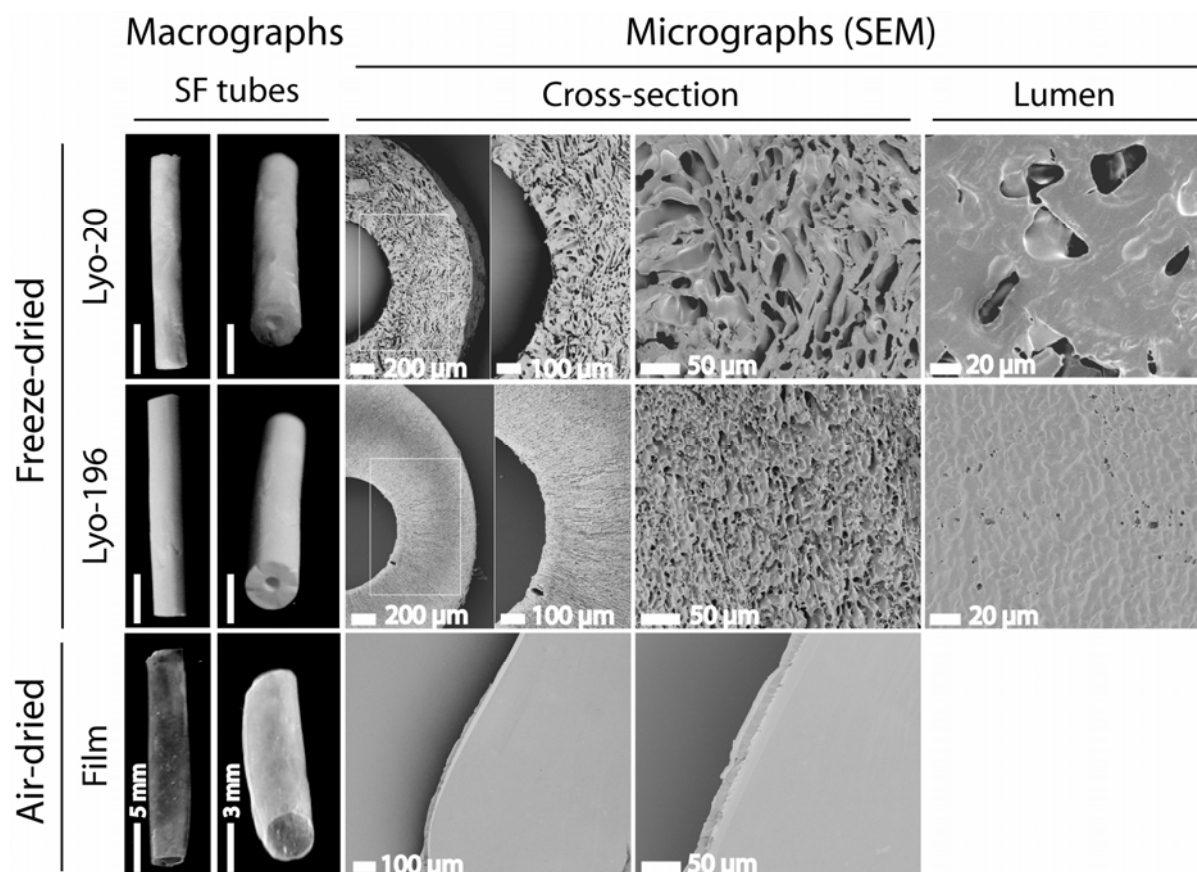


Fig. 3: Macrographs (“SF tubes” in columns 1 and 2) and scanning electron micrographs (“Cross-section” and “Lumen” in columns 3-6) of freeze-dried SF tubes shock-frozen at -196 °C (Lyo-196, row 1) or slowly frozen at -20 °C (Lyo-20, row 3), and of air-dried SF films rolled to a cylindrical matrix (film, row 3).

The induction of crystallinity in the different SF matrices by methanol treatment was examined by differential scanning calorimetry (DSC) and FTIR (**Fig. 4**). DSC thermograms did not show any crystallization or melting before the matrices started to decompose at 190-200 °C, irrespective of the preparation method of the SF matrices (data not shown). FTIR measurement revealed β -sheet conformation in all formulations, as evidenced by a shoulder at 1262 cm^{-1} , corresponding to the amide III band shift (for random coil at 1235 cm^{-1}), and an absorption band at 1630 cm^{-1} , corresponding to the amide I band shift (for random coil at 1660 cm^{-1}).

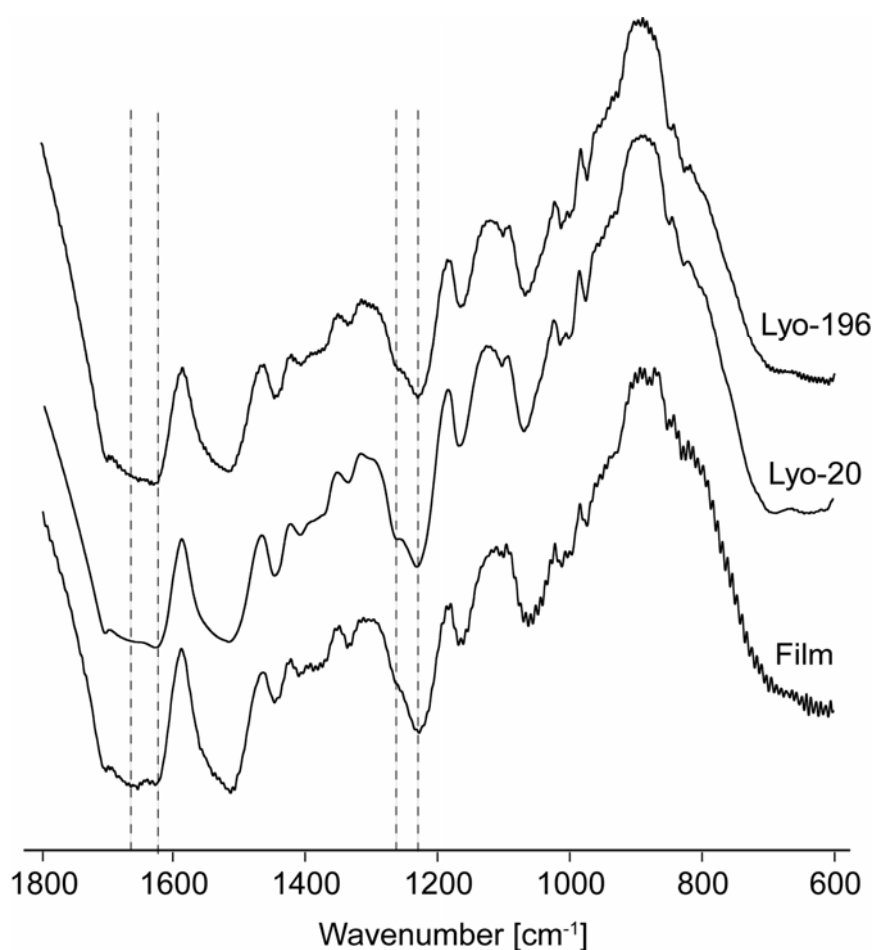


Fig. 4: Fourier transformed infrared spectra (FTIR) of silk fibroin matrices prepared by freeze-drying after shock-freezing at $-196\text{ }^{\circ}\text{C}$ (Lyo-196), freeze-drying after slow freezing at $-20\text{ }^{\circ}\text{C}$ (Lyo-20), or by air-drying (film).

Stability and bioactivity of NGF under process conditions for SF matrix preparation

In view of preparing NGF-loaded SF matrices, NGF stability was assessed upon air-drying of the NGF-SF solution at RT and upon slow and shock freezing (-20 °C for 1 h or -196 °C for 1 min) with subsequent freeze-drying (n=3). In this preliminary experiment, SF was replaced by lactose to avoid any potential interference of SF in the analysis of NGF. After drying, the solid product was re-dissolved in acetate buffer and analyzed by SEC, HPLC and in a PC12 cell bioassay; a fresh solution of equivalent amounts of NGF and lactose was used as control. SEC chromatograms (**Fig. 5**) of the control (Control) and freeze-dried (Lyo-20 and Lyo-196) NGF/lactose showed a main peak at a retention time (RT) of 9.5 min, corresponding to the NGF dimer, and a minor peak at RT of 5.6 min, most probably corresponding to a high molecular weight aggregate of NGF. The air-dried NGF/lactose showed enlarged main and minor peaks with shoulders between 10.5 and 13 min and between 5.1 and 5.3 min, respectively. Data integration revealed statistically similar amounts of air-dried, freeze-dried (Lyo-20 and Lyo-196), and control NGF (data not shown), which was also confirmed by ELISA (**Fig. 6A**). The percentage of high molecular aggregates was calculated from the ratio of areas under the curve (AUC) of the peaks at a retention time of 5.6 min and 9.5 min. The thus calculated percentages of high molecular weight aggregates did not differ significantly between NGF control, air-dried or freeze-dried samples (**Fig. 6B**). Hence, the AUC-values were not sufficiently sensitive to discriminate between the observed differences in the shape of the main peak.

Consequently, we calculated the ratio of the AUC (at RT of 9.5 min) over the corresponding peak height. This ratio was significantly ($p < 0.05$) increased, i.e., broader peak, for air-dried NGF/lactose in comparison to the control NGF and the Lyo-20 freeze-dried NGF/lactose; it was also significantly ($p < 0.05$) increased for Lyo-196 freeze-dried samples in comparison to the control NGF (**Fig. 6C**).

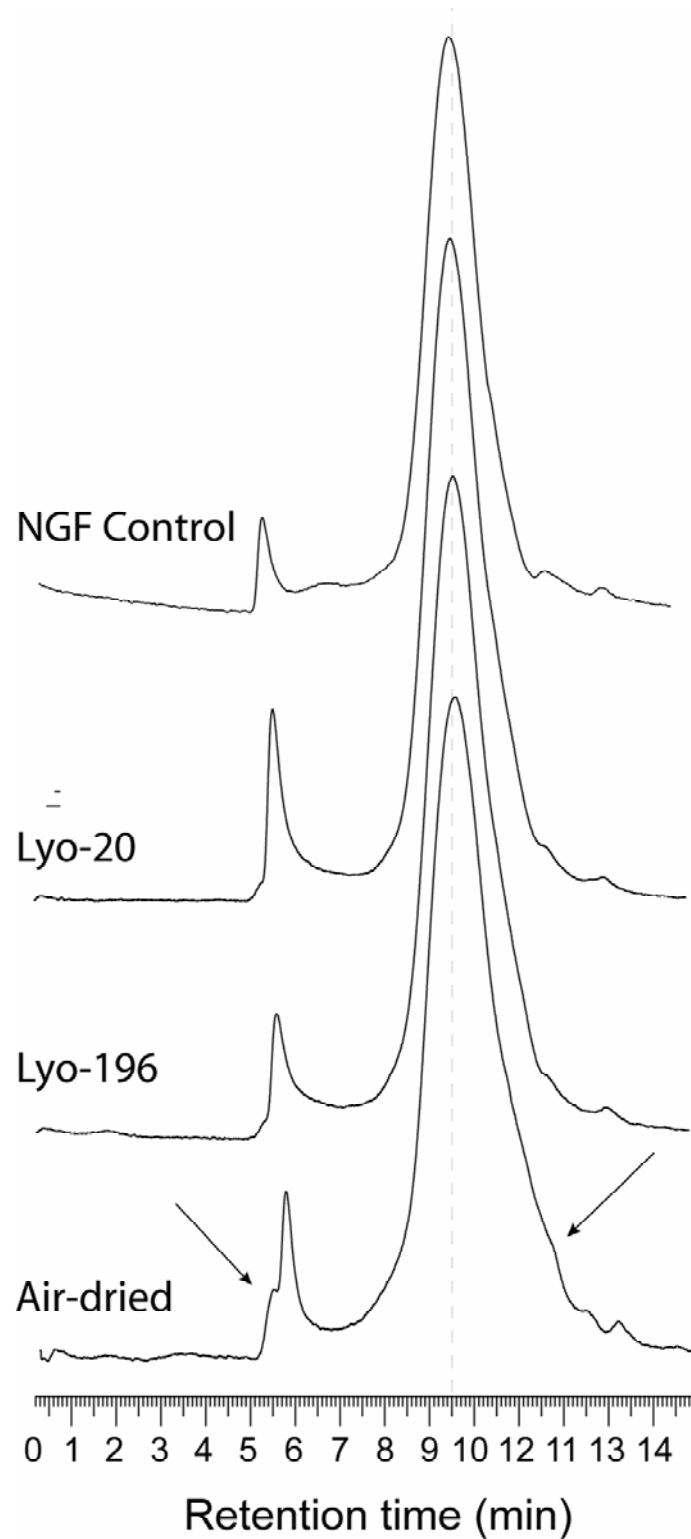


Fig. 5: Size exclusion chromatograms (SEC) of NGF after processing in blends with lactose. Solutions of NGF and lactose in acetate buffer of pH 5.5 were either freeze-dried after shock-freezing at $-196\text{ }^{\circ}\text{C}$ (Lyo-196), freeze-dried after slow freezing at $-20\text{ }^{\circ}\text{C}$ (Lyo-20), or air-dried (air-dried). NGF in acetate buffer (pH 5.5) stored at $4\text{ }^{\circ}\text{C}$ served as control (NGF control). Arrows indicate degradation products.

The testing of the various NGF/lactose formulations and control NGF in a PC12 cell bioassay evidenced a loss of NGF-bioactivity upon air-drying and freeze-drying of NGF/lactose solutions (**Fig. 6D**).

At a nominal NGF concentration of 2.5 ng/ml, none of the processed NGF/lactose blends triggered a significant differentiation of PC12 cells, in contrast to the control NGF. At a NGF concentration of 5 ng/ml, the freeze-dried samples (Lyo-20, Lyo-196) performed significantly ($p < 0.05$) better than the air-dried samples, although all processed samples triggered significantly ($p < 0.05$) less PC12 differentiation than the control NGF. The decreased bioactivity of the processed samples was no longer distinguishable at NGF concentrations of 10 ng/ml (freeze-dried samples) or 100 ng/ml (air-dried samples).

NGF content and bioactivity of rehydrated SF matrices

The amount and bioactivity of NGF that was recoverable from the rehydrated SF matrices were assessed by ELISA and PC12 cell bioassay, respectively (**Fig. 7**). In general, more than 50% of NGF remained unrecoverable from the SF formulations (control SF solution or matrix) when detected by ELISA, suggesting a strong binding between NGF and SF. The amount of recoverable NGF did not significantly differ between the NGF/SF control solution ($33.0 \pm 6.6\%$) and SF matrices (Lyo-20: $49.6 \pm 13.3\%$; Lyo-196: $55.2 \pm 36.5\%$; film: $30.7 \pm 7.5\%$) (**Fig. 7B**). In the bioassay, NGF eluted from freeze-dried matrices (Lyo-20 and Lyo-196) induced low ($< 20\%$) but significant PC12 differentiation at a dilution that corresponded nominally to 2.5 ng/ml NGF, which was not observed with comparable NGF dilutions from the NGF/SF control solution and NGF/SF film (**Fig. 7B**). At a nominal concentration of 5 ng/ml, the elutions from freeze-dried samples yielded a similar bioactivity as the control NGF/SF solution, which was comparable to the bioactivity of the eluted freeze-dried samples diluted to 2.5 ng/ml. At a nominal NGF concentration of 10 ng/ml, all matrix elutions as well as the NGF/SF control solution triggered a significant PC12 differentiation, although the bioactivity of the NGF/SF film elutions was

significantly lower ($48.6\% \pm 25.0$) than the NGF control ($90.6\% \pm 4.5$) and elutions of the matrices frozen at $-196\text{ }^{\circ}\text{C}$ and subsequently freeze-dried (Lyo-196; $87.2\% \pm 5.8$). At NGF dilutions of 100 ng/ml , all matrix elutions as well as the NGF/SF control solution induced comparable differentiation in the order of 80% of all adherent cells.

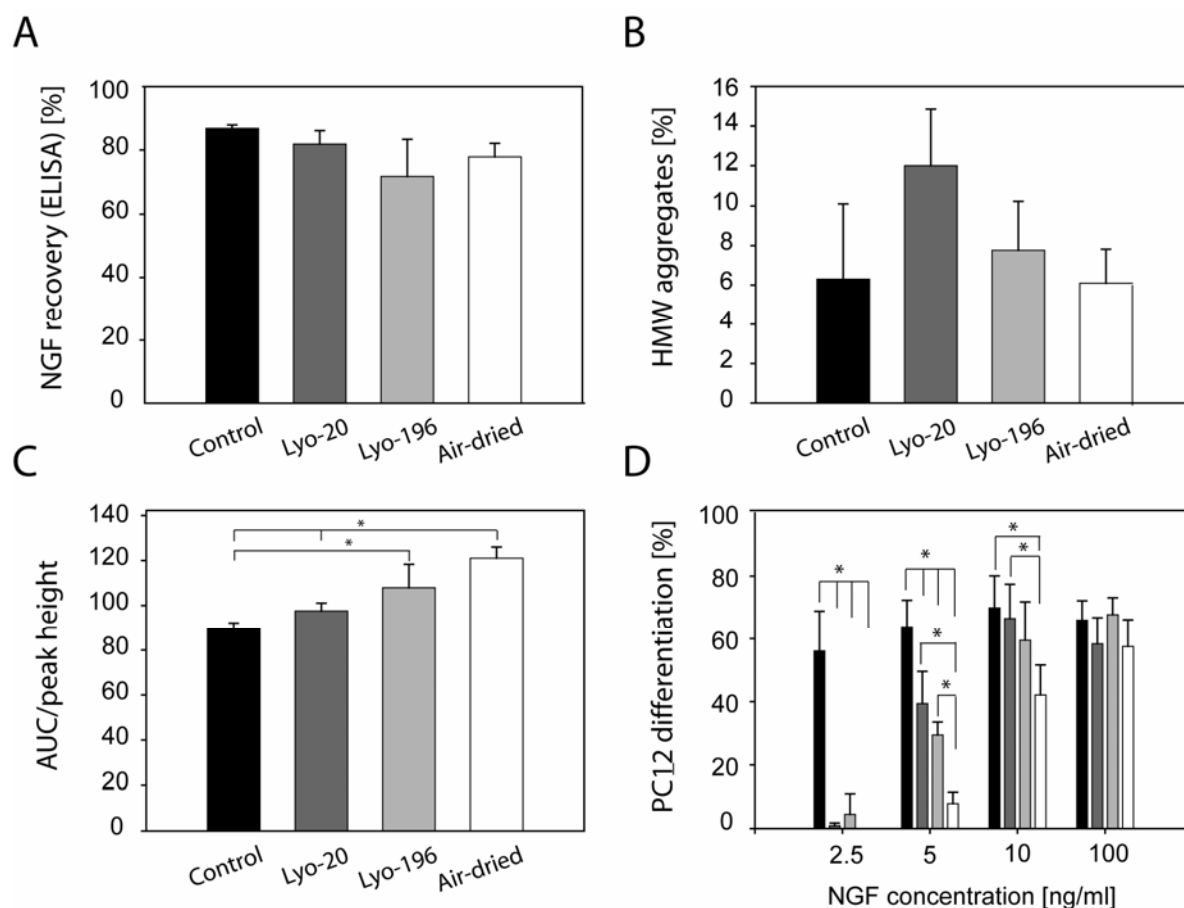


Fig. 6: Stability and bioactivity of NGF after processing in blends with lactose and assessed by ELISA (A), SEC (B, C), and PC12 cell differentiation (D). Solutions of NGF and lactose in acetate buffer of pH 5.5 were either freeze-dried after shock-freezing at $-196\text{ }^{\circ}\text{C}$ (Lyo-196), freeze-dried after slow freezing at $-20\text{ }^{\circ}\text{C}$ (Lyo-20), or air-dried (air-dried); a solution of NGF-lactose in acetate buffer of pH 5.5 stored at $4\text{ }^{\circ}\text{C}$ served as control (Control). (A) NGF quantification by ELISA; the data shows the percentage of recovered NGF relative to the initial amount. (B) SEC-derived percentage of high molecular aggregates of NGF after processing. (C) SEC-derived ratio of AUC/peak height of the NGF homodimer peak. (D) PC12 cell differentiation-derived bioactivity of NGF after processing; note that the different gray shadings of the bars in panel D correspond to those shown in panels A-C.

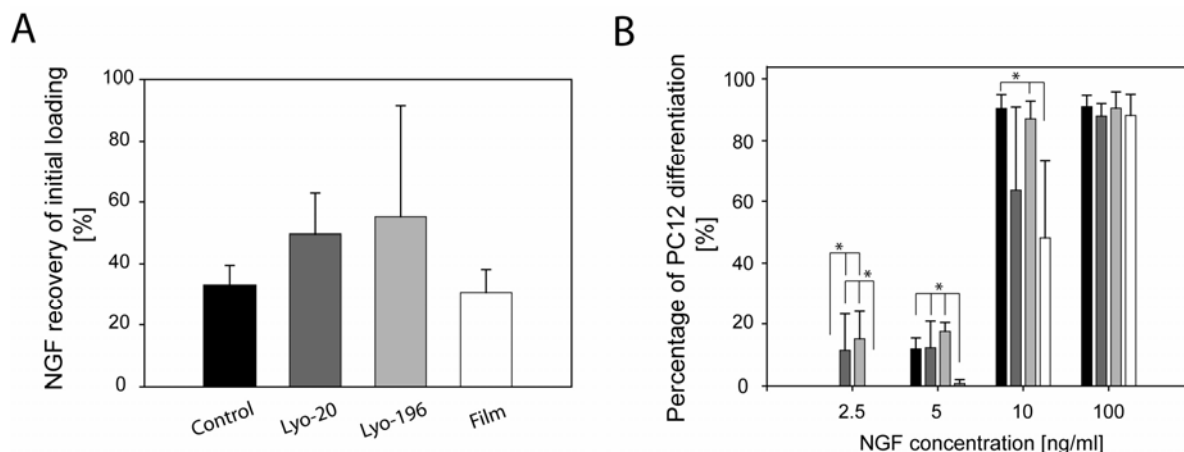


Fig. 7: Amounts of ELISA-responsive (A) and bioactive (B) NGF recovered from processed NGF-silk fibroin (SF) matrices. Solutions of NGF and SF in acetate buffer of pH 5.5 were either freeze-dried after shock-freezing at -196 °C (Lyo-196), freeze-dried after slow freezing at -20 °C (Lyo-20), or air-dried (Film); a solution of NGF-SF in acetate buffer of pH 5.5 stored at 4 °C served as control (NGF-SF-control). Note that the different gray shadings of the bars in panel B correspond to those shown in panel A.

In vitro release kinetics and bioactivity of NGF released from SF matrices

The three NGF/SF matrix types released significantly different absolute amounts, but comparable relative amounts of NGF within the first 4 days (**Fig. 8D**), with Lyo-20 releasing $0.37 \text{ ng} \pm 0.03$ or 78% of total (as measured after 22 days), Lyo-196 releasing $2.607 \text{ ng} \pm 0.69$ or 73% of total, and film releasing $12.8 \text{ ng} \pm 1.33$ or 66% of total). During this initial phase, both freeze-dried matrices released substantially less than 1 ng NGF per mg scaffold and day (**Fig. 8A, B**), whereas the SF film released between 2 and 4.5 ng NGF per mg scaffold and day (**Fig. 8C**). After 5 days, the daily NGF release from all matrices remained very low, though it continued until the end of the experiment. The absolute cumulative release after 22 days differed significantly between the formulations and attained $0.49 \pm 0.09 \text{ ng/mg}$ (Lyo-20 tube), $3.57 \pm 0.78 \text{ ng/mg}$ (Lyo-196 tube), and $23.40 \pm 8.64 \text{ ng/mg}$ (air-dried film). Therefore, the SF film released 49 and 6.5 times more NGF than the Lyo-20 and Lyo-196 SF tubes, respectively.

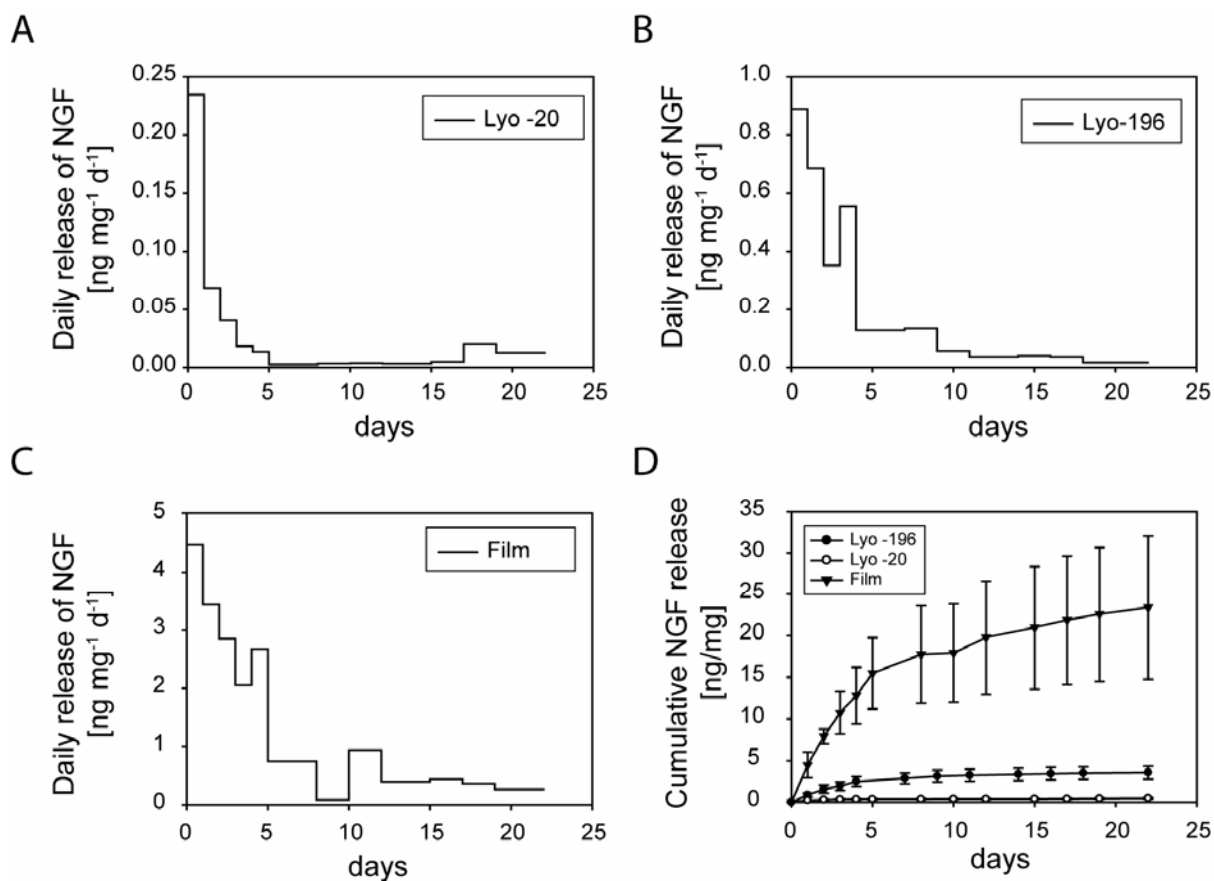


Fig. 8: NGF *in vitro* release from SF matrices in acetate buffer of pH 5.5. (A-C) Daily release of NGF per mg of SF matrix prepared by freeze-drying a NGF-SF solution after slow freezing at -20 °C (A; Lyo-20), or by freeze-drying a NGF-SF solution after shock-freezing at -196 °C (B; Lyo-196), or by air-drying a NGF-SF solution (C; Film). (D) Cumulative release per mg of SF matrix prepared by the aforescribed processes.

Relative to the total NGF dose incorporated into the matrices, the percentages of NGF released after 22 days amounted to $0.27 \pm 0.04\%$, $2.0 \pm 0.4\%$, and $13.0 \pm 4.8\%$ for the Lyo-20, Lyo-196, and air-dried SF matrices, respectively. The bioactivity of released NGF was tested with pre-incubated matrix samples ($n=3$) exposed to release conditions for different time periods prior to transferring the matrix samples to adherent PC12 cultures. Co-incubation of matrix samples with PC12 cells lasted for 4 days. At time zero, i.e., without pre-incubation, all matrices induced a similar extent of PC12 differentiation (approx. 55%), which was slightly lower than that induced by 100 ng/ml NGF (approx. 70%; control) (**Fig. 9**).

The pre-incubated air-dried NGF/SF film and freeze-dried Lyo-196 SF tube sustained sufficient NGF release during the entire 4 week period to trigger a consistently high PC12 cell differentiation. On the contrary, the freeze-dried Lyo-20 NGF/SF tubes induced significantly less cell differentiation already after one week of pre-incubation ($41.7 \pm 16.5\%$), and the bioactivity of the Lyo-20 samples dropped further to 2-20% at weeks 2 to 4 of pre-incubation. In conclusion, the bioactivity results were consistent with the profiles of the daily NGF release (**Fig. 8A-C**).

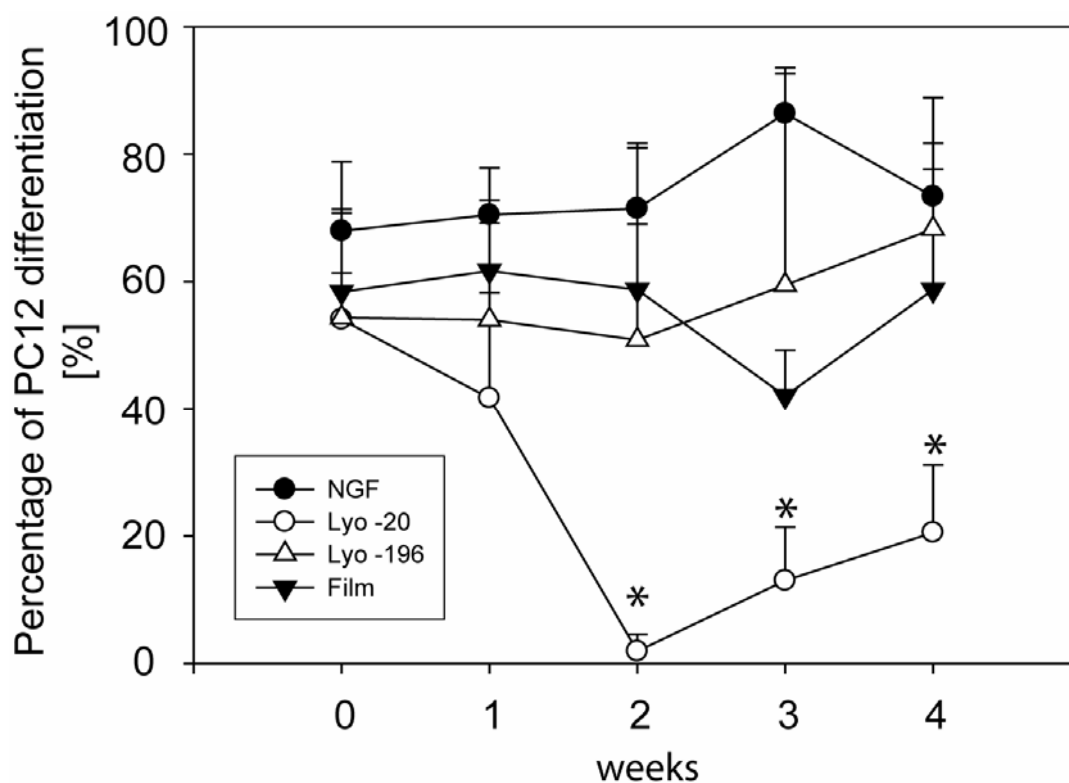


Fig. 9: PC12 cell differentiation-derived bioactivity of 10 mg NGF-SF matrices that had previously been pre-incubated in acetate buffer (pH 5.5) at 37 °C for 0, 1, 2, 3, and 4 weeks. At each time point, the pre-incubated NGF-SF matrices were carefully rinsed and incubated with PC12 cells for 4 days, after which the percentage of PC12 cells showing neurite outgrowth was determined. A solution of NGF in the release medium (100 ng/ml) served as control (NGF). The NGF-SF matrices were prepared as described before.

DISCUSSION

Several authors have reported that NC releasing neurotrophic factors can enhance nerve regeneration across long nerve gaps [29, 45-47]. Maximal benefit from neurotrophic factors can, however, only be achieved with effective and prolonged growth factor delivery [28]. Recent approaches aimed at embedding or encapsulating neurotrophic factors into a polymer [46, 48] or protein [29] matrix, which was subsequently integrated into pre-existing NC with adequate mechanical strength. Depending on the materials, the direct embedding of neurotrophic factors into polymeric NC may suffer from the use of organic solvents or heat; further, single materials generally do not afford optimal properties for both prolonged drug release kinetics and adequate mechanical strength. Consequently, we considered SF for manufacturing NC with appropriate physical and growth factor release properties. SF had already demonstrated excellent biocompatibility both *in vitro* and *in vivo* [34, 35, 49], good mechanical properties [36], and slow biodegradation. The beneficial mechanical properties of SF over those of native and cross-linked collagen have been shown in bone and cartilage tissue engineering [50, 51]. Recent studies have also demonstrated the multifunctionality of SF for drug delivery in the context of tissue engineering [52, 53] and for controlled release of bioactive proteins in general [40]. Thus, in the present work, we evaluated technologies for the embedding of NGF into a SF matrix to produce subsequently a mechanically adequate NC. The SF matrices (films, tubes) were prepared under relatively mild conditions to respect the bioactivity of the embedded NGF and to achieve controlled release of bioactive NGF over several weeks.

Our study demonstrates that SF may indeed be a suitable material for NC, as it supported the proliferation of PC12 cells with subsequent cell differentiation as evidenced by neurite outgrowth. SF supported neurite outgrowth as efficiently as collagen-1 or laminin, materials that were successfully used for NC [54-58]. The suitability of SF as a substrate for cell proliferation and differentiation has

recently been demonstrated also in the differentiation of embryonic stem cells into glial precursor cells [39], cartilage, bone, and ligament cells [50, 51, 59].

SF was also adequate for co-processing with NGF in aqueous medium to produce NGF/SF matrices. Upon freeze-drying, but not upon air-drying, the proportion of high molecular aggregates of NGF remained comparable to that of the NGF stock solution (**Fig. 6**). An important observation concerned the strong interaction between NGF and SF, as compared to NGF and lactose (**Fig. 6**). SF co-dissolved with NGF lowered the availability of the protein to a concentration of 50-70% of the actual amount (180 ng/mg). This interaction affected of course also the availability of NGF from the SF films and tubes (**Fig. 7A,B**). We assume the observed interaction being governed largely by ionic attractions, because NGF carries a positive ($pI = 4.3$ [60]) and SF a negative net charge ($pI = 9.3$ [61]) at isohydric pH.

The NGF - SF ionic interaction must have also affected the NGF release from the SF matrices, which was prolonged over more than three weeks, but remained largely incomplete, i.e., 0.3 - 13% within 22 days. By comparison, insulin-like growth factor-1 (IGF-1) with a lower net charge at isohydric pH ($pI = 8.3$) and a lower molecular weight (7.4 kDa for IGF-1 *versus* 26 kDa for the NGF homodimer) was released more completely from freeze-dried SF matrices, i.e., 20-25% of the actual dose (unpublished data). These findings demonstrate that growth factor release kinetics from SF matrices is likely influenced by both ionic charge and molecular weight of the protein. In a previous study, we showed that dextrans with increasing molecular weight are released slower and less complete [40]. Interestingly, NGF release did not cease entirely even after 3 weeks (**Fig. 8 A, Fig. 9**). At present, it remains elusive whether or not the amount of NGF released between week 1 and 3, and beyond, can exert an effect *in vivo* in the context of nerve growth.

Despite the assumed strong molecular interaction between NGF and SF, the differently prepared NGF/SF matrices exhibited different release profiles. We can only speculate that the freezing of the NGF-SF solution might have temporarily changed the conformation of either or both of the compounds so that a larger

number of functional ionic, polar or H-bonding groups became exposed and available for NGF-SF interaction. While the conformation of NGF during and after the processing was not analyzed, all SF matrices revealed indistinguishable β -sheet conformation, although quantitative data on the proportion of β -sheets is not available (**Fig. 4**). It may be interesting to note also that the total amounts of NGF released from the three matrix types was inversely related to the pore size of the matrices, i.e., the smaller the pore size of the matrix the higher the amount of NGF released. At present, we do not have an explanation for this phenomenon.

CONCLUSIONS

This study evidenced that SF should be a suitable material for NC designed to deliver neurotrophic factors. First, SF was found suitable for supporting PC12 cell proliferation and maturation upon stimulation with NGF. SF was readily shaped into matrices for future use as NC and loaded with NGF. The SF matrices were rendered water-insoluble through treatment with methanol, which induced β -sheet formation. The used methanol treatment did not appear to alter the NGF bioactivity. NGF-release from the SF matrices lasted for more than three weeks, but the total fraction released remained generally very low, i.e., between 0.3% and 13.0%, depending on the preparation method. This incomplete release could not be related to NGF-aggregation. The released NGF remained fully bioactive over the entire release experiment of four weeks and afforded PC12 cell differentiation with neurite outgrowth. Further work will encompass the optimization of mechanical properties and the *in vivo* testing of the SF-NC in terms of their biocompatibility in a peripheral nerve gap and their nerve growth stimulating capacity.

ACKNOWLEDGMENTS

We thank Genentech (South San Francisco, CA, USA) for kind provision of NGF and Trudel (Zurich, Switzerland) for silk cocoons. We further thank Lukas Pfister (Drug Formulation and Delivery Group, ETH Zurich) for his expert advice regarding NGF stability aspects. Financial support was from AO (Davos, AO Biotechnology Research Grant 2003), the Association for Orthopaedic Research, ETH Zurich (TH 26.04-1), and the GEBERT RÜF STIFTUNG (Basel, grant P-033/03).

REFERENCES

1. J.S. Belkas, M.S. Shoichet, R. Midha, Peripheral nerve regeneration through guidance tubes, *Neurol Res* 26 (2) (2004) 151-60.
2. K. Horch, Guidance of regrowing sensory axons after cutaneous nerve lesions in the cat, *J Neurophysiol* 42 (5) (1979) 1437-49.
3. D.A. Abernethy, P.K. Thomas, A. Rud, R.H. King, Mutual attraction between emigrant cells from transected denervated nerve, *J Anat* 184 (Pt 2) (1994) 239-49.
4. A.G. Lumsden, A.M. Davies, Earliest sensory nerve fibres are guided to peripheral targets by attractants other than nerve growth factor, *Nature* 306 (5945) (1983) 786-8.
5. D.H. Kim, K. Han, R.L. Tiel, J.A. Murovic, D.G. Kline, Surgical outcomes of 654 ulnar nerve lesions, *J Neurosurg* 98 (5) (2003) 993-1004.
6. L. de Medinaceli, M. Prayon, M. Merle, Percentage of nerve injuries in which primary repair can be achieved by end-to-end approximation: review of 2,181 nerve lesions, *Microsurgery* 14 (4) (1993) 244-6.
7. B. Battiston, S. Geuna, M. Ferrero, P. Tos, Nerve repair by means of tubulization: literature review and personal clinical experience comparing biological and synthetic conduits for sensory nerve repair, *Microsurgery* 25 (4) (2005) 258-67.
8. P. Aebischer, V. Guenard, S. Brace, Peripheral nerve regeneration through blind-ended semipermeable guidance channels: effect of the molecular weight cutoff, *J Neurosci* 9 (10) (1989) 3590-5.
9. P. Aebischer, V. Guenard, R.F. Valentini, The morphology of regenerating peripheral nerves is modulated by the surface microgeometry of polymeric guidance channels, *Brain Res* 531 (1-2) (1990) 211-8.
10. V. Guenard, R.F. Valentini, P. Aebischer, Influence of surface texture of polymeric sheets on peripheral nerve regeneration in a two-compartment guidance system, *Biomaterials* 12 (2) (1991) 259-63.
11. P.A. Danielsson, L. Adolfsson, L.B. Dahlin, Different effect on axonal outgrowth of application of non-absorbable or absorbable tubes around a nerve repair, *Scand J Plast Reconstr Surg Hand Surg* 35 (4) (2001) 347-53.
12. S. Bunting, L. Di Silvio, S. Deb, S. Hall, Bioresorbable glass fibres facilitate peripheral nerve regeneration, *J Hand Surg* 30 (3) (2005) 242-7.

13. E. Gamez, K. Ikezaki, M. Fukui, T. Matsuda, Photoconstructs of nerve guidance prosthesis using photoreactive gelatin as a scaffold, *Cell Transplant* 12 (5) (2003) 481-90.
14. A. Goraltchouk, T. Freier, M.S. Shoichet, Synthesis of degradable poly(L-lactide-co-ethylene glycol) porous tubes by liquid-liquid centrifugal casting for use as nerve guidance channels, *Biomaterials* 26 (36) (2005) 7555-63.
15. J. Cai, X. Peng, K.D. Nelson, R. Eberhart, G.M. Smith, Synergistic improvements in cell and axonal migration across sciatic nerve lesion gaps using bioresorbable filaments and heregulin-beta1, *J Biomed Mater Res A* 69 (2) (2004) 247-58.
16. P.D. Dalton, L. Flynn, M.S. Shoichet, Manufacture of poly(2-hydroxyethyl methacrylate-co-methyl methacrylate) hydrogel tubes for use as nerve guidance channels, *Biomaterials* 23 (18) (2002) 3843-51.
17. I. Ducic, C.T. Maloney, Jr., A.L. Dellon, Reconstruction of the spinal accessory nerve with autograft or neurotube? Two case reports, *J Reconstr Microsurg* 21 (1) (2005) 29-33; discussion 34.
18. M. Navissano, F. Malan, R. Carnino, B. Battiston, Neurotube for facial nerve repair, *Microsurgery* 25 (4) (2005) 268-71.
19. D.K. Hinckley, C.A. Lyles, D.E. Mattox, Repair of peripheral nerves of unequal diameters, *Laryngoscope* 101 (11) (1991) 1150-4.
20. H.H. Chen, H.M. Liu, The use of collagen polymer tube and fibrin clot in peripheral nerve repair, *Proc Natl Sci Counc Repub China B* 18 (2) (1994) 58-63.
21. S. Itoh, K. Takakuda, S. Kawabata, Y. Aso, K. Kasai, H. Itoh, K. Shinomiya, Evaluation of cross-linking procedures of collagen tubes used in peripheral nerve repair, *Biomaterials* 23 (23) (2002) 4475-81.
22. R.L. Collins, D. Christiansen, G.A. Zazanis, F.H. Silver, Use of collagen film as a dural substitute: preliminary animal studies, *J Biomed Mater Res* 25 (2) (1991) 267-76.
23. G. Lundborg, L.B. Dahlin, N. Danielsen, R.H. Gelberman, F.M. Longo, H.C. Powell, S. Varon, Nerve regeneration in silicone chambers: influence of gap length and of distal stump components, *Exp Neurol* 76 (2) (1982) 361-75.
24. V.B. Doolabh, M.C. Hertl, S.E. Mackinnon, The role of conduits in nerve repair: a review, *Rev Neurosci* 7 (1) (1996) 47-84.

25. M. Ebadi, R.M. Bashir, M.L. Heidrick, F.M. Hamada, H.E. Refaey, A. Hamed, G. Helal, M.D. Baxi, D.R. Cerutis, N.K. Lassi, Neurotrophins and their receptors in nerve injury and repair, *Neurochem Int* 30 (4-5) (1997) 347-74.
26. R.W. Gundersen, J.N. Barrett, Neuronal chemotaxis: chick dorsal-root axons turn toward high concentrations of nerve growth factor, *Science* 206 (4422) (1979) 1079-80.
27. A. Hari, B. Djohar, T. Skutella, S. Montazeri, Neurotrophins and extracellular matrix molecules modulate sensory axon outgrowth, *Int J Dev Neurosci* 22 (2) (2004) 113-7.
28. T. Hadlock, C. Sundback, R. Koka, D. Hunter, M. Cheney, J. Vacanti, A novel, biodegradable polymer conduit delivers neurotrophins and promotes nerve regeneration, *Laryngoscope* 109 (9) (1999) 1412-6.
29. E.G. Fine, I. Decosterd, M. Papaloizos, A.D. Zurn, P. Aebischer, GDNF and NGF released by synthetic guidance channels support sciatic nerve regeneration across a long gap, *Eur J Neurosci* 15 (4) (2002) 589-601.
30. C.B. Nguyen, E. Szonyi, M.D. Sadick, T.E. Hotaling, J.L. Mendoza-Ramirez, E. Escandon, Stability and interactions of recombinant human nerve growth factor in different biological matrices: in vitro and in vivo studies, *Drug Metab Dispos* 28 (5) (2000) 590-7.
31. L. Uebersax, H. Hagenmuller, S. Hofmann, E. Gruenblatt, R. Muller, G. Vunjaknovakovic, D.L. Kaplan, H.P. Merkle, L. Meinel, Effect of Scaffold Design on Bone Morphology in Vitro, *Tissue Eng* 12 (12) (2006) 3417-29.
32. R. Nazarov, H.J. Jin, D.L. Kaplan, Porous 3-D scaffolds from regenerated silk fibroin, *Biomacromolecules* 5 (3) (2004) 718-26.
33. G.H. Altman, F. Diaz, C. Jakuba, T. Calabro, R.L. Horan, J. Chen, H. Lu, J. Richmond, D.L. Kaplan, Silk-based biomaterials, *Biomaterials* 24 (3) (2003) 401-16.
34. L. Meinel, S. Hofmann, V. Karageorgiou, C. Kirker-Head, J. McCool, G. Gronowicz, L. Zichner, R. Langer, G. Vunjak-Novakovic, D.L. Kaplan, The inflammatory responses to silk films in vitro and in vivo, *Biomaterials* 26 (2) (2005) 147-55.
35. B. Panilaitis, G.H. Altman, J. Chen, H.J. Jin, V. Karageorgiou, D.L. Kaplan, Macrophage responses to silk, *Biomaterials* 24 (18) (2003) 3079-85.
36. P.M. Cunniff, S.A. Fossey, M.A. Auerbach, J.W. Song, D.L. Kaplan, W. Adams, R.K. Eby, D. Mahoney, D. Deborah, D.L. Vezie, Mechanical and thermal properties of Dragline Silk from the Spider *Nephila cavipes*, *Polymers for Advanced Technologies* 5 (1994) 401-410.

37. F. Lange, Künstliche Bänder aus Seide., Münch Med Wochenschr (17) (1907) 834-836.
38. F. Lange, Ueber die Sehnenplastik, Verh Dtsch Orthop 2 (1903) 10-12.
39. L. Uebersax, D.E. Fedele, C. Schumacher, D.L. Kaplan, H.P. Merkle, D. Boison, L. Meinel, The support of adenosine release from adenosine kinase deficient ES cells by silk substrates, Biomaterials 27 (26) (2006) 4599-607.
40. S. Hofmann, C.T. Foo, F. Rossetti, M. Textor, G. Vunjak-Novakovic, D.L. Kaplan, H.P. Merkle, L. Meinel, Silk fibroin as an organic polymer for controlled drug delivery, J Control Release 111 (1-2) (2006) 219-27.
41. L.A. Greene, A.S. Tischler, Establishment of a noradrenergic clonal line of rat adrenal pheochromocytoma cells which respond to nerve growth factor, Proc Natl Acad Sci U S A 73 (7) (1976) 2424-8.
42. P. Doherty, D.A. Mann, F.S. Walsh, Cell-cell interactions modulate the responsiveness of PC12 cells to nerve growth factor, Development 101 (3) (1987) 605-15.
43. J.D. Foley, E.W. Grunwald, P.F. Nealey, C.J. Murphy, Cooperative modulation of neuritogenesis by PC12 cells by topography and nerve growth factor, Biomaterials 26 (17) (2005) 3639-44.
44. S. Sofia, M.B. McCarthy, G. Gronowicz, D.L. Kaplan, Functionalized silk-based biomaterials for bone formation, J Biomed Mater Res 54 (1) (2001) 139-48.
45. C.M. Patist, M.B. Mulder, S.E. Gautier, V. Maquet, R. Jerome, M. Oudega, Freeze-dried poly(D,L-lactic acid) macroporous guidance scaffolds impregnated with brain-derived neurotrophic factor in the transected adult rat thoracic spinal cord, Biomaterials 25 (9) (2004) 1569-82.
46. R. Midha, C.A. Munro, P.D. Dalton, C.H. Tator, M.S. Shoichet, Growth factor enhancement of peripheral nerve regeneration through a novel synthetic hydrogel tube, J Neurosurg 99 (3) (2003) 555-65.
47. A. Piotrowicz, M.S. Shoichet, Nerve guidance channels as drug delivery vehicles Biomaterials 27 (9) (2006) 2018-27.
48. Y. Yang, L. De Laporte, C.B. Rives, J.H. Jang, W.C. Lin, K.R. Shull, L.D. Shea, Neurotrophin releasing single and multiple lumen nerve conduits, J Control Release 104 (3) (2005) 433-46.
49. M. Santin, A. Motta, G. Freddi, M. Cannas, In vitro evaluation of the inflammatory potential of the silk fibroin, J Biomed Mater Res 46 (3) (1999) 382-9.

50. L. Meinel, V. Karageorgiou, R. Fajardo, B. Snyder, V. Shinde-Patil, L. Zichner, D. Kaplan, R. Langer, G. Vunjak-Novakovic, Bone tissue engineering using human mesenchymal stem cells: effects of scaffold material and medium flow, *Ann Biomed Eng* 32 (1) (2004) 112-22.
51. L. Meinel, S. Hofmann, V. Karageorgiou, L. Zichner, R. Langer, D. Kaplan, G. Vunjak-Novakovic, Engineering cartilage-like tissue using human mesenchymal stem cells and silk protein scaffolds, *Biotechnol Bioeng* 88 (3) (2004) 379-91.
52. V. Karageorgiou, L. Meinel, S. Hofmann, A. Malhotra, V. Volloch, D. Kaplan, Bone morphogenetic protein-2 decorated silk fibroin films induce osteogenic differentiation of human bone marrow stromal cells, *J Biomed Mater Res A* 71 (3) (2004) 528-37.
53. V. Karageorgiou, M. Tomkins, R. Fajardo, L. Meinel, B. Snyder, K. Wade, J. Chen, G. Vunjak-Novakovic, D.L. Kaplan, Porous silk fibroin 3-D scaffolds for delivery of bone morphogenetic protein-2 in vitro and in vivo, *J Biomed Mater Res A* 78 (2) (2006) 324-34.
54. S. Itoh, A. Matsuda, H. Kobayashi, S. Ichinose, K. Shinomiya, J. Tanaka, Effects of a laminin peptide (YIGSR) immobilized on crab-tendon chitosan tubes on nerve regeneration, *J Biomed Mater Res B Appl Biomater* 73 (2) (2005) 375-82.
55. J.J. Hauw, A.B. Novikoff, P.M. Novikoff, J.M. Boutry, R. Robineaux, Culture of nervous tissue on collagen in Leighton tubes, *Brain Res* 37 (2) (1972) 301-9.
56. H.S. Dresner, T.A. King, H.B. Clark, S.K. Juhn, S.C. Levine, Peripheral facial nerve regeneration using collagen conduit entubulation in a cat model, *Ann Otol Rhinol Laryngol* 115 (8) (2006) 631-42.
57. Z.L. Chen, S. Strickland, Laminin gamma1 is critical for Schwann cell differentiation, axon myelination, and regeneration in the peripheral nerve, *J Cell Biol* 163 (4) (2003) 889-99.
58. K. Matsumoto, K. Ohnishi, T. Kiyotani, T. Sekine, H. Ueda, T. Nakamura, K. Endo, Y. Shimizu, Peripheral nerve regeneration across an 80-mm gap bridged by a polyglycolic acid (PGA)-collagen tube filled with laminin-coated collagen fibers: a histological and electrophysiological evaluation of regenerated nerves, *Brain Res* 868 (2) (2000) 315-28.
59. G.H. Altman, R.L. Horan, H.H. Lu, J. Moreau, I. Martin, J.C. Richmond, D.L. Kaplan, Silk matrix for tissue engineered anterior cruciate ligaments, *Biomaterials* 23 (20) (2002) 4131-41.

60. Q. Cheng, T.Z. Peng, X.B. Hu, C.F. Yang, Charge-selective recognition at fibroin-modified electrodes for analytical application, *Anal Bioanal Chem* 382 (1) (2005) 80-4.
61. K. Herrup, E.M. Shooter, Properties of the beta nerve growth factor receptor of avian dorsal root ganglia, *Proc Natl Acad Sci U S A* 70 (12) (1973) 3884-8.

CHAPTER VI

The support of adenosine release from adenosine kinase deficient ES cells by silk substrates

Lorenz Uebersax¹, Denise Fedele^{1,2}, Claudia Schumacher², David L. Kaplan³,

Hans P. Merkle¹, Detlev Boison⁴, Lorenz Meinel^{1,3}

*¹Institute for Pharmaceutical Sciences, Drug Formulation and Delivery, ETH
Zurich, CH-8093 Zurich, Switzerland*

*²Institute for Pharmacology and Toxicology, University of Zurich, CH-8057
Zurich, Switzerland*

*³Department for Biomedical Engineering, Tufts University, Medford, MA 02155,
USA*

*⁴R.S. Dow Neurobiology Laboratories, Legacy Research, Portland, OR 97232,
USA*

ABSTRACT

Adenosine kinase deficient (Adk^{-/-}) embryonic stem cells (ESC) encapsulated in synthetic polymers have previously been shown to provide therapeutic adenosine release and transient seizure suppression in epileptic rats. Here we explored the utility of biopolymer-substrates to promote long-term adenosine release from Adk^{-/-} ESCs. Three different substrates were studied: (1) type I collagen (Col-1), (2) silk-fibroin (SF), and (3) poly(L-ornithine) (PO) coated tissue culture plastic. Adk^{-/-} or wild type (wt) ESC-derived glial precursor cells were seeded on the substrates and cultured either in proliferation medium containing growth factors or in differentiation medium devoid of growth factors. In proliferation medium cell proliferation was higher and metabolic activity lower on Col-1 and PO substrates as compared to SF. Cells from both genotypes readily differentiated into astrocytes after growth factor removal on all substrates. Adk^{-/-} cells cultured on biopolymers released significantly more adenosine than their wt counterparts at all developmental stages. Adenosine release was similar on SF and PO substrates and the amounts released from Adk^{-/-} cells (>20 ng/ml) were considered to be of therapeutic relevance. Taken together, these results suggest that SF matrices are particularly suitable biomaterials for ESC encapsulation and for the design of adenosine releasing bioincubators for the treatment of epilepsy.

INTRODUCTION

The purine ribonucleoside adenosine is an important modulator of central nervous system functions, exerting primarily inhibitory effects on neuronal activity and suppressing seizure activity in various rodent models of epilepsy [1-3]. However, traditional methods for the administration of adenosine to epileptic patients are limited by severe systemic side effects ranging from a decrease of heart rate, blood pressure, and body temperature to sedation [4]. Recently, new strategies have been developed aiming at the local administration of adenosine by intracerebral implantation of cells engineered to release adenosine [2, 5, 6]. Since self-renewing, totipotent embryonic stem cells (ESC) may provide a virtually unlimited donor source for implantation, mouse ESCs were genetically engineered to lack the main adenosine-metabolizing enzyme, adenosine kinase (Adk), causing the cells to release significant amounts of adenosine [7]. These Adk deficient (Adk^{-/-}) ESCs were subjected to a glial differentiation protocol [8] and the glial precursors could be maintained under proliferative culture conditions for several passages (>20). When allowed to differentiate, Adk^{-/-} glial precursors were shown to mature into primarily astrocytes [7]. When encapsulated and implanted into the brain ventricle of epileptic, electrically kindled rats, the adenosine release from the Adk^{-/-} glial precursors was effective in suppressing seizures for 5-7 days after capsule implantation at which time the cells died and seizures resumed [5].

While these studies demonstrated the effectiveness of local adenosine application for the treatment of epilepsy, they do not offer a therapeutic solution due to disadvantages associated with the material selected for encapsulation, polysulfone derivatives. One main disadvantage is the persistence of the biomaterial which may impact the viability of the encapsulated cells by causing immunogenic reactions and by eliminating activity dependent support from the host cells [9]. Furthermore, cells did not adhere to the polysulfone matrix. To address some of these challenges, protein-based biomaterials with variations related to rates of degradation were investigated in the present study. Adk^{-/-} glial

precursor growth, differentiation, and adenosine release were evaluated on fast degrading type I collagen (Col-1) substrates and slow degrading silk-fibroin (SF) substrates in comparison to poly(L-ornithine) coated tissue culture plastic surfaces, routinely used for culture of these cells.

Collagens have a longstanding tradition as biomaterial substrates for nervous tissue formation in two- [10] and three-dimensional cell culture [11]. Nerve guidance tubes based on collagen or collagen/agarose polymer blends have been used to repair segments in rat distal peripheral nerve increasing the percentage of axons crossing the anastomosis [12, 13]. However, challenges remain, mainly due to the lack of mechanical integrity and rapid degradation rates of collagens. Tubes prepared from untreated collagen were shown to separate into different layers and stenosis of the lumen occurred early after implantation, a problem which could be partly solved by cross-linking the collagen thus stabilizing the tubes [14]. However, cross-linking of collagen is associated with unwanted inflammatory potential, spontaneous and uncontrolled calcification and remaining issues concerning the rapid biodegradation within 8 weeks [15-17].

Silk, which is a mixture of mainly silk fibroin (SF) and sericin, has an extensive history in clinical application as a suture material. Unwanted immune reactions to silk sutures observed early on in their application were assigned to the presence of sericin. However, *in vitro* and *in vivo* evaluations of pure SF films, scaffolds, or fibers demonstrated excellent biocompatibility, while maintaining the distinguishing mechanical features of silks as compared to most synthetic and all biopolymers known [18-22]. The performance of SF might be improved by the addition of cell-binding domains, such as the RGD domain, to increase the release of bioengineered products from terminally differentiated cells, such as interferon-beta release from fibroblasts [23]. However, the use of unmodified SF, which does not contain cell-binding domains and after methanol treatment predominantly forms beta-sheets, might be advantageous for the maintenance of defined differentiation pathways of stem cells or precursor cells. Therefore, unmodified SF should be a particularly suitable substrate for cells in which differentiation needs

to be tightly controlled by exogenous cues. In addition to the biocompatibility of SF and its robust mechanical stability, the slow and complete biodegradation of the material *in vivo* is an important characteristic. This is relevant in light of the estimated time frame for function of bioincubators (release matrices) in epilepsy of 6 – 12 months, and based on previous findings detailing biodegradation at other anatomic sites than the brain [20, 24, 25].

The present study addresses the need for novel biomaterial options as a basis for bioincubator manufacture for clinically applicable treatments of epilepsy. Both protein biomaterials tested here, Col-1 and SF, appeared to be suitable materials as substrates for Adk^{-/-} ESC derived glial precursor cells regarding cellular adherence, metabolic activity, differentiation and adenosine-release. Initial studies of nutrient transport through the silk fibroin membranes, as a prerequisite for survival of encapsulated cells, is also provided to further substantiate the unique applicability of this biomaterial system for applications in the treatment of epilepsy.

MATERIALS AND METHODS

Materials

All cell culture materials including medium, medium supplements and growth factors were purchased from Invitrogene (Carlsbad, CA, USA) unless otherwise noted. The ATP Bioluminescent assay kit, the MTT assay kit, poly(L-ornithine) hydrobromide (MW 30,000-70,000), Triton-X, paraformaldehyde, and EDTA were purchased from Sigma-Aldrich (St. Louis, MO, USA). All primary antibodies used were obtained from Chemicon International (Temecula, CA, USA). Donkey Anti-Mouse Cy3 was purchased from Jackson Immuno Research Laboratories (West Grove, PA, USA). The PicoGreen assay kit was obtained from Molecular Probes Europe BV (Leiden, The Netherlands). In addition, Collagen I (Calf Skin,) and D(+) Glucose anhydrous were purchased from Sigma-Aldrich (St.

Louis, MO, USA). D[1-14C]-Glucose aqueous solution containing 3% ethanol was purchased from Amersham Life Science CFA349, B73L01 (2 GBq/mmol) and Ultima Gold from Perkin Elmer (Boston, MA, USA).

Preparation of silk films

Silk fibroin was prepared as described previously [26]. Briefly, cocoons derived from *Bombyx mori* (Trudel Inc. Zurich, Switzerland) were boiled in 0.02 M Na₂CO₃, rinsed and dissolved in 9M LiBr overnight at 37 °C to generate a 10% (w/v) solution. This solution was dialyzed (Pierce, Rockford, IL; MWCO 2000 g/mol) to give a 3% (w/v) solution. The solution was then sterile filtered through a 0.2 µm filter into 22 mm diameter Teflon molds. The films were dried overnight and subsequently treated with 90% methanol (v/v) for 30 min to induce crystallization and insolubility to the biomaterial matrix in the aqueous culture medium.

Preparation of collagen films

Calf-skin collagen type 1 (Col-1) films were prepared in 12-well non tissue culture treated polystyrene microtiter plates by pipetting 1 ml of 0.5 g/l collagen (in 0.1% v/v acetic acid) into the wells. Films were allowed to dry overnight and were then neutralized by applying 2 ml of 0.1 M Na₂HPO₄ in each well for 1 h and the wells were then washed twice with PBS before cells were seeded. For the immunostaining, glass coverslips were coated twice with 400 µl of collagen solution and sterilized by ethylene oxide after drying.

Preparation of poly(L-ornithine) coated plastic

Tissue culture grade poly(L-ornithine) hydrobromide (30–70 kDa) was used as an aqueous solution at a final concentration of 100 µg/ml. A sufficient volume of the diluted solution was used to cover the bottom of the cell culture vessels (flasks and Petri dishes) and the vessels were incubated for at least 2 h at 37°C.

Immediately before plating the cells, the PO was rinsed from the surface with two washes of PBS and one final wash of DMEM.

Contact angle measurement

To measure the hydrophobicity of the biopolymer membranes, static contact angle measurements were performed on dry SF or Col-1 films and on PO-coated tissue culture plastic (n=3) at ambient temperature using a goniometer (NRL C, Ramé-Hart Inc., Mountain Lakes, NJ, USA). Ultra-pure water droplets were used with a drop volume of approximately 30 μ l.

Cell culture and differentiation

Wt and Adk^{-/-} murine ESCs [7] were stepwise differentiated to the glial precursor stage as previously described [8]. Glial precursor cells were routinely cultured on poly(L-ornithine)-coated (PO-coated) dishes in N3 medium, a 1:1 mixture of DMEM with Ham's F12 supplemented with insulin (25 μ g/ml), human apo-transferrin (100 μ g/ml), progesterone (20 nM), putrescine (100 μ M), sodium selenite (30 nM), penicillin (100 U/ml), and streptomycin (100 μ g/ml). In addition, laminin (1 μ g/ml) was added when plating the cells. To keep the cells in a proliferative state, the growth factors, FGF2 (10 ng/ml) and EGF (20 ng/ml), were added daily and this medium was changed every 48 h. Frozen stocks of undifferentiated glial precursor cells could be kept in liquid nitrogen. To induce the differentiation of glial precursor cells, fresh N3 medium was added without growth factors. Growth factor free medium was replaced every 48 h. After 4-5 days of growth factor withdrawal, the cells had differentiated as was evidenced by immunostaining for GFAP, a marker of mature astrocytes (see below).

To prepare glial precursor cells for seeding onto different biopolymers, cells were thawed and plated onto PO-coated, 25 cm² tissue culture flasks in N3 medium plus growth factors and maintained in a proliferative state until approximately 90% confluent. At this point, the cells were washed 3 times with

PBS, scraped off the plastic in PBS plus 1% DNase, centrifuged and replated on 3 PO-coated 25 cm² flasks in N3 medium plus growth factors. Once the 3 flasks were about 90% confluent the cells were again scraped off, counted and plated onto the appropriate substrate (silk, collagen, or poly(L-ornithine)) in 12-well plates at a concentration of 3×10^5 cells per ml.

MTT assay to determine cell viability and metabolism

ESC derived glial precursor cells were seeded in replicas of 5 in a concentration of 1.5×10^5 cells/cm² on the different substrates and incubated until measurement. At 48 h and 96 h the proliferation of the cells on the different substrates was assessed using a 3-(4,5 dimethylthiazol-2-yl)-2,5-diphenyltetrazolium bromide (MTT) assay. MTT was dissolved in PBS for a final concentration of 5 mg/ml and sterile filtered. The MTT solution was diluted in DMEM medium to a final concentration of 0.5 mg/ml before use. The culture medium was removed from the cells and replaced by 2 ml MTT (0.5 mg/ml in DMEM medium). After 2 h of incubation at 37 °C and 5% CO₂, the solution was removed and 1 ml of acidic isopropyl alcohol (500 ml Isopropyl alcohol + 3.5 ml 6M HCl) was added to the culture to dissolve the crystals that had formed. After 10 min incubation at room temperature, the tubes were centrifuged (300 g, 1 min, 4 °C) and 100 µl of the supernatant were transferred to a 96 well plate. The absorbance was assessed at 570 nm and the background (630 nm) was subtracted using a Thermomax microplate reader (Molecular Devices Corporation, Sunnyvale, CA).

PicoGreen assay to determine cell number

The PicoGreen assay quantifies double-stranded DNA in solution using a fluorescent nucleic acid stain. A defined concentration of DNA (100 µg/ml) was diluted in Tris-EDTA (TE) assay buffer to provide a standard curve of 0–1000 ng/ml DNA. ESC derived glial precursor cells (n=5) were seeded in a

concentration of 1.5×10^5 cells/cm² on the appropriate substrates and maintained in N3 medium plus growth factors. After 48 and 96 h the supernatant was removed and cell samples were disrupted by addition of 1 ml lysis buffer [Triton-X (0.2%) + 5mM MgCl₂] to each well with incubation in the dark for 48 h. The lysate was then transferred to a tube and centrifuged at 3000 g for 10 min at RT. Subsequently, 41 µl of the supernatant were transferred to a new tube and 166.6 µl of diluted PicoGreen solution (PicoGreen stock solution in dimethylsulfoxide; diluted 200 times in TE assay buffer) were added. After vortexing for 3 min, 100 µl of the solution were transferred to a 96-well plate. Plates were then incubated for 5 min in the dark. Standards/samples were excited at 485 nm and the fluorescence emission intensity measured at 530 nm in a FluoroCount™ plate reader (Packard instrument, Downes Gore, IL).

Immunofluorescence staining for the assessment of the differentiation of glial precursor cells

ESC derived glial precursor cells were plated in a concentration of 1.5×10^5 cells/cm² on glass cover slips coated with PO or collagen or on silk films in a 12-well plate. After culturing the cells for 96 h in N3 medium with growth factors the differentiation was induced by 5 days of growth factor withdrawal. Cells were then fixed with 4% paraformaldehyde. The following primary antibodies were used: anti-mouse GFAP (1:10,000) to stain astrocytes, anti-mouse O4 (1:50) to stain oligodendrocytes, and anti-mouse βIII tubulin (1:1000) to stain early neurons. Donkey anti-mouse Cy3 (1:500) was used as the secondary antibody. To stain the nucleus of all the cells in the culture, Hoechst 33258 (1:10,000) was used. Immunofluorescence analyses were performed using a Zeiss fluorescence microscope (Karl Zeiss AG, Jena, Germany) with Openlab imaging. Images were acquired with a resolution of 512×512 pixels.

Quantification of adenosine release

Single cell suspensions of ESC derived glial precursors were plated at a density of 1.5×10^5 cells/cm² onto the different substrates in 12-well plates (n = 6 wells per substrate) and maintained under culture conditions supporting proliferation at 37 °C under 5% CO₂. After 48 h and 96 h the medium was exchanged, and 2 h thereafter 150 µl of the medium were collected from each well and stored at -20 °C for subsequent analysis. After the 96 h samples were taken, the medium was changed to N3 medium without growth factors to induce the differentiation of the cells. On the fifth day after growth factor withdrawal, the medium was changed and 2 h later 150 µl samples of the medium were collected. Adenosine was quantified using an enzyme-coupled bioluminescence assay as previously described [27].

Permeation of ¹⁴C-D-glucose through silk fibroin films

Silk fibroin films were prepared from 8% (w/w) aqueous silk fibroin solutions, casted on Teflon surfaces and carefully transferred to a diffusion chamber (Crown Glass Co., Somerville, NJ, USA) (n = 4). The receiver chamber was filled with 3 ml PBS and 3 ml of glucose solution (4.5 mg/ml) in PBS containing 1 µl of ¹⁴C-d-glucose (2 GBq/mmol) was added to the donor chamber. Samples (3 ml) were taken at the receiver side every day for two days. One ml of sample was mixed with 6 ml of Ultimate Gold and measured in a Beta Counter (Packard Instruments, Downers Grove, IL, USA).

Statistical analysis

Statistical data analysis was performed by one-way analysis of variance (ANOVA) and Tukey-Kramer procedure for *post hoc* comparison. $p < 0.05$ was considered statistically significant.

RESULTS

Hydrophobicity of poly(L-ornithine), collagen, and silk fibroin substrates

The hydrophobicity of non-coated, non tissue culture treated plastic was compared to that of poly(L-ornithine)-coated (PO-coated) tissue culture plastic, collagen (Col-1) and silk fibroin (SF) by contact angle measurements (**Fig. 1**). PO coated tissue culture plastic was significantly ($p < 0.01$) less hydrophobic (contact angle of $43 \pm 1.41^\circ$) than non-coated, non tissue culture treated plastic (contact angle of $77 \pm 0.84^\circ$). The resulting contact angle was significantly lower than the contact angle measured on Col-1 ($58 \pm 0.73^\circ$) and SF ($52 \pm 0.89^\circ$).

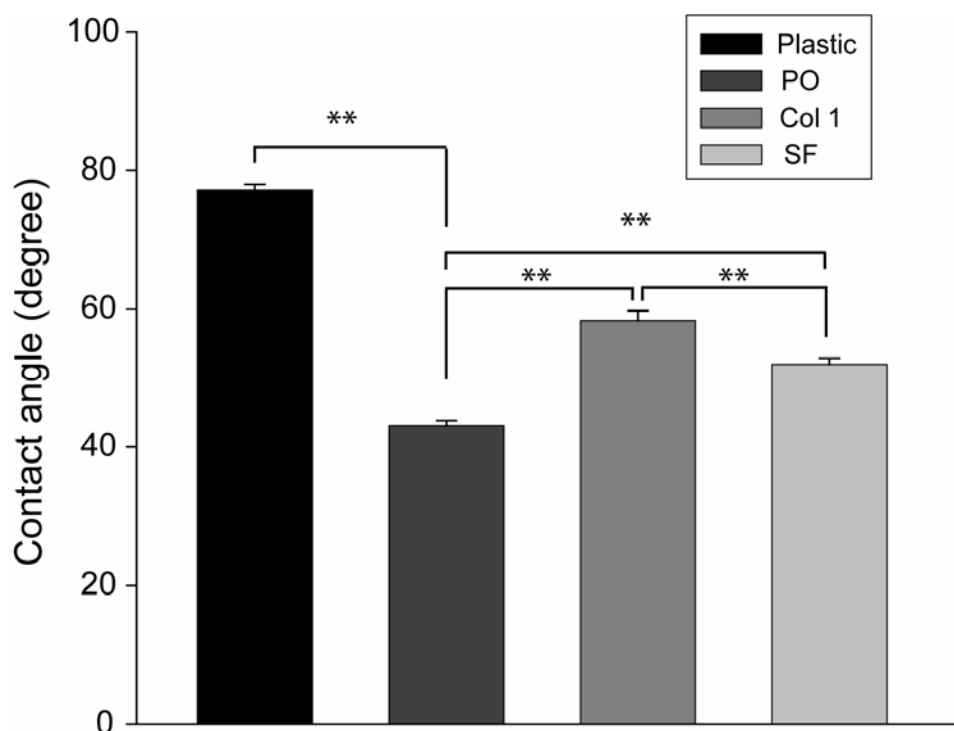


*Fig. 1: Contact angle measurement on non tissue culture treated plastic (Plastic), poly(L-ornithine) coated plastic (PO), collagen I (Col-1) and silk fibroin (SF) films (** $p < 0.01$).*

Adherence and morphology of proliferating wt and Adk^{-/-} ESC derived glial precursor cells on SF, Col-1, and PO substrates

Wt and Adk^{-/-} glial precursor cells were plated on SF, Col-1, and PO coated tissue culture plastic (n=5, for each combination). After 24 h, both wt and Adk^{-/-} glial precursor cells adhered to SF and Col-1 to the same degree as that observed in control, PO-coated, wells. Cellular morphology was comparable on all three substrates with the cells spreading homogeneously on the surfaces. After 48 and 96 h, glial precursor cells of both genotypes grown on SF and Col-1 covered approximately 30 - 40% or 80 - 90% of the available surface, respectively, whereas the density of cells grown on PO was slightly higher at both time points as assessed qualitatively (**Fig. 2**). Cellular morphologies did not differ between SF, Col-1, and PO substrates, time points (48 and 96 h post seeding) or genotypes (wt or Adk^{-/-}) - and there were no signs of cell death.

Metabolic activity and proliferation of Adk^{-/-} ESC derived glial precursor cells cultured on PO, Col-1, and SF

To evaluate the influence of different substrates on the metabolic activity of undifferentiated glial precursor cells, Adk^{-/-} glial precursor cells were plated (n=5) on SF, Col-1 and (PO). Metabolic conversion of MTT was measured, using the MTT assay and comparing relative units of absorbance (rU_{MTT}) (**Fig. 3A**). 48 h after plating on SF, Adk^{-/-} cells showed a conversion of 0.066 ± 0.019 rU_{MTT}. This value was significantly lower than those obtained from cells cultured on Col-1 (0.116 ± 0.039 rU_{MTT}) and PO (0.186 ± 0.009 rU_{MTT}). MTT conversion measured after 96 h were as follows: SF: 0.628 ± 0.152 rU_{MTT}; Col-1: 0.333 ± 0.042 rU_{MTT}; PO: 0.404 ± 0.068 rU_{MTT}.

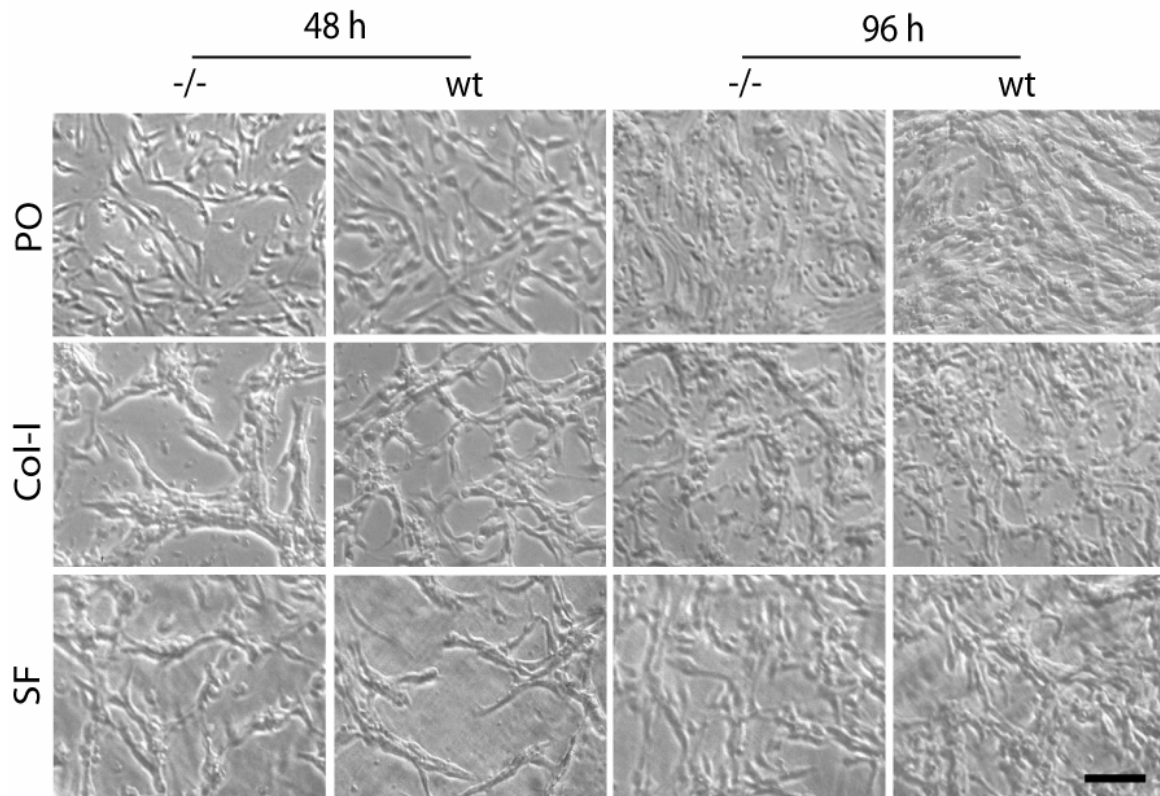


Fig. 2: Adherence of *Adk*^{-/-} (-/-) and *wt* ES derived glial precursor cells on poly(L-ornithine) (PO), collagen I (Col-I) and silk fibroin (SF) after 48 h and 96 h; scale bar = 20 μ m.

On all substrates cells showed a significant ($p < 0.01$) increase of absorbance after 96 h as compared to 48 h of culture. This increase was most evident in *Adk*^{-/-} cell cultures on SF, increasing almost 10-fold (48 h: 0.066 ± 0.019 rU_{MTT}; 96 h: 0.628 ± 0.152 rU_{MTT}). Compared to cells on PO and Col-1, MTT conversion of glial precursor cells on SF was significantly higher ($p < 0.05$ or $p < 0.01$, respectively) after 96 h of culture.

To evaluate changes in cell numbers across substrates and time in culture, DNA content of the cell cultures was assessed with the PicoGreen assay (Fig. 3B). After 48 h, the DNA content in *Adk*^{-/-} glial precursor cells was similar on all substrates (SF: 0.557 ± 0.135 ng; Col-1: 0.421 ± 0.037 ng; PO: 0.479 ± 0.0433 ng). DNA content of *Adk*^{-/-} cell cultures on PO and, to a lesser extent, on Col-1 increased significantly (** $p < 0.01$) at 96 h (Col-1: 4.669 ± 2.323 ng; PO: $9.086 \pm$

6.474 ng) when compared to the 48 hour time point. However, on SF, the Adk^{-/-} cell numbers remained essentially the same at 96 h (0.755 ± 0.175 ng).

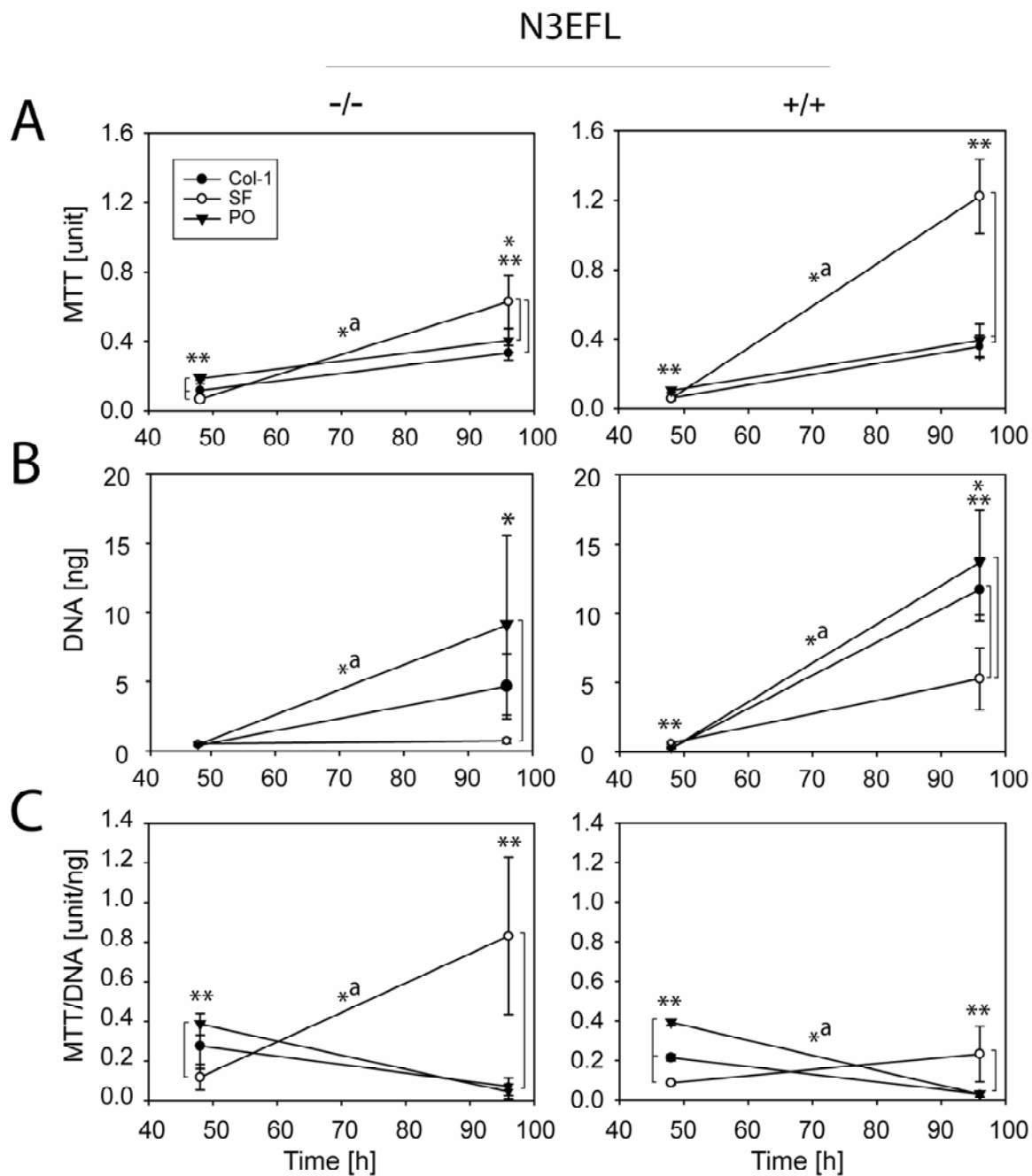


Fig. 3: Metabolism and DNA content of Adk^{-/-} (-/-) and wild type (+/+) ES derived glial precursor cell cultures on poly(L-ornithine) (PO), collagen 1 (Col-1) and silk fibroin (SF) after 48 h and 96 h ($p < 0.05$, ** $p < 0.01$).*

To assess the metabolic activity irrespective of cell viability, the conversion of MTT (rU_{MTT}) was normalized according to the DNA content of the cultures ($rU_{\text{MTT}}/\text{ng DNA}$). The normalized metabolic activity of Adk^{-/-} cells was significantly increased ($p < 0.01$) on the SF films at 96 h ($0.831 \pm 0.396 rU_{\text{MTT}}/\text{ng DNA}$) when compared to 48 h ($0.119 \pm 0,064 rU_{\text{MTT}}/\text{ng DNA}$). The normalized metabolic activity of Adk^{-/-} glial precursor cells grown on Col-1 and on PO decreased significantly ($p < 0.01$) at 96 h (Col-1: $0.071 \pm 0.039 rU_{\text{MTT}}/\text{ng DNA}$; PO: $0.044 \pm 0.039 rU_{\text{MTT}}/\text{ng DNA}$) when compared to 48 h (Col-1: $0.276 \pm 0.116 rU_{\text{MTT}}/\text{ng DNA}$; PO: $0.387 \pm 0.055 rU_{\text{MTT}}/\text{ng DNA}$) of culture, a time point when the normalized metabolic activity of the cells grown on Col-1 and PO was slightly higher than that of the cells grown on SF ($0.119 \pm 0,064 rU_{\text{MTT}}/\text{ng DNA}$). Adk^{-/-} glial precursor cells cultured on SF for 96 h showed a significantly ($p < 0.01$) higher normalized metabolic rate as compared to the respective cells cultured for 96 h on Col-1 or PO surfaces (**Fig. 3C**).

Differentiation of wt and Adk^{-/-} ESC derived glial precursor cells on SF and

Col-1

To determine the impact of SF and Col-1 on stem cell derived glial precursor differentiation in comparison to that on PO, cells of both genotypes were plated on the different substrates ($n=5$), differentiated by growth factor withdrawal and immunostained with markers indicative of astrocytes (GFAP), oligodendrocytes (O4) and early neurons (β III-tubulin). The majority of wt and Adk^{-/-} glial precursor cells cultured on the PO-coated tissue culture plastic stained positive for GFAP (**Fig. 4A**). Wt and Adk^{-/-} cells cultured on Col-1 (**Fig. 4B**) and SF (**Fig. 4C**) also stained almost exclusively for GFAP. Minimal or no positive staining was observed for O4 and β III-tubulin (data not shown).

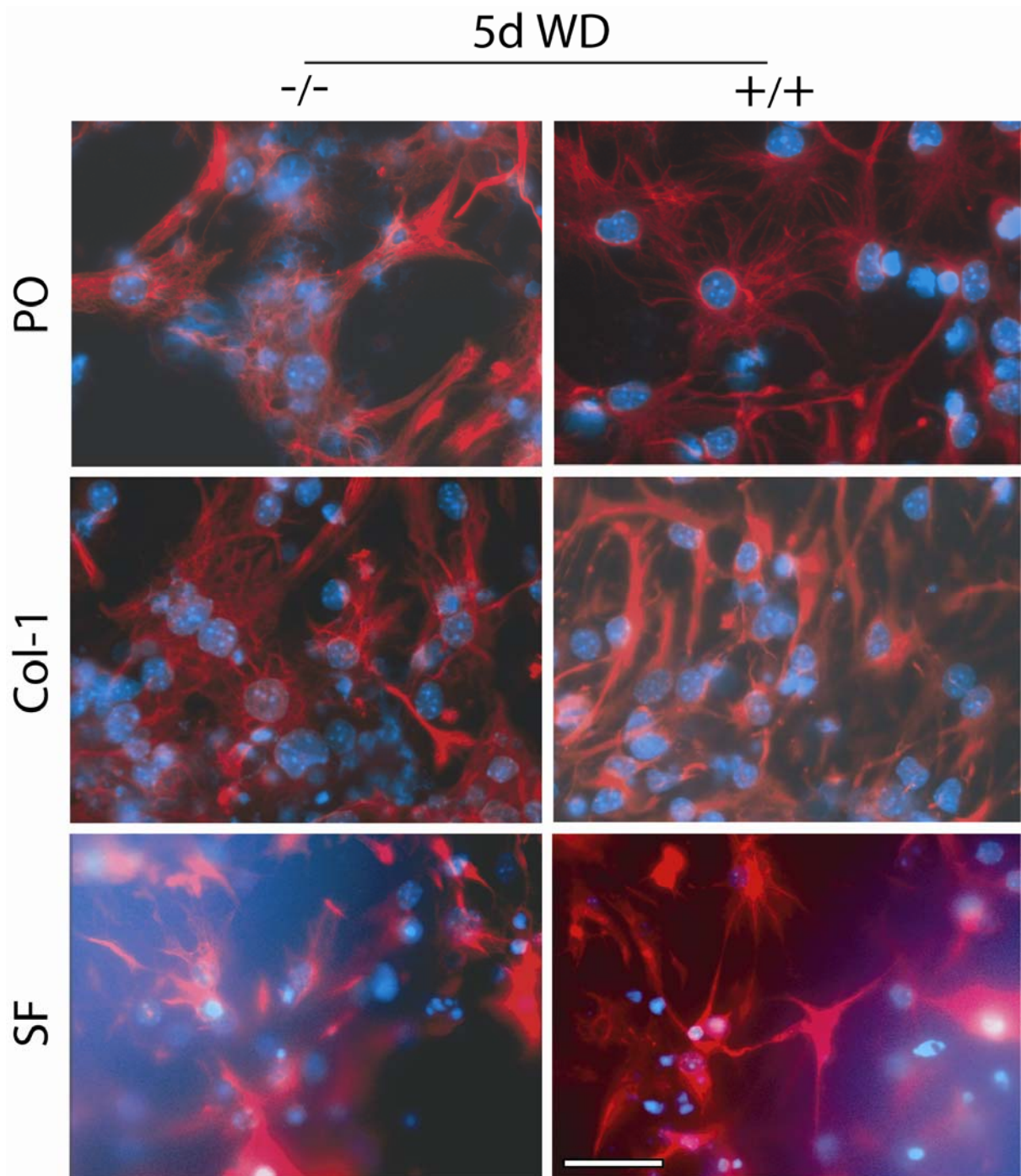


Fig. 4: Immunohistochemical staining of GFAP localization in differentiated Adk^{-/-} (-/-) and wt (+/+) ES derived glial precursor cells after 5 days growth factor withdrawal (5d WD) on poly(L-ornithine) (PO), collagen 1 (Col-1) and silk fibroin (SF); scale bar = 20 μ m.

Adenosine release from wt and Adk^{-/-} ESC derived glial precursor cells cultured on SF and PO

To determine the influence of SF on adenosine release from Adk^{-/-} cells, a bioluminescence assay was used. Wt and Adk^{-/-} cells were cultured on SF and PO (n=6) and samples of medium were taken 2 h after medium change. Overall, Adk^{-/-} cells on SF released significantly more adenosine than the respective wt cells on all substrates. This was comparable to the adenosine release from cells cultured on PO (**Fig. 5**). Adenosine release from Adk^{-/-} cells cultured for 48 h was 43.9 ± 13.9 ng/ml on SF and 48.1 ± 11.0 ng/ml on PO compared to 10.5 ± 3.1 ng/ml and 10 ± 0.7 ng/ml from the respective wt cells ($p < 0.01$). At the 96 hour time point, Adk^{-/-} cells cultured on SF released 68.6 ± 12.0 ng/ml adenosine and Adk^{-/-} cells on PO released 74.0 ± 9.7 ng/ml adenosine as compared to the respective wt cells, which released 23.5 ± 4.5 ng/ml adenosine on SF and 10.5 ± 2.3 ng/ml adenosine on PO ($p < 0.01$). After 5 days of withdrawal from growth factors allowing the cells to differentiate into glial cells, Adk^{-/-} cells on SF released 44.3 ± 12.7 ng/ml adenosine while Adk^{-/-} cells on PO released 40.2 ± 6.1 ng/ml adenosine. The respective wt cells after 5 days of differentiation released significantly less adenosine, 10.5 ± 7.6 ng/ml on SF and 11.7 ± 3.1 ng/ml on PO ($p < 0.01$).

Glucose permeation through silk films

To evaluate nutrient transport through the silk films, we measured the diffusion of radioactively tagged glucose through the films. The initial concentration of glucose in the donor chamber was set at 4.5 mg/ml, which was equivalent to the glucose concentration in the cell culture medium (DMEM). The rate of glucose diffusing through the silk films was constant over 48 h. The flux per unit surface, as calculated by linear regression, was $8.6 \mu\text{g mm}^{-2} \text{h}^{-1}$ (**Fig. 6**).

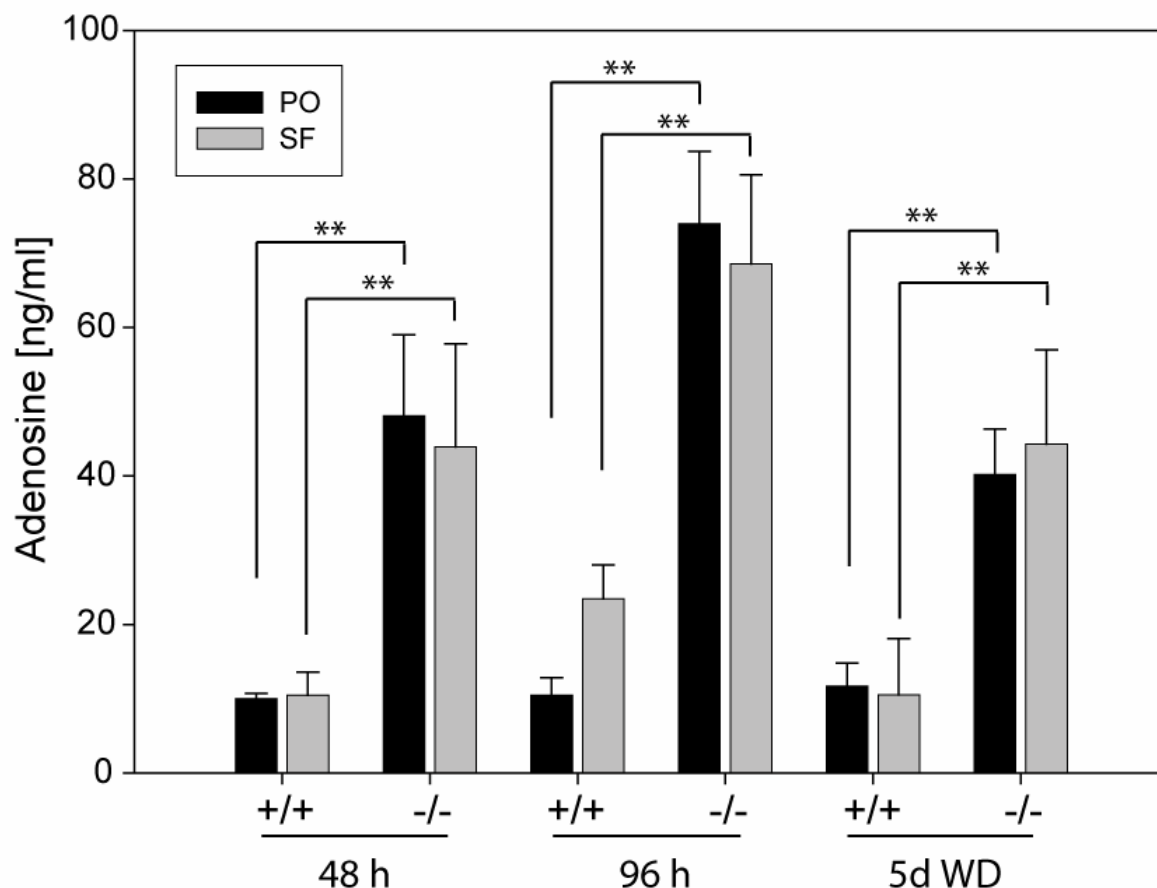


Fig. 5: Adenosine release from *Adk*^{-/-} (-/-) and wt (+/+) ES derived glial precursor cells on poly(L-ornithine) (PO) and silk fibroin (SF) before (48 h, 96 h) and after 5 days growth factor withdrawal (5d WD) (***p* < 0.01).

DISCUSSION

Local cell-mediated adenosine release has been demonstrated to represent an effective strategy to suppress seizures in the rat kindling model of epilepsy [5, 6, 27]. In these previous studies, cells were engineered to release adenosine based on a genetic disruption of adenosine kinase (*Adk*^{-/-}). The cells were encapsulated into a semipermeable, synthetic polyethersulfone membrane and implanted into the lateral brain ventricle of kindled rats. While this approach proved that paracrine cell-mediated adenosine release into the lateral ventricle was an efficacious treatment of epilepsy, the therapeutic effect did not persist because of limited cell viability within the polymer capsules.

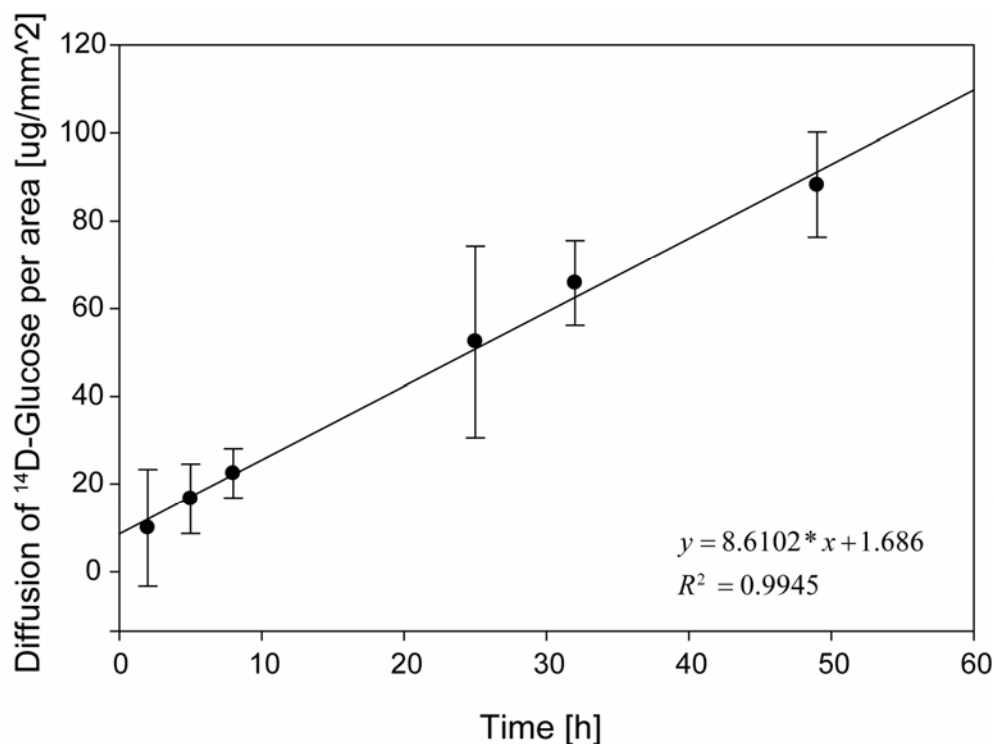


Fig. 6: Glucose permeation through silk films over 2 days. Glucose flux was $8.6 \mu\text{g mm}^{-2} \text{h}^{-1}$.

Furthermore, the system faced limitations due to the persistent nature of polysulfone, demanding a second surgical intervention if the bioreactor had to be replaced. New approaches in cell therapy must consider the long-term maintenance of cells on a biopolymeric substrate, which exhibits mechanical strength, biocompatibility, slow degradation, little or no immune or inflammatory response from the host tissue, and allow for cell adherence to the biomaterial matrix.

Collagens have already proven their compatibility in nervous tissue [10-14]. However, they exhibit weak mechanical stability, fast biodegradation and may not be stable enough to maintain cell cultures *in vivo*. Silk fibroin (SF) may offer an alternative to fill the niche due to its distinguished mechanical properties and optimal biodegradation times, adjustable between 6–12 months or more [24]. In addition, cells adhere directly to SF matrices and inflammatory reactions were less as compared to collagens or synthetic polymers [19, 20, 25, 26, 28]. Here we compared silk fibroin (SF) and fast degrading collagen (Col-1) with poly(L-

ornithine) (PO) coated tissue culture plastic as substrates for Adk^{-/-} embryonic stem cell (ESC) derived glial precursor cell culture in an effort to determine the feasibility of such substrates for clinically relevant epilepsy treatment.

While the hydrophobicity of PO coated tissue culture plastic appeared to be significantly lower than non-coated plastic, it was comparable to that of SF and Col-1 (**Fig. 1**). Therefore, in terms of hydrophilic interactions with the cells, SF and Col-1 appear equally capable compared to the traditional substrate used for cell culture, PO. Corroborating these findings, we observed that both Adk^{-/-} and control (wt) ESC derived glial precursor cells cultured on SF and Col-1 appeared to adhere and spread on the substrate to a similar degree as that observed on PO (**Fig. 2**). Therefore, SF and Col-1 are able to support the initial adherence and culture of ESC derived glial precursor cells.

To assess relative metabolic activity and proliferation of cells attached to various substrates we used the MTT assay [29, 30]. In order to compare the metabolic activity of cells under the various conditions irrespective of the number or viability of the cells, we performed a Pico Green DNA assay to normalize the metabolic activity to DNA content of the cultures. Thus, the relative metabolic activity $[rU_{\text{MTT}}]$ divided by DNA amount $[\text{ng DNA}]$ allowed us to assess the normalized metabolic activity of the cells $[rU_{\text{MTT}}/\text{ng DNA}]$, which takes into account the possible different proliferation rates and viability of the cells during the time period of assessment.

Our results demonstrate that both the relative (**Fig. 3A**) as well as the normalized (**Fig. 3C**) metabolic activity of the cells grown on Col-1 and PO was slightly higher than that of the cells grown on SF for 48 h. Since the relative metabolic activity can be indicative of cell proliferation, we observe a corresponding increase in cell number at 96 h compared to 48 h on Col-1 and PO. Such an increase in cell number was not observed on SF at the 96 hour time point compared to the 48 hour time point; therefore, the normalized metabolic activity of the cells increased significantly at this later time point. The normalized metabolic activity further revealed the dramatic increase in metabolism of cells

grown on SF at 96 h compared to 48 h and compared to the other substrates at the 96 h time point. This indicates that there is a slight delay in cells grown on SF to reach their maximal metabolic activity and we would expect the number of cells on SF to increase accordingly after the 96 hour time point.

Despite an initial delay in cell proliferation of cultures grown on SF, cells on all substrates differentiated into astrocytes after growth factor withdrawal for 5 days (**Fig. 4**), as indicated by the positive stain for GFAP, a marker of astrocytes, and the phenotypic change indicative of astrocytic differentiation. This suggests that both Col-1 and SF supported the capacity of the glial precursor cells to differentiate into astrocytes to the same extent as that observed on PO coated tissue culture plastic surfaces. Since our SF membranes are mainly in beta-sheet conformation and do not contain any cell binding domains, such as RGD domains, cell differentiation processes were not expected to be influenced by the film itself, a prediction that was confirmed here. This is an important finding since the differentiation of ES cell derived glial progenitor cells into astrocytes needs to be controlled by exogenous cues [7, 8]. As determined previously for terminally differentiated cells [23], the inclusion of cell binding domains or of Pronectin-F or Pronectin-L into the silk membrane may help to augment the release of bioengineered products.

To assess whether SF supports the release of adenosine in the absence of such cell binding domains, adenosine release was determined from Adk^{-/-} glial precursor cells grown on SF and PO. Adk^{-/-} cells cultured on SF for 48 and 96 h and after 5 days of differentiation released the same amount of adenosine as the respective Adk^{-/-} cells cultured on PO. Thus, the inclusion of cell binding domains is not necessary to promote cell mediated adenosine release. In contrast to our previous study, here we observed that differentiated cells do not release significantly more adenosine than proliferating cells [7]. One difference between the two experiments is the time period the cells were in culture before sampling the medium. In the previous study adenosine release was measured 24 h after plating of glial precursor cells on PO, and glial differentiation was initiated 24 h

after plating. Therefore, the delayed sampling of adenosine performed in the present study resulted in higher levels of adenosine release from the proliferating cells when compared to the differentiated cells. Since in the present study the actual number of cells growing on SF could not be determined, cell counts were replaced by DNA quantification with the PicoGreen assay. Therefore, it is difficult to compare the current release data with that of our previous study, where the release was normalized according to cell numbers.

Glucose permeability studies demonstrated a high glucose flux through the SF films used in the present work. Recent diffusion studies, including small molecular drugs and oxygen permeation through silk fibroin membranes [31], further support the quality of silk fibroin and its possible application as a material for bioincubators suitable for cell based drug delivery.

CONCLUSION

The results of this study demonstrate that the differentiation of adenosine kinase deficient ES cell derived glial precursor cells into astrocytes was efficient on silk fibroin. We demonstrated that silk fibroin supports the release of adenosine from the differentiated Adk^{-/-} astrocytes. We conclude that silk fibroin constitutes a suitable substrate for the directed differentiation of ES cell derived progeny and for the cell-mediated therapeutic release of adenosine. Thus, future developments might allow the construction of silk- and Adk^{-/-} stem cell-based bioincubators for the treatment of partial epilepsies.

ACKNOWLEDGEMENTS

We thank Trudel Inc. (Zurich, Switzerland) for providing the silk cocoons. Financial support was from the Association for Orthopaedic Research, from ETH Zurich (TH project), the US National Science Foundation (grant # 0436490), the NIH grant P41 (EB002520), the NIH grant R01 NS047622-01A2, the Good

Samaritan Hospital Foundation, the Swiss National Science Foundation (grant # 3100A0-100841), and the NCCR on Neural Plasticity and Repair.

REFERENCES

1. G. Akay, M.A. Birch, M.A. Bokhari, Microcellular polyHIPE polymer supports osteoblast growth and bone formation in vitro, *Biomaterials* 25 (18) (2004) 3991-4000.
2. E. Tsuruga, H. Takita, H. Itoh, Y. Wakisaka, Y. Kuboki, Pore size of porous hydroxyapatite as the cell-substratum controls BMP-induced osteogenesis, *J Biochem (Tokyo)* 121 (2) (1997) 317-24.
3. V. Karageorgiou, D. Kaplan, Porosity of 3D biomaterial scaffolds and osteogenesis, *Biomaterials* 26 (27) (2005) 5474-91.
4. S.F. Hulbert, F.A. Young, R.S. Mathews, J.J. Klawitter, C.D. Talbert, F.H. Stelling, Potential of ceramic materials as permanently implantable skeletal prostheses, *J Biomed Mater Res* 4 (3) (1970) 433-56.
5. M.C. Wake, C.W. Patrick, Jr., A.G. Mikos, Pore morphology effects on the fibrovascular tissue growth in porous polymer substrates, *Cell Transplant* 3 (4) (1994) 339-43.
6. K.A. Athanasiou, G.G. Niederauer, C.M. Agrawal, Sterilization, toxicity, biocompatibility and clinical applications of polylactic acid/polyglycolic acid copolymers, *Biomaterials* 17 (2) (1996) 93-102.
7. J.O. Hollinger, J. Brekke, E. Gruskin, D. Lee, Role of bone substitutes, *Clin Orthop Relat Res* (324) (1996) 55-65.
8. L.D. Harris, B.S. Kim, D.J. Mooney, Open pore biodegradable matrices formed with gas foaming, *J Biomed Mater Res* 42 (3) (1998) 396-402.
9. H. Suh, Recent advances in biomaterials, *Yonsei Med J* 39 (2) (1998) 87-96.
10. F. DeLustro, J. Dasch, J. Keefe, L. Ellingsworth, Immune responses to allogeneic and xenogeneic implants of collagen and collagen derivatives, *Clin Orthop Relat Res* (260) (1990) 263-79.
11. S. Srivastava, S.D. Gorham, D.A. French, A.A. Shivas, J.M. Courtney, In vivo evaluation and comparison of collagen, acetylated collagen and collagen/glycosaminoglycan composite films and sponges as candidate biomaterials, *Biomaterials* 11 (3) (1990) 155-61.
12. P.M. Cunniff, S.A. Fossey, M.A. Auerbach, J.W. Song, D.L. Kaplan, W. Adams, R.K. Eby, D. Mahoney, D. Deborah, D.L. Vezie, Mechanical and thermal properties

- of Dragline Silk from the Spider *Nephila cavipes*, *Polymers for Advanced Technologies* 5 (1994) 401-410.
13. S. Sofia, M.B. McCarthy, G. Gronowicz, D.L. Kaplan, Functionalized silk-based biomaterials for bone formation, *J Biomed Mater Res* 54 (1) (2001) 139-48.
 14. L. Meinel, S. Hofmann, V. Karageorgiou, C. Kirker-Head, J. McCool, G. Gronowicz, L. Zichner, R. Langer, G. Vunjak-Novakovic, D.L. Kaplan, The inflammatory responses to silk films in vitro and in vivo, *Biomaterials* 26 (2) (2005) 147-55.
 15. B. Panilaitis, G.H. Altman, J. Chen, H.J. Jin, V. Karageorgiou, D.L. Kaplan, Macrophage responses to silk, *Biomaterials* 24 (18) (2003) 3079-85.
 16. G.H. Altman, F. Diaz, C. Jakuba, T. Calabro, R.L. Horan, J. Chen, H. Lu, J. Richmond, D.L. Kaplan, Silk-based biomaterials, *Biomaterials* 24 (3) (2003) 401-16.
 17. L. Meinel, S. Hofmann, V. Karageorgiou, L. Zichner, R. Langer, D. Kaplan, G. Vunjak-Novakovic, Engineering cartilage-like tissue using human mesenchymal stem cells and silk protein scaffolds, *Biotechnol Bioeng* 88 (3) (2004) 379-91.
 18. L. Meinel, V. Karageorgiou, R. Fajardo, B. Snyder, V. Shinde-Patil, L. Zichner, D. Kaplan, R. Langer, G. Vunjak-Novakovic, Bone tissue engineering using human mesenchymal stem cells: effects of scaffold material and medium flow, *Ann Biomed Eng* 32 (1) (2004) 112-22.
 19. L. Meinel, V. Karageorgiou, S. Hofmann, R. Fajardo, B. Snyder, C. Li, L. Zichner, R. Langer, G. Vunjak-Novakovic, D.L. Kaplan, Engineering bone-like tissue in vitro using human bone marrow stem cells and silk scaffolds, *J Biomed Mater Res A* 71 (1) (2004) 25-34.
 20. N. Minoura, S. Aiba, M. Higuchi, Y. Gotoh, M. Tsukada, Y. Imai, Attachment and growth of fibroblast cells on silk fibroin, *Biochem Biophys Res Commun* 208 (2) (1995) 511-6.
 21. F. Lange, Ueber die Sehnenplastik, *Verh Dtsch Orthop* 2 (1903) 10-12.
 22. F. Lange, Künstliche Bänder aus Seide., *Münch Med Wochenschr* (17) (1907) 834-836.
 23. M. Tsukada, F. Cuiulinao, M. Norihiko, A. Ciulia, Preparation and Application of Porous Silk Fibroin Materials, *Journal of Applied Polymer Science* 54 (1994) 507-514.
 24. R. Nazarov, H.J. Jin, D.L. Kaplan, Porous 3-D scaffolds from regenerated silk fibroin, *Biomacromolecules* 5 (3) (2004) 718-26.

25. U.J. Kim, J. Park, H.J. Kim, M. Wada, D.L. Kaplan, Three-dimensional aqueous-derived biomaterial scaffolds from silk fibroin, *Biomaterials* 26 (15) (2005) 2775-85.
26. H.J. Kim, U.J. Kim, G. Vunjak-Novakovic, B.H. Min, D.L. Kaplan, Influence of macroporous protein scaffolds on bone tissue engineering from bone marrow stem cells, *Biomaterials* 26 (21) (2005) 4442-52.
27. L. Meinel, O.E. Illi, J. Zapf, M. Malfanti, H. Peter Merkle, B. Gander, Stabilizing insulin-like growth factor-I in poly(D,L-lactide-co-glycolide) microspheres, *J Control Release* 70 (1-2) (2001) 193-202.
28. ICH, *Q3C(R3) - Guidelines for residual solvents*.
29. Z. Ma, C. Gao, Y. Gong, J. Shen, Paraffin spheres as porogen to fabricate poly(L-lactic acid) scaffolds with improved cytocompatibility for cartilage tissue engineering, *J Biomed Mater Res B Appl Biomater* 67 (1) (2003) 610-7.
30. V.J. Chen, P.X. Ma, Nano-fibrous poly(L-lactic acid) scaffolds with interconnected spherical macropores, *Biomaterials* 25 (11) (2004) 2065-73.
31. J. Magoshi, Y. Magoshi, Physical Properties and Structure of Silk. The Glass Transition and Conformational Changes of Tussah Silk Fibroin, *J. Appl Polym. Sci.* 21 (1977) 2405-2407.
32. U.S. Pharmacopeia, *Chapter (467): Organic volatile impurities - Residual solvents*, in *USP XXVIII*. 2006, The United States Pharmacopeia Convention, Inc.
33. P. Ruegsegger, B. Koller, R. Muller, A microtomographic system for the nondestructive evaluation of bone architecture, *Calcif Tissue Int* 58 (1) (1996) 24-9.
34. T. Hildebrand, A. Laib, R. Muller, J. Dequeker, P. Ruegsegger, Direct three-dimensional morphometric analysis of human cancellous bone: microstructural data from spine, femur, iliac crest, and calcaneus, *J Bone Miner Res* 14 (7) (1999) 1167-74.
35. R. Muller, T. Hildebrand, P. Ruegsegger, Non-invasive bone biopsy: a new method to analyse and display the three-dimensional structure of trabecular bone, *Phys Med Biol* 39 (1) (1994) 145-64.
36. N.V. Bhat, G.S. Nadiger, Crystallinity in Silk Fibers: Partial Acid Hydrolysis and Related Studies., *J. Appl. Polym. Sci.* 25 (1979) 921-932.
37. R.B. Martin, D.B. Burr, N.A. Sharkey, *Skeletal tissue mechanics*. 1998: Springer-Verlag New York, Inc.

38. A. Bigi, G. Cojazzi, S. Panzavolta, A. Ripamonti, N. Roveri, M. Romanello, K. Noris Suarez, L. Moro, Chemical and structural characterization of the mineral phase from cortical and trabecular bone, *J Inorg Biochem* 68 (1) (1997) 45-51.
39. M.J. van Luyn, P.B. van Wachem, L.H. Olde Damink, P.J. Dijkstra, J. Feijen, P. Nieuwenhuis, Secondary cytotoxicity of cross-linked dermal sheep collagens during repeated exposure to human fibroblasts, *Biomaterials* 13 (14) (1992) 1017-24.
40. M. van Luyn, P. van Wachem, O. Damink L, J. Dijkstra P, J. Feijen, P. Nieuwenhuis, Relations between *in vitro* cytotoxicity and crosslinked dermal sheep collagens., *J Biomed Mater Res* 26 (1992) 1091–1110.
41. T. Asakura, A. Kuzuhara, Conformation Characterization of Bombyx mori Silk Fibroin in the Solid State by High-Frequency ¹³C Cross Polarization-Magic Angle Spinning NMR, X-ray Diffraction, and Infrared Spectroscopy, *Macromolecules* 18 (1984) 1841-1845.
42. L. Mingzhong, L. Shenzhou, W. Zhengyu, Y. Haojing, M. Jingyu, W. Lihong, Studies on porous silk fibrion materials. I. Fine structure of freeze dried silk fibrion, *Journal of Applied Polymer Science* 79 (1999) 2185-2191.
43. R. Valluzzi, S.P. Gido, W. Muller, D.L. Kaplan, Orientation of silk III at the air-water interface, *Int J Biol Macromol* 24 (2-3) (1999) 237-42.
44. R. Valluzzi, S. Winkler, D. Wilson, D.L. Kaplan, Silk: molecular organization and control of assembly, *Philos Trans R Soc Lond B Biol Sci* 357 (1418) (2002) 165-7.
45. A.S. Lin, T.H. Barrows, S.H. Cartmell, R.E. Guldberg, Microarchitectural and mechanical characterization of oriented porous polymer scaffolds, *Biomaterials* 24 (3) (2003) 481-9.
46. L. Moroni, J.R. de Wijn, C.A. van Blitterswijk, 3D fiber-deposited scaffolds for tissue engineering: Influence of pores geometry and architecture on dynamic mechanical properties, *Biomaterials* 27 (7) (2006) 974-85.
47. J.C. Le Huec, T. Schaefferbeke, D. Clement, J. Faber, A. Le Rebeller, Influence of porosity on the mechanical resistance of hydroxyapatite ceramics under compressive stress, *Biomaterials* 16 (2) (1995) 113-8.
48. D.F. Meaney, Mechanical properties of implantable biomaterials, *Clin Podiatr Med Surg* 12 (3) (1995) 363-84.
49. F.P. Barry, R.E. Boynton, S. Haynesworth, J.M. Murphy, J. Zaia, The monoclonal antibody SH-2, raised against human mesenchymal stem cells, recognizes an epitope on endoglin (CD105), *Biochem Biophys Res Commun* 265 (1) (1999) 134-9.

50. M.K. Majumdar, V. Banks, D.P. Peluso, E.A. Morris, Isolation, characterization, and chondrogenic potential of human bone marrow-derived multipotential stromal cells, *J Cell Physiol* 185 (1) (2000) 98-106.
51. W. Judd, C.A. Poodry, J.L. Strominger, Novel surface antigen expressed on dividing cells but absent from nondividing cells, *J Exp Med* 152 (5) (1980) 1430-5.
52. L.C. Kuhn, A. McClelland, F.H. Ruddle, Gene transfer, expression, and molecular cloning of the human transferrin receptor gene, *Cell* 37 (1) (1984) 95-103.
53. H.M. DeLisser, P.J. Newman, S.M. Albelda, Platelet endothelial cell adhesion molecule (CD31), *Curr Top Microbiol Immunol* 184 (1993) 37-45.
54. R.S. Negrin, K. Atkinson, T. Leemhuis, E. Hanania, C. Juttner, K. Tierney, W.W. Hu, L.J. Johnston, J.A. Shizurn, K.E. Stockerl-Goldstein, K.G. Blume, I.L. Weissman, S. Bower, R. Baynes, R. Dansey, C. Karanes, W. Peters, J. Klein, Transplantation of highly purified CD34+Thy-1+ hematopoietic stem cells in patients with metastatic breast cancer, *Biol Blood Marrow Transplant* 6 (3) (2000) 262-71.
55. G.J. Spangrude, S. Heimfeld, I.L. Weissman, Purification and characterization of mouse hematopoietic stem cells, *Science* 241 (4861) (1988) 58-62.
56. S.L. Ishaug, G.M. Crane, M.J. Miller, A.W. Yasko, M.J. Yaszemski, A.G. Mikos, Bone formation by three-dimensional stromal osteoblast culture in biodegradable polymer scaffolds, *J Biomed Mater Res* 36 (1) (1997) 17-28.
57. I. Martin, V.P. Shastri, R.F. Padera, J. Yang, A.J. Mackay, R. Langer, G. Vunjak-Novakovic, L.E. Freed, Selective differentiation of mammalian bone marrow stromal cells cultured on three-dimensional polymer foams, *J Biomed Mater Res* 55 (2) (2001) 229-35.
58. G. Vunjak-Novakovic, B. Obradovic, I. Martin, P.M. Bursac, R. Langer, L.E. Freed, Dynamic cell seeding of polymer scaffolds for cartilage tissue engineering, *Biotechnol Prog* 14 (2) (1998) 193-202.
59. S.J. Lee, Cytokine delivery and tissue engineering, *Yonsei Med J* 41 (6) (2000) 704-19.
60. W.L. Murphy, M.C. Peters, D.H. Kohn, D.J. Mooney, Sustained release of vascular endothelial growth factor from mineralized poly(lactide-co-glycolide) scaffolds for tissue engineering, *Biomaterials* 21 (24) (2000) 2521-7.
61. M.J. Whitaker, R.A. Quirk, S.M. Howdle, K.M. Shakesheff, Growth factor release from tissue engineering scaffolds, *J Pharm Pharmacol* 53 (11) (2001) 1427-37.

62. T.A. Holland, Y. Tabata, A.G. Mikos, Dual growth factor delivery from degradable oligo(poly(ethylene glycol) fumarate) hydrogel scaffolds for cartilage tissue engineering, *J Control Release* 101 (1-3) (2005) 111-25.
63. D.D. Hile, M.L. Amirpour, A. Akgerman, M.V. Pishko, Active growth factor delivery from poly(D,L-lactide-co-glycolide) foams prepared in supercritical CO₂, *J Control Release* 66 (2-3) (2000) 177-85.

GENERAL DISCUSSION AND CONCLUSION

Biomaterial scaffolds used as artificial tissue substitutes should be biocompatible and bioresorbable but still provide enough mechanical integrity and cell adherence to physically support and guide tissue formation. For further improvement of their biological performance such as their potential to activate and support natural tissue (re)generation, the concomitant delivery of growth factors (GFs) would be highly beneficial. Yet, many synthetic biomaterials provide weak cell adherence, doubtful biocompatibility and limited bioresorption in contrast to most natural biopolymers [1-3]. Collagens from mammalian origin, e.g., have a longstanding tradition as biocompatible tissue substitutes and delivery platforms for GFs providing excellent interaction with cells and tissue. Unfortunately, their application is limited by weak mechanical properties and rapid biodegradation, and they frequently fail to physically guide and support tissue (in)growth [4-8]. In contrast, scaffolds from silk fibroin (SF) as obtained from *Bombyx mori* represent an interesting alternative to collagen because of its nearly unlimited availability and slow bioresorption, and the excellent mechanical strength and sustained integrity of its scaffolds after implantation. Previously observed undesired immune reactions to silk materials were assigned to the presence of the glycoprotein sericin and resolved by the exhaustive elimination of this component from SF. Since then, SF has been demonstrated to produce 3D scaffolds with controlled macroscopic porosity to support tissue formation and guidance over an extended period of time both *in vitro* and *in vivo* [5, 9, 10]. SF scaffolds have been successfully used to adsorb GFs by soak-loading or chemical crosslinking thus largely improving the osteoinductivity of the scaffolds again *in vitro* and *in vivo* [11, 12]. However, during soak-loading or covalent coupling to SF scaffolds significant amounts of GFs are being lost. Also the efficiency of SF scaffolds to sustain the release of GFs is poor, resulting in burst-like and fast release within the first days. Safe embedment of GFs in the SF matrix is, therefore, a promising strategy to improve the efficiency to load the scaffolds with GFs and to better sustain their release from the matrix. Though, existing SF scaffolding protocols

are frequently unacceptable for direct embedment of GFs in 3D SF matrices. Process parameters such as large salt concentrations, elevated temperatures or presence of organic solvents during scaffolding are likely to corrupt the bioactivity of GFs.

Against this background, the main objective of this PhD thesis was the development of novel scaffolding techniques for SF implants, featuring:

- (i) spatial guidance of tissue (re)generation *in vitro* and *in vivo*, (re)producing complex topological features.
- (ii) sustained release of embedded bioactive GFs, improving the biological performance of the implant and, therefore, rate and quality of tissue (re)generation.

As a proof of principle our group has recently shown that films prepared by casting and air drying aqueous SF solution were capable to sustain the release and maintain the bioactivity of embedded model proteins [13]. Fabrication of GF loaded SF scaffolds by air drying, however, lacks technical feasibility because of two reasons: (i) simple airflow is insufficient to evaporate large amounts of SF solution casted in a complex 3D mold, as a SF film will initially form at the surface and hinder the drying of underlying solution (ii), The GF is exposed for a prolonged time to room temperature or above during air drying. The dissolved GF is likely to adsorb to the mold surface or aggregate and denature under these conditions.

An additional issue is the implementation of a process that controls the formation of a macroscopic pore architecture during SF scaffolding while avoiding the degradation or the leaching of embedded GFs. Previously studied scaffolding processes utilizing foaming or freeze drying of aqueous SF solutions to produce porous scaffolds showed unsatisfactory control of the resulting pore diameter and interconnectivity [14], both parameters being essential for cellular ingrowth and formation of new bone *in vivo* [15-17]. To overcome this limitation, here we introduced a novel scaffolding technology, namely freeze drying of highly concentrated aqueous SF solutions using paraffin spheres as porogen which were

readily extracted with hexane after freeze-drying. The protocol ensured the requested porous and interconnective architecture of the scaffolds. When appropriately processed, SF is highly water soluble and allows to prepare aqueous solutions in concentrations of up to 30% (w/w) whereas the aqueous solubility of other proteins, such as collagen, is often below 1% (w/w). High protein concentrations are key for the preparation of the scaffolds as they ensure sufficient mechanical stability of the freeze dried scaffolds. For instance, porous SF scaffolds produced with a 10% (w/w) SF solution yielded half the compressive modulus at 2% strain than a scaffold produced with a 20% solution (data not shown in this thesis). Moreover, the presence of proteins at high concentration is likely to stabilize any admixed GF during processing under relatively mild conditions (drying at -30 °C).

The pore size of the SF scaffolds was predetermined by the diameter of the paraffin spheres used as porogen, whereas the interconnectivity of the pores was controlled by careful sintering of the paraffin spheres at certain temperatures. Presetting the pore diameter and the interconnectivity ensured sufficient cell ingrowth and eventually guided the deposition of bone-like tissue after seeding with human mesenchymal stem cells (hMSC) and cell culture under osteogenic conditions. This approach appears especially suitable to guide complex bone morphologies and restore tissue function. SF scaffolds with wide interconnective pore diameters showed improved osteoconductivity when implanted in cancellous bone of sheep and promoted the ingrowth of local networks of interconnected trabecular-like bone tissue.

Hexane residuals, originating from the paraffin leaching, were below the official limit of 200 ppm [18] and had no effect on the good biocompatibility of the SF scaffolds, neither *in vitro* nor *in vivo*. Nevertheless, when considering their prospective application as an implant, it may be wise to avoid the use of hexane. Replacement - if possible - with other solvents would be preferable. Furthermore, leaching the porogen with a solvent, at least to some degree, entails the risk to wash out or denature embedded GFs. In this context, we hypothesized that issues

associated with porogen leaching could be obviated by the use of a degradable porogen, such as a biopolymer with inherently fast *in vivo* resorption. This would allow to implant semi-erosive scaffolds directly after fabrication. A resorbable porogen (e.g. gelatine spheres) could be enzymatically degraded by ingrowing cells leaving the porous structure of the SF scaffold to guide tissue growth.

The sterilisation of GF loaded SF scaffolds is another important issue to be addressed. SF *per se* remains very stable at elevated temperature and allows straightforward autoclaving at standard conditions (121 °C, 20 min), in sharp contrast to a majority of natural biopolymers and biodegradable synthetic polymers. In this work, autoclaved SF scaffolds exerted excellent biocompatibility. Nevertheless, autoclaving is likely to denature embedded GFs. Therefore, the implementation of more appropriate sterilization methods is crucial to further develop GF loaded SF scaffolds. We have initially investigated ethylenoxide (EO) sterilization of SF scaffolds. It has been previously reported that the EO sterilization of BMP-2 loaded collagen scaffolds is clinically feasible, even retaining the potency of the embedded GF [19]. However, sterilization of porous SF implants by EO led to poor biocompatibility after implantation in sheep or mice, and was not further considered (data not included in this thesis). At this point it is still elusive whether the sterilization times for SF were too long, or degassing after sterilization was insufficient. This could have either led to covalent coupling of EO to SF or to traces of EO remaining in SF, which could have increased the observed foreign body reaction to SF. To assure the sterility of GF loaded SF scaffolds, the implants were either fabricated under aseptic conditions or sterilized by gamma irradiation, with the latter being even less detrimental to embedded GFs than EO [20].

To improve the biological activity of the SF scaffolds, insulin-like growth factor I (IGF-I) was admixed to highly concentrated aqueous SF solutions (20%) and embedded using the novel scaffolding process. IGF-I is an abundant GF present in many tissues, exerting mitogenic activity on various cell types such as progenitor cells in bone and cartilage under *in vitro* and *in vivo* conditions [21-24].

Therefore, IGF-I was expected to improve the biological performance of the novel SF implants in both bone and cartilage tissue engineering. The potency of embedded IGF-I was maintained upon gamma irradiation of the scaffolds. Bioactive IGF-I was released from porous SF scaffolds for 29 days and improved the chondrogenesis of hMSC in contrast to unloaded scaffolds. However, only a fraction of 20 to 26% of the initially loaded IGF-I was released from the scaffolds. It yet remains to be clarified whether the unavailable fraction of IGF-I remained physically entrapped in the scaffold or was irreversibly bound or denatured through interaction with SF.

To enlarge the excellent mechanical features of SF, its slow biodegradation and GF delivery properties to other GFs and tissues, SF was also used to produce nerve conduits (NC) to guide the regeneration of peripheral nerves after injury. NC should bridge the incidental gaps between the transected nerves stumps, and physically guide and support the ingrowth of Schwann cells, while physically protecting the sprouting axonal cones during regeneration. Nerve growth factor (NGF) is a known neurotrophic factor involved in the maintenance and survival of neurons, stimulating and spatially guiding ingrowing Schwann cells and the sprouting axon, which is especially beneficial to enhance the regeneration of larger nerve gaps (>10 mm). SF-NC were prepared by either air drying or freeze drying of aqueous SF solution. Embedded bioactive NGF was released from SF-NC for more than 4 weeks under physiological conditions and triggered differentiation of PC12 cells during the entire release. However, the total cumulative release of NGF was well below the release of IGF-I embedded under the same conditions.

It has been previously reported that the total cumulative release of embedded molecules from SF matrices is negatively correlated with their molecular weight [13]. Moreover, SF exerts a negative net charge [25] at isohydric pH and is likely to bind and retain GFs carrying a positive net charge. By comparison, IGF-I exerts a lower MW but also a lower net charge at isohydric pH in contrast to the larger NGF dimer with a higher negative net charge at isohydric

pH [26]. Probably both the higher MW of NGF as well as its stronger ionic interaction with SF must have slowed down the release of NGF from SF matrices. To further elucidate the impact of GF-SF interactions, NGF was processed in SF solution as well as in solutions containing lactic acid and subsequently resuspended in buffer to assess both the changes in NGF availability and its activity as monitored by ELISA, HPLC and PC12 bioactivity assay, respectively. GFs formulated with SF solution lost about 60% of their initial availability and activity in contrast to the GFs formulated in solutions containing lactic acid. At this moment it is still elusive, whether the GF bound reversible or irreversibly to SF, and whether the GF underwent denaturation when interacting with negatively charged and highly hydrophobic SF molecules.

Consequently, improvements in SF-GF interactions hold great potential to further optimize GF delivery properties of SF matrices. In this context, SF was blended with collagen (Col) to introduce more hydrophilic moieties for GF stabilization. SF blended with collagen at a ratio of 90:10 led to a release of 80% of the initially loaded horse radish peroxidase (HRP) being in sharp contrast to only 15% from pure SF films (results not included in this thesis). The release of HRP from SF films correlated well with the release of NGF. However, HRP, serving as a model for GF, was quickly released within 5 days approximating the observed release from SF within this period. This pattern indicated a good sustainment of its potency but poor and unspecific retention of the protein itself. Nevertheless, the blending of SF with low amounts of ECM molecules such as collagen, hyaluronic acid or heparin holds the potential to improve the retention of specific GF with inherent affinity for these ECM molecules, such as BMP-2, TGF-beta or FGF-2, respectively [21, 27, 28]. Such modifications could help to further sustain the potency of GF during embedment and release as well as improve the loading and retention of the GF. Through such additives, also the adsorption of GFs on SF could be enhanced obviating for certain applications the complicated embedment of GF and the drawbacks associated with this process. However, a successful incorporation of additives that endow SF with improved GF

interactions - by blending, chemical modification or genetic engineering of SF – makes it necessary to circumvent negative interactions between SF and GFs. Ongoing projects, such as the sulfation of SF are aimed to provide more hydrophilic interaction sites for GF binding. In analogy to sulfated glycosaminoglycans (GAG), addition of heparin may improve SF-GF interactions, maintain GF stability and modify GF delivery. An optimization of the fundamental interactions between GF and SF is crucial for the implementation of more complex release mechanisms. Improvements in this area will be crucial for clinical applications of SF towards GF delivery systems for tissue repair.

In conclusion, the present work is a contribution to the current know-how regarding the application of SF as a scaffold for GF delivery in tissue engineering, particularly with respect to (i) SF scaffolding technologies, (ii) sustainment of GF potency and release, (iii) the interactions between GFs and SF and (iv) the importance of controlled GF delivery in tissue engineering.

REFERENCES

- [1] P. Giusti, L. Lazzeri, S. De Petris, M. Palla, M.G. Cascone, Collagen-based new bioartificial polymeric materials, *Biomaterials* 15 (15) (1994) 1229-33.
- [2] M.G. Cascone, N. Barbani, C. Cristallini, P. Giusti, G. Ciardelli, L. Lazzeri, Bioartificial polymeric materials based on polysaccharides, *J Biomater Sci Polym Ed* 12 (3) (2001) 267-81.
- [3] N. Bhattarai, H.R. Ramay, J. Gunn, F.A. Matsen, M. Zhang, PEG-grafted chitosan as an injectable thermosensitive hydrogel for sustained protein release, *J Control Release* 103 (3) (2005) 609-24.
- [4] S. Itoh, K. Takakuda, S. Kawabata, Y. Aso, K. Kasai, H. Itoh, K. Shinomiya, Evaluation of cross-linking procedures of collagen tubes used in peripheral nerve repair, *Biomaterials* 23 (23) (2002) 4475-81.
- [5] L. Meinel, V. Karageorgiou, R. Fajardo, B. Snyder, V. Shinde-Patil, L. Zichner, D. Kaplan, R. Langer, G. Vunjak-Novakovic, Bone tissue engineering using human mesenchymal stem cells: effects of scaffold material and medium flow, *Ann Biomed Eng* 32 (1) (2004) 112-22.
- [6] S. Srivastava, S.D. Gorham, D.A. French, A.A. Shivas, J.M. Courtney, In vivo evaluation and comparison of collagen, acetylated collagen and collagen/glycosaminoglycan composite films and sponges as candidate biomaterials, *Biomaterials* 11 (3) (1990) 155-61.
- [7] S. Srivastava, S.D. Gorham, J.M. Courtney, The attachment and growth of an established cell line on collagen, chemically modified collagen, and collagen composite surfaces, *Biomaterials* 11 (3) (1990) 162-8.
- [8] R.L. Collins, D. Christiansen, G.A. Zazanis, F.H. Silver, Use of collagen film as a dural substitute: preliminary animal studies, *J Biomed Mater Res* 25 (2) (1991) 267-76.
- [9] L. Meinel, V. Karageorgiou, S. Hofmann, R. Fajardo, B. Snyder, C. Li, L. Zichner, R. Langer, G. Vunjak-Novakovic, D.L. Kaplan, Engineering bone-like tissue in vitro using human bone marrow stem cells and silk scaffolds, *J Biomed Mater Res A* 71 (1) (2004) 25-34.
- [10] S. Hofmann, H. Hagenmuller, A.M. Koch, R. Muller, G. Vunjak-Novakovic, D.L. Kaplan, H.P. Merkle, L. Meinel, Control of in vitro tissue-engineered bone-like

- structures using human mesenchymal stem cells and porous silk scaffolds, *Biomaterials* 28 (6) (2007) 1152-62.
- [11] V. Karageorgiou, M. Tomkins, R. Fajardo, L. Meinel, B. Snyder, K. Wade, J. Chen, G. Vunjak-Novakovic, D.L. Kaplan, Porous silk fibroin 3-D scaffolds for delivery of bone morphogenetic protein-2 in vitro and in vivo, *J Biomed Mater Res A* 78 (2) (2006) 324-34.
- [12] V. Karageorgiou, L. Meinel, S. Hofmann, A. Malhotra, V. Volloch, D. Kaplan, Bone morphogenetic protein-2 decorated silk fibroin films induce osteogenic differentiation of human bone marrow stromal cells, *J Biomed Mater Res A* 71 (3) (2004) 528-37.
- [13] S. Hofmann, C.T. Foo, F. Rossetti, M. Textor, G. Vunjak-Novakovic, D.L. Kaplan, H.P. Merkle, L. Meinel, Silk fibroin as an organic polymer for controlled drug delivery, *J Control Release* 111 (1-2) (2006) 219-27.
- [14] R. Nazarov, H.J. Jin, D.L. Kaplan, Porous 3-D scaffolds from regenerated silk fibroin, *Biomacromolecules* 5 (3) (2004) 718-26.
- [15] F.R. Rose, L.A. Cyster, D.M. Grant, C.A. Scotchford, S.M. Howdle, K.M. Shakesheff, In vitro assessment of cell penetration into porous hydroxyapatite scaffolds with a central aligned channel, *Biomaterials* 25 (24) (2004) 5507-14.
- [16] B. Flautre, M. Descamps, C. Delecourt, M.C. Blary, P. Hardouin, Porous HA ceramic for bone replacement: role of the pores and interconnections - experimental study in the rabbit, *J Mater Sci Mater Med* 12 (8) (2001) 679-82.
- [17] J.X. Lu, B. Flautre, K. Anselme, P. Hardouin, A. Gallur, M. Descamps, B. Thierry, Role of interconnections in porous bioceramics on bone recolonization in vitro and in vivo, *J Mater Sci Mater Med* 10 (2) (1999) 111-20.
- [18] ICH, *Q3C(R3) - Guidelines for residual solvents*.
- [19] Y.C. Tyan, J.D. Liao, S.P. Lin, C.C. Chen, The study of the sterilization effect of gamma ray irradiation of immobilized collagen polypropylene nonwoven fabric surfaces, *J Biomed Mater Res A* 67 (3) (2003) 1033-43.
- [20] T. Pekkarinen, O. Hietalal, T. Jamsa, P. Jalovaara, Gamma irradiation and ethylene oxide in the sterilization of native reindeer bone morphogenetic protein extract, *Scand J Surg* 94 (1) (2005) 67-70.
- [21] S. Mohan, D.J. Baylink, Bone growth factors, *Clin Orthop Relat Res* (263) (1991) 30-48.

- [22] S. Yakar, P. Pennisi, Y. Wu, H. Zhao, D. LeRoith, Clinical relevance of systemic and local IGF-I, *Endocr Dev* 9 (2005) 11-6.
- [23] L. Meinel, E. Zoidis, J. Zapf, P. Hassa, M.O. Hottiger, J.A. Auer, R. Schneider, B. Gander, V. Luginbuehl, R. Bettschart-Wolfisberger, O.E. Illi, H.P. Merkle, B. von Rechenberg, Localized insulin-like growth factor I delivery to enhance new bone formation, *Bone* 33 (4) (2003) 660-72.
- [24] L. Longobardi, L. O'Rear, S. Aakula, B. Johnstone, K. Shimer, A. Chytil, W.A. Horton, H.L. Moses, A. Spagnoli, Effect of IGF-I in the chondrogenesis of bone marrow mesenchymal stem cells in the presence or absence of TGF-beta signaling, *J Bone Miner Res* 21 (4) (2006) 626-36.
- [25] Q. Cheng, T.Z. Peng, X.B. Hu, C.F. Yang, Charge-selective recognition at fibroin-modified electrodes for analytical application, *Anal Bioanal Chem* 382 (1) (2005) 80-4.
- [26] K. Herrup, E.M. Shooter, Properties of the beta nerve growth factor receptor of avian dorsal root ganglia, *Proc Natl Acad Sci U S A* 70 (12) (1973) 3884-8.
- [27] Y. Zhu, A. Oganessian, D.R. Keene, L.J. Sandell, Type IIA procollagen containing the cysteine-rich amino propeptide is deposited in the extracellular matrix of prechondrogenic tissue and binds to TGF-beta1 and BMP-2, *J Cell Biol* 144 (5) (1999) 1069-80.
- [28] M. Maccarana, B. Casu, U. Lindahl, Minimal sequence in heparin/heparan sulfate required for binding of basic fibroblast growth factor, *J Biol Chem* 268 (32) (1993) 23898-905.

*CURRICULUM VITAE***Lorenz Uebersax**

MSc, Dipl Ing. Biotech ESBS

University of Strasbourg, France and University of Basel, Switzerland

Born February 20th 1976 in Basel, Switzerland

Luisenstrasse 18

CH-8005 Zürich

Education & position held

- | | |
|-----------------|---|
| 07/2004-10/2007 | PhD student and teaching assistant
Swiss Federal Institute of Technology Zurich, ETH Zurich, Zurich
Switzerland
Department of Chemistry and Applied Biosciences (D-CHAB)
Institute of Pharmaceutical Sciences
Drug Formulation & Delivery
(Prof. Dr. Hans P. Merkle, Dr. Dr. Lorenz Meinel) |
| 10/2003 | MSc in molecular and cellular biology and Dipl. Ing. Biotech ESBS |

- 2000-2003 Tri-national Master program (EUCOR) in Biotechnology hosted by the Ecole Supérieure de Biotechnologie de Strasbourg (ESBS), Strasbourg, France and University of Basel, Basel Switzerland.
- 1998-2000 Undergraduate studies in Biology II (BSc)
University of Basel, Basel, Switzerland
Biozentrum
- 1997-1998 Undergraduate studies in Law
University of Basel, Basel, Switzerland
Juristische Fakultät
- 1992-1996 High School
Gymnasium Oberwil (BL)
Typus C (Science)

Scientific Internships

-
- 2006-2007 Swiss National Science foundation (SNF) fellowship
Tufts University, Medford, MA, USA
Department of Biomedical Engineering
Tufts-MIT Tissue Engineering Resource Center (TERC)
(Prof. Dr. David L. Kaplan)
-
- 2003-2004 Scientific internship (6 month): Novel strategies for stable and transient gene expression
Ecole Polytechnique Fédérale de Lausanne, EPFL, Lausanne Switzerland, School of Life Science
Laboratory of Cellular Biotechnology (LBTC)
(Prof. Dr. Florian M. Wurm)

- 2002-2003 Master Thesis (9 months): On-chip reverse transfection array for neuronal cell lines and stem cells.
National Institute of Advance Science and Technology (AIST), Amagasaki, Japan, Tissue Engineering Research Center (TERC)
Gene Technology Team
(Dr. Jun Myiake, Dr. Masato Myiake)
- 6-7/2001 Scientific intership (2 month)
Enzymatic screening in *Saccharomyces cerevisia*
University of Lund, Lund, Sweden, Chemistry Center
(Prof. Dr. Bärbel Hahn-Hägerdahl)
- 10/2002 Scientific internship (1 month): Database of Small molecular ligands for modeling of receptor-ligand interaction
Institute de Génétique et de Biologie Moléculaire et Cellulaire, IGBMC, Illkirch, France, Department of Bioinformatics
(Dr. Wurtz)

Scientific publications

Journal publications

Uebersax L, Apfel Tanja, Kaplan DL, Auer J, Meinel L, Merkle HP, von Rechenberg B. *Biocompatibility and osteoconduction of macroporous silk fibroin implants in cortical defects in sheep*. To be submitted to Biomaterials

Uebersax L, Merkle HP, Meinel L. *Insulin-like growth factor I releasing silk fibroin scaffolds induce chondrogenic differentiation of human mesenchymal stem cells*. J. Control. Release. 2007, 27(1):12-21.

Uebersax L, Mattotti M, Papaloizos M, Merkle HP, Gander B, Meinel L. *NGF-releasing silk fibroin implants for peripheral nerve repair*. Biomaterials. 2007; 28:4449–4460

Schneider OD, Loher S, Brunner T, Uebersax L, Simonet M, Grass RN, Merkle HP, Stark WJ. *Surgeon/patient-tailored, flexible, cotton-like composite biomaterials: In vitro bioactivity and osteogenic differentiation of human mesenchymal stem cells*. J Biomed Mater Res B Appl Biomater. 2007 Jul 6; [Epub ahead of print]

Yamada S, Nomura T, Uebersax L, Matsumoto K, Fujita S, Miyake M, Miyake J. *Retinoic acid induces functional c-Ret tyrosine kinase in human neuroblastoma*. Neuroreport. 2007 Mar 5; 18(4):359-63.

Uchimura E, Yamada S, Uebersax L, Fujita S, Miyake M, Miyake J. *Method for reverse transfection using gold colloid as a nano-scaffold*. J Biosci Bioeng. 2007 Jan; 103(1):101-3.

Uebersax L, Hagenmüller H, Hofmann S, Gruenblatt M, Müller R, Vunjak-Novakovic G, Kaplan DL, Merkle HP, Meinel L. *Effect of scaffold design on bone morphology in vitro*. Tissue Eng. 2006 Dec; 12(12):3417-29.

Uebersax L, Fedele D, Schumacher C, Merkle HP, Kaplan DL, Boison D, Meinel L. *The support of adenosine release from adenosine kinase deficient ES cells by silk substrates*. Biomaterials. 2006 Sep; 27(26):4599-607.

Uchimura E, Yamada S, Uebersax L, Yoshikawa T, Matsumoto K, Kishi M, Funeriu DP, Miyake M, Miyake J. *On-chip transfection of PC12 cells based on the rational understanding of the role of ECM molecules: efficient, non-viral transfection of PC12 cells using collagen IV*. Neurosci Lett. 2005 Apr 11; 378(1):40-3.

Hunt L, Hacker DL, Grosjean F, De Jesus M, Uebersax L, Jordan M, Wurm FM. *Low temperature pausing of cultivated mammalian cells*. Biotechnol Bioeng. 2005 Jan 20; 89(2):157-63.

Scientific Review & book chapter

Uebersax L, Merkle H. P., Meinel L. *Biopolymer based growth factor delivery: From natural concepts to engineered systems*. Manuscript in preparation

Poster Presentation

Uebersax L, Kaplan DL, Merkle HP. *Collagen blended silk fibroin materials: In vitro degradation and delivery of bioactive proteins*. Material resource center meeting, ETH Zurich, Zurich, June 27, 2007

Uebersax L, Mattotti M, Merkle H.P, Gander B, Meinel L. *Influence of processes parameters on release kinetics and bioactivity of NGF embedded in silk fibroin matrices for peripheral nerve repair*. GPEN Kansas University, October 24, 2006

Uebersax L, Merkle HP, Kaplan DL, Meinel L. *Macroporous silk implants for drug delivery in tissue engineering*. 33rd Annual Meeting & Exposition of the Controlled release society (CRS), July 21, 2006

Hagenmüller H, Uebersax L, Glettig D, Merkle HP, Meinel L, Müller R. *3-D imaging of silk fibroin scaffolds with micro-computed tomography* Dreiländertagung der deutschen, österreichischen und schweizerischen Gesellschaft für biomedizinische Technik, September 6, 2006

Uebersax L, Hagenmüller H, Hofmann S, Gruenblatt M, Müller R, Vunjak-Novakovic G, Kaplan DL, Merkle HP, Meinel L. *Effect of scaffold design on morphology of bone in vitro*. Material resource center meeting, ETH Zurich, Zurich, June 29, 2006

Hofmann S, Uebersax L, Mueller M, Merkle H.P, Meinel L. *Silk biomaterials mimicking the spider*. Electron microscopy center (EMEZ), ETH Hönggerberg, Zurich, April 22, 2005

Uebersax L, Hofmann S, Hagenmüller H, Müller R, Merkle HP, Meinel L. *Highly porous silk scaffolds for bone repair*. General assembly of the Swiss Society for Biomaterials (SSB), May 2005

Oral presentations

Uebersax L. *Silk fibroin scaffolding for growth factor delivery in tissue engineering*. PhD student symposium, Institute of Pharmaceutical Sciences, ETH Zurich, Zurich Switzerland, October 2007

Uebersax L. *Silk-based Bone Implants*. Zurich-Geneva Joint Seminar Series on Drug Formulation & Drug Delivery, Zurich, Switzerland, October 07 – 08, 2004.

Awards

Swiss National Foundation (SNF) research exchange fellowship for prospective researchers: Uebersax L., Kaplan DL, Merkle HP. *Characterization and application of silk fibroin/collagen blends*. SNF May 2006

First price for the best presentation (Dr. Wander Preis): Uebersax L., Gander B, Kaplan DL, von Rechenberg B, Meinel L, Merkle HP. *Silk fibroin scaffolding for growth factor delivery in tissue engineering*. Doktorandentag, Institute for Pharmaceutical Sciences, Department of Chemistry and Applied Biosciences, ETH Zurich, October 2006

First price for the best presentation: Uebersax L., Hofmann S, Hagenmüller H, Müller R, Merkle HP, Meinel L. *Highly porous silk scaffolds for bone repair*. General assembly of the Swiss Society for Biomaterials (SSB), May 2005

Additional scientific training

- Sterile manufacturing under GMP guidelines (certificated by Concept Heidelberg)
- Training in production of liquid formulations in the 'Armee Apotheke' (AApot)

Organisations involved

- Member, former board of the Pharmaceutical Scientists' Association (PSA)
- Member and co-founder of the Young European Biotech Network (YEBN)

Languages

German: Mother tongue

English: Fluent in reading and writing. TOEIC (A)

French: Fluent in reading and writing

Japanese: Intermediate (Certificate for passed Beginners class at the Language School of ETH/Uni Zürich)

Hobbies

Rock climbing, randonee skiing, hiking, jogging, cooking, and wine

ACKNOWLEDGMENTS

My deepest gratitude goes to Prof. Hans P. Merkle, head of the Drug Formulation & Delivery group at ETH Zurich, for giving me the opportunity to perform my PhD in this interesting area and for his constant support. I appreciated his kind personality, his inexhaustible patience and greatly benefited from his editorial work on my manuscripts.

I am further indebted to my supervisor PD Dr. Dr Lorenz Meinel, from the Drug Formulation & Delivery group at ETH Zurich, for his introduction into the interesting research at the interface of tissue engineering and drug delivery and for sharing his large scientific network. He has been a mentor of my personal skills throughout my PhD.

I would like to express my sincerest gratitude to Prof. David L. Kaplan at Tufts University, for taking on the responsibility of co-examination and for hosting me in his group at Tufts University during my internship. He provided various valuable contributions to my work.

Furthermore, I would like to thank Prof. Dr. Brigitte von Rechenberg and her group at the Vetsuisse Faculty, University of Zurich. I greatly enjoyed the insights I have gained in the planning and evaluation of animal studies and appreciated the time I have spent with her group members.

I am grateful to Prof. Dr. Wendelin J. Stark at ETH Zurich for taking the responsibility of co-examination of my thesis and for letting me participating in his project on functional nanomaterials.

My sincerest thanks and gratitude goes to Prof. Dr Bruno Gander for his friendly support and great contribution to our joint publication, which is included in chapter V of my PhD thesis.

I am further grateful to PD Dr. Detlev Boison, Dr. Denise Fedele, Claudia Schumacher (formerly University of Zurich) for the interesting collaboration on embryonic stem cells and the joint publication, which is included in chapter VI of this thesis.

I greatly appreciated the contribution and company of my Erasmus and diploma students: Marta Mattotti, Emanuel Gruenblatt, Cristina Fernandez, Michael Drechsler and Cindy Baumann.

Special thanks goes to Dr. Sandra Hofmann for the introduction into *in vitro* tissue engineering using human mesenchymal stem cells and her good company, Dr. Lukas Pfister for many fruitful discussions on material science and peripheral nerve regeneration, and in general the members of the silk group, Ester Wenk, Anne Wandrey, Henri Hagenmueller, Dr. Marcos Garcia and Dr. Chunmei Li, for a good atmosphere in the lab as well as many meals and subsequent coffees at the student restaurant. I would further like to express my gratitude to all other current and former members of the Drug Formulation & Delivery group I did not personally mention in here.

Furthermore, I would like to thank my other collaborators and colleagues I had the opportunity to meet and to work with. My gratitude goes out to Dr. vet. Roland Schubotz, Dr. vet. Tanja Apfel, PD Dr. vet. Katja Nuss (former Equine Hospital Zurich). I am very grateful to John Kluge, Brian Lawrence, Dr. Amanda Murphy, Debby Cheng and Dr. Sourabh Gosh from the Kaplan-group at Tufts, for a warm atmosphere during a cold winter in Boston. Moreover, I have greatly appreciated the dynamic collaboration with Dr. Stefan Loher, Dr. Tobias Brunner, and Oliver Schneider from the Stark-group at ETH Zurich.

Last but not least, I would like to thank my parents, family and friends for their constant support, and for being a valuable balance to my scientific adventures.